Performance Analysis and Resource Allocation in Underlaid Device-to-Device Cellular Networks

Hung V. Vu

Department of Electrical & Computer Engineering
McGill University
Montréal, Canada

December 2020

A thesis submitted to McGill University in partial fulfillment of the requirements for the degree of Doctor of Philosophy.

Abstract

Device-to-device (D2D) communications enables direct connection between nearby cellular users without traversing through the base-station (BS). Potential benefits of D2D communications in cellular networks are multi-folds, ranging from enhancing spectrum efficiency, reducing network congestion, shortening packet delay, saving power, to enabling location-based applications and services. D2D-enabled networking not only has been required for public safety networks when the cellular coverage is not available, but also developed as supporting technologies for Internet of Things (IoT) and Vehicle-to-Everything (V2X) connections. As D2D is allowed to operate in the same spectrum with cellular users, the more resources (e.g., time-frequency) are shared between D2D and cellular transmission, the more interference will be present, yet higher potential spectral efficiency gains will be provided if the interference can be effectively managed. This thesis considers underlaid D2D schemes where the D2D links fully reuse time-spectrum resources that currently occupied by the cellular transmission. Our focus is to investigate the benefits offered by underlaid D2D in terms of spectral efficiency gains via performance analysis and sum-rate maximizing resource allocation algorithms.

First, this thesis develops a Gaussian-Mixture (GM) model to represent the aggregate interference at a typical D2D receiver in underlaid D2D cellular networks. From information theoretical point-of-view, the corresponding D2D link can be thought of as an additive quadrature GM channel. We then study the characterization of optimal input and the computation of capacity of such GM channel under an average power constraint. It is shown that the capacity-achieving input distribution has a uniformly distributed phase, while the optimal amplitude distribution includes a finite number of mass points. Our numerical examples illustrate that, in many cases, the capacity-achieving distribution consists of only one or two mass points.

Second, the analysis of achievable sum-rate offered by D2D communications is extended from link to network level. Both single- and multi-cell settings are considered in which multiple D2D links reuse the channel (time-frequency resources) currently occupied by *one* cellular uplink transmission. In addition, we assume full-duplex (FD) operation at D2D links to ease the channel assignment for underlaid D2D as FD D2D only requires one carrier frequency for both transmitting and receiving signals. Utilizing stochastic geometry based models to capture the randomness and mobility of D2D/cellular users, analytical sum-rate expressions are derived and applied to investigate the effects of network parameters on the achieved sum-rates. It is demonstrated that, from an average throughput perspective, FD D2D brings performance improvements as compared to the half-duplex (HD) counterpart and pure cellular systems (in absence of D2D).

Third, the single-antenna multi-cell network model is expanded to include multi-antenna trans-

mission equipped base-stations and to further study the coexistence between massive multiple-input multiple-output (MIMO) *downlink* and underlaid D2D transmission. The focus is on joint beamforming and power allocation design for achievable sum-rate (per cell) maximization while considering the effects of interference to both cellular and D2D transmission. The problem formulation leads to a nonconvex vector-variable optimization problem, where we develop an efficient solution using a fractional programming (FP) based approach. It is shown that, in agreement with previous uplink analysis, integrating FD D2D in cellular downlink also provides a significant sum-rate improvement as compared to the HD counterpart and pure cellular systems.

Finally, motivated by the fact that resource allocation algorithms in D2D-enabled cellular networks require global channel state information (CSI) at central controllers and thus exhibit high overhead (i.e., high latency), this thesis utilizes multi-agent reinforcement learning (RL) and proposes a distributed algorithm to tackle this challenge. We focus on cellular vehicle-to-everything (C-V2X), a D2D-based technology whose characteristics are fast channel variation and low latency connection to which centralized optimization solutions are not viable. The proposed algorithm allows the vehicles to collaborate and collectively learn the environment; so optimal channels and transmit powers can be obtained independently at each vehicle, based solely on local CSI acquisition. A comparison between the learning and centralized optimization algorithms is also made to demonstrate the advantages of proposed RL approach over traditional optimization techniques.

Sommaire

Les communications d'appareil à appareil (D2D) permettent une connexion directe entre les utilisateurs cellulaires à proximité sans passer par la station de base (BS). Les avantages potentiels des communications D2D dans les réseaux cellulaires sont multiples, allant de l'amélioration de l'efficacité du spectre, à la réduction de la congestion du réseau, au raccourcissement du délai de transmission des paquets, à l'économie d'énergie, à la mise en place d'applications et de services basés sur la localisation. La mise en réseau compatible D2D a non seulement été requise pour les réseaux de sécurité publique lorsque la couverture cellulaire n'est pas disponible, mais a également été développée en tant que technologies de prise en charge pour les connexions Internet des objets (IoT) et véhicule à tout (V2X). Comme D2D est autorisé à fonctionner dans le même spectre avec les utilisateurs cellulaires, plus les ressources (par exemple, temps-fréquence) sont partagées entre D2D et la transmission cellulaire, plus il y aura d'interférences, mais des gains d'efficacité spectrale potentiels plus élevés seront fournis si les interférences peuvent être gérées efficacement. Cette thèse considère les schémas D2D sous-jacents dans lesquels les liaisons D2D réutilisent entièrement les ressources du spectre temporel actuellement occupées par la transmission cellulaire. Notre objectif est d'étudier les avantages offerts par le D2D sous-jacent en termes de gains d'efficacité spectrale via une analyse de performance et des algorithmes d'allocation de ressources maximisant le taux de somme.

Premièrement, cette thèse développe un modèle de mélange de Gaussiennes (GM) pour représenter l'interférence globale sur un récepteur D2D typique dans des réseaux cellulaires D2D sous-jacents. Du point de vue théorique de l'information, la liaison D2D correspondante peut être considérée comme un canal GM en quadrature additive. Nous étudions ensuite la caractérisation de l'entrée optimale et le calcul de capacité d'un tel canal GM sous une contrainte de puissance moyenne. On montre que la distribution d'entrée permettant d'atteindre la capacité a une phase uniformément distribuée, tandis que la distribution d'amplitude optimale comprend un nombre fini de points de masse. Nos exemples numériques illustrent que, dans de nombreux cas, la distribution de capacité à atteindre se compose d'un ou deux points de masse seulement.

Deuxièmement, l'analyse du taux de somme réalisable offert par les communications D2D est étendue du niveau de la liaison au niveau du réseau. Les paramètres à cellule unique et à cellules multiples sont considérés dans lesquels plusieurs liaisons D2D réutilisent le canal (ressources temps-fréquence) actuellement occupé par une transmission de liaison montante cellulaire. De plus, nous supposons un fonctionnement en duplex intégral (FD) sur les liaisons D2D pour faciliter l'affectation de canal pour le D2D sous-jacent, car FD D2D ne nécessite qu'une seule fréquence porteuse pour les signaux d'émission et de réception. En utilisant des modèles basés

sur la géométrie stochastique pour capturer le caractère aléatoire et la mobilité des utilisateurs D2D/cellulaires, des expressions de taux de somme analytiques sont dérivées et appliquées pour étudier les effets des paramètres de réseau sur les taux de somme obtenus. Il est démontré que, du point de vue du débit moyen, FD D2D apporte des améliorations de performances par rapport à l'homologue semi-duplex (HD) et aux systèmes cellulaires purs (en l'absence de D2D).

Troisièmement, le modèle de réseau multicellulaire à antenne unique est élargi pour inclure des stations de base équipées de transmission multi-antenne et pour étudier plus avant la coexistence entre les liaisons descendantes de multi-entrée multi-sortie (MIMO) massif et la transmission D2D sous-jacente. L'accent est mis sur la conception conjointe de la formation de faisceaux et de l'allocation de puissance pour une maximisation réalisable du débit somme (par cellule) tout en tenant compte des effets des interférences sur la transmission cellulaire et D2D. La formulation du problème conduit à un problème d'optimisation à variable vectorielle non convexe, où nous développons une solution efficace en utilisant une approche basée sur la programmation fractionnaire (FP). Il est montré que, en accord avec l'analyse de liaison montante précédente, l'intégration de FD D2D dans la liaison descendante cellulaire fournit également une amélioration significative du taux de somme par rapport à l'homologue HD et aux systèmes cellulaires purs.

Enfin, motivée par le fait que les algorithmes d'allocation de ressources dans les réseaux cellulaires compatibles D2D nécessitent des informations globales sur l'état du canal (CSI) au niveau des contrôleurs centraux et présentent donc une surcharge élevée (c.-à-d., forte latence), cette thèse utilise l'apprentissage par renforcement multi-agents (RL) et proposer un algorithme distribué pour relever ce défi. Nous nous concentrons sur le véhicule cellulaire à tout (C-V2X), une technologie basée sur D2D dont les caractéristiques sont une variante de canal rapide et une connexion à faible latence pour lesquelles les solutions d'optimisation centralisées ne sont pas viables. L'algorithme proposé permet aux véhicules de collaborer et d'apprendre collectivement l'environnement. Ainsi, des canaux et des puissances d'émission optimaux peuvent être obtenus indépendamment au niveau de chaque véhicule, uniquement sur la base d'une acquisition CSI locale. Une comparaison entre les algorithmes d'apprentissage et d'optimisation centralisée est également faite pour démontrer les avantages de l'approche RL proposée par rapport aux techniques d'optimisation traditionnelles.

Acknowledgments

I would like to express my gratitude and appreciation to the people who have helped me throughout the journey of completing my Ph.D.. I owe my deepest gratitude to my supervisor, Prof. Tho Le-Ngoc, for his support, encouragement, and advice during my graduate study at McGill University. Without his assistance and dedicated involvement in every steps throughout the process, this thesis would have never been accomplished. I also learned very much from his vast knowledge, genuine enthusiasm toward research, hard work, and his sense of humour.

I am grateful to Dr. Nghi Tran, whose suggestions and enormous knowledge in wireless communications and mathematics have benefited me tremendously. I would also like to thank Prof. Benoit Champagne, Prof. Jun Cai, and Prof. Ioannis Psaromiligkos for being in my thesis committee and for helpful comments and suggestions. I am especially indebted to Prof. Benoit Champagne and Prof. Jun Cai and for their valuable time and efforts devoted in reviewing this thesis. I would also like to express my appreciation to Prof. Hannah Michalska for her feedback and comments in my research seminar, which have significantly improved the quality of this thesis. I am also thankful to Dr. Subramaniya I. Harihara and Prof. M. Cenk Gursoy for the collaborations.

I would like to acknowledge McGill Engineering Doctoral Award (MEDA), Natural Sciences and Engineering Research Council (NSERC) of Canada, and Huawei Technologies for the financial support throughout my doctorate.

I would like to thank the entire faculty of Department of Electrical & Computer Engineering for creating the great learning atmosphere. I am also thankful to all my colleagues, especially Berri, Ahmed, Robert, Quang, Mobeen, Harry, Asil, Tuong, Ngon, Tuan, Atoosa, Ruikai, Tri, Zheyu, and Kevin, who made my years at the McGill University full of fun.

Finally, it is my greatest honour to thank my parents and my brother for all the love and support they have provided. I would also like to thank my wife's family for their support and for making me feel like a welcomed family member. The last word of acknowledgment is dedicated to my wife and best friend, Trang, who motivated me to explore new places and enjoy life. Her constant love and support allowed me to complete this journey.

Contents

List of Figures

List of Tables

List of Acronyms

2G	2nd Generation Mobile Networks
3GPP	3rd Generation Partnership Project
5G	5th Generation Mobile Networks
AWGN	Additive White Gaussian Noise
BG	Bernoulli-Gaussian
BS	Base-Station
CCDF	Complementary Cumulative Distribution Functions
CF	Characteristic Function
CR	Cognitive Radio
CSI	Channel State Information
CU	Cellular User
C-V2X	Cellular Vehicle-to-Everything
D2D	Device-to-Device
DC	Difference of Convex
DNN	Deep Neural Network
DQN	Deep Q-Network
DSRC	Dedicated Short Range Communications
FD	Full-Duplex
FFR	Fractional Frequency Reuse
FP	Fractional-Programming
GM	Gaussian-Mixture
HD	Half-Duplex
IoT	Internet of Things
ITS	Intelligent Transportation Systems
KTC	Kuhn-Tucker Conditions
LTE	Long-Term Evolution

MDP	Markov Decision Process
MIMO	Multiple-Input-Multiple-Output
ML	Machine Learning
MRT	Maximum Ratio Transmission
P25	Project 25
P2P	Peer-to-Peer
PDF	Probability Density Function
PPP	Poisson Point Process
PSD	Power Spectral Density
QAM	Quadrature Amplitude Modulation
QoS	Quality-of-Service
QPSK	Quadrature Phase-Shift Keying
RA	Resource Allocation
RL	Reinforcement Learning
RSU	Roadside Unit
RV	Random Variable
SE	Spectral Efficiency
SFR	Standard Frequency Reuse
SGD	Stochastic Gradient Descent
SI	Self-Interference
SIC	Self-Interference Cancellation
SINR	Signal-to-Interference-plus-Noise
SIPR	Self-Interference-to-Power-Ratio
SNR	Signal-to-Noise-Ratio
TDD	Time Division Multiplexing
TETRA	Terrestrial Trunked Radio
UE	User Equipment
UFR	Universal Frequency Reuse
ULA	Uniform Linear Array
V2I	Vehicle-to-Infrastructure
V2V	Vehicle-to-Vehicle
V2X	Vehicle-to-Everything
WLAN	Wireless Local Area Network
ZF	Zero-Forcing

List of Symbols

a_t	Action in reinforcement learning
$d_{\min}, d_{\max}$	Minimum and maximum distances of D2D links
$h, \mathbf{h}$	Complex scalar and vector channel fading gains
$g, \mathbf{g}$	Real scalar and vector channel power gains
L	Large-scale fading gain including path-loss and/or shadowing
k, m, n	User/link index values
M	Number of cellular/V2I links
N, K	Number of D2D/V2V links
p_c, p_d	Coverage probabilities of cellular and D2D links
P_c, P_d	Maximum transmit powers of cellular and D2D users
P_n	Transmit power of D2D user n in optimization problem
Q^{π}	Q-function in reinforcement learning
$R_m^{(\mathrm{c})}, R_n^{(\mathrm{d})}$	Achievable rates of cellular link m and D2D link n
R_c, R_d	Achievable sum-rates of cellular and D2D links
$\overline{R}_c, \overline{R}_d$	Ergodic sum-rates of cellular and D2D links
r_t, R_t	Rewards in reinforcement learning
s_t	State in reinforcement learning
T	Latency constraint
$\mathbf{v}$	Beamforming vector
α	Path-loss exponent
β	Self-interference-to-power-ratio in full-duplex mode
γ_c, γ_d	Target SINRs at cellular and D2D receivers
ϵ	Convergence threshold in iterative algorithm
$\lambda_b, \lambda_c, \lambda_d$	Densities of base-stations, cellular links, and D2D links
π	Policy in reinforcement learning
σ_c^2, σ_d^2	Noise powers at cellular and D2D receivers

Mathematical Notation

A, a	Non-bold variables denote scalars
$\mathbf{a}$	Lower-case bold variables denote vectors
$\mathbf{A}$	Upper-case bold variables denote matrices
$\overline{a}$	Complex conjugate of complex number a
$\mathbf{a}^{\mathsf{H}}$	Conjugate transpose of vector $\mathbf{a}$
$\mathbf{a}^{\mathsf{T}}$	Transpose of vector $\mathbf{a}$
$\lvert a \rvert$	Magnitude of scalar a
$\lvert \mathbf{a} \rvert$	Norm of vector $\mathbf{a}$
$\lvert \mathcal{A} \rvert$	Cardinality of set $\mathcal{A}$
$\mathbb{C}$	Complex number space
$\mathcal{CN}(0, \sigma^2)$	Complex Gaussian distribution with zero mean and variance σ^2
$\mathbb{E}[\cdot]$	Expected value operation
$\exp(1)$	Exponential distribution with unit parameter
$\mathbf{I}$	Identity matrix
$\ln, \log_2, \log$	Logarithmic function base e, 2, and 10
$\mathcal{L}\{\cdot\}$	Laplace transform operation
$\mathbf{0}$	Zero matrix
$\mathcal{O}(\cdot)$	Big-O notation
$\mathbb{P}(A \geq a)$	Probability that $A \geq a$
$\mathbb{R}$	Real number space
$\mathbb{R}_+$	Nonnegative and real number space
$\mathrm{Re}(\cdot)$	Real part of complex number
$\sup$	Supremum operation
$\{\cdot\}$	Set notation

Chapter 1

Introduction

This chapter starts with a brief introduction to device-to-device (D2D) communications in Section 1.1, including the motivation behind recent surge of interest in D2D networking and its relevant development in the industry. Section 1.2 compares two resource sharing modes of cellular and D2D transmission called overlay and underlay that lead to the focus of this thesis on underlaid D2D communications. Section 1.3 describes the use of half-duplex (HD) and full-duplex (FD) operation in D2D. Section 1.4 introduces cellular vehicle-to-everything (C-V2X) communications, a D2D-based solution for intelligent transportation systems. Finally, Section 1.5 provides an overview of the contributions of this thesis and a brief description of thesis organization.

1.1 Device-to-Device Services in Cellular Systems

Existing technologies supporting direct connections between cellular devices in proximity can be broadly referred as peer-to-peer (P2P) solutions in which WiFi Direct and Bluetooth are most popular [1]. However, both technologies are limited in scalability. Since WiFi Direct and Bluetooth use the unlicensed spectrum, they suffer from the uncontrolled interference generated by other devices sharing the same spectrum such as microwave ovens and wireless speakers. As a result, they provide D2D connectivity with low densities (< 10 users). Further, due to its two-step discovery process (i.e., operating and dealing with uncontrolled interference from other devices using the same unlicensed spectrum), the battery impact in Wi-Fi Direct increases exponentially with the number of users, and hence hurting its energy efficiency [1].

The limitations of existing direct-connectivity technologies give rise to the interest of D2D services in cellular systems where direct communications between two mobile users are enabled without traversing through the base-station (BS). From the technical perspective, incorporating

D2D services into cellular network can provide multiple benefits. Instead of routing data through base-stations (BSs), D2D users communicate directly with each other, thus not only enhancing spectrum utilization but also saving energy. Further, bypassing the BS helps offload the cellular traffic and reduce the network congestion. Given the short range of D2D networking, D2D users may transmit in high data-rate and low end-to-end delay. D2D communications also helps extend the range of cellular link via user-to-user relaying. When the cellular coverage is not available, a group of D2D users can communicate in a self-organizing manner in which a user acts as a clusterhead and helps synchronization, manages radio resources, and schedules transmission. In Fig. 1.1, we illustrate potential benefits of D2D communications in cellular systems.

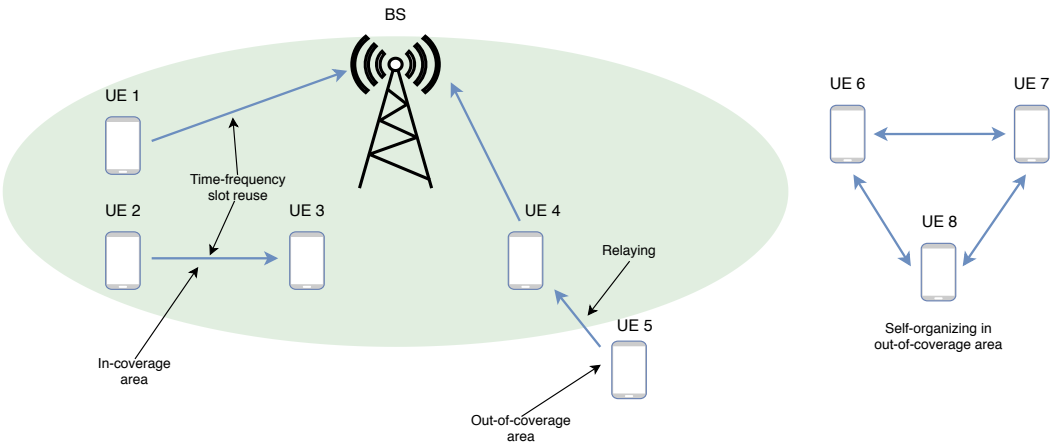

Fig. 1.1 Potential benefits of D2D communications in cellular systems.

Given the benefits of D2D networking, significant efforts in industry have been made to promote this novel feature into the future cellular systems. For instance, a D2D communication system called FlashLinQ has been developed and implemented by Qualcomm to enable proximity-aware networking among devices [2, 3]. In addition, the Third Generation Partnership Project (3GPP) has first included the D2D networking in Long-Term Evolution (LTE) Release 12 [4]. Specifically, motivated by the fact that the current public safety networks are still operated by the obsolete 2G technologies like Project 25 (P25) and Terrestrial Trunked Radio (TETRA), D2D feature in LTE has been proposed to be a promising solution for public safety networks [5], providing direct networking among mobile devices when the cellular coverage is unavailable. D2D platforms for consumers also have been developed for consumer-based applications with the capability of discovering $1,000$s of nearby devices/services within 500 m as well as allowing direct networking between cellular users. Such D2D discovery and networking have been enhanced to include the device-to-network relays for public safety networks and more flexible discovery such as re-

stricted/private and inter-frequency for consumer-based services. Further, additional D2D-enabled capability, i.e., multi-hop for Internet of Things (IoT) applications, has also been studied [6], along with modifying the D2D communication platforms for reliable vehicle-to-everything (V2X) systems [7, 8].

1.2 Overlaid and Underlaid Device-to-Device Communications

D2D communications can operate on either the licensed cellular spectrum (i.e., inband D2D) or unlicensed spectrum (i.e., outband D2D). Based on spectrum sharing manner between D2D and cellular users, inband D2D can be classified further into two categories:

- Overlay: Cellular and D2D users use orthogonal time or frequency resources.
- Underlay: D2D users reuse the time and/or frequency resources currently occupied by the cellular transmission.

The main advantage of overlaid D2D is that the interference between cellular and D2D transmission is essentially neglected due to orthogonal resource allocation, so the primary cellular transmission can be protected from the newly integrated D2D feature. Nevertheless, this mode requires dedicated cellular time/frequency resources assigned to the D2D transmission, thus preventing the cellular user to transmit at its maximum capacity. In contrast to the overlaid mode, interference is a fundamental limiting factor in underlaid D2D. When the cellular time-frequency resources are fully reused by D2D transmission, cellular links experience the interference from both cellular and D2D transmission, while D2D links have to combat the interference caused by not only cellular transmission but also other co-channel D2D links. Thus, interference management is essential to ensure a harmonious co-existence of D2D and cellular networking. Yet, as multiple D2D links are capable of reusing the channel of an active cellular user, significant spectral efficiency gains can be offered by the underlaid mode. This thesis focuses on underlaid D2D communications in cellulars networks where D2D transmission simultaneously operates in the same time-frequency resources with cellular uplink/downlink.

1.3 Half-Duplex and Full-Duplex Device-to-Device Communications

D2D feature will fundamentally alter the cellular architecture, reducing the primacy of cellular networking and enabling direct communications between mobile users. Conventional D2D cellular systems apply half-duplex (HD) transmission in which a D2D user can only transmit and receive

signals in separate time and/or frequency slots. It follows that the incorporation of a underlaid and bidirectional D2D link into existing cellular systems would require two time-frequency slots currently used by the uplink/downlink cellular transmission, which further complicates the D2D-enabled cellular architecture design. The employment of full-duplex (FD) in D2D communications has been considered as an attractive solution to address this challenge. FD D2D transmission enables D2D nodes to transmit and receive signals simultaneously over a single channel (i.e., over the same frequency at the same time). As a result, the use of FD D2D operation not only substantially enhances the spectrum efficiency, but more importantly, lowers the number of carrier frequencies needed for underlaid D2D transmission. FD transmission incurs additional interference, known as residual self-interference, from the transmitter to the receiver of the same node, as shown in Fig. 1.2. Typically, the self-interference power is significantly higher than that of received signal, hurting the performance of D2D transmission and preventing the sum-rate gains. Given a number of encouraging self-interference cancellation (SIC) designs (e.g., see [9–12]), the FD approach lends itself well into the concept of D2D transmission as FD D2D essentially does not require high SIC levels at the transmitters due to the short distance of D2D link. However, the integrating FD operation into D2D transmission will increase interference to both cellular and D2D receivers due to the increasing number of interfering D2D nodes, so effective interference management is needed. Moreover, a comparison between FD and HD D2D in terms of offered sum-rates should also be made to justify the benefits of FD D2D feature. In this thesis, we consider both HD and FD D2D transmission modes.

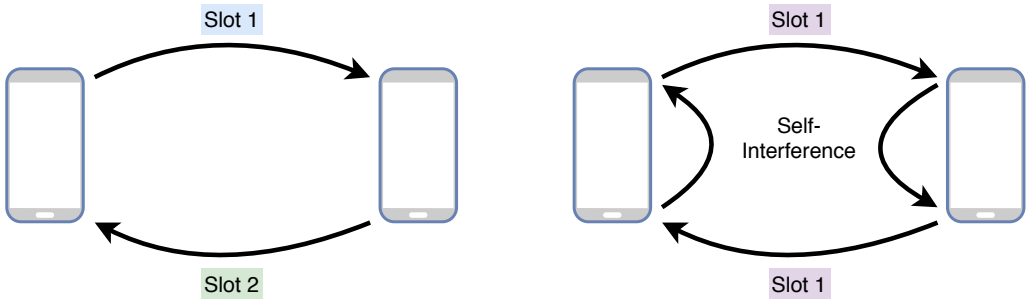

(a) Half-duplex D2D transmission (b) Full-duplex D2D transmission

Fig. 1.2 Half-duplex and full-duplex D2D transmission.

1.4 Cellular Vehicle-to-Everything Communications

Vehicle-to-Everything (V2X) refers to the vehicle-based communications in the intelligent transportation systems (ITS) to support the cooperation among the vehicles [13]. Early technologies, e.g., dedicated short-range communications (DSRC) [14] and ITS-G5 [15], were developed based on IEEE 802.11p standard to support vehicular *ad hoc* networks. However, recent research [16, 17] have demonstrated that, because DSRC and ITS-G5 were built upon IEEE 802.11p that was originally designed for wireless local area network (WLAN) with low mobility nodes, IEEE 802.11p-based technologies such as DSRC and ITS-G5 eventually exhibit several limitations including short-lived V2I transmission, lack of quality of service (QoS) guarantee, and high latency due to delay in medium (channel) access. Such limitations motivate the development of cellular vehicle-to-everything (C-V2X), a vehicular communication paradigm via the cellular networks supported by 3GPP [18]. High bandwidth and dynamic resource allocation in cellular networks allow to tackle the challenge of QoS guarantee and short-lived V2I transmission [19], while D2D communications, backed by the long-standing cellular architecture, is capable of ensuring the stringent latency requirement of V2V applications [16].

Typically, a C-V2X system includes vehicle-to-infrastructure (V2I) and vehicle-to-vehicle (V2V) transmission. As illustrated in Fig. 1.3, the V2I transmission connects the vehicles to BS or BS-typed roadside unit (RSU), while the V2V transmission provides direct information exchange among the vehicles in proximity. In C-V2X architecture, the V2I and V2V connections are implemented via the cellular (Uu) and sidelink (PC5) interfaces, respectively, which were originally developed for D2D communications [20]. In standards [7, 8], C-V2X systems are envisioned to provide high data-rate connectivity to vehicle/cellular users of V2I links for entertainment services (e.g., gaming and video streaming). Meanwhile, dynamic coordination between vehicles of V2V links is required for advanced driving applications (e.g., autonomous driving). In order to support advanced driving applications, safety messages should be periodically exchanged among neighboring vehicles via V2V communications with high reliability and extremely low latency. The safety messages usually include vehicle-related information such as its position, speed, and destination in order to improve the mutual awareness of all vehicles in the same local driving environment [8]. Apart from conventional D2D communications, the key characteristics of C-V2X systems are high user mobility and fast channel variations, so satisfying their requirements is challenging, and hence, calling for intelligent resource allocation designs. Following the underlaid mode in D2D services, this thesis considers spectrum sharing between V2I and V2V links with necessary interference management to simultaneously support high data-rate V2I transmission and reliable V2V connections. Instead of traditional optimization techniques extensively used in ex-

isting research, we will adopt a reinforcement learning approach to interference management in C-V2X systems.

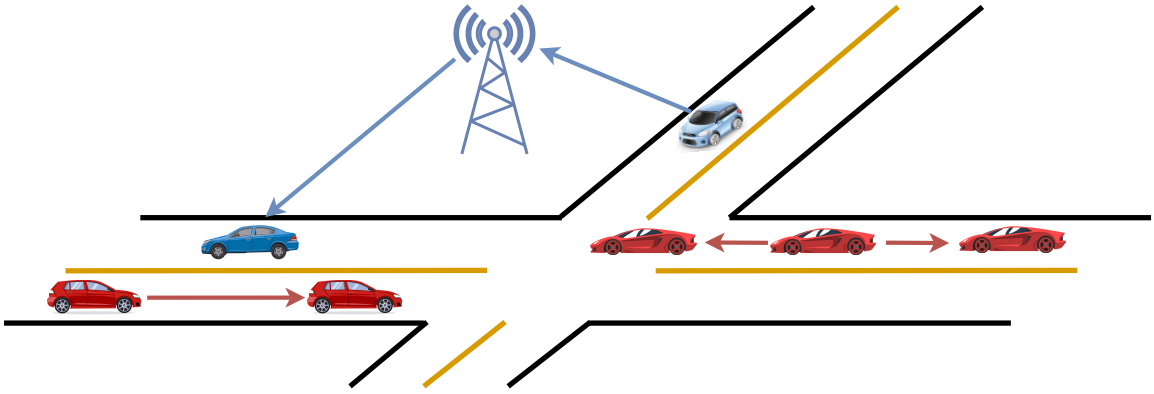

Fig. 1.3 An illustrative example of a C-V2X system (red arrow: V2V link, blue arrow: V2I link).

1.5 Contributions and Organization

Integrating underlaid D2D communications into existing cellular systems increases the interference but also provides the potential spectral efficiency gains if the interference can be effectively managed. The goal of this thesis is to investigate the benefits of D2D-enabled communications via performance analysis and dynamic resource allocation.

The remainder of this thesis is organized as follows. Chapter 2 reviews the relevant literature on achievable D2D rate analysis at single link level under the focus of capacity analysis of additive Gaussian-Mixture channel as well as achievable sum-rate analysis at network level based on stochastic geometry approach. Additionally, related works on sum-rate maximizing algorithms in underlaid D2D cellular networks and learning-based resource allocation in C-V2X systems are also included.

In Chapter 3, we focus on the link level and analyze the capacity of a single D2D link in underlaid D2D cellular networks where a D2D link intends to communicate by sharing the frequency-time resources with a cellular user. In this context, the additive Gaussian channels have been adopted extensively in literature to model the D2D link communications. This results from a common assumption that, when treated as noise, the aggregate D2D-to-cellular interference is

Gaussian distributed. However, such a Gaussian channel model is only valid if the D2D transmitters use the Gaussian codebooks in their transmit signals. For more practical transmit schemes (e.g., discrete constellations), the Gaussian channel may not be an accurate model of the D2D link in considered D2D cellular networks. Thus, from information-theoretic perspective, the conventional result that Gaussian distributed input is capacity-achieving for a single D2D link in underlaid D2D environment will no longer hold true. This issue requires rethinking of well-known models and assumptions currently used in existing research. This motivates us to address the challenge of developing an accurate channel model called additive Gaussian-Mixture (GM) channel for a point-to-point D2D link in underlaid D2D cellular networks. Under the consideration of additive GM channel, we then attempt to characterize the capacity-achieving input and compute the corresponding channel capacity. The achieved channel capacity is also compared to that of traditional Gaussian channel so as to confirm the validity of considered GM model.

Chapter 4 extends the study of achievable rate at the link level to a network level to calculate the achievable sum-rates of both cellular and D2D links in a single-cell setting. Toward this end, we first propose a random network model that takes into consideration the random mobility of cellular and D2D users and the distribution of channel state information (CSI). In addition, we assume that the D2D links use full-duplex (FD) transmission due to its significant benefits. As aforementioned, FD is appealing in D2D networking as it allows the D2D node to transmit and receive simultaneously in a single channel, thus substantially enhancing the spectrum efficiency of the network. Since the FD D2D node uses a single carrier frequency in both transmitting and receiving signals, the use of FD operation reduces the cellular frequency resources consumed by the underlaid D2D networking. Given the random network models, we then analytically characterize important network metrics including coverage probabilities of cellular and D2D links and achievable sum-rate of D2D links. Power allocation is also performed in both centralized and distributed manners to further improve the sum-rate objective and it is taken into account while computing the network metrics. The achieved network metrics allow to investigate the benefits of integrating D2D services into cellular networks as well as FD D2D over the half-duplex (HD) counterpart.

In Chapter 5, we extend the single-cell setting into a multi-cell network to rigorously study the benefits of incorporating D2D transmission into cellular networks. Toward this end, we provide an analytical performance characterization of underlaid D2D cellular networks where D2D users operate in FD mode under the presence of residual self-interference. In considered networks, the base-stations (BSs) are distributed according to a hexagonal grid, while the locations of cellular and D2D users follow Poisson point processes (PPPs). Based on the stochastic-geometry approach, we develop the approximations of key performance metrics including coverage proba-

bilities and achievable sum-rates of both cellular and D2D links, and such approximations involve quickly commutable integrals. Under a special case in which the number of D2D links is sufficiently large, the obtained approximations can be simplified to closed-form expressions, allowing characterize the sum-rate behaviors under the effects of various system parameters. We show that underlaid D2D communications in cellular network can offer a significant spectral efficiency gain as compared to pure cellular transmission. With a sufficiently low self-interference cancellation (SIC) level, FD D2D can offer a substantial spectral efficiency improvement over the HD counterpart. Further, the resulting performance metrics are compared with multi-cell networks operating in standard and fractional frequency reuse modes, and we observe that frequency reuse offers improved coverage probabilities of both cellular and D2D links, but substantially reduces the D2D sum-rate performance.

In cellular networks, separate sets of carrier frequencies are allocated to the uplink and downlink transmission. The underlaid D2D services generally favor the use of uplink spectrum [21]. The main reason is that, in downlink transmission, the cellular receivers are typically located close to the D2D transmitters, thus reusing the downlink spectrum can substantially increase the D2D-to-cellular interference. Moreover, high transmit power levels at the BS can also cause severe interference to the D2D receivers. Hence, interference management is crucial to enable the underlaid D2D services in cellular downlink transmission. In Chapter 6, the focus is shifted from the cellular uplink to downlink being underlaid by D2D communications. To address the challenge of interference management, we consider the case of BS's equipped with large antenna arrays in multi-cell networks with D2D services. More specifically, under the assumption of uniform linear array (ULA), we focus on joint beamforming and power allocation design for achievable network sum-rate (per cell) maximization in presence of interference to both cellular downlink and D2D transmission. The problem formulation leads to a nonconvex vector-variable optimization problem, where we develop an efficient solution using a fractional programming (FP) based approach. Numerical results show that, at sufficiently high SIC levels, the FD D2D transmission provides a significant sum-rate improvement as compared to the HD counterpart and pure cellular systems in absence of D2D transmission.

An implicit assumption made in Chapters 4 and 6 is that the resource allocation algorithms (e.g., power allocation and/or beamforming design) are performed in a centralized manner. The optimization algorithms are based on the procedure that first estimating the interfering channels between D2D and cellular transmitters/receivers, collecting the global CSI at central controllers, then optimizing the beamformers and transmit powers. This approach suffers from a shortcoming that the channel estimation is resource-intensive and eventually exhibits high overhead. As

a result, traditional optimization algorithms may not be viable in D2D-based applications whose key characteristics are high user mobility, fast channel variations, and low latency requirement, e.g., C-V2X systems. Chapter 7 is dedicated to develop a distributed resource allocation algorithm to resolve the joint channel assignment and power allocation problem in underlaid C-V2X systems where multiple V2I uplinks share the time-frequency resources with multiple V2V platoons. Based on a reinforcement learning approach, we model the resource allocation as a multi-agent system. Each platoon leader acts as an agent who collectively interacts with each other to achieve a common reward. In addition, we utilize the deep Q-learning algorithm to train the agents so as to maximize the V2I sum-rate while satisfying the packet delivery probability of each V2V link over a desired latency limitation. We select the well-known exhaustive search algorithm as a benchmark to demonstrate the benefit of newly developed learning algorithm. Compared to the centralized exhaustive search approach, the developed learning algorithm can be employed in a distributed fashion, i.e., it only requires local CSI estimation, while being capable of providing a close delivery probability performance.

Finally, Chapter 8 provides some concluding remarks and summarizes the key results of this thesis.

Before processing further, we should note that the contributions of Chapters 3, 4, and 5 have been published in peer-reviewed journals and refereed conferences, which are provided as follows

Journal papers

- H. V. Vu, N. H. Tran, M. C. Gursoy, T. Le-Ngoc, and S. I. Hariharan, "Capacity-achieving input distributions of additive quadrature Gaussian Mixture noise channels," *IEEE Trans. Commun.*, vol. 63, pp. 3607–3620, Oct. 2015

- H. V. Vu, N. H. Tran, and T. Le-Ngoc, "Full-duplex device-to-device cellular networks: Power control and performance analysis," *IEEE Trans. Veh. Tech.*, vol. 68, pp. 3952–3966, Apr. 2019

- H. V. Vu and T. Le-Ngoc, "Performance analysis of underlaid full-duplex D2D cellular networks," *IEEE Access*, vol. 7, pp. 176233–176247, 2019

Conference papers

- H. V. Vu, N. H. Tran, M. C. Gursoy, T. Le-Ngoc, and S. I. Hariharan, "Characterization of optimal input distributions for Gaussian-mixture noise channels," in *Proc. IEEE Can. Work. on Infor. Theory (CWIT)*, pp. 32–35, 2015

- H. V. Vu, N. H. Tran, and T. Le-Ngoc, "On coverage probabilities and sum-rate of full-duplex device-to-device cellular networks," *Proc. IEEE Int. Conf. Commun. (ICC)*, pp. 4042–4047, 2018

- H. V. Vu and T. Le-Ngoc, "Underlaid full-duplex D2D cellular networks: Modeling and analysis," in *Proc. Int. Symp. on Personal, Indoor and Mobile Radio Commun. (PIMRC)*, pp. 1–6, 2019

In all of these publications, the first author, Hung V. Vu, proposed the idea, formulated the problem, developed the algorithms, implemented simulations and prepared the first draft of the manuscripts. The co-authors, Dr. Nghi. H. Tran and Prof. Tho Le-Ngoc reviewed the works and assisted with the editing and writing of the final manuscripts. The other co-authors, Dr. Subramaniya I. Harihara and Prof. M. Cenk Gursoy provided constructive comments to improve the quality of manuscripts [22] and [25].

Meanwhile, the contributions of Chapters 6 and 7 are currently in preparation for refereed conference submissions. In these chapters, the author, Hung V. Vu, proposed the idea, formulated the problem, developed the algorithms, implemented simulations and prepared the writing. Prof. Tho Le-Ngoc reviewed the works and assisted with the editing and writing of the final manuscripts. In Chapter 7, Mr. Zheyu Liu, the undergraduate student in 2020 Summer Undergraduate Research in Engineering program (SURE 2020), assisted with the simulations.

Chapter 2

D2D Communications: A Literature Review

This chapter provides a short literature review of the state-of-the-art approaches in performance analysis and resource allocation in D2D communications. In Section 2.1, we review related works on the capacity analysis of GM channels adopted to model, at the link level, the channel of a single D2D link in simple underlaid D2D cellular networks where one D2D and one cellular links attempt to share a time-frequency slot. Section 2.2 extends to the scenario where multiple D2D links are capable of fully reusing a time-frequency slot currently occupied by the cellular link. We then focus on the achievable sum-rate analysis of underlaid D2D cellular networks at network levels, emphasizing on the stochastic geometry approach. In Section 2.3, we review the related works on resource allocation methods, focusing on joint beamforming and/or power allocation designs, in underlaid D2D communications coexisting with massive MIMO equipped BSs. Finally, Section 2.4 provides a literature review of both traditional optimization and reinforcement learning approaches on distributed resource allocation in D2D-based V2X systems.

2.1 Optimal Input Distribution and Capacity Analysis of Single D2D Link

In this section, we consider simple underlaid D2D cellular networks where a cellular link and a point-to-point D2D link operate in the same sub-band and both use the HD transmission mode. We will demonstrate shortly that, from an information theoretic perspective, the D2D link can be modeled as an additive GM channel. As a result, we will review related works on the characterization of capacity-achieving input and channel capacity of general GM channels in literature. Before processing further, we should note that, this D2D-enabled scenario has been studied in prior works (e.g., see [28–30]), but mostly dedicated to rate-maximizing resource allocation.

For the illustrative purpose, let us consider a scenario with one uplink cellular user (CU) and

two D2D users who establish (D2D) communications via the same time-frequency slot. The received signal at the D2D receiver is then given by

$$y_d = h_d r_d^{-\frac{\alpha}{2}} x_d + h_c r_c^{-\frac{\alpha}{2}} x_c + z_d, \tag{2.1}$$

where y_d denotes the received signal at the D2D receiver; x_c and x_d are the transmitted signals of cellular user and D2D transmitter, respectively; z_d denotes the additive white Gaussian noise (AWGN) at D2D receiver following the distribution $\mathcal{CN}(0, \sigma^2)$; h_c and h_d denote the fading coefficients from cellular user and D2D transmitter to D2D receiver, respectively. We assume that the fading coefficients are independently distributed as $\mathcal{CN}(0, 1)$. Further, we model the distance dependent path-loss as $r_c^{-\alpha}$ and $r_d^{-\alpha}$ where r_c and r_d refer to the distances from cellular user and D2D transmitter to the D2D receiver, respectively; and α refers to the path-loss exponent.

Supposing that a Gaussian-distributed signal is transmitted from cellular user, the cellular-to-D2D interference and subsequently the interference-plus-noise at D2D receiver is also Gaussian distributed. Thus, it is straightforward that an additive Gaussian channel can be used to model the D2D link in this case. Nevertheless, if a discrete constellation signal is used at cellular transmitter, such a Gaussian channel model will no longer be valid. This is because, under this assumption, the cellular-to-D2D interference will follow a GM distribution. More specifically, assuming that the transmitted signal x_c of cellular user is represented by a modulated signal which can take M different values $u_1, \ldots, u_M$ with corresponding probabilities $p_1, \ldots, p_M$, the faded signal from cellular user to D2D receiver is distributed as a GM random variable (RV) with the following probability density function (PDF):

$$f_w(w) = \sum_{i=1}^{M} \frac{p_i}{2\pi\sigma_i^2} \exp\left(-\frac{|w|^2}{2\sigma_i^2}\right), \tag{2.2}$$

where $w = r_c^{-\alpha/2} h_c x_c$ and $\sigma_i^2 = r_c^{-\alpha/2}|u_i|^2$, $i = 1, \ldots, M$. Based on the fact that sum of a GM RV and a Gaussian RV is also a GM RV, we can conclude that the aggregate interference-plus-noise $r_c^{-\alpha/2} h_c x_c + z_d$ is also GM distributed; and therefore the corresponding channel of the underlaid D2D link can be represented as an additive GM channel model when the information of channel states and users' locations are available at the central controller.

In existing research, the GM model is also considered as one of the most general models for aggregate interference in other wireless systems [31–36]. For instance, the GM model includes both single-carrier and multi-carrier Bernoulli-Gaussian (BG) and Middleton Class-A impulsive noise channels as special cases [37]. This GM model can also be used to represent multiple-access inter-

ference in wireless communications [34,35]. As demonstrated in [38], GM model is generally rich enough to accurately approximate a wide variety of interference in cognitive radio (CR) networks under imperfect spectrum sensing. The aggregate interference generated by femtocell to macrocell wireless networks also follows GM distribution because of some dominant interferers [39]. Such a distinctive trait of GM model motivates us to study the general additive GM channel from an information theory perspective. More specifically, we are interested in characterizing the optimal inputs and calculating the corresponding capacities of the GM channels.

The characterization of the optimal input and the computation of the channel capacity have been fundamental topics in information theory since Shannon's pioneering work [40]. Up to date, most of the studies have focused on the AWGN channels. For instance, it has been well-known that under the average power constraint, Gaussian signaling achieves the capacity of the AWGN channel. When both peak and average power constraints are considered, Smith in [41] demonstrated that the optimal input distribution has a discrete nature with a finite number of mass points for a real AWGN channel. Shamai *et al.* in [42] extended these results to the quadrature Gaussian channel and the corresponding capacity-achieving input was shown to have uniformly distributed phase and discrete amplitude with a finite number of levels. The discreteness of the optimal input distributions with either finite or infinite support has also been observed in AWGN channels under other constraints, such as rapid phase variations [43], duty cycle [44], or under additional impairments such as fading [45–47]. Similar results were also obtained in [48] for a conditionally Gaussian channel, which serves as a general channel model for various practical communications systems with AWGN.

While statistical-physical models of GM [31, 32, 34, 35, 49] and its special cases such as BG [37, 50], $\epsilon-$mixture [51], and Middleton Class-A [52–54] have been well developed to empirically fit the first order statistics of aggregate noise and interference, these non-Gaussian channels are not fully understood from an information-theoretic perspective. For example, even for the simplest BG noise channel and equivalently $\epsilon-$mixute noise channel (i.e., GM channels consist of two elements in the GM PDF), while Gaussian distributed input signals have been shown to be asymptotically optimal under the average power constraint [55–57], the optimal input signaling and the capacity for a given finite input power level still remain unknown. The same drawbacks are also observed for the Middleton Class-A model (i.e., a GM channel with infinite elements) [53], which is considered to be the most credited model with direct physical interpretation that fits well to a variety of impulsive interference measurements [52, 53]. Recently, by using the heavy-tailed property [58] of α-stable noise, Fahs and Abou-Faycal [59] have shown that the optimal input distribution has finite support. However, for other models such as the BG noise, Middleton Class-A

noise, or more generally, GM noise, the noise distributions are neither heavy-tailed nor light-tailed. Also, it is worth mentioning that there exist other works addressing the optimal distributions for real non-Gaussian channels [60–63] such as the real Poisson channel in [60] and the inverse Gaussian noise channel in [62]. However, these results cannot be used for additive GM channels. Therefore, in general, obtaining a detailed characterization of a capacity-achieving input for GM channels still remains a challenging task.

2.2 Achievable Sum-Rate Analysis in Underlaid D2D Cellular Networks

In existing research, the consideration of underlaid D2D transmission in cellular networks in terms of achievable rate analysis at network levels has received some interest, but mostly dedicated to static models in which the locations of D2D/cellular users generally are assumed to be placed deterministically (please see e.g. [64, 65]). For more realistic results, it is also of great interest to investigate the benefits offered by D2D in non-deterministic network models where the randomness of user positions is taken into consideration. Toward this end, the stochastic geometry approach has been adopted as a tractable solution for analyzing the achievable rate in D2D cellular networks. In stochastic geometry based model, the locations of D2D/cellular users are randomly distributed according to some Poisson point processes (PPPs), and hence, under very general assumption, resulting analytical expressions for the signal-to-interference-plus-noise (SINR) distribution and mean rate. The achieved expressions involve quickly computable integrals, and, in some practical special cases, can be reduced to simple closed-form expressions. As a result, the behaviors of achievable sum-rate under the effects of important system parameters can be effectively characterized, providing useful insights into the network design.

During the last few years, many research have been undertaken to study the effect of incorporating D2D feature into existing cellular systems at the network levels using stochastic geometry. For example, Lee *et al.* in [66] studied the key performance metrics including coverage probabilities of both cellular and D2D users and sum-rates of D2D links via power control in a single-cell network. The coexistence of D2D and cellular users has also been studied for multi-cell settings [67–69]. The performance of multicast D2D transmission was examined in [67] using a stochastic geometry approach. The spectrum sharing problem was investigated in [68] for both overlaid and underlaid D2D cellular networks, while the impact of underlaid D2D transmission on the cellular networks via power allocation was studied in [69]. Under this line of works, it is shown that underlaid D2D communications can offer a significant performance improvement. The cognitive-radio assisted D2D transmission was developed in [70] with the consideration of a mixed overlaid-underlaid

spectrum sharing. It follows that the pivotal performance metrics including coverage probabilities and maximum allowable density of D2D devices were derived to provide useful insights into system design.

In prior works [66–70], the D2D studies have developed and evaluated under the consideration of half-duplex (HD) D2D communications, where a D2D user can either transmit or receive on a single channel, but not simultaneously. Given a number of encouraging full-duplex (FD) designs (e.g., see [9–12]), the integration of FD in D2D communications is an attractive solution for the development of new architectures and algorithms in cellular networks. FD D2D operation is appealing in such a context that the employment of FD to D2D transmission essentially does not require high self-interference cancellation level at the transmitters due to the short distance of D2D link. Since the FD D2D node uses a single carrier frequency in both transmitting and receiving signals, the use of FD D2D operation not only substantially enhances the spectrum efficiency but it also lowers the number of carrier frequencies needed for D2D transmission. Recently, the integration of FD operation into D2D transmission has received some interest, but only a few efforts have been dedicated to combine FD and D2D at the network level. For instance, in a recent work [71], the authors evaluated the performance of overlaid D2D multi-cell networks where cellular and D2D links use FD transmission. This work, however, suffers from a shortcoming that it did not take into account the consideration of fading, which is an important channel component. The benefits of FD D2D transmission in multi-cell networks in terms of throughput improvement were also investigated in [72]. Under this line of work, a D2D receiver is assumed to be at a fixed distance from the D2D transmitter with its location being followed a PPP. The performance of underlaid D2D cellular networks with single-cell setting was also of interest in [73, 74]. The performance of single-cell D2D cellular networks in terms of throughput was analyzed in [73], taking into account the joint pairing and mode selection in FD D2D communications. The throughput analysis was also presented in [74] where D2D links either operate in HD or FD modes based on their corresponding distances, and D2D users were assumed to form multiple clusters.

2.3 Resource Allocation in Underlaid D2D Cellular Networks

Interference is the main limiting factor in underlaid D2D cellular networks. To ensure a harmonious co-existence of D2D and cellular networking, interference management is essential. In cellular systems, the employment of massive multiple-input multiple-output (MIMO) equipped BSs in conjunction with coordinated resource allocation between cellular and D2D transmitters is an appealing solution to address this challenge. With a sufficiently large number of antennas and

intelligent beamformer design, the BS is capable of forming very narrow beams aiming toward the intended cellular receivers, thereby resulting in extremely low interference to co-channel cellular/D2D users. Meanwhile, implementing resource allocation strategies at D2D transmitters allow to effectively mitigate the interference caused by the D2D transmission at both cellular and D2D receivers. Accordingly, this section focuses on resource allocation, emphasizing on power allocation and/or beamforming designs, that attempts to maximize the achievable sum-rate of underlaid D2D cellular networks (equivalently maximize the SINR or conversely minimize the overall power consumption under fixed rate constraints).

In existing research, there has been considerable interest in designing power allocation techniques for underlaid D2D cellular networks. In primary works, D2D studies have developed and evaluated under the consideration of HD D2D communications, where the D2D node transmit and receive signal in the separate time-frequency slot. For instance, a simple power allocation scheme was developed in [30] for a single-cell setting, adapting both cellular and D2D transmit powers to protect the existing cellular transmission while maximizing the overall network sum-rate. In [30], the focus was on a simple spectrum sharing scheme in which one D2D link reuses the spectrum currently used by one cellular uplink, and hence, leading to a close-formed solution of optimal transmit powers. Similarly, given single D2D link transmission being underlaid with a cellular uplink, a power allocation mechanism at a single D2D link was considered in [75] which adjusts the D2D transmit power via BS to mitigate the interference caused by D2D transmission and protect the cellular users. For a more complex spectrum sharing scheme, the single-cell setting was extended in [66] to include multiple D2D links sharing the same time-frequency slot with one cellular uplink. A SINR maximizing algorithm based on standard convex optimization techniques was proposed to perform in a centralized fashion. Meanwhile, a distributed on-off power control algorithm was also developed to maximize the sum-rate of D2D links. A D2D user who only knows the channel quality of its direct link would transmit the signals if such link quality is good (beyond a certain threshold) and vise versa.

For FD D2D cellular networks, the power control problems were also of interest [76–78]. In [76], maximum allowed transmit powers were employed at D2D transceivers to mitigate the interference from BS, while, for interference management from cellular transmission to the D2D link, the concept of interference limited area is used. Multiple underlaid FD D2D links were considered in [77] for a single-cell setting. Based on the K-Mean algorithm that limits the D2D-to-cellular interference, achievable network sum-rate was maximized while constraining on the minimum required SINR at each cellular/D2D user. The single-cell setting was also investigated in [78] where multiple FD D2D links could reuse different channels from cellular transmission.

Similar to [77], achievable sum-rate maximization was considered, yet the optimization problem was expanded to include channel assignment in conjunction with power control at cellular and D2D users. This work began by rewriting the sum-rate objective function (e.g., f) as the difference of two convex functions (i.e., $f = u - v$). The convex function v was approximated by an affine function, denoted as $\tilde{v}$, thus f was subsequently approximated by the convex function $\tilde{f} = u - \tilde{v}$. It follows that the optimal solution of the nonconvex optimization problem could be approximately located by an iterative algorithm in which each iteration more closely approximates the (locally) optimal solution.

Under the prior line of works, single antenna transmission was adopted at both D2D and cellular users. For multiple-antenna systems, research efforts have also been made to develop the beamforming and/or power allocation techniques for underlaid D2D cellular networks with massive and multi-user MIMO equipped BSs. Assuming a single-cell setting without out-of-cell interference, Mirza *et al.* focused on joint beamforming and power allocation to optimize the transmit powers at both cellular and D2D users [79]. Interestingly, numerical results in [79] showed that the solution of joint beamforming and power allocation converged to that of power control with fixed beamforming schemes (zero-forcing (ZF), regularized ZF, and hybrid ZF and maximum ratio transmission (MRT)). For single-cell massive MIMO cellular systems being underlaid by D2D users, Chen *et al.* in [80] proposed a simple rate adaptation method based on stochastic geometry approach to minimize the interference to cellular users. Also, in the single-cell setting, [81] studied a joint pilot design and power control problem to minimize the D2D data transmit power. Rate adaptation based on a stochastic geometry approach was extended for the multi-cell setting in [82]. Power control at both cellular and D2D users with fixed beamformers (ZF and MRT) was investigated in [83] for multi-cell massive MIMO systems with underlaid D2D in order to maximize the minimum spectral efficiency (SE) and the product of SINRs. For underlaid D2D systems in absent of cellular transmission, Shen *et al.* adopted the matrix fractional programming (FP) techniques, solving the coordinated joint scheduling, power control, and beamforming so as to optimize the network sum-rate [84]. In this system, each D2D link was equipped with single-user MIMO transmission, and the mappings between the transmitters and the corresponding receivers were one-to-one. By introducing some suitable auxiliary variables q_n, the proposed FP-based approach essentially transformed the sum-rate objective function, which is represented in a multiple sum-ratio form, e.g., $\sum_n f\left(A_n/B_n\right)$, to a convex objective function $\sum_n f\left(2q_nA_n - q_n^2B_n\right)$. As a result, the original nonconvex optimization problem could be recast as a sequence of convex subproblems, and it could be effectively solved in an iterative fashion.

2.4 Resource Allocation in C-V2X Systems

This section provides a short literature review of the state-of-the-art approaches on distributed resource allocation including both traditional optimization and trending reinforcement learning (RL) approaches, under the emphasis on sum-rate maximizing problems in D2D-based C-V2X systems. As discussed in Section 1.4, fast changing channel condition is the main limiting factor in designing efficient and practical resource allocation (RA) strategies in vehicular communication environment. As a result, centralized optimization methods relying on the global CSI knowledge at the central controller will no longer be feasible in C-V2X systems due to the high CSI overhead. To address this challenge, distributed RA algorithms have been developed to relieve the global CSI requirement. For instance, a distributed spatial spectrum reuse scheme was considered in [85] for D2D-based vehicular networks, while throughput maximizing algorithms were proposed in [86, 87], utilizing the slowly-varying aspect of large-scale fading channels in order to reduce the CSI overhead. Achievable sum-rate of V2I links has been maximized with V2V reliability guarantee using large-scale fading channel information in [88] or CSI from periodic feedback in [89]. Novel graph-based approaches were further developed in [90, 91] for sum-rate maximization in V2X-related RA problems.

Beside traditional optimization methods, the last few years have seen a surge of interest in RL approach to tackle the distributed RA challenge in C-V2X systems. Such an interest comes from a motivation that many service requirements in C-V2X systems are hard to ensured by using traditional optimization approach. For instance, the problem of joint channel assignment and power allocation to simultaneously maximize the V2I sum-rate and V2V transmission reliability, defined as the successful delivery probability of messages having size B within the time latency constraint T, is generally difficult find the exact optimal solutions. The prior works [86–88, 91] proposed to transform the requirement into SINR constraint at each time step t of time constraint T and adopt various optimization methods to locate the optimal solution. These techniques, however, suffer from a limitation that the balance of V2I and V2V performances across the time duration T can be lost, thus degrading the sum-rate performance. Existing research have demonstrated that the RL approach can effectively tackle the challenge of hard-to-model problems in C-V2X systems. The RL approach allows to address sequential decision making over the time limitation T via trial-and-error interaction with the vehicular environment. At each time step t, the transmitter, defined as an agent, learns an optimal policy to adjust its action (e.g., sub-band and/or transmit power) so as to maximize a reward function, which essentially correlates with the optimization objectives. The flexibility of reward function design enables the RL to deal with problems that are difficult to formulate and solve by the traditional optimization methods.

In underlaid C-V2X systems where V2V links are allowed to autonomously reuse the time-frequency resources currently assigned to the V2I transmission, intelligent power and spectrum allocation is crucial to manage the interference and optimize the throughput. To investigate the spectrum sharing in C-V2X systems where multiple V2V links reuse the spectrum preoccupied by V2I transmission, [92, 93] modeled the joint channel assignment and power allocation problem as a multi-agent RL problem. Such a RL problem was then solved by utilizing the deep Q-learning technique that can be implemented in a distributed fashion. Each V2V link, who was assigned as an agent, made its decisions to choose an optimal solution in a predefined set of discrete sub-bands and power levels for transmission without requiring the global CSI. In [92], the single Q-learning algorithm was used, where the agents used an identical deep Q-network to adjust their actions. The optimization objective of [92] was satisfying the stringent latency constraints on V2V links and minimizing the interference to V2I transmission. [93] extended the RL algorithm in [92] to a multiple Q-learning approach in which each agent adopted a separate deep Q-network. At each time step, the agents acted simultaneously to maximize both the achievable sum-rate of V2I links and successful payload delivery probability of each V2V link. The multi-agent DQN approach was also of interest in [94] under the optimization objective of maximizing the overall capacity of V2I links while ensuring the transmission delay of V2V links. Each V2V link who acted as an agent collectively interacted with the environment so as to find the optimal cellular/D2D transmission mode and transmit power level. Instead of allowing only one vehicle user to be served from only one access point (AP), [95] proposed the concept of virtual cell formation so that a user could be served from multiple APs simultaneously. A distributed single-agent RL algorithm based on Q-learning was then developed to efficiently optimize joint user association and power allocation of the APs in a highly mobile vehicular network. We should also note that, in the context of D2D transmission, the RL-based approach to power allocation problems was also studied [96–98].

2.5 Concluding Remarks

In this chapter, we have provided a literature survey for achievable rate/sum-rate analysis and resource allocation techniques in underlaid D2D cellular networks and C-V2X systems. For a simple link level setup in which one D2D link and one cellular link simultaneously operate in the same time-frequency slot, the single D2D link can be effectively modeled by additive GM channels. Beside D2D transmission, various types of aggregate interference in other wireless systems also exhibit the GM structure; and it has been seen that optimal input distribution and corresponding capacity of such GM channels have not been characterized yet.

For underlaid D2D transmission at network level in which multiple D2D links are capable of reusing a sub-band currently occupied by the cellular user, the concept of stochastic geometry was introduced. This concept is relevant to both HD and FD D2D. When the underlaid D2D feature is integrated into existing cellular systems, achievable sum-rate analysis, taking into account the random distribution of cellular/D2D user locations and channels, is essential in realizing the benefits offered by D2D transmission.

For interference management in underlaid D2D cellular networks, proposed approaches including power allocation and/or beamforming designs at massive MIMO equipped BSs were discussed, allowing to maximize the achievable sum-rate while ensuring reliable transmission at D2D and cellular users.

Finally, the concept of reinforcement learning for resource allocation in the C-V2X system, a D2D-based vehicular network, was discussed. In general, C-V2X systems require stringent latency on V2V transmission, which is not realizable by time-consuming centralized techniques in practice, and hence, calling for the development of distributed resource management to which the learning approach can be effectively applied.

The above literature review provides some motivation for the research topics presented in this thesis. Chapter 3 characterizes the capacity-achieving distribution and correspondingly computes the channel-capacity for a single D2D link modeled by the GM channel. Chapters 4 and 5 utilize the stochastic geometry approach to study the achievable sum-rates and spectral efficiency gains for FD D2D in single- and multi-cell systems, respectively. Chapter 6 develops effective beamforming and power allocation algorithms for network sum-rate maximization in underlaid D2D cellular networks with massive MIMO equipped BSs, while Chapter 7 adopts the multi-agent reinforcement learning to address the challenge of distributed resource management in C-V2X systems.

Chapter 3

Capacity Analysis of Single D2D link [1]

3.1 Introduction

As demonstrated in Chapter 2, the additive Gaussian-Mixture (GM) channels can be used to model the single D2D link in a simple underlaid D2D cellular network where a D2D link reuses a time-frequency slot currently allocated to a cellular user. This chapter is dedicated to study the characterization of the optimal input and the computation of the capacity of additive quadrature GM channels under an average power constraint. While we follow a similar methodology proposed in [41, 42], which was also adopted in other works for Gaussian channels under other additional constraints, the following aspects make our contributions stand out from the previously used tools and ideas.

We first show that the use of a uniformly distributed input phase that is independent with the input amplitude is optimal. While the result is similar to that obtained in [42] for quadrature Gaussian channels, the extension to general GM channels is not trivial and requires new derivations.

The second contribution of this work is to prove the existence and uniqueness of the optimal distribution of the input amplitude. As in the previous studies in [42, 45] for Gaussian channels, we apply tools in complex analysis to show the weak* continuity [2] of mutual information function with respect to the input amplitude distribution. Different from the Gaussian channels, one of the main challenges for GM channels is to establish an integrable upper bound on the absolute function of the integrand in the output entropy equation so that the Dominated Convergence Theorem [99] can be applied.

More importantly, we have comprehensively characterized the discrete nature of the optimal

[1] Parts of Chapter 3 have been presented at the 2015 IEEE Canadian Workshop on Information Theory (CWIT) [25] and published in the IEEE Transaction on Communications [22].

[2] The definition of weak* convergence (correspondingly weak* continuity) is given in Appendix 3.6.1.

input amplitude distribution. Similar to the method considered in [42, 43, 100], we use the Kuhn-Tucker conditions (KTC) to examine the number of mass points in the optimal input amplitude distribution. However, while the previous works in Gaussian channels rely on additional constraints such as peak constraint or fading to show the discreteness of the optimal input amplitude, the consideration of GM channels under only an average power constraint makes the problem of interest much more challenging and requires new approaches. To this end, we first show that if the optimal input amplitude distribution contains an infinite number of mass points on a bounded interval, the channel output must be Gaussian distributed. However, by using Bernstein's theorem [101], we examine the completely monotonic condition and show that such Gaussian-distributed output does not exist. As a result, there is always a finite number of mass points on any bounded interval in the optimal amplitude distribution.

Further, we also demonstrate that it is not possible for the optimal amplitude input to be discrete with an infinite number of mass points. That gives us the unique solution of an optimal input having discrete amplitude with a finite number of mass points. While we rely on the Envelope Theorem proposed earlier in [43, 100], care must be taken into account to establish a upper bound on the Lagrange multiplier and a lower bound on the KTC.

Finally, we propose a simple way to compute the discrete optimal input amplitude and the corresponding capacity. To this end, we first show that the mutual information achieved by a given discrete input amplitude and a uniformly distributed input phase in GM channels can be effectively calculated using Gauss-Laguerre quadrature formulas. A simple gradient descent based method is then adopted to locate the mass points of the optimal input amplitude. Our numerical examples show that in many cases, a capacity-achieving distribution consists of only one or two mass points. As the signal-to-noise-ratio (SNR) increases, the number of mass points increases monotonically but the optimal input distribution remains discrete at any SNR.

The remainder of this chapter is organized as follows. Section 3.2 introduces the GM channel model. In Section 3.3, a detailed characterization of optimal input distributions is presented under an average power constraint. Section 3.4 details a simple method to compute the optimal input distribution and the corresponding capacity. Numerical results are also presented in this section to confirm the analysis. Finally, Section 3.5 concludes the chapter.

3.2 Gaussian-Mixture Channel

3.2.1 Channel Model

We can modify the considered system model of D2D link in Section 2.1 by considering a general input/output model of an additive GM channel as

$$y = x + z. \tag{3.1}$$

In (3.1), $x \in \mathbb{C}$ is the complex channel input, $y \in \mathbb{C}$ is the complex channel output, and $z \in \mathbb{C}$ is the zero mean GM noise with unit variance $\mathbb{E}[|z|^2] = 1$ with $|\cdot|$ being the magnitude of a complex number. For simplicity, the time index in (3.1) is omitted. The probability density function (PDF) of the GM noise is a weighted sum of Gaussian component densities and it can be expressed as [49]

$$f_Z(z) = \sum_{n=1}^{N} \frac{\varepsilon_n}{2\pi\sigma_n^2} \exp\left(-\frac{|z|^2}{2\sigma_n^2}\right), \tag{3.2}$$

where $\sigma_1, \sigma_2, \ldots, \sigma_N > 0$, $\varepsilon_n \in (0,1)$ for $n = 1, \ldots, N$, $N \geq 2$ and

$$\sum_{n=1}^{N} \varepsilon_n = 1, \tag{3.3a}$$

$$\sum_{n=1}^{N} \varepsilon_n \sigma_n^2 = \frac{1}{2}. \tag{3.3b}$$

Without the loss of generality, it is assumed that $\sigma_1 = \max\{\sigma_n\}_{n=1}^N$ and $\sigma_N = \min\{\sigma_n\}_{n=1}^N$ and $\sigma_1 > \sigma_N > 0$.

Note that when the PDF in (3.2) consists of only two terms, we obtain the PDF of $\epsilon-$mixute noise [51] and Bernoulli-Gaussian noise [50]. For a given overlapping factor A and power ratio Ω, we have the Middleton Class A model with $\varepsilon_n = \exp(-A)\frac{A^n}{n!}$ and $\sigma_n = \frac{n/A+\Omega}{1+\Omega}$ as $N \to \infty$ [37, 52].

3.2.2 Channel Capacity

In this chapter, we are interested in the optimal signaling scheme and the corresponding D2D channel capacity under the average power constraint

$$\mathbb{E}[|x|^2] \leq P_d. \tag{3.4}$$

Under this constraint, the channel capacity, which is the supremum of the mutual information between the channel input and output over the set of all input distributions, can be expressed as

$$C = \sup_{\substack{F_X(\cdot) \\ \mathbb{E}[|x|^2] \leq P_d}} I(x;y) = \sup_{\substack{F_X(\cdot) \\ \mathbb{E}[|x|^2] \leq P_d}} H(y) - H(y|x), \tag{3.5}$$

where $F_X(\cdot)$ denotes the input distribution function, $H(y)$ is the entropy of the channel output and $H(y|x) = H(z)$ is the GM noise entropy. Note that for a given GM noise PDF in (3.2), $H(z)$ is a constant. Therefore, the optimal input that achieves the capacity shall maximize the output entropy $H(y)$.

Using the polar coordinates, the channel input x and output y can be represented as $x = re^{i\theta}$ and $y = ue^{i\psi}$, respectively. The output entropy can then be calculated as [42, equ. (6)]:

$$H(y) = H(u,\psi) + \int_0^\infty f_U(u) \ln u \, \mathrm{d}u, \tag{3.6}$$

where $H(u,\psi)$ is the joint differential entropy of u and ψ and $f_U(u)$ is the PDF of u.

3.3 Capacity-Achieving Input Distributions

In this section, we will investigate in detail the structure of the optimal input distribution of the additive GM noise channel under the average power constraint. To this end, we first establish a result on the optimality of the uniformly distributed input phase θ that is independent of the input amplitude r in Section 3.3.1, and the existence and uniqueness of the optimal distribution of the input amplitude r in Section 3.3.2. The optimality of a discrete input amplitude distribution having a finite number of mass points is then given in Section 3.3.3.

3.3.1 Optimal Phase Distribution

First, we write the joint PDF $f_{U,\Psi}(u,\psi)$ of u and ψ as follows:

$$f_{U,\Psi}(u,\psi) = \int_0^\infty \int_0^{2\pi} f_{U,\psi|R,\Theta}(u,\psi|r,\theta) f_{R,\Theta}(r,\theta) \mathrm{d}\theta \mathrm{d}r. \tag{3.7}$$

Here, $f_{R,\Theta}(r,\theta)$ is the joint PDF of r and θ. Furthermore, $f_{U,\psi|R,\Theta}(u,\psi|r,\theta)$ is the joint PDF of u and ψ conditioned on r and θ and it is given as

$$f_{U,\psi|R,\Theta}(u,\psi|r,\theta) = \sum_{n=1}^{N} \frac{\varepsilon_n}{2\pi\sigma_n^2} \exp\left(-\frac{u^2+r^2-2ur\cos(\psi-\theta)}{2\sigma_n^2}\right). \tag{3.8}$$

Then by integrating (3.7) over ψ, we obtain the marginal PDF $f_U(u)$ as

$$\begin{aligned} f_U(u) &= \int_0^{2\pi} f_{U,\Psi}(u,\psi)d\psi \\ &= \int_0^{\infty} u \sum_{n=1}^{N} \frac{\varepsilon_n}{\sigma_n^2} \exp\left(-\frac{u^2+r^2}{2\sigma_n^2}\right) I_0\left(\frac{ur}{\sigma_n^2}\right) \mathrm{d}F_R(r). \end{aligned} \tag{3.9}$$

where $I_0(\cdot)$ is the zeroth-order modified Bessel function defined as $I_0(z) = \frac{1}{\pi}\int_0^{\pi} e^{z\cos(t)}dt$. The following proposition then provides the preliminary result on the optimal phase distribution of the input.

Proposition 1. *For the additive GM noise channel (3.1) under the average power constraint (3.4), a uniformly distributed phase θ that is independent of the input amplitude r is capacity-achieving.*

Proof. Using the independence bound on the entropy, we first have the following inequality:

$$H(u,\psi) \le H(u) + H(\psi) \tag{3.10a}$$

$$\le H(u) + \ln(2\pi). \tag{3.10b}$$

The equality in (3.10a) is achieved if and only if (iff) u and ψ are independent, and we have the equality in (3.10b) iff ψ is uniformly distributed. Now, let assume that r and θ are independent and θ is uniformly distributed, we obtain

$$f_{R,\Theta}(r,\theta) = f_R(r)f_\Theta(\theta) = \frac{1}{2\pi} f_R(r). \tag{3.11}$$

From (3.8), the joint PDF of output can be expressed as follows:

$$\begin{aligned} f_{U,\Psi}(u,\psi) &= \frac{1}{2\pi}\sum_{n=1}^{N}\int_0^\infty\int_0^{2\pi}\frac{u\varepsilon_n}{2\pi\sigma_n^2}\exp\left(-\frac{u^2+r^2-2ur\cos(\psi-\theta)}{2\sigma_n^2}\right)\mathrm{d}\theta f_R(r)\mathrm{d}r \\ &= \frac{1}{2\pi}\sum_{n=1}^{N}\int_0^\infty\frac{u\varepsilon_n}{\sigma_n^2}\exp\left(-\frac{u^2+r^2}{2\sigma_n^2}\right)I_0\left(\frac{ur}{\sigma_n^2}\right)\mathrm{d}F_R(r) \\ &= \frac{1}{2\pi}f_U(u), \end{aligned} \tag{3.12}$$

where the last equality in (3.12) comes from (3.9). It can be seen from (3.12) that the selection of uniformly distributed θ that is independent of r results in independent u and uniformly distributed ψ. Such selection of the inputs r and θ is therefore optimal. □

3.3.2 Existence and Uniqueness of Optimal Amplitude Distribution

Next, we will examine the input amplitude. With a slight abuse of notation, let F_R be the distribution of the amplitude r. Also, let $v \triangleq u^2/2$. The mutual information between the channel input and output can then be rewritten as

$$I(F_R) \triangleq I(x;y) = -\int_0^\infty f_V(v;F_R)\ln f_V(v;F_R)\mathrm{d}v + \ln(2\pi) - H(z), \tag{3.13}$$

where $f_V(v;F_R)$ is the PDF of the output v for a given input distribution F_R. Using the concept of kernel function $K_N(\cdot,\cdot)$ [42], this PDF can be expressed as

$$f_V(v;F_R) = \int_0^\infty K_N(v,r)\mathrm{d}F_R(r). \tag{3.14}$$

With the transformation $v = u^2/2$, we have $f_V(v;F_R) = f_U(u)/u$. Then by combining (3.14) and (3.9), we obtain the kernel function $K_N(v,r)$ in closed-form for the considered GM noise channel as

$$K_N(v,r) = \sum_{n=1}^{N}\frac{\varepsilon_n}{\sigma_n^2}\exp\left(-\frac{2v+r^2}{2\sigma_n^2}\right)I_0\left(\frac{\sqrt{2v}r}{\sigma_n^2}\right) \tag{3.15}$$

with $I_0(\cdot)$ being the zeroth-order modified Bessel function.

Now, let $\mathcal{F}$ denote the set of probability functions satisfying the average power constraint (3.4). Then from [45, Appendix I.A], $\mathcal{F}$ is weak* compact in the Levy metric topology and convex. We

then have the following important lemma:

Lemma 1. *The function $I(\cdot)$ in (3.13) is a weak* continuous function on $\mathcal{F}$ and the capacity-achieving input amplitude distribution exists and is unique.*

Proof. Let the notation $F_n \xrightarrow{w^*} F$ indicate that a sequence $F_n(r)$ converges weak*[3] to the distribution function $F(r)$. The weak* continuity of $I(\cdot)$ is equivalent to the fact that if $F_n \xrightarrow{w^*} F$, we will have $I(F_n) \to I(F)$, i.e.,

$$F_n \xrightarrow{w^*} F \Rightarrow I(F_n) \to I(F). \tag{3.16}$$

Since the function $K_N(v, r)$ in (3.15) is a bounded continuous function for all $v, r \geq 0$, by the weak* convergence, we have

$$F_n \xrightarrow{w^*} F \Rightarrow f_V(v; F_n) \to f_V(v; F). \tag{3.17}$$

Therefore,

$$\int_0^\infty \lim_{n\to\infty} f_V(v; F_n) \ln f_V(v; F_n) \mathrm{d}v = \int_0^\infty f_V(v; F) \ln f_V(v; F) \mathrm{d}v. \tag{3.18}$$

Furthermore, as we show in Appendix 3.6.2, an integrable upper bound on $|f_V(v; F_n) \ln f_V(v; F_n)|$ can always be established. Then by using Dominated Convergence Theorem [99], we obtain

$$\lim_{n\to\infty} \int_0^\infty f_V(v; F_n) \ln f_V(v; F_n) \mathrm{d}v = \int_0^\infty \lim_{n\to\infty} f_V(v; F_n) \ln f_V(v; F_n) \mathrm{d}v. \tag{3.19}$$

It then follows that

$$\lim_{n\to\infty} \int_0^\infty f_V(v; F_n) \ln f_V(v; F_n) \mathrm{d}v = \int_0^\infty f_V(v; F) \ln f_V(v; F) \mathrm{d}v, \tag{3.20}$$

which is equivalent to (3.16). It means that the function $I(\cdot)$ in (3.13) is weak* continuous over $\mathcal{F}$. Furthermore, the mutual information $I(F_R)$ is a strictly concave function of F_R [45]. Therefore, following [45, Theorem 1] and [41, Optimization Theorem (p. 207)], $I(\cdot)$ achieves its maximum over $\mathcal{F}$ at a unique point $F_0 \in \mathcal{F}$, proving the existence and uniqueness of the capacity-achieving amplitude distribution. □

[3]The definition of weak* convergence is given in Appendix 3.6.1

3.3.3 Characterization of Optimal Amplitude Distribution

Based on the results obtained in the previous subsection, this subsection shall study the detailed characterization of the capacity-achieving input amplitude distribution. To proceed further, let us first present the key result of this subsection in the following theorem.

Theorem 1. *For the additive GM noise channel (3.1) under the average power constraint (3.4), the capacity-achieving input amplitude distribution is discrete with a finite number of mass points.*

The remaining part of this subsection is devoted to the proof of Theorem 1. Instead of proving it directly, we will show Theorem 1 by an alternative approach. In particular, for the optimal input distribution F_0, there are only two possible cases for the support set E_0 as follows:

1. E_0 contains an infinite number of mass points on a bounded interval. This case includes a continuous distribution F_0 and a mixed continuous and discrete distribution F_0 as special cases.

2. E_0 contains only a finite number of mass points on any bounded interval.

In the following, using the Kuhn-Tucker condition, we will first demonstrate that the first case is not possible. Specifically, we show that if E_0 contains an infinite number of mass points on a bounded interval, the output must be Gaussian distributed. However, using Bernstein's theorem to examine the completely monotonic condition, we rule out this possibility. Then focusing on the second case, we show that E_0 cannot have an infinite number of mass points. This results in an optimal discrete input amplitude having a finite number of mass points.

Case 1

Assume that E_0 contains an infinite number of mass points on a bounded interval. We first have the following proposition that provides a necessary and sufficient condition for the amplitude distribution F_0 to be optimal.

Proposition 2. *[Kuhn-Tucker Condition (KTC)] For the additive GM channel under an average power constraint, F_0 is a capacity-achieving amplitude distribution iff there exists $\lambda \geq 0$ such that the following is satisfied*

$$\Phi(r) \triangleq \int_0^\infty K_N(v,r) \ln f_V(v;F_0) dv + \lambda(r^2 - P_d) + H_0 \geq 0, \quad \forall r \geq 0 \tag{3.21}$$

with the equality being achieved when $r \in E_0$, the support set of F_0. Here, H_0 is the output entropy achieved by F_0.

Proof. The proof follows closely the arguments in [100], with some slight modifications to the considered GM channel. For completeness, the detail is provided in Appendix 3.6.3. □

The next two theorems address the analytic property of $\Phi(r)$ in (3.21), which is useful in determining F_0.

Theorem 2. *For each compact subset $\mathcal{K}$ of $\mathbb{C}$, where $\mathbb{C}$ is the set of complex numbers, the integral*

$$\int_0^\infty K_N(v,z)\ln f_V(v;F_0)dv \tag{3.22}$$

is uniformly convergent for all $z \in \mathcal{K}$.

Proof. By definition, the integral $\int_0^\infty f(t,z)\mathrm{d}t$ is said to be uniformly convergent for all $z \in \mathcal{K}$ if $\lim_{B\to\infty}\int_B^\infty |f(t,z)|\mathrm{d}t = 0, \forall z \in \mathcal{K}$ [100, Lemma C.2]. As we show in Appendix 3.6.4, the density function $f_V(v;F_R)$ for a given F_R can be lower bounded as $f_V(v;F_R) \geq d\exp\left(-\frac{2v+P_d}{2\sigma_N^2}\right)$, with $d = \sum_{n=1}^{N}\frac{\varepsilon_n}{\sigma_n^2}$. Also, as we showed earlier, $f_V(v;F_R) \leq d$ (please see Appendix 3.6.2). Therefore,

$$|\ln f_V(v;F_0)| \leq \max\left\{\left|\ln d - \frac{2v+P_d}{2\sigma_N^2}\right|, |\ln d|\right\}. \tag{3.23}$$

It then follows that

$$\begin{aligned}\int_0^\infty |K_N(v,z)\ln f_V(v;F_0)|\,\mathrm{d}v &\leq \int_0^\infty |K_N(v,z)| \times \max\left\{\left|\ln d - \frac{2v+P_d}{2\sigma_N^2}\right|, |\ln d|\right\}\mathrm{d}v \\ &= \int_0^\infty \left|\sum_{n=1}^{N}\frac{\varepsilon_n}{\sigma_n^2}e^{-\frac{2v+z^2}{2\sigma_n^2}}I_0\left(\frac{\sqrt{2v}z}{\sigma_n^2}\right)\right| \times \max\left\{\left|\ln d - \frac{2v+P_d}{2\sigma_N^2}\right|, |\ln d|\right\}\mathrm{d}v \\ &< \infty, \qquad \forall z \in \mathcal{K}.\end{aligned} \tag{3.24}$$

The inequality in (3.24) is obtained from the fact that every compact set $\mathcal{K}$ in the complex plane is closed and bounded and we use the following two integrals [102, 6.643.2]

$$\int_0^\infty e^{-\alpha x}I_0\left(2\beta\sqrt{x}\right)\mathrm{d}x = \alpha^{-1}e^{\beta^2/\alpha} \tag{3.25}$$

and

$$\int_0^\infty xe^{-\alpha x}I_0\left(2\beta\sqrt{x}\right)\mathrm{d}x = \alpha^{-3}e^{\beta^2/\alpha}\left(\beta^2+\alpha\right). \tag{3.26}$$

Since the integrand is a positive function and the integral is finite, we obtain

$$\lim_{B\to\infty}\int_{B}^{\infty}\left|K_N(v,z)\ln f_V(v;F_0)\right|\mathrm{d}v=0.$$

The theorem is therefore proved. □

Theorem 3. *For the GM noise channel, the function $\Phi(z)$ in (3.21) is analytic for all $z\in\mathbb{C}$.*

Proof. From (3.21), it can be seen that it is sufficient to show that

$$H\left(z;F_0\right)=\int_{0}^{\infty}K_N(v,z)\ln f_V(v;F_0)\mathrm{d}v \tag{3.27}$$

is analytic for all $z\in\mathbb{C}$. For all $v\geq 0$, it can be verified that the kernel function $K_N(v,z)$ is analytic in the entire complex plane. It is because the exponential functions $\exp\left(-\frac{2v+z^2}{2\sigma_n^2}\right)$ and the modified Bessel function $I_0(\cdot)$ are analytic, since they can be expanded as power series. Therefore, given the result in Theorem 2 and the fact $K_N(v,z)$ is analytic, we can conclude that $H\left(z;F_0\right)$ is analytic in $\mathbb{C}$ by using the Differentiation Lemma [103, Section XV], [100]. Therefore, $\Phi(z)$ is analytic for all $z\in\mathbb{C}$. □

Since the support set E_0 contains an infinite number of mass points on a bounded interval, by Bolzano-Weierstrass Theorem [42], E_0 contains a limit point and all the elements in E_0 are confined to $[0,\,\infty)$. From the Identity Theorem [42], we know that if two analytic functions are identical on an infinite set of points in a region along with their limit points, these two functions will be identical in the entire region. Therefore, by combining the results from Proposition 2, Theorem 3, and the Identity Theorem, we obtain the following integral

$$\begin{aligned}\Phi(r)&=\int_{0}^{\infty}K_N(v,r)\ln f_V(v;F_0)\mathrm{d}v+\lambda(r^2-P_d)+H_0\\&=0,\quad\forall r\in\mathbb{R}\end{aligned} \tag{3.28}$$

with $\mathbb{R}$ being the set of real numbers.

In the following, we show that (3.28) can be solved to give a unique and closed-formed solution of $f_V(v;F_0)$. This solution is optimal as long as the corresponding input distribution F_0 is a valid distribution and λ is nonnegative because this solution satisfies the KTC in Proposition 2. To this end, the following lemma first states an important property of an integral equation of the kernel function.

Lemma 2. *The integral equation*

$$\int_0^\infty K_N(v,r)g(r)dr = 0, \quad \forall v \geq 0, \tag{3.29}$$

with $g(\cdot)$ being a continuous function, has the only solution $g(r) = 0, \forall r \geq 0$. Similarly, the integral equation

$$\int_0^\infty K_N(v,r)g(v)dv = 0, \quad \forall r \geq 0 \tag{3.30}$$

has $g(v) = 0, \forall v \geq 0$, as its only solution.

Proof. We first focus on (3.29). Taking the Laplace transform of (3.29) with respect to v gives

$$\int_0^\infty \int_0^\infty e^{-vs} K_N(v,r)g(r)\mathrm{d}v\mathrm{d}r = 0, \quad \forall s \geq 0. \tag{3.31}$$

Using (3.25), we have

$$\begin{aligned}\sum_{n=1}^{N} \frac{\varepsilon_n}{\sigma_n^2} \int_0^\infty e^{-vs} \cdot e^{-\frac{2v+r^2}{2\sigma_n^2}} I_0\left(\frac{\sqrt{2v}r}{\sigma_n^2}\right) \mathrm{d}v &= \sum_{n=1}^{N} \frac{\varepsilon_n}{\sigma_n^2} \int_0^\infty e^{-v\left(s+1/\sigma_n^2\right)} \cdot e^{-r^2/\sigma_n^2} I_0\left(2\sqrt{\frac{r^2}{2\sigma_n^4}v}\right) \mathrm{d}v \\ &= \sum_{n=1}^{N} \frac{\varepsilon_n}{\sigma_n^2 s + 1} \exp\left(-\frac{r^2 s}{2\left(\sigma_n^2 s + 1\right)}\right).\end{aligned}$$

Thus, (3.31) can be rewritten as

$$\int_0^\infty \left[\sum_{n=1}^{N} \frac{\varepsilon_n}{\sigma_n^2 s + 1} \exp\left(-\frac{r^2 s}{2\left(\sigma_n^2 s + 1\right)}\right)\right] g(r)\mathrm{d}r = 0, \quad \forall s \geq 0. \tag{3.32}$$

Let $x = r^2/2$ and $q(x) = \sqrt{2x}g(\sqrt{2x})$. Then (3.32) becomes

$$\int_0^\infty K(s,x)q(x)\mathrm{d}x = 0, \quad \forall s \geq 0, \tag{3.33}$$

where

$$K(s,x) = \sum_{n=1}^{N} \frac{\varepsilon_n}{\sigma_n^2 s + 1} \exp\left(-x \cdot \frac{s}{(\sigma_n^2 s + 1)}\right).$$

Let $Q(t) \triangleq \mathcal{L}\{q'(x)\}$ and $h \triangleq 1/s + \sigma_1^2$ be the Laplace transform at t of the first-order derivative

of $q(x)$. Then (3.32) becomes

$$\sum_{n=1}^{N} \varepsilon_n Q\left(\frac{1}{h-d_n}\right) = 0, \quad \forall h \in (\sigma_1^2, \infty) \tag{3.34}$$

with $d_n = \sigma_1^2 - \sigma_n^2 \geq 0$. Also changing the functional notation as $F(h) = Q(1/h)$, we obtain

$$\sum_{n=1}^{N} \varepsilon_n F(h-d_n) = 0, \quad \forall h \in (0, 1/\sigma_1^2).$$

Taking the inverse Laplace transform of the above equality yields

$$\sum_{n=1}^{N} \varepsilon_n e^{d_n y} f(y) = 0, \tag{3.35}$$

where

$$f(y) = \mathcal{L}^{-1}\{F(h)\} = \frac{1}{2\pi i} \lim_{T\to\infty} \int_{\gamma-iT}^{\gamma+iT} e^{hy} F(h) \mathrm{d}h.$$

Thus, we conclude $f(y) = 0$. By taking the Laplace transform of (3.35), we obtain $F(h) = 0$, $\forall h \in (0, 1/\sigma_1^2)$ and subsequently $Q(h) = 0$, $\forall h \in (\sigma_1^2, \infty)$. Finally, using the transformation $s = \frac{1}{h-\sigma_1^2}$, we have $Q(s) = 0$, $\forall s \in (0, \infty)$ and $q'(x) = 0$. Since $\int_0^\infty q(x)\mathrm{d}x = 0$, we have $q(x) = 0$. Equivalently, $g(r) = 0$, $\forall r \geq 0$. For (3.30), by changing the variables as $x = \sqrt{v/2}$ and $y = r^2/2$, we obtain a similar integral as in (3.29). The proof then follows similarly. □

From Lemma 2, it can be seen that there exists a unique solution to (3.28). In addition, by using (3.25) and (3.26), it is straightforward to show that the density function

$$f_V(v; F_0) = c(\lambda) e^{-2\lambda v}, \tag{3.36}$$

with $c(\lambda) \triangleq e^{\lambda P_d + \lambda - H_0}$ satisfies (3.28). As such, $f_V(v; F_0) = c(\lambda)e^{-2\lambda v}$ is an optimal output distribution. Now, if $\lambda = 0$, we have $f_V(v; F_0) = c(0) = e^{-H_0}$ and the optimal input amplitude distribution is $f_R(r) = re^{-H_0}$. However, it is an invalid PDF. Therefore, $\lambda > 0$ and v follows an exponential distribution $f_V(v; F_0) = 2\lambda e^{-2\lambda v}$, and λ can be verified to be $\lambda = \frac{1}{P_d+1}$. Hence, the distribution of the output amplitude u can be expressed as

$$f_U(u) = \frac{2u}{P_d+1} e^{-\frac{u^2}{P_d+1}}. \tag{3.37}$$

which is a Rayleigh distribution. As a result, the channel output y must be Gaussian distributed. To further understand the characterization of the corresponding optimal input, we now study whether there exists an input distribution that leads to a Gaussian output.

From (3.2), the characteristic function (CF) of the noise z can be expressed as

$$\psi_n(\omega_1, \omega_2) = \sum_{n=1}^{N} \varepsilon_n \exp(-\sigma_n^2(\omega_1^2 + \omega_2^2)/2). \tag{3.38}$$

If the output distribution is Gaussian, the CF of input x can be written as follows:

$$\begin{aligned}\psi_x(\omega_1, \omega_2) &= \frac{\psi_y(\omega_1, \omega_2)}{\psi_n(\omega_1, \omega_2)} \\ &= \frac{\exp\left(-\left(P_d + 2\sum\limits_{n=1}^{N} \varepsilon_n \sigma_n^2\right)(\omega_1^2 + \omega_2^2)/4\right)}{\sum\limits_{n=1}^{N} \varepsilon_n \exp\left(-\sigma_n^2(\omega_1^2 + \omega_2^2)/2\right)}.\end{aligned} \tag{3.39}$$

In order to check whether the above CF is valid, we first use the Euclidean norm transformation $t = \sqrt{(\omega_1^2 + \omega_2^2)}$ to obtain the transformed univariate function as

$$\varphi_x(t) = \frac{\exp\left(-\left(P_d + 2\sum\limits_{n=1}^{N} \varepsilon_n \sigma_n^2\right) t^2/4\right)}{\sum\limits_{n=1}^{N} \exp(-\sigma_n^2 t^2/2)}. \tag{3.40}$$

It can be observed that this function is a radial function [104]. Therefore, as shown in [105], the necessary and sufficient condition to have a valid CDF in (3.39) is the completely monotone property of the function $\psi_x(t) = \varphi_x(\sqrt{t})$, which is given as

$$\begin{aligned}\psi_x(t) &= \frac{\exp\left(-\left(P_d + 2\sum\limits_{n=1}^{N} \varepsilon_n \sigma_n^2\right) t/4\right)}{\sum\limits_{n=1}^{N} \varepsilon_n \exp(-\sigma_n^2 t/2)} \\ &= \frac{\exp\left(-\left(P_d + 2\sum\limits_{n=1}^{N-1} \varepsilon_n (\sigma_n^2 - \sigma_N^2)\right) t/4\right)/\varepsilon_N}{1 + \sum\limits_{n=1}^{N-1} \frac{\varepsilon_n}{\varepsilon_N} \exp(-(\sigma_n^2 - \sigma_N^2) t/2)}.\end{aligned} \tag{3.41}$$

Note that in (3.41), $\sigma_n^2 - \sigma_N^2 \geq 0$ for $n = 1, \ldots, N-1$, because $\sigma_N = \min\{\sigma_n\}_{n=1}^{N}$. In general,

checking the monotone property presents some challenges, since one needs to check the non-negativity of any l^{th} derivative $(-1)^l \psi_x^{(l)}(t)$ for any $t \geq 0$ [105]. In the following, we consider an alternative approach using Bernstein's theorem [101, Theorem 1.4].

By Bernstein's theorem [101, Theorem 1.4], a function $g(\cdot)$ is completely monotonic iff it has the following representation:

$$g(r) = \int_0^\infty e^{-tr}\, d\mu(t) \tag{3.42}$$

for a unique Borel measure μ on $[0, \infty]$. We then have the following theorem:

Theorem 4. *The function $g(r)$, $r > 0$,*

$$g(r) = \frac{e^{-br}}{1 + \sum_{m=1}^{M} d_m e^{-a_m r}} \tag{3.43}$$

with $M \geq 1$, $b > 0$, the positive sets $\{d_m\}$, and the nonnegative set $\{a_m\}$ with $\max\{a_m\} > 0$, is not completely monotonic.

Proof. Assume that $g(r)$ in (3.43) is completely monotonic. Using (3.42), for a positive σ, we have:

$$\frac{g(r+\sigma)}{g(r)} = \frac{\int_0^\infty e^{-t\sigma} e^{-tr}\, d\mu(t)}{\int_0^\infty e^{-tr}\, d\mu(t)}. \tag{3.44}$$

Using this representation, it has been shown in [106] that a completely monotone $g(r)$ is either in the form of $\alpha e^{-\beta r}$ for some $\alpha, \beta \geq 0$, or $g(r+\sigma)/g(r)$ must be a strictly increasing function of r. It is obvious that $g(r)$ in (3.43) cannot be represented as $g(r) = \alpha e^{-\beta r}$. The ratio $g(r+\sigma)/g(r)$ can then be expressed as

$$\frac{g(r+\sigma)}{g(r)} = e^{-b\sigma} \cdot \frac{1 + \sum_{m=1}^{M} d_m e^{-a_m r}}{1 + \sum_{m=1}^{M} d_m e^{-a_m (r+\sigma)}}. \tag{3.45}$$

Taking its first derivative with respect to r yields

$$\frac{\partial \left[g(r+\sigma)/g(r) \right]}{\partial r} = e^{-b\sigma} \cdot \frac{\sum_{m=1}^{M} d_m a_m e^{-a_m r} \left(e^{-a_m \sigma} - 1 \right)}{\left[1 + \sum_{m=1}^{M} d_m e^{-a_m (r+\sigma)} \right]^2} < 0.$$

where the inequality comes from the fact that $\max\{a_m\} > 0$. Therefore, $g(r+\sigma)/g(r)$ is a decreasing function of r, which results in a contradiction. As a consequence, $g(r)$ in (3.43) is not completely monotonic. □

Using Theorem 4, it can be seen that $\psi_x(t)$ in (3.41) is not completely monotonic. Therefore, the CF function $\psi_x(\omega_1, \omega_2)$ in (3.39) is not a valid one. As such, there does not exist an input distribution that results in a Gaussian distributed output for the GM noise channel. Equivalently, it is not possible to have an F_0 with an infinite number of mass points on a bounded interval. Instead, there is always a finite number of mass points on any bounded interval. This second case shall be examined further in the following.

Case 2

Now, we consider the case of having an F_0 with a finite number of mass points on any bounded interval. For this case, there are still two possibilities: i) F_0 has an infinite number of mass points, but finitely many of them on any bounded interval; ii) F_0 has a finite number of mass points. To shed some further light on F_0, the next Lemma establishes a upper bound on the parameter λ in (3.21) of the KTC.

Lemma 3. *For the optimal discrete distribution F_0, λ in the KTC in (3.21) is smaller than one, i.e., $\lambda < 1$.*

Proof. Using similar arguments as in [54, 107], we can interpret the additive GM noise channel as a Markov chain whose state space $\mathcal{S} = \{s_1, s_2, \ldots, s_N\}$ corresponds to N memoryless AWGN channels with noises $\{\mathcal{CN}(0, 2\sigma_n^2)\}$. If these channel states are perfectly known at both receiver and transmitter, we have the following achievable rate which is the capacity of the finite-state Markov channel [54]:

$$C_A = \sum_{n=1}^{N} \varepsilon_n \ln\left(1 + \frac{P_d}{2\sigma_n^2}\right).$$

From the above interpretation, it can be seen that C_A is a upper bound on the channel capacity C. For convenience, let us denote the capacity C, the rate C_A and λ as a function of P_d, i.e., $C(P_d)$, $C_A(P_d)$, and $\lambda(P_d)$. By the Envelope Theorem [108] and the KTC, $\lambda(P_d)$ is the derivative of $C(P_d)$. Since $C_A(0) = C(0) = 0$ and $\frac{\partial C_A(P_d)}{\partial P_d}\Big|_{P_d=0} = 1$, we must have $\lambda(0) \leq 1$. Otherwise we can find a small enough P_d such that $C(P_d)$ would exceed $C_A(P_d)$. Furthermore, as we demonstrate in Appendix 3.6.5, $C(P_d)$ is a strictly concave function of P_d. Hence $\lambda(P_d) < \lambda(0) \leq 1$. The lemma is therefore proved. □

Given that the optimal input distribution is discrete, the integral in (3.14) becomes a sum and the output PDF can be expressed as $f_V(v;F_0)=\sum_{i\in\mathcal{I}} p_i K_N(v,r_i)$ where $\mathcal{I}$ is the set of mass points, and $\{p_i\}$ and $\{r_i\}$, $i\in\mathcal{I}$, are the probabilities and locations of mass points, respectively. Let p_k and r_k be the probability and location of a given $k-$th finite mass point, we then have a lower bound on $f_V(\cdot;\cdot)$ as follows:

$$\begin{aligned} f_V(v;F_0) > p_k K_N(v,r_k) &= p_k \sum_{n=1}^{N} \frac{\varepsilon_n}{\sigma_n^2} e^{-\frac{2v+r_k^2}{2\sigma_n^2}} I_0\left(\frac{\sqrt{2v}r_k}{\sigma_n^2}\right) \\ &\geq p_k \sum_{n=1}^{N} \frac{\varepsilon_n}{\sigma_n^2} e^{-\frac{2v+r_k^2}{2\sigma_n^2}} \qquad (3.46a) \\ &> p_k \frac{\varepsilon_1}{\sigma_1^2} e^{-\frac{2v+r_k^2}{2\sigma_1^2}} \\ &\geq p_k \frac{\varepsilon_1}{\sigma_1^2} e^{-2v-r_k^2}, \qquad (3.46b) \end{aligned}$$

where (3.46a) is obtained by using $I_0(x)\geq 1$, $\forall x\geq 0$ and (3.46b) is obtained from the fact that $\sigma_1^2\geq\frac{1}{2}$. We can then establish the following lower bound on $\Phi(\cdot)$ in (3.21):

$$\begin{aligned} \Phi(r) &> \int_0^\infty \ln\left(\frac{p_k\varepsilon_1}{\sigma_1^2}e^{-r_k^2}\right) K_N(v,r)\mathrm{d}v - \int_0^\infty 2vK_N(v,r)\mathrm{d}v + \lambda(r^2-P_d)+H_0 \\ &= \ln\left(\frac{p_k\varepsilon_1}{\sigma_1^2}\right) - r_k^2 - (r^2+1) + \lambda(r^2-P_d)+H_0 \qquad (3.47a) \\ &= (1-\lambda)r^2 + \ln\left(\frac{p_k\varepsilon_1}{\sigma_1^2}\right) - r_k^2 - 1 + \lambda P_d + H_0, \qquad (3.47b) \end{aligned}$$

where we have used the integrals in (3.25) and (3.26) to arrive at (3.47a).

Since $\lambda<1$, we have $1-\lambda>0$. Therefore, the lower bound in (3.47b) grows without bound as r increases and this leads to the fact that there exists a finite value r_{max} such that $\Phi(r)>0$ for all $r\in(r_{max},\infty)$. Thus, all the mass points of the optimal distribution are located in the bounded interval $[0,r_{max}]$.

Combining the above results, it can be seen that the capacity-achieving input amplitude distribution is discrete with a finite number of mass points as stated in Theorem 1. This result makes GM noise fundamentally different from Gaussian noise. It is because for the considered GM channel, only an average power constraint is imposed on the input rather than an average power constraint together with additional constraints such as peak constraint or fading studied earlier for Gaussian channels.

3.4 Optimal Input and Capacity Computation

Given the discrete nature of the optimal input, it is certainly of further interest to find the locations and the probabilities of the mass points. However, analytically finding these values for the optimal input distribution and the corresponding capacity is a very challenging task. It is because in general, the locations and the probabilities of the mass points are SNR-dependent. Therefore, in this section, we resort to numerical methods to find the discrete optimal input and the capacity. In the following, we first present a simple way to calculate the mutual information between the input and output for a given discrete input distribution without the need of time-consuming Monte Carlo simulations. A simple gradient descent-based optimization method is then presented to find the optimal distribution and to calculate the capacity. Numerical examples are finally provided to confirm our analysis.

3.4.1 Mutual Information and Optimal Input/Capacity Computation

To find the optimal input, let us first consider a given discrete input F_R with a fixed number of mass points P. Furthermore, assume that the amplitude mass points are located at $\{r_k\}_{k=1}^{P}$ with the corresponding probabilities $\{p_k\}_{k=1}^{P}$. With this input distribution, the mutual information between the channel input and output can be expressed as

$$\begin{aligned} I(F_R) &= -\int_0^\infty f_V(v;F_R)\ln f_V(v;F_R)\mathrm{d}v + \ln(2\pi) - H(z) \\ &= -\sum_{n=1}^{N} I_n + \ln(2\pi) - H(z), \end{aligned} \tag{3.48}$$

with

$$I_n = \int_0^\infty e^{-\frac{v}{\sigma_n^2}} \sum_{k=1}^{P} p_k \frac{\varepsilon_n}{\sigma_n^2} e^{-\frac{r_k^2}{2\sigma_n^2}} I_0\left(\frac{\sqrt{2v}r_k}{\sigma_n^2}\right) \times \ln \sum_{k=1}^{P} p_k K_N(v, r_k)\mathrm{d}v. \tag{3.49}$$

Since it is not possible to obtain I_n in closed-form, we use the Gauss-Laguerre quadrature formulas to evaluate it [109]. Specifically, let $Q = \int_0^\infty e^{-x} q(x)\mathrm{d}x$ for a given function $q(x)$. We can then approximate Q as follows:

$$Q \approx \sum_{i=1}^{G} w_i q(x_i). \tag{3.50}$$

In (3.50), $\{x_i\}$ are the roots of Laguerre polynomial $L_G(x) = \frac{e^x}{G!}\frac{\mathrm{d}^G}{\mathrm{d}x^G}(e^{-x}x^G) = 0$. In addition, for each x_i, the weight w_i is given by $w_i = \frac{x_i}{(G+1)^2[L_{G+1}(x_i)]^2}$. For each value of G, the sets $\{x_i\}$ and $\{w_i\}$ can be pre-calculated as in [109]. As shown in [109], an accurate approximation to Q can be achieved by using $G = 15$. Therefore, using the transformation $x = v/\sigma_n^2$, I_n in (3.49) and subsequently $I(F_R)$ in (3.48) can be calculated effectively via (3.50).

Given that $I(F_R)$ can be easily evaluated for a given input F_R using Gauss-Laguerre quadrature formulas, a gradient descent-based method [41, 45, 46] can now be used to find the optimal input. Note that we need to maximize over the number of mass points P, the set of mass point locations and their probabilities under the average power constraint. This method has been shown to be more effective than the well-known Arimoto-Blahut algorithm [45]. Specifically, we can start by maximizing the mutual information over the set of one or two mass point distributions and their probabilities satisfying the input constraints using the vector optimization technique. This solution is, however, only considered as a local maximizer. It is because we do not know whether the optimization problem is convex over the space of the mass point locations and probabilities. To enhance the algorithm and to achieve the capacity-achieving solution F_0, for a given SNR, the obtained solution is then verified with the Kuhn-Tucker condition in (3.21), which is a necessary and sufficient condition for optimality. If this distribution satisfies the Kuhn-Tucker condition, it is globally optimal. On the other hand, if the Kuhn-Tucker condition does not hold, we will increase the number of mass points by one and repeat the optimizing process until the Kuhn-Tucker condition is satisfied. We observe via numerous numerical simulations that the convergence to the global solution happens very fast, especially at low and medium SNRs. As we demonstrate shortly, at low and medium SNRs, a capacity-achieving amplitude distribution consists of only one or two mass points. Note that as soon as the optimal distribution F_0 is obtained, it can be used in (3.48) to effectively calculate the channel capacity using the Gauss-Laguerre quadrature formulas.

3.4.2 Numerical Examples

In the following, we provide numerical results to confirm the theoretical derivations and calculations developed in the previous sections.

Capacity-Achieving Distributions

We first consider a popular Bernoulli-Gaussian impulsive noise channel where the total noise consists of two components, the thermal background noise and the impulsive noise. The noise parameters are selected as $\varepsilon_1 = 1-p = 0.6$, $\varepsilon_2 = p = 0.4$, and $\sigma_2^2 = 20\sigma_1^2$. Fig. 3.1 shows the magnitude and the probability of the optimal input as a function of signal-to-total-noise ratio $\mathrm{SNR} = \frac{P_d}{\mathbb{E}[|z|^2]}$.

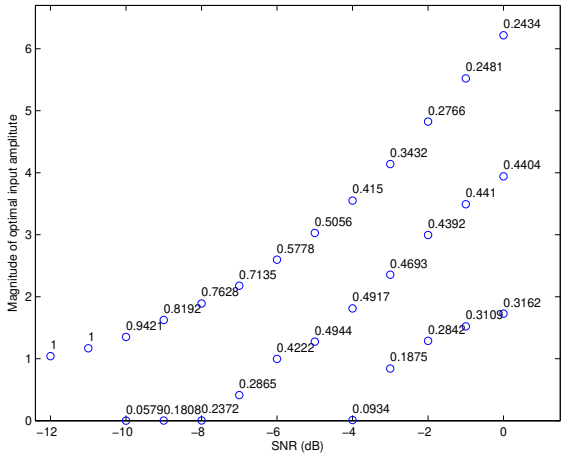

Fig. 3.1 The magnitudes and corresponding probabilities of optimal input amplitude for different values of SNRs.

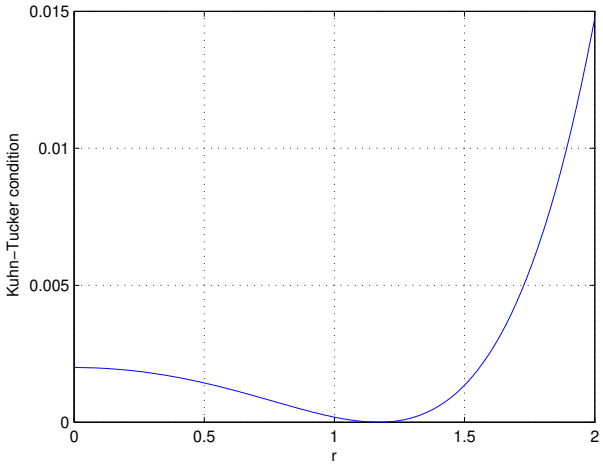

Fig. 3.2 The KTC at $\mathrm{SNR} = -11\,\mathrm{dB}$ for $f_R(r) = \delta(r - 1.1689)$, i.e., a single mass point at $r = 1.1689$.

We have verified that these distributions satisfy the KTC in (3.21). As an illustrative example, the LHS of the KTC in (3.21) is plotted in Figs. 3.2 and 3.3 as a function of r at $\mathrm{SNR} = -11\,\mathrm{dB}$ and $\mathrm{SNR} = -5\,\mathrm{dB}$, respectively.

It can be observed from Fig. 3.1 at low and medium SNRs, the optimal amplitude distribution contains only 1 or 2 mass points. We observe via extensive numerical results that at sufficiently low SNRs, the optimal distribution consists of a single mass point located at $\sqrt{P_d}$, and therefore the information is sent via uniform phase. As the SNR is increased, the number of mass points increases monotonically, e.g., there are 3 mass points when $\mathrm{SNR} = 0\,\mathrm{dB}$.

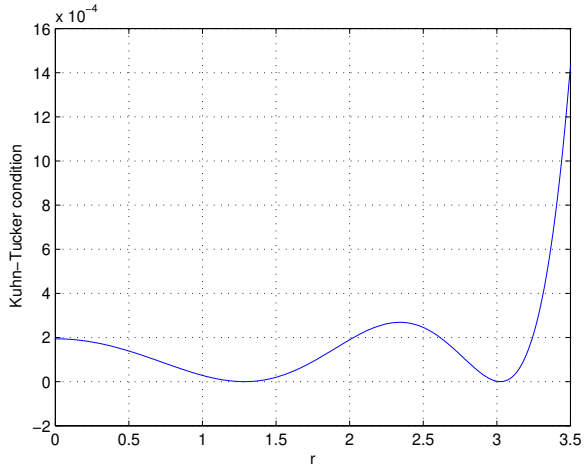

Fig. 3.3 The KTC at SNR $= -5\,\mathrm{dB}$ for $f_R(r) = 0.4944\,\delta(r - 1.2752) + 0.5056\,\delta(r - 3.0279)$, i.e., we have two mass points at $r = 1.2752$ and $r = 3.0279$, with the two corresponding probabilities 0.4944 and 0.5056, respectively.

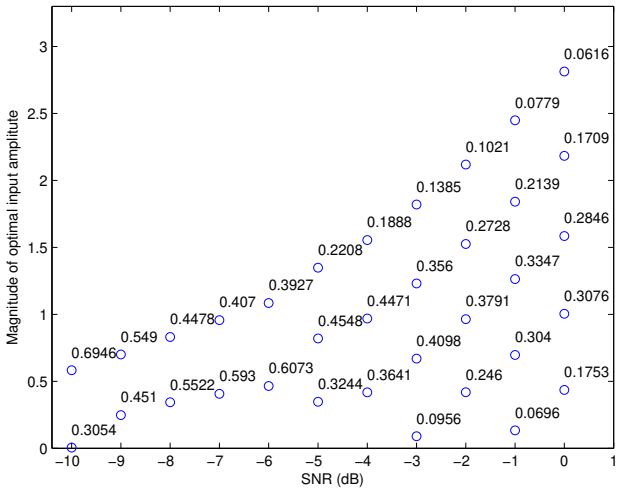

Fig. 3.4 The magnitudes and corresponding probabilities of optimal input amplitude of GM noise channel for different values of SNRs.

Similar results are also obtained for more general GM channels. Specifically, Fig. 3.4 presents the magnitudes and the corresponding probabilities of the optimal input as a function of SNR for a GM channel having three Gaussian components with $\varepsilon_1 = 0.8$, $\varepsilon_2 = 0.1$, $\varepsilon_3 = 0.1$, $\sigma_2^2 = 10\sigma_1^2$, and $\sigma_3^2 = 10\sigma_2^2$. It can be seen that the optimal amplitude distribution consists of only a few mass point at low SNRs. At higher SNRs, the number of mass points gradually increases, e.g., at SNR $= 0\,\mathrm{dB}$, the optimal input amplitude distribution consists of 5 mass points for the considered GM

channel.

Capacity and Information Rates

Given the above results, it is also interesting to compare the capacity achieved by the capacity-achieving input and the information rates obtained by using other types of inputs. Fig. 3.5 presents such results for the Bernoulli-Gaussian impulsive noise channel. Specifically, besides the capacity per channel use (in nats), shown in Fig. 3.5 are the information rates C_{GI} and C_{QPSK} obtained by using the Gaussian input and QPSK modulation scheme, respectively. As illustrated in Fig. 3.5, the information rate achieved by the Gaussian input approaches very close to the capacity in a wider range of SNRs, which is in agreement with earlier results that the Gaussian input has been shown to be asymptotically optimal at sufficiently low and high SNRs for this channel [55–57]. However, such a channel capacity can be effectively achieved via the optimal codebook determined in Fig. 3.1, while the Gaussian codebook is not viable in practice. It is also important to note that the plotted rates are in the units of nats per channel use, i.e., the rates are normalized. For a system with bandwidth B, the rates in bits per second will be B times the normalized rates we have in the plots. As such, the rate gap between C and C_{GI} can be more significant if we consider rates in bits/s, which is what the user experiences. The capacity-achieving discrete input outperforms QPSK input, especially when the SNR increases.

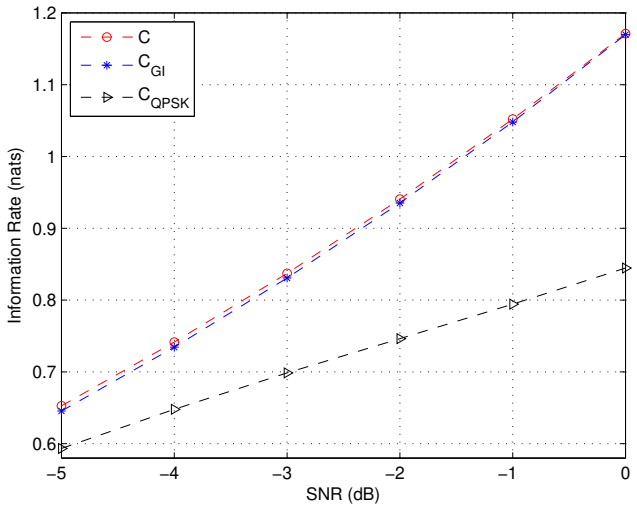

Fig. 3.5 The capacity and information rates per channel use achieved by different input distributions in the BG noise channel.

Finally, Fig. 3.6 shows the capacity and the information rates per channel use achieved by the

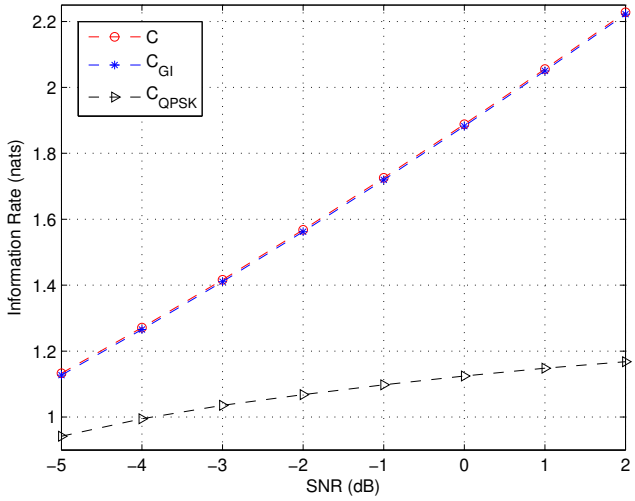

Fig. 3.6 The capacity and information rates per channel use achieved by different input distributions in the GM noise channel.

Gaussian distributed input and QPSK modulation scheme for the GM channel having 3 Gaussian components chosen before. It can be seen from Fig. 3.6 that the capacity and information rates follow the same trend for the considered GM channel.

3.5 Concluding Remarks

In this chapter, additive quadrature GM channels have been adopted to effectively model the channel of a single D2D link in underlaid D2D cellular networks. Given the GM model, we have characterized the capacity-achieving input distribution and computed the corresponding capacity of the GM channels under an average power constraint. To this end, we have first shown that the optimal input distribution is unique and it has a uniformly distributed phase that is independent of the amplitude. We have then further demonstrated that it is not possible to have an optimal input with an infinite number of mass points on any bounded interval. The result is developed using Bernstein's theorem to examine the completely monotonic condition of the input characteristic function. In addition, by applying a bounding technique on the KTC and using the Envelope Theorem, we have demonstrated that the optimal input amplitude distribution must have a finite number of mass points. We have also proposed a simple method to compute the discrete optimal input and the corresponding capacity. Numerical results are also provided to confirm the analysis.

Before processing further, we should note that, while we are able to demonstrate the discreteness of the optimal input amplitude at a given SNR, this result allows to construct a capacity-

achieving codebook for a single D2D channel under the effect of interference caused by discrete-constellation based cellular transmission. On the other hand, if conventional Gaussian distributed input is adopted at cellular transmitter, the optimal input of D2D channel is also Gaussian distributed. As it was demonstrated that the capacities of a D2D link (as an additive GM channel) obtained by discrete and Gaussian-distributed inputs are almost identical, the capacity expression derived via the Gaussian input can be effectively used to accurately estimate the channel capacity of the D2D link, under the consideration of both discrete and Gaussian distributed inputs at the cellular transmitter. From the channel capacity computation perspective, such a capacity expression is generally much simpler than that obtained by the discrete input (e.g., (3.48)), thus being more tractable to analyze the achievable cellular/D2D sum-rate at the network level in which the distance and channel distribution of multiple D2D links will be taken into consideration. It follows that, in subsequent chapters where multiple D2D links operates in a time-frequency slot currently used by cellular transmission, we shall assume that both cellular and D2D links use Gaussian inputs to transmit their signals.

3.6 Appendix

3.6.1 Useful Definitions

In this appendix, several definitions in optimization and probability theories are provided, which are useful for the development of the analytical framework in this chapter.

Definition 1. *- Weak* Convergence [108, Section 5.10] and [100, Section A.1] - Consider a probability measure F and a sequence of probability measures $\{F_n\}$. The sequence $\{F_n\}$ is said to converge weak* to F, which is denoted as $F_n \overset{w^*}{\to} F$, if*

$$\int_{\mathbb{R}} f(r) dF_n(r) \to \int_{\mathbb{R}} f(r) dF(r)$$

for every continuous bounded function f on $\mathbb{R}$ with $\mathbb{R}$ being the set of real numbers.

Definition 2. *- Weak Differentiability [41] - Let Ω be a convex space, f be a function from Ω into the real line $\mathbb{R}$, X_0 be an element of Ω, and θ is a real number in $[0, 1]$. Suppose there exists a mapping $f'_{X_0} : \Omega \to \mathbb{R}$ such that*

$$f'_{X_0}(X) \triangleq \lim_{\theta \to 0} \left\{ \frac{f[(1-\theta)X_0 + \theta X] - f[X_0]}{\theta} \right\},$$

for all X in Ω. Then f is said to be weakly differentiable in Ω at X_0, and f'_{X_0} is the weak derivative in Ω at X_0.

3.6.2 Integrable Bound on $|f_V(v;F_n)\ln f_V(v;F_n)|$

Since $I_0(x) \leq \exp(x)$ for all $x \geq 0$, we obtain the following upper bound on the kernel function

$$K_N(v,r) \leq \sum_{n=1}^{N} \frac{\varepsilon_n}{\sigma_n^2} = d, \quad \forall v, r \geq 0. \tag{3.51}$$

It then follows that

$$\begin{aligned} f_V(v;F_n) &= \int_0^\infty K_N(v;F_n)\mathrm{d}F_n(r) \\ &\leq d\int_0^\infty \mathrm{d}F_n(r) = d. \end{aligned} \tag{3.52}$$

Now, consider two possible cases for the values of d as follows:

1. $d \leq 1$. Using the inequality $|x\ln x| \leq 4x^{0.9}$ for $0 \leq x \leq 1$ [100, Lemma A.3], we have

$$\begin{aligned} |f_V(v;F_n)\ln f_V(v;F_n)| &\leq 4[f_V(v;F_n)]^{0.9} \\ &\leq 4d^{0.9}, \end{aligned} \tag{3.53}$$

   where $4d^{0.9}$ is an integrable upper bound.

2. $d > 1$. For this case, we first have the following proposition:

   Proposition 3. *For any $0 < x \leq d < \infty$, there always exists constants B and μ such that*

$$|x\ln x| \leq Bx^{1-\mu}. \tag{3.54}$$

   Proof. If $0 < x \leq 1$, we have $|x\ln x| \leq 4x^{0.9}$. Next, let us consider $x > 1$, the inequality (3.54) can be rewritten as $x^\mu \ln x \leq B$ for all $1 < x \leq d$. Therefore, for any $\mu \in (0,1)$ the choice $B = d^\mu \ln d$ is sufficient to achieve (3.54). □

   Therefore, we obtain $|f_V(v;F_n)\ln f_V(v;F_n)| \leq 4[f_V(v;F_n)]^{0.9} \leq 4d^{0.9}$ for $0 < f_V(v;F_n) \leq 1$ and $|f_V(v;F_n)\ln f_V(v;F_n)| \leq Bx^{1-\mu} \leq Bd^{1-\mu}$ for $1 < f_V(v;F_n) \leq d$. Note that both $4d^{0.9}$ and $Bd^{1-\mu}$ are integrable.

Given the above results, it can be seen that an integrable bound on $|f_V(v;F_n)\ln f_V(v;F_n)|$ can always be established.

3.6.3 Proof of Proposition 2

By Lagrangian Theorem [100, Theorem B.2], there exists $\lambda \geq 0$ such that

$$\begin{aligned} C &= \sup_{\substack{F_R\in\mathcal{F}\\ \mathbb{E}[r^2]\leq P_d}} I(F_R) \\ &= \sup_{F_R\in\mathcal{F}} \left[I(F_R) - \lambda\left(\int_0^\infty r^2 \mathrm{d}F_R - P_d\right)\right]. \end{aligned} \tag{3.55}$$

Given the definition of weak differentiability in Appendix 3.6.1 and following a similar analysis in [100], it can be verified that the function $I(\cdot)$ is weakly differentiable at $F_0 \in \mathcal{F}$ with weak derivative

$$I'_{F_0} = -\int_0^\infty f_V\left(v;F_R\right)\ln f_V\left(v;F_0\right)\mathrm{d}v - H_0. \tag{3.56}$$

Furthermore, from [100, Lemma B.1], the function $\phi(F_R) \triangleq \int_0^\infty r^2 \mathrm{d}F_R - P_d$ is weakly differentiable at F_0 with weak derivative

$$\phi'_{F_0}(F_R) = \phi(F_R) - \phi(F_0). \tag{3.57}$$

Therefore, the function $I(F_R) - \lambda\phi(F_R)$ is weakly differentiable at F_0. Then by [100, Theorem B.1], F_0 achieves the supremum in (3.55) iff

$$I'_{F_0}(F_R) - \lambda\phi'_{F_0}(F_R) \leq 0, \quad \forall F_R \in \mathcal{F}. \tag{3.58}$$

By the Lagrangian Theorem [100, Theorem B.2], we have

$$\lambda\left(\int_0^\infty r^2 \mathrm{d}F_0(r) - P_d\right) = 0. \tag{3.59}$$

Then substituting (3.56), (3.57) and (3.59) into (3.58) and using the fact that $f_V(v;F_R) = \int_0^\infty K_N(v,r)\mathrm{d}F_R$ yields

$$\int_0^\infty \left(\int_0^\infty K_N(v,r)\ln f_V(v;F_0)\mathrm{d}v\right)\mathrm{d}F_R(r) + \lambda\int_0^\infty \left(r^2 - P_d\right)\mathrm{d}F_R(r) + H_0 \geq 0, \quad \forall F_R \in \mathcal{F}. \tag{3.60}$$

Finally, using the same steps in [45, Appendix II, Theorem 4], Proposition 2 is proved.

3.6.4 Lower Bound on $f_V(v; F_R)$

We first have

$$\begin{aligned} f_V(v;F_R) &= \sum_{n=1}^{N} \frac{\varepsilon_n}{\sigma_n^2} \int_0^\infty e^{-\frac{2v+r^2}{2\sigma_n^2}} I_0\left(\frac{\sqrt{2v}r}{\sigma_n^2}\right) \mathrm{d}F_R(r) \\ &\geq \sum_{n=1}^{N} \frac{\varepsilon_n}{\sigma_n^2} e^{-\frac{v}{\sigma_n^2}} \int_0^\infty e^{-\frac{r^2}{2\sigma_n^2}} \mathrm{d}F_R(r) \\ &= \sum_{n=1}^{N} \frac{\varepsilon_n}{\sigma_n^2} e^{-\frac{v}{\sigma_n^2}} \mathbb{E}\left[\exp\left(-\frac{r^2}{2\sigma_n^2}\right)\right], \end{aligned} \tag{3.61}$$

with $d = \sum_{n=1}^{N} \frac{\varepsilon_n}{\sigma_n^2}$ and the inequality is obtained by using $I_0(x) \geq 1$ for all $x \geq 0$. Then by applying Jensen's inequality $\mathbb{E}[e^{-ax}] \geq e^{-a\mathbb{E}[x]}$ for all $a, x \geq 0$ and $\mathbb{E}[r^2] \leq P_d$ to (3.61), we have

$$\begin{aligned} f_V(v;F_R) &\geq \sum_{n=1}^{N} \frac{\varepsilon_n}{\sigma_n^2} e^{-\frac{v}{\sigma_n^2}} \cdot e^{-\frac{\mathbb{E}[r^2]}{2\sigma_n^2}} \\ &\geq \sum_{n=1}^{N} \frac{\varepsilon_n}{\sigma_n^2} e^{-\frac{2v+P_d}{2\sigma_n^2}}. \end{aligned} \tag{3.62}$$

Finally, since $\sigma_N = \min\{\sigma_n\}_{n=1}^N$, we obtain

$$\begin{aligned} f_V(v;F_R) &\geq \left(\sum_{n=1}^{N} \frac{\varepsilon_n}{\sigma_n^2}\right) \exp\left(-\frac{2v+P_d}{2\sigma_N^2}\right) \\ &= d \exp\left(-\frac{2v+P_d}{2\sigma_N^2}\right). \end{aligned} \tag{3.63}$$

3.6.5 Strict Concavity of $C(P_d)$

Let F_1 and F_2 be the capacity achieving input distributions at two different power constraints $\int_0^\infty r^2 \mathrm{d}F_1(r) \leq P_1$ and $\int_0^\infty r^2 \mathrm{d}F_2(r) \leq P_2$, respectively. Define $F_\theta = \theta F_1 + (1-\theta)F_2$ with $\theta \in (0,1)$. It can be verified that F_θ satisfies the average power constraint $\int_0^\infty r^2 \mathrm{d}F_\theta(r) \leq \theta P_1 +$

$(1-\theta)P_2$. From the strict concavity of the mutual information $I(\cdot)$, we have

$$\begin{aligned} C(\theta P_1 + (1-\theta)P_2) &\geq I(F_\theta) \\ &> \theta I(F_1) + (1-\theta) I(F_2) \\ &= \theta C(P_1) + (1-\theta) C(P_2), \end{aligned}$$

which implies that $C(\cdot)$ is strictly concave.

Chapter 4

Power Allocation and Performance Analysis of Full-Duplex D2D Cellular Networks in Single-Cell Setting [1]

4.1 Introduction

Chapter 3 focused on HD D2D transmission at the link level in which one D2D link and one cellular link share the time-frequency slot. This chapter extends the study of achievable D2D sum-rate into a network level to include multiple D2D transceivers, which simultaneously occupy the cellular resources. Additionally, we focus on FD D2D transmission in which the signals are transmitted and received simultaneously over the same frequency at the same time, as discussed in Chapter 1. Apart from the link level, the achievable rate analysis at network level takes into account the random mobility of both cellular and D2D users and the distribution of CSI. As a result, the GM interference models in Chapter 3, when adopted to such a network level analysis, is not tractable. For more tractable models, we assume the aggregate interference at cellular and D2D receivers shall be treated as noise, to which the well-known Gaussian models can be applied.

In existing research, only a few efforts have been dedicated to combine FD and D2D at the network level. For instance, in a recent work in [71], the authors evaluated the performance of overlaid D2D multi-cell networks where cellular and D2D links use FD transmission. However, the considered power allocation scheme and corresponding performance metrics in [71] ignored the effect of small-scale fading, which is the main factor that affects the network performance.

[1] Parts of Chapter 3 have been presented at the 2018 IEEE International Conference on Communications (ICC) [26] and published in the IEEE Transaction on Vehicular Technology [23].

The benefits of FD D2D transmission in multi-cell networks in terms of throughput improvement were also investigated in [72]. Under this line of work, a D2D receiver was assumed to be at a fixed distance from the D2D transmitter with its location following a Poison point process (PPP). Furthermore, to provide a basic quality of service for cellular users, the authors in [72] proposed a mechanism that prevents D2D transmission when D2D users are in the guard areas of the base-stations without considering power control algorithms.

In this chapter, we investigate the integration of FD in a practical underlaid cellular D2D network where multiple FD D2D users intend to communicate simultaneously by sharing the uplink spectrum with a cellular user as in [66]. While there exists other modes in which multiple cellular users can co-exist with D2D users, such as FD D2D systems co-existing with a multiple antenna equipped base-station [110, 111] and cellular networks being underlaid by relay-assisted D2D transmission [112–114], our considered model can be directly applied to a cellular network with multiple cellular users where each user is assigned a separate frequency-time slot. For completeness, we shall adopt both the centralized and on-off power control methods [66]. However, different from [66] that only studied a HD network with fixed distances of D2D links, we consider a more realistic model where D2D users' locations are modeled by homogeneous spatial PPPs, and the selection of D2D users is based on the maximum allowed distance for D2D communications to be enabled. In addition, we take into account the effect of residual self-interference due to FD transmission. Given the considered random network model, we are interested in studying the key performance metrics including the coverage probabilities of both cellular and D2D links and the sum-rate of D2D links. Our main contributions are provided as follows.

Our first focus is on the centralized power allocation mechanism. Toward this end, we first formulate an optimization problem that maximizes the D2D link sum-rate under the constraint on minimum target SINR at each user. Since the problem is nonconvex, a two-step approach is then proposed to approximately locate the global optimal point. Specifically, an admission control method is first employed to guarantee that a feasible solution always exists. Our main idea is to remove D2D links that potentially cause high interference to the BS until the constraints are satisfied. In the next step, we apply the difference of convex (DC) based method [115,116] to transform the highly nonconvex power allocation problem into a sequence of convex subproblems, which can be solved efficiently by a converged iterative algorithm with low complexity. The optimal solutions then allow us to calculate the coverage probabilities of both cellular and D2D links and the average sum-rate of D2D links. Our numerical results show that the proposed centralized power control achieves a very high coverage probability of cellular link while successfully supporting a large number of active D2D links. Furthermore, the centralized power control also significantly

improves the overall network throughput via optimizing the sum-rate of newly underlaid D2D links.

In the second part of the chapter, we consider a distributed power control where only the local CSI of direct link between respective D2D users is needed. By utilizing the tools of stochastic geometry, we derive closed-form approximations of coverage probabilities for both cellular and D2D links. In general, the coverage probabilities involve multiple integrals, since one needs to take the average over the distributions of transmit power, wireless fading, and link distances [66,68,71]. To overcome this issue, we apply Laplace transforms and novel approximations that accurately approximate the expected values of fractional and exponential functions of random variables to obtain the distribution functions of SINRs at the BS and D2D users in closed-form. By further taking the average over the distributions of cellular and D2D link distances, we then arrive at the closed-form approximations of cellular and D2D coverage probabilities. In addition, based on the approximation of D2D link coverage probability, an analytical expression for the D2D link sum-rate is also obtained, and it can be effectively calculated. Further, optimal transmit thresholds that maximize the D2D link sum-rate are derived when the on-off power control is used at D2D users. Our results show that the integration of FD in D2D transmission provides significant sum-rate improvement over the HD D2D counterpart.

The remainder of this chapter is organized as follows. In Section 4.2, we describe the system model of interest and define the key performance metrics. Section 4.3 focuses on the developments of these metrics under the centralized power control. Extension to the on-off power control allocation is considered in Section 4.4. Numerical results are given in Section 4.5 to confirm our analysis. Finally, Section 4.6 concludes the chapter.

4.2 System Model and Performance Metrics

4.2.1 System Model

We consider a single-cell network with one uplink cellular user (CU) C_0 and N pairs of cellular users who wish to establish D2D communications using FD mode via the same radio resource, i.e., there are N potential D2D user pairs $\{x_n, y_n\}_{n=1}^{N}$. In this model, the BS is centered at the origin, and its coverage region is a circular disk $\mathcal{C}$ with radius R. The cellular user is assumed to be located uniformly in this region. To model the potential D2D users, we assume the locations of D2D users $\{x_n\}_{n=1}^{N}$ and $\{y_n\}_{n=1}^{N}$ of corresponding potential D2D links are both distributed in the whole $\mathbb{R}^2$ plane according to two separate homogeneous PPPs with the same density λ. Note that this parameter is related to the average number of D2D links per cell, and it can be estimated at the

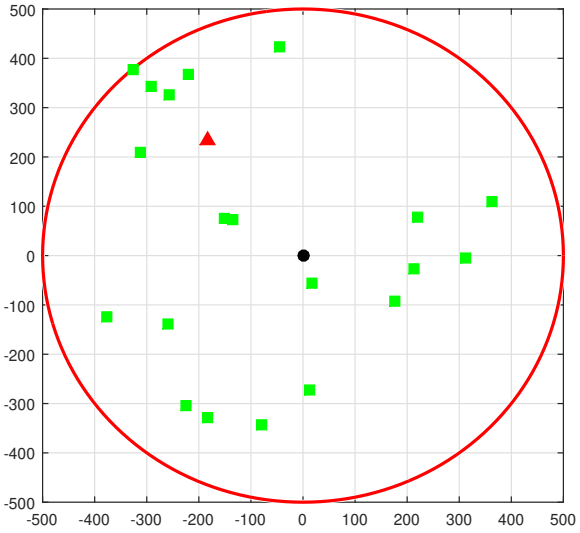

Fig. 4.1 A underlaid D2D cellular network with a single-cell setting (black circle: BS, red triangle: cellular user, green square: D2D transceiver)

base station in the process of D2D link establishment [20, 21, 66, 117]. This estimated parameter can then be sent to the D2D users using a control channel. Given that, the number of potential D2D links in $\mathcal{C}$ is a Poisson random variable (RV) with mean $\mathbb{E}[N] = \lambda\pi R^2$.

For each potential FD D2D pair x_n and y_n, $n = 1, \ldots, N$, the links from x_n to y_n and y_n to x_n are called the forward and reverse links, respectively. Furthermore, x_n and y_n are referred to as f-D2D and r-D2D users, respectively. Hereafter, the term D2D user is used to refer to both f-D2D and r-D2D users. In addition, we adopt a distance-based D2D mode selection from [68]. Specifically, a D2D mode can only be established if and only if (iff) the link distance r does not exceed a certain value $d_{\max}$. While a CSI-based criterion, such as signal power-based D2D mode selection, can potentially be used to further enhance the accuracy and performance, such a scenario requires cooperation/coordination between D2D users and the base station to acquire perfect CSI of the D2D link. As we shall explain shortly, for a simple distributed on-off power allocation considered in this chapter, only the local CSI of the direct link between respective D2D users is needed, and the distance-based D2D link construction is more feasible.

Given the maximum distance constraint $d_{\max}$, the operating f-D2D and r-D2D users both form PPPs with the same density $\lambda_d = \lambda\mathbb{P}(r \leq d_{\max})$ where $\mathbb{P}(r \leq d_{\max})$ denotes the probability that $r \leq d_{\max}$. Suppose that K out of N potential D2D links satisfy the maximum distance constraint, then the average number of operating D2D links is $\mathbb{E}[K] = \mathbb{P}(r \leq d_{\max})\lambda\pi R^2$. When these K pairs communicate in FD mode, there exists residual self-interference (SI) due to FD operation

that affects the D2D communications. Recently, several realistic SI models have been developed (please see [71, 118–123] and references therein). In this thesis, we adopt an SI model in which the residual interference is reflected in the self-interference-to-power-ratio (SIPR) β as in [71, 122].

For FD D2D links, $d_{k,k}$ denotes the link distance between a f-D2D user k and r-D2D user k. In addition, $d_{l,k}^{(f\to r)}$, $d_{l,k}^{(f\to f)}$, $d_{l,k}^{(r\to f)}$ and $d_{l,k}^{(r\to r)}$ are the distances between f-D2D user l and r-D2D user k, f-D2D user l and f-D2D user k, r-D2D user l and f-D2D user k and r-D2D user l and r-D2D user k, respectively, $l, k \in \{1, \ldots, K\}$. For the cellular users, we use $d_{0,0}$, $d_{0,k}^{(\mathrm{r})}$ and $d_{0,k}^{(\mathrm{f})}$ as the distances from CU to BS, r-D2D user k and f-D2D user k, respectively. Similarly, $d_{0,k}^{(\mathrm{r})}$ and $d_{0,k}^{(\mathrm{f})}$ are the distances from BS to r-D2D user k and f-D2D user k, respectively. Furthermore, $P_k^{(\mathrm{f})}$ and $P_k^{(\mathrm{r})}$ are the transmit powers at the f-D2D user k and r-D2D user k, respectively. For convenience, we use the notation $g_{l,k}^{(z)}$ with $z \in \{f, r, f \to r, f \to f, r \to f, r \to r\}$ and $l, k \in \{0, 1, \ldots, K\}$ to refer to the corresponding channel power gains. Specifically, $g_{k,k}^{(\mathrm{f})}$ and $g_{k,k}^{(\mathrm{r})}$ are the gains from f-D2D user k to its intended r-D2D k and vice versa. Also, $g_{l,k}^{(f\to r)}$, $g_{l,k}^{(f\to f)}$, $g_{l,k}^{(r\to f)}$ and $g_{l,k}^{(r\to r)}$ are the channel power gains from f-D2D user l to r-D2D user k, f-D2D l to f-D2D user k, r-D2D user l to f-D2D user k and r-D2D user l to r-D2D user k, respectively. For CU, $g_{0,0}$ is the channel power gain of the CU-BS link. In addition, $g_{0,k}^{(\mathrm{r})}$ and $g_{0,k}^{(\mathrm{f})}$ are the gains from CU to r-D2D user k and f-D2D user k. Similarly, $g_{0,k}^{(\mathrm{r})}$ and $g_{0,k}^{(\mathrm{f})}$ are the gains from r-D2D user k and f-D2D user k to BS. In this chapter, we consider Rayleigh fading where all channel power gains follow an exponential distribution with unit parameter.

As we can see from the above, in underlaid FD D2D cellular networks, D2D transmission is impaired by various sources of interference [124]. These include the aggregate interference caused by the cross-tier interference from cellular user, intra-tier interference between D2D users, and the residual SI due to FD operation. Meanwhile, cellular transmission suffers from the cross-tier interference from D2D links. These interferences need to be taken into account explicitly in developing key performance metrics, as we demonstrate in the following.

4.2.2 Power Allocation and Performance Metrics

Centralized and Distributed Power Allocation Schemes

In this work, we consider two power allocation schemes, namely the centralized and distributed power allocations as in [66], which are described in the following.

The centralized power allocation, which is implemented at the BS, aims to find the optimal transmit power $P_k^{(\mathrm{f})}$ and $P_k^{(\mathrm{r})}$ that maximize the sum-rate of D2D links while satisfying the minimum SINR at each forward/reverse-D2D link. Note that the centralized power control requires

the knowledge of global CSI at the BS. As we describe shortly, while D2D and cellular users do not fully coordinate as in [125–127], this information enables the cooperation between D2D and cellular users to enhance the D2D sum-rate. Certainly, it is not always practical to assume such a perfect knowledge of CSI and the nodes' locations given their dynamic and mobility. However, such an assumption has been considered in the literature as a useful and important criterion to compare different schemes [66]. It is because this consideration can serve as a system benchmark, e.g., the ultimate performance or a upper bound, to other systems with imperfect channel knowledge.

On the other hand, the distributed on-off power allocation requires no cooperation between D2D and cellular users, as it only needs the direct CSI of D2D link between the corresponding transmitter and receiver [66]. In particular, the power used at the D2D link k is P_d when the quality of forward/reverse link satisfies $g_{k,k}^{(z)} d_{k,k}^{-\alpha} \geq G_{\min}$, $z \in \{f, r\}$, with α being the path-loss exponent. Here, $G_{\min}$ is a nonnegative threshold that is known at all D2D users. Otherwise, the power is 0. Equivalently, transmit power at D2D users k can be expressed as

$$\{P_k^{(\mathrm{f})}, P_k^{(\mathrm{r})}\} = \begin{cases} P_d \text{ with probability } p_t\left(d_{k,k}\right), \\ 0 \quad \text{with probability } 1 - p_t\left(d_{k,k}\right), \end{cases} \tag{4.1}$$

where $p_t\left(d_{k,k}\right)$ denotes the transmit probability at D2D users, and it can be calculated as

$$p_t\left(d_{k,k}\right) = \mathbb{P}\left[g_{k,k}^{(z)} d_{k,k}^{-\alpha} \geq G_{\min}\right] = \exp(-G_{\min} d_{k,k}^{\alpha}), \tag{4.2}$$

where $z \in \{f, r\}$. Note that through out this work, as similar to [66], we assume that the transmit power at cellular user is fixed at P_c. Certainly, the power level used at the cellular user will have an impact on the overall performance. If a power mechanism can be performed at the cellular user, further improvement will be achieved. But this process requires a certain type of coordination among the D2D users, the BS, and the cellular user. As a result, there is a trade-off between performance and complexity that needs to be investigated, and it goes beyond the scope of this work.

Key Performance Metrics

For a given power allocation scheme with $P_k^{(\mathrm{f})}$ and $P_k^{(\mathrm{r})}$ at D2D users, we now define the corresponding network performance metrics, including coverage probabilities of cellular and D2D links and D2D link sum-rate. As such, the instantaneous SINRs at the r/f-D2D user k and the BS for the

cellular user-BS link can be expressed as follows:

$$\text{SINR}_k^{(\text{r})} = \frac{g_{k,k}^{(\text{f})} d_{k,k}^{-\alpha} P_k^{(\text{f})}}{g_{0,k}^{(\text{r})} \left(d_{0,k}^{(\text{r})}\right)^{-\alpha} P_c + I_k^{(f\to r)} + I_k^{(r\to r)} + \beta P_k^{(\text{r})} + \sigma_d^2},$$

$$\text{SINR}_k^{(\text{f})} = \frac{g_{k,k}^{(\text{r})} d_{k,k}^{-\alpha} P_k^{(\text{r})}}{g_{0,k}^{(\text{f})} \left(d_{0,k}^{(\text{f})}\right)^{-\alpha} P_c + I_k^{(f\to f)} + I_k^{(r\to f)} + \beta P_k^{(\text{f})} + \sigma_d^2},$$

$$\text{SINR}_0 = \frac{g_{0,0} d_{0,0}^{-\alpha} P_c}{I_0^{(\text{f})} + I_0^{(\text{r})} + \sigma_c^2},$$

where σ_d^2 and σ_d^2 are the noise powers at D2D and cellular receivers, repetitively. Furthermore, $I_k^{(z)}$ with $z \in \{f \to r, f \to f, r \to f, r \to r\}$ and $I_0^{(z)}$, $z \in \{f, r\}$, are the corresponding interference powers defined by

$$I_k^{(z)} = \sum_{l=1, l\neq k}^{K} g_{l,k}^{(z)} \left(d_{l,k}^{(z)}\right)^{-\alpha} P_l^{(\text{f})},\ z \in \{f \to r, f \to f\},$$

$$I_k^{(z)} = \sum_{l=1, l\neq k}^{K} g_{l,k}^{(z)} \left(d_{l,k}^{(z)}\right)^{-\alpha} P_l^{(\text{r})},\ z \in \{r \to f, r \to r\},$$

$$I_0^{(z)} = \sum_{k=1}^{K} g_{0,k}^{(z)} (d_{0,k}^{(z)})^{-\alpha} P_k^{(z)},\ z \in \{f, r\}.$$

The coverage probabilities for cellular user $p_c(\gamma_c)$ and D2D users $p_d(\gamma_d)$ are then defined as

$$p_c(\gamma_c) = \mathbb{E}\left[\mathbb{P}\left(\text{SINR}_0 \geq \gamma_c\right)\right], \tag{4.3}$$

$$p_d(\gamma_d) = \mathbb{E}\left[\mathbb{P}\left(\text{SINR}_k^{(z)} \geq \gamma_d\right)\right],\ z \in \{f, r\}. \tag{4.4}$$

Here, γ_c and γ_d represent the target SINR at cellular/D2D link, respectively, and $\mathbb{E}[\cdot]$ denotes the expectation over locations of cellular and D2D users. In addition, $\mathbb{P}(\text{SINR}_0 \geq \gamma_c)$ and $\mathbb{P}(\text{SINR}_k^{(z)} \geq \gamma_d)$, $z \in \{f, r\}$, are the complementary cumulative distribution functions (CCDFs) conditioned on the locations of cellular user, f-D2D user k and r-D2D user k, respectively. Note that for centralized power control, the coverage probability can be calculated as the average fraction of cellular/D2D links that can achieve a target SINR over many network realizations [128]. It is because in this case, the locations of cellular and D2D users are different in each network realization. On the other hand, for distributed power control, the calculation of coverage probabil-

ities involves the estimation of CCDFs of SINR_0, $\text{SINR}_k^{(\text{f})}$, and $\text{SINR}_k^{(\text{r})}$ and the expectations over distance distributions of cellular and D2D links.

Assuming that Gaussian signaling schemes are used at all the users, the interference is also Gaussian distributed. Thus, the ergodic sum-rate of D2D links can be written as

$$\overline{R}_d = \mathbb{E}\left[\sum_{k=1}^{K}\left(\log_2\left(1+\text{SINR}_k^{(\text{r})}\right)+\log_2\left(1+\text{SINR}_k^{(\text{f})}\right)\right)\right],$$

where the expectation is taken over the network realizations and the SINR distribution for centralized and distributed power control schemes, respectively. We should emphasize that in this work, it is of our interest to only study the sum-rate of D2D users instead of the total sum-rate of D2D and cellular users. The reason for that is because we consider a single cellular user in the network. As we will describe shortly, in the case of the centralized power algorithm, this cellular user is always guaranteed a minimum quality of service. For the distributed power control, we assume a fixed power at the cellular user, and focus mainly on an effective power control method for D2D users and their performance.

Before closing this section, we should also note that while K potential D2D links are established, a pair of specific D2D users is not necessarily forced to make a D2D communications right away. Depending on whether that D2D communications is helpful to enhance the spectral efficiency/coverage probability and/or to protect the preexisting cellular link, it might be removed from the D2D mode. This process is reflected in detail in the solutions of the two proposed power allocation schemes that shall be studied in the subsequent parts of the chapter.

4.3 Centralized Power Control

In this section, we shall develop a centralized power control algorithm that maximizes the sum-rate of D2D links while satisfying the target SINR constraints at both cellular user-BS link and D2D users. Note that different with the *ad hoc* network, in D2D cellular system, the centralized power control is performed at the central controller [66], where the global CSI and locations of both cellular and D2D users are available at the BS. For a given network realization, the achievable rate of D2D link k is given as follows:

$$R_k = \log_2\left(1+\text{SINR}_k^{(\text{f})}\right)+\log_2\left(1+\text{SINR}_k^{(\text{r})}\right). \tag{4.5}$$

For simplicity, we assume that D2D users have the same minimum target SINR γ_d, while the minimum quality service of the cellular user is reflected in γ_c, the minimum target SINR for the cellular user-BS link. The sum-rate optimization problem is then formulated as

$$\max_{\{P_k^{(\mathrm{r})},P_k^{(\mathrm{f})}\}_{k=1}^K} \quad R_d = \sum_{k=1}^K R_k \tag{4.6a}$$

$$\text{s.t.} \quad \mathrm{SINR}_k^{(z)} \geq \gamma_d,\ z \in \{f,r\}, k = 1,\ldots,K, \tag{4.6b}$$

$$\mathrm{SINR}_0 \geq \gamma_c, \tag{4.6c}$$

$$0 \leq P_k^{(\mathrm{f})}, P_k^{(\mathrm{r})} \leq P_d,\ k = 1,\ldots,K. \tag{4.6d}$$

Before solving (4.6), the following lemma first establishes necessary conditions to ensure that the feasible solution set of (4.6) is always nonempty.

Lemma 4. *The feasible solution of optimization problem (4.6) exists if the following two conditions are satisfied*

$$\frac{g_{0,0}d_{0,0}^{-\alpha}}{\sum\limits_{k=1}^K\left[g_{0,k}^{(f)}\left(d_{0,k}^{(f)}\right)^{-\alpha}+g_{0,k}^{(r)}\left(d_{0,k}^{(r)}\right)^{-\alpha}\right]+\sigma_c^2} \geq \frac{\gamma_c P_d}{P_c}, \tag{4.7a}$$

$$\textit{and} \quad \lambda_{\max} < 1. \tag{4.7b}$$

Here, $\lambda_{\max}$ is the maximum positive real eigenvalue of a $2K \times 2K$ matrix $\mathbf{F}$ defined as

$$\mathbf{F}_{l,k} = \begin{cases} 0, & k = l,\ k = 1,\ldots,2K, \\ \beta, & l = k+K,\ k = 1,\ldots,K, \\ \dfrac{g_{l,k}^{(f\to r)}\left(d_{l,k}^{(f\to r)}\right)^{-\alpha}}{g_{k,k}^{(r)}d_{k,k}^{-\alpha}}, & k \neq l;\ l,k = 1,\ldots,K, \\ \dfrac{g_{l,k-K}^{(r\to r)}\left(d_{l,k-K}^{(r\to r)}\right)^{-\alpha}}{g_{k,k}^{(r)}d_{k,k}^{-\alpha}}, & k = 1,\ldots,K;\ l = K+1,\ldots,2K, \\ \beta, & l = k-K,\ k = K+1,\ldots,2K, \\ \dfrac{g_{k-l,k}^{(f\to f)}\left(d_{k-l,k}^{(f\to f)}\right)^{-\alpha}}{g_{k-K,k-K}^{(f)}d_{k-K,k-K}^{-\alpha}}, & k = K+1,\ldots,2K, \\ & l = 1,\ldots,K, \\ \dfrac{g_{k-l,k-K}^{(f\to r)}\left(d_{k-l,k-K}^{(f\to r)}\right)^{-\alpha}}{g_{k-K,k-K}^{(f)}d_{k-K,k-K}^{-\alpha}}, & l,k = K+1,\ldots,2K; k \neq l. \end{cases} \tag{4.8}$$

Note that in (4.8), $g_{k,k}^{(z)}\left(d_{k,k}^{(z)}\right)^{-\alpha} = 0$ for $k = 1,\ldots,K$ and $z \in \{f \to f, r \to r\}$.

Proof. Condition (4.7a) comes directly from the constraints (4.6c) and (4.6d). Condition (4.7b) can be obtained by utilizing the well-known Perron-Frobenius theorem [129] and constraint (4.6b). Specifically, we first rewrite (4.6b in a vector form by

$$(\mathbf{I}-\mathbf{F})\,\mathbf{p} \geq \mathbf{b}^{\mathsf{T}}, \tag{4.9}$$

where $\mathbf{p} = \left[P_1^{(\mathrm{f})},\ldots,P_K^{(\mathrm{f})},P_1^{(\mathrm{r})},\ldots,P_K^{(\mathrm{r})}\right]^{\mathsf{T}}$ denotes the nonnegative power vector and $\mathbf{I}$ is the identity matrix. Further, the target SINR vector $\mathbf{b}$ is defined as

$$\mathbf{b}_k = \begin{cases} \dfrac{\gamma_d\left(\sigma^2+g_{0,k}^{(\mathrm{r})}\left(d_{0,k}^{(\mathrm{r})}\right)^{-\alpha}P_c\right)}{g_{k,k}^{(\mathrm{r})}d_{k,k}^{-\alpha}}, & k=1,\ldots,K, \\ \dfrac{\gamma_d\left(\sigma^2+g_{k-0,k}^{(\mathrm{f})}\left(d_{k-0,k}^{(\mathrm{f})}\right)^{-\alpha}P_c\right)}{g_{k-K,k-K}^{(\mathrm{f})}d_{k-K,k-K}^{-\alpha}}, & k=K+1,\ldots,2K. \end{cases}$$

The matrix $\mathbf{F}$ defined in (4.8) is irreducible because all D2D users are transmitting and interfering each others. From (4.9) and the fact that $\mathbf{b} > 0$, we obtain the inequality $(\mathbf{I}-\mathbf{F})\mathbf{p} > 0$, which is equivalent to $\mathbf{F}\mathbf{p} < \mathbf{p}$. Condition (4.7b) then can be achieved by Perron-Frobenius theorem [129]. □

Because the number of D2D links and corresponding locations of D2D users are randomly distributed in each network realization, there is a possibility that the conditions (4.7a) and (4.7b) are not met, which results in an empty feasible set of the optimization problem in (4.6). To overcome this issue, we can first implement an admission control method to ensure that the solution of (4.6) is feasible by selecting a subset of active D2D links. In particular, the BS first checks the two conditions (4.7a) and (4.7b). If they are not satisfied, BS removes the D2D link that potentially causes highest interference to it. To do so, BS simply drops the D2D link k that results in the maximum value of $g_{0,k}^{(\mathrm{r})}\left(d_{0,k}^{(\mathrm{r})}\right)^{-\alpha}+g_{0,k}^{(\mathrm{f})}\left(d_{0,k}^{(\mathrm{f})}\right)^{-\alpha}$, $k=1,\ldots,K$, to protect the preexisting cellular link. BS will continue to remove D2D links until the conditions (4.7a) and (4.7b) are met. Note that the problem to select the subset of D2D links satisfying the conditions (4.7a) and (4.7b) can be solved by the well-known brute-force algorithm with the required number of condition computations being $\sum_{k=1}^{K}\binom{N}{k}$. As such, the computational complexity of the conventional brute-force algorithm grows exponentially with the number of D2D links K. Meanwhile, the computational complexity of proposed admission control scheme only increases linearly with K, which is more efficient.

Given the above admission control mechanism, we are now ready to address the optimal solution of (4.6). Because the objective function (4.6a) is nonconcave, (4.6) is a nonconvex optimization problem. As such, it is not possible to directly obtain the globally optimal solution. As

an alternative, our idea is to apply the difference of convex (DC)-based approach [115, 116] to transform (4.6) into a sequence of convex problems where each problem can be solved effectively by standard convex optimization techniques. The idea of this DC-based approach is to exploit the DC structure of the objective function so that we can develop a sequential convex programming algorithm that approximately locates the globally optimal point with a low complexity. Such an approach represents the objective function f of the nonconvex optimization problem as a difference of two convex functions u and v, i.e., $f = u - v$, and the linear approximation to v can then be applied. The function f is then approximated by a convex function and the corresponding optimization problem becomes convex. As a result, the global optimal solution can be achieved by solving a sequence of convex optimization problems. The detailed procedure is given as follows.

We first rewrite (4.6) as the following minimization problem

$$\begin{aligned} \min_{\mathbf{p}} \quad & -R_d \\ \text{s.t.} \quad & \text{(4.6b) - (4.6d).} \end{aligned} \tag{4.10}$$

Here, the R_d can be expressed in a DC form as

$$-R_d(\mathbf{p}) = U(\mathbf{p}) - V(\mathbf{p}), \tag{4.11}$$

where

$$\begin{aligned} U(\mathbf{p}) = & -\frac{1}{\ln(2)} \sum_{k=1}^{K} \ln\left(g_{k,k}^{(\mathrm{f})} d_{k,k}^{-\alpha} P_k^{(\mathrm{f})} + g_{0,k}^{(\mathrm{r})} \left(d_{0,k}^{(\mathrm{r})} \right)^{-\alpha} P_c + I_k^{(f\to r)} + I_k^{(r\to r)} + \beta P_k^{(\mathrm{r})} + \sigma_d^2 \right) \\ & -\frac{1}{\ln(2)} \sum_{k=1}^{K} \ln\left(g_{k,k}^{(\mathrm{r})} d_{k,k}^{-\alpha} P_k^{(\mathrm{r})} + g_{0,k}^{(\mathrm{f})} \left(d_{0,k}^{(\mathrm{f})} \right)^{-\alpha} P_c + I_k^{(f\to f)} + I_k^{(r\to f)} + \beta P_k^{(\mathrm{f})} + \sigma_d^2 \right), \\ V(\mathbf{p}) = & -\frac{1}{\ln(2)} \sum_{k=1}^{K} \ln\left(g_{0,k}^{(\mathrm{r})} \left(d_{0,k}^{(\mathrm{r})} \right)^{-\alpha} P_c + I_k^{(f\to r)} + I_k^{(r\to r)} + \beta P_k^{(\mathrm{r})} + \sigma_d^2 \right) \\ & -\frac{1}{\ln(2)} \sum_{k=1}^{K} \ln\left(g_{0,k}^{(\mathrm{f})} \left(d_{0,k}^{(\mathrm{f})} \right)^{-\alpha} P_c + I_k^{(f\to f)} + I_k^{(r\to f)} + \beta P_k^{(\mathrm{f})} + \sigma_d^2 \right). \end{aligned}$$

The functions U and V are convex. Now, we approximate $-R_d$ as $-R_d \approx U(\mathbf{p}) - V'(\mathbf{p})$ where $V'(\cdot)$ is the first-order Taylor's series of V at $\mathbf{p} = \tilde{\mathbf{p}}$. Specifically, we have

$$V(\mathbf{p}) \approx V'(\mathbf{p}) = V(\tilde{\mathbf{p}}) + \langle \nabla V(\tilde{\mathbf{p}}), \mathbf{p} - \tilde{\mathbf{p}} \rangle \tag{4.12}$$

with $\nabla V(\cdot)$ being the gradient of V, and it is calculated as

$$\nabla V\left(P_l^{(z)}\right) = -\frac{1}{\ln(2)}\sum_{k=1}^{K}\frac{\mathbf{e}_l^{(z)}(k)}{g_{0,k}^{(\mathrm{r})}\left(d_{0,k}^{(\mathrm{r})}\right)^{-\alpha}P_c + I_k^{(f\to r)} + I_k^{(r\to r)} + \beta P_k^{(\mathrm{r})} + \sigma_d^2} - \frac{1}{\ln(2)}\sum_{k=1}^{K}\frac{\mathbf{v}_l^{(z)}(k)}{g_{0,k}^{(\mathrm{f})}\left(d_{0,k}^{(\mathrm{f})}\right)^{-\alpha}P_c + I_k^{(f\to f)} + I_k^{(r\to f)} + \beta P_k^{(\mathrm{f})} + \sigma_d^2},$$

for $z \in \{f, r\}$. The vectors $\mathbf{e}_l^{(z)}, \mathbf{v}_l^{(z)} \in \mathbb{R}^K$ are defined by

$$\mathbf{e}_l^{(\mathrm{f})}(k) = \begin{cases} 0 & \text{for } k = l, \\ g_{l,k}^{(f\to r)}\left(d_{l,k}^{(f\to r)}\right)^{-\alpha} & \text{for } l \neq k, \end{cases}$$

$$\mathbf{v}_l^{(\mathrm{f})}(k) = \begin{cases} \beta & \text{for } k = l, \\ g_{l,k}^{(f\to f)}\left(d_{l,k}^{(f\to f)}\right)^{-\alpha} & \text{for } l \neq k, \end{cases}$$

$$\mathbf{e}_l^{(\mathrm{r})}(k) = \begin{cases} \beta & \text{for } k = l, \\ g_{l,k}^{(r\to r)}\left(d_{l,k}^{(r\to r)}\right)^{-\alpha} & \text{for } l \neq k, \end{cases}$$

$$\mathbf{v}_l^{(\mathrm{r})}(k) = \begin{cases} 0 & \text{for } k = l, \\ g_{l,k}^{(r\to f)}\left(d_{l,k}^{(r\to f)}\right)^{-\alpha} & \text{for } l \neq k. \end{cases}$$

When $\tilde{\mathbf{p}}$ is close to $\mathbf{p}$, the approximation (4.12) is tight. Further, the function $U(\mathbf{p}) - V'(\mathbf{p})$ is convex since $V'(\mathbf{p})$ is linear. Therefore, the nonconvex optimization problem (4.10) can be approximated effectively by the following convex optimization problem

$$\begin{aligned} \min_{\mathbf{p}} \quad & U(\mathbf{p}) - V'(\mathbf{p}) \\ \text{s.t.} \quad & \text{(4.6b) - (4.6d).} \end{aligned} \tag{4.13}$$

Given (4.13), an iterative algorithm can be developed to solve (4.6) as follows. The algorithm generates a sequence $\mathbf{p}^{(n)}$ to improve the optimal solutions. From the first feasible solution $\mathbf{p}^{(0)}$ that is randomly generated, at $n-$th iteration, we obtain an optimal solution of the following convex

program

$$\begin{aligned} \min_{\mathbf{p}} \quad & U(\mathbf{p}) - V\left(\mathbf{p}^{(n)}\right) - \left\langle \nabla V\left(\mathbf{p}^{(n)}\right), \mathbf{p} - \mathbf{p}^{(n)} \right\rangle \\ \text{s.t.} \quad & \text{(4.6b) - (4.6d)}, \end{aligned} \tag{4.14}$$

which can be solved effectively by using standard convex programming tools. Because the constraint set (4.6b) - (4.6d) is compact, the sequence $\{\mathbf{p}^{(n)}\}$ always converges by Cauchy theorem [115]. We can set to stop the iterative algorithm when there is no rate improvement, i.e., $\left|R_d(\mathbf{p}^{(n)}) - R_d(\mathbf{p}^{(n-1)})\right| \leq \epsilon$, with ϵ being a chosen threshold. Following the same analysis as in [115, 116], it can be verified that the complexity of iterative power allocation algorithm is $\mathcal{O}(K^3)$. For convenience, the centralized power control algorithm including admission control method and iterative power allocation algorithm is summarized in Algorithm 1.

Algorithm 1 Iterative DC-based algorithm

1: Set the initial square matrix $\mathbf{F}^K$, assuming K D2D links are transmitting.
2: **repeat**
3: Test the condition (4.7a) and (4.7b).
4: Remove the D2D link k such that $k = \arg\max_{k=1,\ldots,K} g_{0,k}^{(\mathrm{r})} \left(d_{0,k}^{(\mathrm{r})}\right)^{-\alpha} + g_{0,k}^{(\mathrm{f})} (g_{0,k}^{(\mathrm{f})})^{-\alpha}$.
5: Assign $K = K - 1$ and update $\mathbf{F}^K$.
6: **until** (4.7a) and (4.7b) are satisfied
7: Set $n = 0$, randomly initialize $\mathbf{p}^{(0)}$ and choose ϵ.
8: **repeat**
9: Calculate $R_d(\mathbf{p}^{(n)}) = V\left(\mathbf{p}^{(n)}\right) - U(\mathbf{p}^{(n)})$ and update $U(\mathbf{p}) - V\left(\mathbf{p}^{(n)}\right) - \left\langle \nabla V\left(\mathbf{p}^{(n)}\right), \mathbf{p} - \mathbf{p}^{(n)} \right\rangle$.
10: Solve the convex program (4.13) to obtain the solution $\mathbf{p}^\star$ and calculate $-R_d(\mathbf{p}^\star) = U(\mathbf{p}^\star) - V(\mathbf{p}^\star)$.
11: Assign $n = n + 1$ and $\mathbf{p}^{(n)} = \mathbf{p}^\star$.
12: **until** R_d converges, i.e., $\left|R_d(\mathbf{p}^{(n)}) - R_d(\mathbf{p}^\star)\right| \leq \epsilon$

Finally, given the optimal solutions of centralized power control, the coverage probabilities of cellular/D2D links can be obtained by averaging the fraction of cellular/D2D links that achieve the corresponding target SINRs over time. In addition, the average sum-rate of D2D links can also be obtained in a similar manner.

4.4 Distributed Power Control

In this section, we turn our attention to the distributed power control provided in (4.1). The focus is on the calculation of $p_c(\cdot)$ and $p_d(\cdot)$. In the following, we will start with the coverage probability for cellular user $p_c(\cdot)$ before extending the results to the coverage probability for D2D users $p_d(\cdot)$. Finally, an effective way to compute the D2D link sum-rate $\overline{R}_d$ is given. Based on this analytical result, the optimal threshold $G_{\min}$ maximizing $\overline{R}_d$ is also derived.

4.4.1 Cellular Link Coverage Probability

The first step to calculate $p_c(\cdot)$ is to evaluate the distribution of SINR_0. It is easy to see that the probability density function (PDF) of the distance $d_{0,0}$ from CU to BS is

$$f_{d_{0,0}}(r) = \begin{cases} \frac{2r}{R^2}, & \text{if } 0 \le r \le R \\ 0, & \text{otherwise.} \end{cases} \tag{4.15}$$

Thus, for a fixed $d_{0,0} = r$, we obtain

$$\begin{aligned} \mathbb{P}\left(\text{SINR}_0 \ge \gamma_c\right) &= \mathbb{P}\left(\frac{g_{0,0} r^{-\alpha} P_c}{I_0^{(\text{f})} + I_0^{(\text{r})} + \sigma_c^2} \ge \gamma_c\right) \\ &= \mathbb{E}\left[\exp\left(-r^{\alpha} P_c^{-1} \gamma_c \left(I_0^{(\text{f})} + I_0^{(\text{r})} + \sigma_c^2\right)\right)\right], \end{aligned} \tag{4.16}$$

where the above expectation is taken over the distributions of $g_{0,k}^{(z)}, d_{0,k}^{(z)}$, and $P_k^{(z)}$, $z \in \{f, r\}$. For convenience, we rewrite (4.16) as the product of two expectations as follows:

$$\begin{aligned} \mathbb{P}\left(\text{SINR}_0 \ge \gamma_c\right) &= \exp\left(-r^{-\alpha} P_c^{-1} \gamma_c \sigma_c^2\right) \mathbb{E}\left[\exp\left(-r^{-\alpha} P_c^{-1} \gamma_c I_0^{(\text{f})}\right)\right] \mathbb{E}\left[\exp\left(-r^{-\alpha} P_c^{-1} \gamma_c I_0^{(\text{r})}\right)\right] \\ &= \exp\left(-r^{-\alpha} P_c^{-1} \gamma_c \sigma_c^2\right) \mathbb{E}\left[\left(-r^{-\alpha} P_c^{-1} \gamma_c \sum_{k=1}^{K} g_{0,k}^{(\text{f})} \left(d_{0,k}^{(\text{f})}\right)^{-\alpha} P_k^{(\text{f})}\right)\right] \\ &\times \mathbb{E}\left[\exp\left(-r^{-\alpha} P_c^{-1} \gamma_c \sum_{k=1}^{K} g_{0,k}^{(\text{r})} \left(d_{0,k}^{(\text{f})}\right)^{-\alpha} P_k^{(\text{r})}\right)\right]. \end{aligned} \tag{4.17}$$

To simplify (4.17) further, we apply the following Laplace transform [66]

$$\begin{aligned}\mathcal{L}_{\Phi}(s) &= \mathbb{E}_{g_{0,k}^{(z)},d_{0,k}^{(z)},P_k^{(z)}}\left[\exp\left(-s\sum_{k=1}^{K} g_{0,k}^{(z)}\left(d_{0,k}^{(z)}\right)^{-\alpha} P_k^{(z)}\right)\right] \\ &= \left(-\frac{\pi}{\mathrm{sinc}(\frac{2}{\alpha})}\lambda_d s^{-\frac{2}{\alpha}}\mathbb{E}\left[(P_k^{(z)})^{-\frac{2}{\alpha}}\right]\right), \end{aligned} \tag{4.18}$$

where $z \in \{f, r\}$ and $\mathrm{sinc}(y) = \sin(\pi y)/(\pi y)$, and λ_d is the density of operating D2D links. It then follows that

$$\mathbb{P}\left(\mathrm{SINR}_0 \geq \gamma_c\right) = \exp\left(-r^{\alpha}P_c^{-1}\gamma_c\sigma_c^2 - \frac{\pi\lambda_d\gamma_c^{\frac{2}{\alpha}}}{\mathrm{sinc}(\frac{2}{\alpha})}r^2 P_c^{-\frac{2}{\alpha}}\left(\mathbb{E}\left[(P_k^{(\mathrm{f})})^{-\frac{2}{\alpha}}\right] + \mathbb{E}\left[(P_k^{(\mathrm{r})})^{-\frac{2}{\alpha}}\right]\right)\right). \tag{4.19}$$

To calculate λ_d, we note that $\lambda_d = \mathbb{P}\left(r \leq d_{\max}\right)\pi\lambda R^2$, where $\mathbb{P}\left(r \leq d_{\max}\right)$ is the probability that the distance between two nodes placed randomly within a circle with radius R not exceeding $d_{\max}$. This probability is given in the following lemma.

Lemma 5. *Denoting $v = r_{\max}^2/(2R)$, $\mathbb{P}\left(r \leq d_{\max}\right)$ can be calculated in closed-form as follows:*

$$\begin{aligned}\mathbb{P}\left(r \leq d_{\max}\right) = &-\frac{2}{\pi}\left[\sqrt{1-v^2}\left(2v^3 - v\right)\arcsin\left(v\right)\right] \\ &+ \frac{4}{\pi}\left[-v\sqrt{1-v^2} + 2v^2\arccos\left(v\right) + \arcsin\left(v\right)\right]. \end{aligned} \tag{4.20}$$

Proof. See Appendix 4.7.1. □

Furthermore, in (4.19), $\mathbb{E}\left[(P_k^{(\mathrm{r})})^{-\frac{2}{\alpha}}\right]$ and $\mathbb{E}\left[(P_k^{(\mathrm{f})})^{-\frac{2}{\alpha}}\right]$ can be approximated as $\overline{p}_t P_d^{-\frac{2}{\alpha}}$. Here, $\overline{p}_t$ is the average transmit probability, which can be effectively computed as

$$\overline{p}_t = \mathbb{E}_{d_{k,k}}\left[p_t\left(d_{k,k}\right)\right] = \int_0^{d_{\max}} \frac{p_t(r)f_d(r)}{\mathbb{P}\left(r \leq d_{\max}\right)}\mathrm{d}r. \tag{4.21}$$

As a result, we obtain

$$\mathbb{P}\left(\mathrm{SINR}_0 \geq \gamma_c\right) = \exp\left(-r^{-\alpha}P_c^{-1}\gamma_c\sigma_c^2 - \frac{2\pi\lambda_d\gamma_c^{\frac{2}{\alpha}}}{\mathrm{sinc}(\frac{2}{\alpha})}r^2\left(\frac{P_d}{P_c}\right)^{\frac{2}{\alpha}}\overline{p}_t\right).$$

Given that, the coverage probability of cellular link can be computed by taking average of $\mathbb{P}\left(\mathrm{SINR}_0 \geq \gamma_c\right)$

over the cellular link distance distribution as follows:

$$p_c(\gamma_c) = \int_0^R \exp\left(-\frac{r^{-\alpha}\gamma_c\sigma_c^2}{P_c}\right) \exp\left(-\frac{2\pi\lambda_d\gamma_c^{\frac{2}{\alpha}}}{\text{sinc}(\frac{2}{\alpha})} r^2 \left(\frac{P_d}{P_c}\right)^{\frac{2}{\alpha}} \overline{p}_t\right) \frac{2r}{R^2}\mathrm{d}r. \tag{4.22}$$

Since $-r^{-\alpha}\gamma_c\sigma_c^2/P_c$ is small, we can approximate $\exp(-r^{-\alpha}\gamma_c\sigma_c^2/P_c)$ as $1 - r^{-\alpha}\gamma_c\sigma_c^2/P_c$. $p_c(\gamma_c)$ can then be effectively calculated in closed-form as

$$\begin{aligned} p_c(\gamma_c) &\approx \int_0^R \left(1 - \frac{r^{\alpha}\gamma_c\sigma_c^2}{P_c}\right) \exp\left(-\frac{2\pi\lambda_d\gamma_c^{\frac{2}{\alpha}}}{\text{sinc}(\frac{2}{\alpha})} r^2 \left(\frac{P_d}{P_c}\right)^{\frac{2}{\alpha}} \overline{p}_t\right) \frac{2r}{R^2}\mathrm{d}r \\ &= \frac{1}{R^2}\int_0^{R^2} \left(1 - x^{\alpha/2}P_c^{-1}\gamma_c\sigma_c^2\right) \exp\left(-\frac{2\pi\lambda_d\gamma_c^{\frac{2}{\alpha}}}{\text{sinc}(\frac{2}{\alpha})} x \left(\frac{P_d}{P_c}\right)^{\frac{2}{\alpha}} \overline{p}_t\right) \mathrm{d}x \\ &\overset{(a)}{=} \frac{\text{sinc}(\frac{2}{\alpha})\left(1 - \exp\left(-\frac{a_1}{a_2}\right)\right)}{a_1} - R^{-2}\text{sinc}\left(\frac{2}{\alpha}\right)^{\frac{(2+\alpha)}{2}} \sigma_c^2(\pi\lambda_d)^{-\frac{\alpha}{2}}(2\overline{p}_t)^{-\frac{\alpha}{2}}P_d \\ &\times \left[\Gamma\left(\frac{(2+\alpha)}{2}\right) - \Gamma\left(\frac{(2+\alpha)}{2}, \frac{a_1}{a_2}\right)\right], \end{aligned} \tag{4.23}$$

where $a_1 = 2\pi\lambda_d R^2\gamma_c^{-\frac{2}{\alpha}}\overline{p}_t P_d^{-\frac{2}{\alpha}}$ and $a_2 = P_c^{-\frac{2}{\alpha}}\text{sinc}(\frac{2}{\alpha})$. Furthermore, in (a) we use the transformation $x = r^2$ and (4.23) follows from the integral equation $\int_0^c e^{-ax}x^b\mathrm{d}x = \frac{\Gamma(b+1)-\Gamma(b+1,ac)}{a^{b+1}}$ with $\Gamma(\cdot)$ and $\Gamma(\cdot,\cdot)$ being the Gamma function and incomplete Gamma function, respectively.

We next derive simple bounds on cellular coverage probability in the following lemma.

Lemma 6. *The cellular coverage probability is bounded by*

$$\exp\left(-\frac{2R^{\alpha}\gamma_c\sigma_c^2}{(2+\alpha)P_c} - \frac{a_1}{a_2}R^2\left(\frac{2}{2+\alpha}\right)^{2\alpha}\right) \leq p_c(\gamma_c) \leq \frac{1-\exp\left(-a_1R^2/a_2\right)}{a_1R^2/a_2}. \tag{4.24}$$

Proof. See Appendix 4.7.2. □

Lemma 6 gives intuition into the effect of underlaid FD D2D communication on the performance of cellular systems via important parameters. For instance, a clear observation is that the coverage probability $p_c(\cdot)$ depends on two parameters related to D2D, namely the D2D links density λ_d of and the $\frac{2}{\alpha}$-th moment of transmit power $\overline{p}_t P_d^{\frac{2}{\alpha}}$ at D2D users. More specifically, $p_c(\cdot)$ decreases exponentially as λ_d and $\overline{p}_t P_d^{\frac{2}{\alpha}}$ increase and vise versa.

4.4.2 D2D Link Coverage Probability

Now, for the D2D link coverage probability, conditioned on link distance $d_{k,k} = r$ and transmit power $P_k^{(\mathrm{f})} = P$, the conditional distribution function of SINR at a r-D2D user k can be calculated as

$$\begin{aligned}\mathbb{P}\left(\mathrm{SINR}_k^{(\mathrm{r})} \geq \gamma_d \,\middle|\, P_k^{(\mathrm{f})} = P\right) &= \mathbb{E}\left[\exp\left(-r^{-\alpha}P^{-1}\gamma_d(d_{0,k}^{(\mathrm{r})})^{-\alpha}P_c + I_k^{(f\to r)} + I_k^{(r\to r)} + \beta P_k^{(\mathrm{r})} + \sigma_d^2)\right)\right] \\ &= \mathbb{E}\left[\exp\left(-r^{-\alpha}P^{-1}\gamma_d g_{0,k}^{(\mathrm{r})}\left(d_{0,k}^{(\mathrm{r})}\right)^{-\alpha}P_c\right)\right]\mathbb{E}\left[\exp\left(-r^{-\alpha}P^{-1}\gamma_d(\beta P_k^{(\mathrm{r})} + \sigma_d^2)\right)\right] \\ &\times \mathbb{E}\left[\exp\left(-r^{-\alpha}P^{-1}\gamma_d I_k^{(f\to r)}\right)\right]\mathbb{E}\left[\exp\left(-r^{-\alpha}P^{-1}\gamma_d I_k^{(r\to r)}\right)\right]. \end{aligned} \tag{4.25}$$

Note that each expectation in (4.25) is taken over the distributions of link distances, fading gains, and D2D transmit powers. Let us consider the first expectation $\mathbb{E}\left[e^{-r^{-\alpha}P^{-1}\gamma_d g_{0,k}^{(\mathrm{r})}\left(d_{0,k}^{(\mathrm{r})}\right)^{-\alpha}P_c}\right]$. Since the CU and r-D2D user k are both placed uniformly within the cell, the distance between CU and a r-D2D user and the D2D link distance must follow the same distribution, i.e., $f_{d_{0,k}^{(\mathrm{r})}}(l) = f_d(l)$, $l \in [0, 2R]$, where $f_d(\cdot)$ is given in (4.38). Therefore, we have

$$\begin{aligned}\mathbb{E}\left[\exp\left(-r^{-\alpha}P^{-1}\gamma_d g_{0,k}^{(\mathrm{r})}\left(d_{0,k}^{(\mathrm{r})}\right)^{-\alpha}P_c\right)\right] &= \int_0^{2R}\int_0^{\infty}\exp\left(-r^{-\alpha}P^{-1}\gamma_d P_c g l^{-\alpha} - g\right) f_{d_{0,k}^{(\mathrm{r})}}(l)\mathrm{d}g\mathrm{d}l \\ &= \int_0^{2R}\frac{f_{d_{0,k}^{(\mathrm{r})}}(l)}{1 + r^{-\alpha}P^{-1}\gamma_d P_c l^{-\alpha}}\mathrm{d}l \\ &\approx \frac{1}{1 + r^2 P^{-\frac{2}{\alpha}}\gamma_d^{-\frac{2}{\alpha}}P_c^{-\frac{2}{\alpha}}\mathbb{E}\left[d_{0,k}^{(\mathrm{r})}\right]^{-2}}. \end{aligned} \tag{4.26}$$

In (4.26), we have used the approximation

$$\int_0^{2R}\frac{f_{d_{0,k}^{(\mathrm{r})}}(l)}{1 + a\left(d_{0,k}^{(\mathrm{r})}\right)^{-\alpha}}\mathrm{d}l = \mathbb{E}\left[\frac{1}{1 + \frac{a}{\left(d_{0,k}^{(\mathrm{r})}\right)^{\alpha}}}\right] \approx \frac{1}{1 + \frac{a^{-\frac{2}{\alpha}}}{\mathbb{E}\left[d_{0,k}^{(\mathrm{r})}\right]^2}},$$

for $a \geq 0$. Also, note that $\mathbb{E}\left[d_{0,k}^{(\mathrm{r})}\right] = \frac{128R}{45\pi}$ [130]. Regarding the second expectation in (4.25), it can be calculated as

$$\begin{aligned}\mathbb{E}\left[\exp\left(-r^{-\alpha}P^{-1}\gamma_d(\beta P_k^{(\mathrm{r})}+\sigma_d^2)\right)\right] &\approx \exp\left(-r^{-\alpha}P^{-1}\gamma_d\mathbb{E}_{P_k^{(\mathrm{r})}}\left[\beta P_k^{(\mathrm{r})}+\sigma_d^2\right]\right)\\ &= \exp\left(-r^{-\alpha}P^{-1}\gamma_d(p_t(r)\beta P_d+\sigma_d^2)\right). \end{aligned} \tag{4.27}$$

For the third and fourth expectations in (4.25), applying the Laplace transform as in (4.18), we have

$$\begin{aligned}&\mathbb{E}\left[\exp\left(-r^{-\alpha}P^{-1}\gamma_d I_k^{(f\to r)}\right)\right]\mathbb{E}\left[\exp\left(-r^{-\alpha}P^{-1}\gamma_d I_k^{(r\to r)}\right)\right]\\ &= \mathbb{E}_{g_{l,k}^{(f\to r)},d_{l,k}^{(f\to r)},P_l^{(\mathrm{f})}}\left[\exp\left(-r^{-\alpha}P^{-1}\gamma_d\sum_{l\neq k}^{K} g_{l,k}^{(f\to r)}(d_{l,k}^{(f\to r)})^{-\alpha}P_l^{(\mathrm{f})}\right)\right]\\ &\times \mathbb{E}_{g_{l,k}^{(f\to r)},d_{l,k}^{(f\to r)},P_l^{(\mathrm{f})}}\left[\exp\left(-r^{-\alpha}P^{-1}\gamma_d\sum_{l\neq k}^{K} g_{l,k}^{(r\to r)}(d_{l,k}^{(r\to r)})^{-\alpha}P_l^{(\mathrm{r})}\right)\right]\\ &= \exp\left(-\frac{\pi}{\mathrm{sinc}\left(\frac{2}{\alpha}\right)}\lambda_d\gamma_d^{-\frac{2}{\alpha}}r^2P^{-\frac{2}{\alpha}}\left(\mathbb{E}\left[\left(P_l^{(\mathrm{r})}\right)^{-\frac{2}{\alpha}}\right]+\mathbb{E}\left[\left(P_l^{(f)}\right)^{-\frac{2}{\alpha}}\right]\right)\right)\\ &= \exp\left(-\frac{2\pi}{\mathrm{sinc}\left(\frac{2}{\alpha}\right)}\lambda_d\gamma_d^{-\frac{2}{\alpha}}r^2\left(\frac{P}{P_d}\right)^{-\frac{2}{\alpha}}p_t(r)\right). \end{aligned} \tag{4.28}$$

Then by substituting (4.26), (4.27) and (4.28) into (4.25), we obtain

$$\begin{aligned}&\mathbb{P}\left(\mathrm{SINR}_k^{(\mathrm{r})}\geq\gamma_d\,\middle|\,P_k^{(\mathrm{f})}=P\right)\approx F(d,p)\\ &= \frac{\exp\left(-r^{-\alpha}P^{-1}\gamma_d(p_t(r)\beta P_d+\sigma_d^2)-\frac{2\pi}{\mathrm{sinc}\left(\frac{2}{\alpha}\right)}\lambda_d\gamma_d^{\frac{2}{\alpha}}r^2\left(\frac{P}{P_d}\right)^{-\frac{2}{\alpha}}p_t(r)\right)}{1+r^2\left(\frac{P_c}{P}\right)^{\frac{2}{\alpha}}\gamma_d^{\frac{2}{\alpha}}\left(\frac{128R}{45\pi}\right)^{-2}}.\end{aligned}$$

By taking the average over both the link distance d and the transmit power p, the D2D coverage

probability is given by

$$\begin{aligned} p_d(\gamma_d) &\approx \mathbb{E}_r\left[p_t(r)F(d,P_d)+(1-p_t(r))F(d,0)\right] \\ &= \mathbb{E}_r\left[p_t(r)F(d,P_d)\right] \\ &= \int_0^{d_{\max}} \frac{\exp\left(-r^{-\alpha}P_d^{-1}\gamma_d(p_t(r)\beta P_d+\sigma_d^2)-\frac{2\pi}{\text{sinc}\left(\frac{2}{\alpha}\right)}\lambda_d\gamma_d^{\frac{2}{\alpha}}r^2p_t(r)\right)}{1+r^2\gamma_d^{-\frac{2}{\alpha}}\left(\frac{P_c}{P_d}\right)^{\frac{2}{\alpha}}\left(\frac{128R}{45\pi}\right)^{-2}}\cdot\frac{p_t(r)f_d(d)}{\mathbb{P}(d\le d_{\max})}\mathrm{d}r, \end{aligned} \tag{4.29}$$

where the third equation comes from the fact that $F(l,0)=0$. Furthermore, $p_t(\cdot)$, $f_d(\cdot)$ and $\mathbb{P}\left(r\le d_{\max}\right)$ are given in (4.2), (4.38) and (4.20), respectively. The expression in (4.29) can be simplified further, which is stated in the following lemma.

Lemma 7. *The coverage probability of a typical D2D user can be approximated as*

$$\begin{aligned} p_d(\gamma_d) \approx \overline{p}_t\exp\left(-\left(\frac{128R}{45\pi}\right)^{\alpha/2}P_d^{-1}\gamma_d(\overline{p}_t\beta P_d+\sigma_d^2)\right) \\ \times\frac{e^{A/B}}{B}E_i\left(-(A/B)(x+1)\right)|_{x=0}^{x=BC}, \end{aligned} \tag{4.30}$$

where $A=\frac{2\pi}{sinc\left(-\frac{2}{\alpha}\right)}\lambda_d\gamma_d^{-\frac{2}{\alpha}}\overline{p}_t$, $B=2\mu^2\mathbb{P}\left(r\le d_{\max}\right)\left(1+\gamma_d^{-\frac{2}{\alpha}}\left(\frac{P_c}{P_d}\right)^{-\frac{2}{\alpha}}x\left(\frac{128R}{45\pi}\right)^{-2}\right)$, $C=d_{\max}^2$, *and* $E_i(z)=\int_{-z}^{\infty}\frac{e^{-t}}{t}dt$ *is the exponential integral function.*

Proof. See Appendix 4.7.3. □

4.4.3 Achievable Sum-Rate of D2D links

Given the results in the previous subsection, in this subsection, we analyze the sum-rate of D2D links and characterize the optimal transmit thresholds. Let $S=\lambda_d\mathbb{P}\left[g_{k,k}^{(\mathrm{f})}d_{k,k}^{-\alpha}\ge G_{\min}\right]\pi R^2=\lambda_d\mathbb{P}\left[g_{k,k}^{(\mathrm{r})}d_{k,k}^{-\alpha}\ge G_{\min}\right]\pi R^2$ be the number of active D2D links (either forward link or reverse link).

The achievable sum-rate of FD D2D links can be estimated as follows:

$$\begin{aligned}\overline{R}_d^{(FD)} &= \mathbb{E}\left[\sum_{k=1}^{K}\left(\log_2(1+\text{SINR}_k^{(\text{f})})+\log_2(1+\text{SINR}_k^{(\text{r})})\right)\right]\\ &\overset{(a)}{=} \frac{S}{\ln(2)}\,\mathbb{E}\left[\ln\left(1+\text{SINR}_k^{(\text{f})}\right)+\ln\left(1+\text{SINR}_k^{(\text{r})}\right)\right]\\ &= \frac{2S}{\ln(2)}\int_0^{\infty}\ln(1+x)\mathrm{d}\left(\mathbb{E}_{d_{k,k}}\left[\mathbb{P}\left(\text{SINR}_k^{(\text{f})}\geq x\right)\right]\right)\\ &\overset{(b)}{=} \int_0^{\infty}\frac{2S\mathbb{E}_{d_{k,k}}\left[\mathbb{P}\left(\text{SINR}_k^{(\text{f})}\geq x\right)\right]}{\ln(2)(1+x)}\mathrm{d}x,\end{aligned} \tag{4.31}$$

where (a) is from the Slivynak's Theorem and (b) is obtained from integration by parts. Combining (4.29) into (4.31), the average sum-rate of D2D links can be written as

$$\begin{aligned}\overline{R}_d^{(FD)} \approx 2\lambda_d\pi R^2\int_0^{\infty}\int_0^{d_{\max}}&\frac{p_t(r)^2}{\ln(2)(1+x)}\exp\left(-r^{-\alpha}P_d^{-1}x(p_t(r)\beta P_d+\sigma_d^2)\right)\\ \times&\frac{\exp\left(-\frac{2\pi}{\text{sinc}\left(-\frac{2}{\alpha}\right)}\lambda_d x^{\frac{2}{\alpha}}r^2p_t(r)\right)}{1+r^2x^{\frac{2}{\alpha}}\left(\frac{P_c}{P_d}\right)^{\frac{2}{\alpha}}\left(\frac{128R}{45\pi}\right)^{-2}}\frac{f_d(d)}{\mathbb{P}\left(r\leq d_{\max}\right)}\,\mathrm{d}r\,\mathrm{d}x.\end{aligned} \tag{4.32}$$

Note that while (4.32) still involves a double integral, it can be effectively calculated. It is because the limits of inside integral of (4.32) is finite and the integrand of (4.32) goes to 0 as $x\to\infty$.

Given the approximation of D2D link sum-rate in (4.32), it is possible to derive an optimal transmit threshold $G_{\min}^{\star}$ by maximizing the instantaneous sum-rate $R_d^{(FD)}(\gamma_d,d_{k,k})$ at the SINR target $x=\gamma_d$ and the link distance $r=d_{k,k}$. The optimal threshold $G_{\min}^{\star}$ is provided in the following lemma.

Lemma 8. *When the on-off power allocation is employed at D2D users, the optimal threshold $G_{\min}^{\star}$ at a target SINR γ_d and D2D link distance $d_{k,k}$ that maximizes the instantaneous sum-rate $R_d^{(FD)}(\gamma_d,d_{k,k})$ is*

$$G_{\min}^{\star}=-d_{k,k}^{-\alpha}\ln(p_t^{\star}), \tag{4.33}$$

where $p_t^\star$ denotes the optimal transmit probability and it is expressed as

$$p_t^\star = \min\left\{1, \frac{2}{d_{k,k}^\alpha \gamma_d \beta + \frac{2\pi}{sinc\left(\frac{2}{\alpha}\right)} \lambda_d \gamma_d^{-\frac{2}{\alpha}} d_{k,k}^2}\right\}. \tag{4.34}$$

Proof. At a given target SINR γ_d and a typical D2D link distance $d_{k,k}$, the instantaneous sum-rate $R_d^{(FD)}(\gamma_d, d_{k,k})$ is written as follows:

$$\begin{aligned} R_d^{(FD)}(\gamma_d, d_{k,k}) &\approx \frac{2\lambda_d \pi R^2 p_t^2 \log_2(1+\gamma_d)}{1 + d_{k,k}^2 \gamma_d^{\frac{2}{\alpha}} \left(\frac{P_c}{P_d}\right)^{\frac{2}{\alpha}} \left(\frac{128R}{45\pi}\right)^{-2}} \\ &\times \exp\left(-d_{k,k}^\alpha P_d^{-1} \gamma_d (p_t \beta P_d + \sigma_d^2) - \frac{2\pi}{\text{sinc}\left(\frac{2}{\alpha}\right)} \lambda_d \gamma_d^{-\frac{2}{\alpha}} d_{k,k}^2 p_t\right) \end{aligned} \tag{4.35}$$

with $p_t = \exp(-G_{\min} d_{k,k}^\alpha)$ being the transmit probability of a typical D2D link k. To obtain the optimal transmit threshold $G_{\min}^\star$, we need to find the optimal probability $p_t^\star$ that maximizes the sum-rate (4.35). To this end, taking the first derivative of (4.35) with respect to (w.r.t.) p_t yields

$$\frac{\partial R_d^{(FD)}(\gamma_d)}{\partial p_t} = 2B_1 p_t e^{-B_2 p_t}(2 - B_2 p_t), \tag{4.36}$$

where

$$B_1 = \frac{2\lambda_d \pi R^2 \log_2(1+\gamma_d) \exp\left(-d_{k,k}^\alpha P_d^{-1} \gamma_d \sigma_d^2\right)}{1 + d_{k,k}^2 \gamma_d^{-\frac{2}{\alpha}} \left(\frac{P_c}{P_d}\right)^{\frac{2}{\alpha}} \left(\frac{128R}{45\pi}\right)^{-2}}, \tag{4.37a}$$

$$B_2 = d_{k,k}^\alpha \gamma_d \beta + \frac{2\pi}{\text{sinc}\left(\frac{2}{\alpha}\right)} \lambda_d \gamma_d^{-\frac{2}{\alpha}} d_{k,k}^2. \tag{4.37b}$$

From (4.36), $R_d^{(FD)}(\cdot,\cdot)$ is a decreasing function w.r.t. p_t when $p_t \geq 2/B_2$. In addition, from the fact that $p_t \in [0,1]$, the sum-rate $R_d^{(FD)}(\cdot,\cdot)$ achieves its maximum value at $p_t^\star = \min\{1, 2/B_2\}$. Combining with $G_{\min} = -d_{k,k}^{-\alpha} \ln(p_t)$, we obtain (4.33). Therefore, lemma 8 is proved. □

Lemma 8 provides an optimal mechanism to employ the on-off power control at each D2D user. In particular, for a typical D2D link k, let $\gamma_d^\star$ be the solution of equation $d_{k,k}^\alpha \gamma_d \beta + \frac{2\pi}{\text{sinc}\left(-\frac{2}{\alpha}\right)} \lambda_d \gamma_d^{-\frac{2}{\alpha}} d_{k,k}^2 = 2$. When the target SINR is small, i.e., $\gamma_d \leq \gamma_d^\star$, D2D users should transmit at their maximum powers in order to achieve the maximum sum-rate. Otherwise, when $\gamma_d > \gamma_d^\star$, they should use the on-off power control with transmit probability $p_t^\star$ given in (4.34).

4.5 Illustrative Results

In this section, numerical results are provided to confirm our calculation of the performance metrics for the considered D2D cellular network using centralized and distributed power allocation methods. For each power allocation mechanism, comparisons with HD counterparts are also made to demonstrate the benefits of FD operation. Our Monte Carlo simulations are performed as follows. The cellular and D2D users are dropped according to PPPs within a circle where the BS is located at origin $(0, 0)$ and the radius is R. We then select the D2D links having distances not exceed $d_{\max}$. The channel gains are generated independently according to an exponential distribution with unit parameter. In our simulations, we assume that the cellular user uses a constant transmit powers P_c while D2D users can use power control (either centralized or on-off power control). In centralized power control algorithm, we choose the maximum transmit power at D2D users and the rate improvement threshold as P_d and ϵ, respectively. If the on-off power control is employed at D2D user k, they use the transmit power $P_k = P_d$, $k = 1, \ldots, K$, when the link qualities are not below the threshold $G_{\min}$. Otherwise, they stop transmitting. The path-loss exponent is chosen as α. Furthermore, the self-interference-to-power-ratio (SIPR) is chosen as β. Simulation results are averaged over $2,000$ independent network realizations. Unless state otherwise, Table 4.1 summarizes the numerical values of parameters used in our simulations.

Note that in the simulation for the HD network, we adopt a similar setup as in [66] using the same parameters as in the considered FD D2D network. However, different from [66], locations of both D2D transmitters and receivers are generated using two independent PPPs, and the D2D link selection is based on the distance-based model.

Table 4.1 Simulation Parameters

Cell radius R	500 m
Density of D2D links λ_d	10 and 40 links/km^2
Maximum D2D link distance $d_{\max}$	50 m
Path-loss exponent α	4
Cellular transmit power P_c	100 mW
Maximum D2D transmit power P_d	0.2 mW
Noise variance for 1 MHz bandwidth	-143.97 dBm
Self-interference-to-power-ratio β	-80 dB
Number of network realizations	$2,000$
Rate improvement threshold ϵ	10^{-5}

4.5.1 Centralized Power Control

Let first consider the centralized power control. For completeness, we consider both sparse and dense deployment of D2D links where the corresponding link densities are chosen as $\lambda_d = 10$ and $\lambda_d = 40$ links/km^2, respectively. The average numbers of underlaid D2D links are therefore $\mathbb{E}[K] = \pi\lambda_d R^2 = 8$ and $\mathbb{E}[K] = \pi\lambda_d R^2 = 31$, respectively. For convenience, we assume that the minimum target SINR for D2D users γ_d and cellular user γ_c are the same.

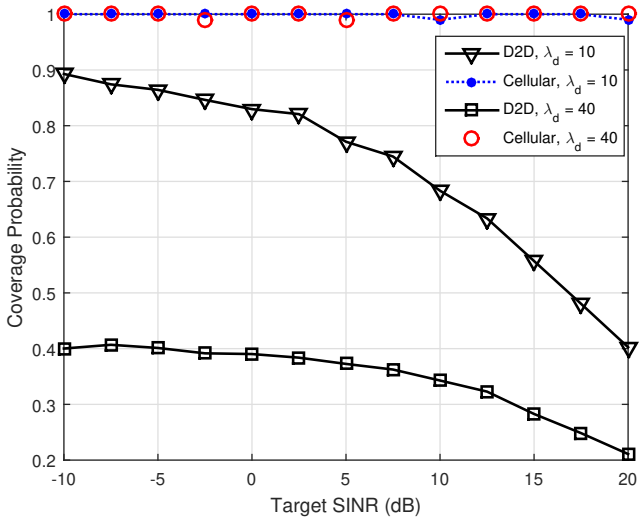

Fig. 4.2 Coverage probabilities of cellular and D2D links versus target SINR via centralized power control.

Fig. 4.2 first shows the coverage probabilities of cellular and D2D links. It is interesting to see from Fig. 4.2 that the centralized power control provides a nearly perfect coverage probability for the cellular link in a wide range of target SINRs, while successfully supporting the underlaid D2D communication. It can be seen that when the density of D2D users increases, the D2D coverage probability, which is the fraction of D2D links that achieves a certain target SINR, is reduced. It is because more D2D links have been removed from the potential D2D list established initially. For example, when the target SINR is 5 dB, the D2D coverage probabilities are 0.77 and 0.37 when $\lambda_d = 10$ and $\lambda_d = 40$ links/km^2, respectively.

The corresponding sum-rates of D2D links are presented in Fig. 4.3 for two realistic FD operations with SIPRs $\beta = -80$ dB and $\beta = -100$ dB. For comparison, the result with a perfect self-interference cancellation is also provided. As illustrated in Fig. 4.3, incorporating underlaid FD D2D communications into cellular network significantly improves the overall cellular network throughput while ensuring the reliable transmission at preexisting cellular link. To further demon-

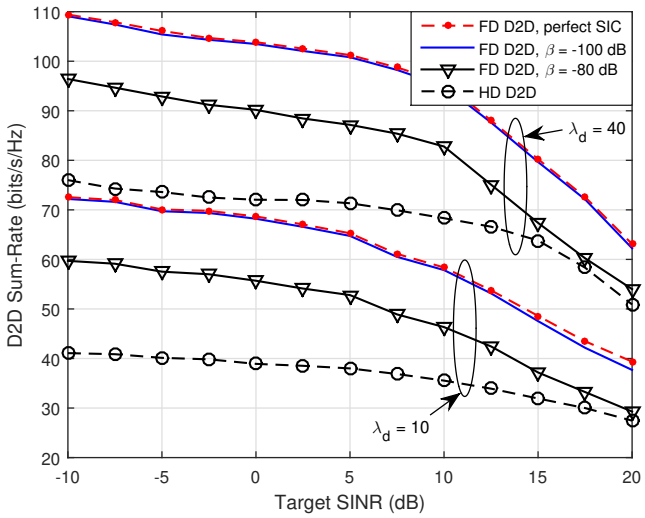

Fig. 4.3 Sum-rate of D2D links versus target SINR via centralized power control.

strate the benefits of FD over HD, the sum-rates of HD D2D links are also included in Fig. 4.3 for two D2D link densities of $\lambda_d = 10$ and $\lambda_d = 40$ links/km^2. It is shown in Fig. 4.3 that, compared to the HD counterpart, a significant sum-rate improvement can be achieved by integrating FD into D2D communications. For example, if a self-interference cancellation (SIC) level of 100 dB can be achieved, FD to HD D2D sum-rate gain ratio of 1.4 at $\lambda_d = 40$ links/km^2 can be achieved at the SINR of 5 dB. It can also be seen that the sum-rates of D2D links at SIC of 100 dB and perfect SIC are almost identical. It indicates that a SIC level of 100 dB is sufficient to exploit the benefit offered by FD. Note that the gain ratio is slightly higher at lower SINRs. For other setups and/or SINRs, the gain might not be as good as that. Therefore, as a future work, it is interesting to rigorously quantify the gain of FD over HD under different environments.

4.5.2 Distributed Power Control

In the case of distributed power control, to validate our approximation of coverage probability of cellular link in (4.23), Fig. 4.4 first shows this approximation and corresponding coverage probability obtained by Monte Carlo simulation over wide range of SINRs and two different D2D link densities, $\lambda_d = 10$ and $\lambda_d = 40$ links/km^2. The tightness of the approximation in (4.23) is clearly observed.

In Fig. 4.5, we plot the approximation of coverage probability of D2D link in (4.30) with simulation result. As shown in Fig. 4.5, the proposed approximation is very tight when $\lambda_d = 10$ links/km^2, i.e. the D2D link deployment is sparse. In dense D2D link deployment with $\lambda_d = 40$

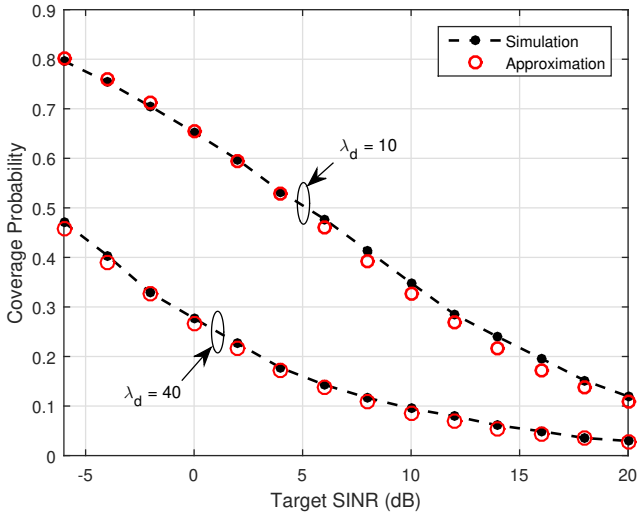

Fig. 4.4 Coverage probability of cellular link versus target SINR.

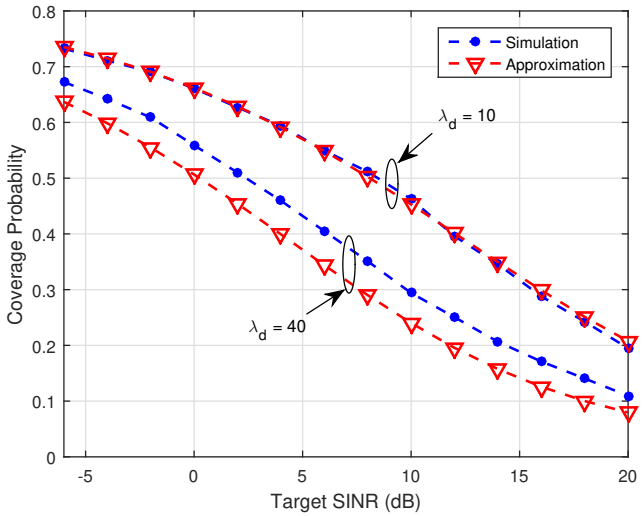

Fig. 4.5 Coverage probability of D2D link versus target SINR.

links/km^2, the approximation is not as tight as the case of $\lambda_d = 10$ links/km^2. The main reason for the variation in the gap between simulation and approximation of $p_d(\cdot)$ when λ_d changes is because of multiple approximations we have adopted to arrive at the closed-form approximation of $p_d(\cdot)$ in (4.30). It is certainly of much interest to analytically quantify the error of approximation compared to exact $p_d(\cdot)$ with regard to λ_d and, eventually, obtain a better approximation of $p_d(\cdot)$. This is indeed an interesting yet challenging problem, and we believe it deserves further studies. However, we would like to note that the obtained results are still sufficiently accurate to approximate the

coverage probability.

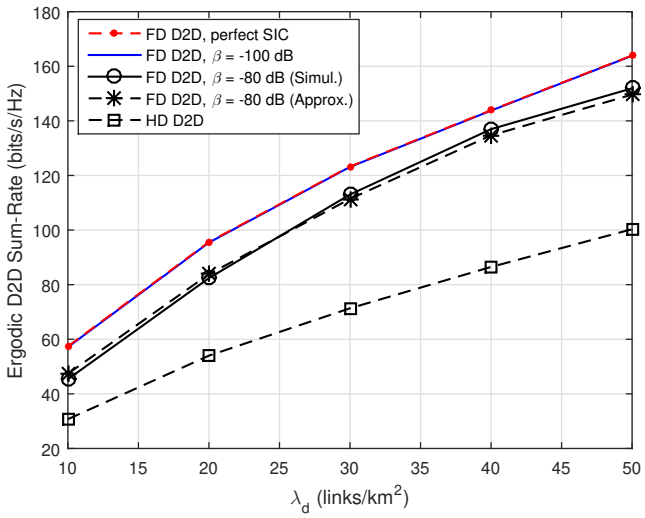

Fig. 4.6 Ergodic sum-rates of FD and HD D2D links versus D2D link density.

Fig. 4.6 plots the D2D link sum-rate obtained by using (4.32) for different densities of D2D links $\lambda_d \in \{10, 20, 30, 40, 50\}$ links/km^2 under various SIC levels, selected as 80 dB, 100 dB, and perfect SIC, i.e., $\beta \in \{-80, -100, -\infty\}$ dB. For comparison, the sum-rate achieved by the HD counterpart is also included. In Fig. 4.6, the rates obtained by Monte Carlo simulations with $\beta = -80$ dB are also presented. It can be seen from Fig. 4.6 that the approximated and simulated results are almost identical. A similar behavior is also observed for the case of $\beta = -100$ dB and perfect SIC. But for a clearer presentation, we omit the Monte Carlo simulation results in such cases. It is obvious that the proposed approximations can be used effectively as accurate system benchmarks. The advantage of FD over HD is also clearly observed from Fig. 4.6. For instance, with $\beta = -80$ dB and $\beta = -100$ dB, FD D2D can offer sum-rate gain ratios of 1.6 and 1.9, respectively, at $\lambda_d = 10$ links/km^2.

4.5.3 Comparison Between Different Power Control Methods

Given the above results, it is also interesting to compare the performances achieved by different power allocation schemes. In particular, Figs. 4.7(a) and 4.7(b) show the coverage probabilities of cellular and D2D links using three PC schemes, namely the centralized PC, the on-off PC and no PC with $\lambda_d = 10$ and $\lambda_d = 40$ links/km^2, respectively. Note that no PC corresponds to the scenario that D2D users always transmit with maximum power P_d, while cellular user uses the

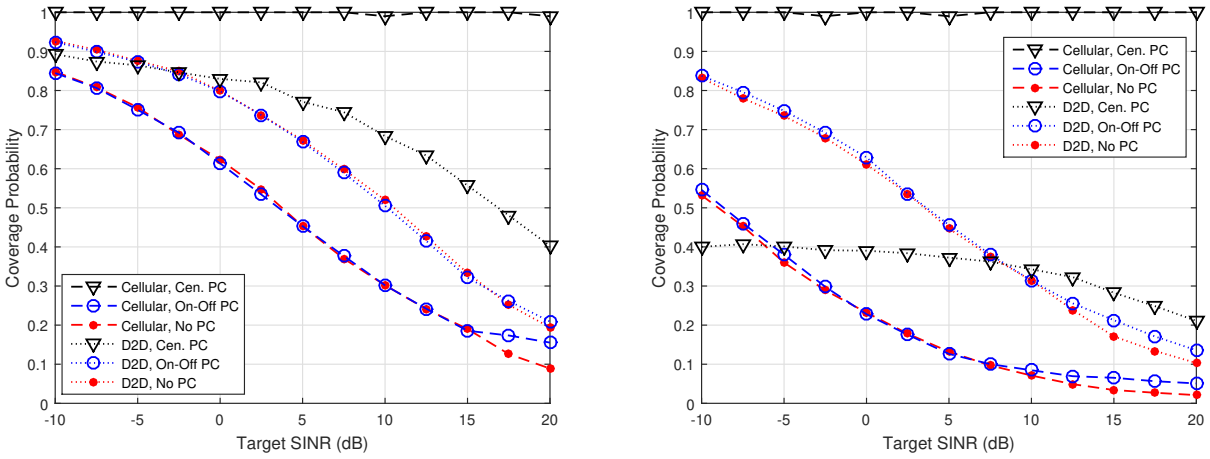

(a) $\lambda_d = 10$ links/km^2 (b) $\lambda_d = 40$ links/km^2

Fig. 4.7 Coverage probabilities of the cellular and D2D links via different power control (PC) methods.

fixed transmit power P_c. Also, in all the simulations, the optimal link quality threshold $G_{\min}$ is given as in (4.33).

As shown in Fig. 4.7, the centralized PC provides a near perfect coverage probability for the cellular user. In addition, with regards to the coverage probability for D2D users, the centralized PC outperforms the other two PC schemes when D2D link deployment is sparse, e.g., when $\lambda_d = 10$ links/km^2. For a denser D2D deployment, the D2D coverage probability offered by the the centralized PC scheme is not that good as compared to the on-off PC scheme, especially in the low SINR region. It is because at low SINRs, the sum-rate is more sensitive to the allocated power. While both schemes try to maximize the sum-rate, the centralized PC has more flexibilities to exploit the benefit of global CSI knowledge for better power allocations. As a result, compared to the on-off PC scheme, the centralized PC can simply choose a fewer yet the best D2D links that yield to a better sum-rate. On the other hand, at a sufficiently high SINR, the sum-rate becomes less sensitive to power allocation. Therefore, the advantage of flexible power control in the centralized PC scheme helps to provide a higher sum-rate, which results in more supported D2D links. Given the cost associated with the process of attaining global CSI knowledge, the centralize PC is therefore preferred only in sparse D2D link deployments. It can also be observed from Fig. 4.7 that the coverage probability in no PC is almost the same as that of the distributed on-off PC. The reason for that is because the objective of the proposed on-off PC scheme is to maximize the D2D sum-rate but not the coverage probability.

To further demonstrate the rate advantage of the distributed on-off PC over no PC, Fig. 4.8

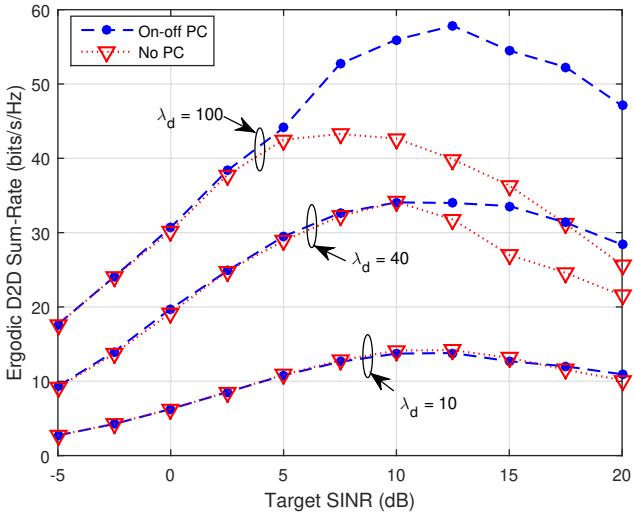

Fig. 4.8 Sum-rate of FD D2D links via optimal on-off and no PC.

shows the D2D sum-rate achieved by these two schemes with three different densities of D2D links $\lambda_d \in \{10, 40, 100\}$ links/km^2 with the SIC of 80 dB. It can be seen from Fig. 4.8 that the rate gain offered by the distributed on-off PC is significant in dense D2D link deployments. However, under sparse D2D link deployment, e.g., $\lambda_d = 10$ links/km^2, the sum-rate improvement is negligible. These results indicate that the distributed PC is more suitable for a network having dense D2D link deployments.

4.6 Concluding Remarks

In this chapter, we have studied the performances of a underlaid cellular D2D network where D2D users operate in FD mode under centralized and distributed power control mechanisms. The locations of D2D users were modeled as homogeneous spatial Poisson point process. Specifically, we first proposed a centralized power allocation scheme that maximizes the D2D throughput while protecting the D2D and cellular link. To deal with the non-convexity of the problem, a DC-based method was proposed to transform the problem into a sequence of convex subproblems, which can be solved efficiently. In the case of distributed on-off power allocation, the closed-form approximations of SINRs at both BS and D2D users were first derived. The coverage probabilities of both cellular and D2D links were then obtained. In addition, based on the approximation of D2D link coverage probability, an analytical expression for the D2D link sum-rate and optimal transmit thresholds that maximizes such sum-rate were also achieved. Simulation results confirmed the an-

alytical results and revealed that significant performance gains can be achieved in the considered FD network as compared to the HD counter part.

4.7 Appendix

4.7.1 Proof of Lemma 5

The PDF of distance between two D2D users within the cell is given in [130] as

$$f_d(l) = \frac{2l}{R^2}\left(\frac{2}{\pi}\arccos\left(\frac{l}{2R}\right) - \frac{l}{\pi R}\sqrt{1-\frac{l^2}{4R^2}}\right) \tag{4.38}$$

for $l \in [0, 2R]$. Thus, the probability that the distance d of a D2D link will not exceed $d_{\max}$ can be estimated as

$$\begin{aligned}\mathbb{P}\left(d \le d_{\max}\right) &= \int_0^{d_{\max}} f_d(l)\mathrm{d}l \\ &= \frac{16}{\pi}\int_0^{\frac{d_{\max}}{2R}} (x\arccos(x) - x^2\sqrt{1-x^2})\mathrm{d}x, \end{aligned} \tag{4.39}$$

where (4.39) is obtained by using the variable transformation $x = l/(2R)$. Applying the integral equations $\int_0^a x\arccos(x)\mathrm{d}x = (-\sqrt{1-a^2}a + 2a^2\arccos(a) + \arcsin(a))/4$ and $\int_0^a x^2\sqrt{1-x^2}\mathrm{d}x = (a\sqrt{1-a^2}(2a^2-1) + \arcsin(a))/8$ to (4.39) yields (4.20).

4.7.2 Proof of Lemma 6

Let first consider the lower bound. The cellular coverage probability given in (4.22) can be rewritten as follows:

$$\begin{aligned} p_c(\gamma_c) &= \int_0^R \exp\left(-\frac{r^{-\alpha}\gamma_c\sigma^2}{P_c} - \frac{a_1}{a_2}r^2\right)\frac{2r}{R^2}\mathrm{d}r \\ &= \mathbb{E}_x\left[\exp\left(-c_1x - c_2x^{-\frac{2}{\alpha}}\right)\right], \end{aligned} \tag{4.40}$$

where $x = r^{-\alpha}$, $c_1 = \gamma_c\sigma^2/P_c$ and $c_2 = a_1/a_2$. Furthermore, it can be verified that the second derivation of $\exp(-c_1x - c_2x^{-\frac{2}{\alpha}})$ is nonnegative when $\alpha > 2$ and $x \ge 0$ [66]. Therefore, $\exp(-c_1x - c_2x^{-\frac{2}{\alpha}})$ is a convex function. Using Jensen's inequality, (4.40) can be lower bounded

as

$$\mathbb{E}_x\left[\exp\left(-c_1 x - c_2 x^{-\frac{2}{\alpha}}\right)\right] \leq \exp\left(-c_1\mathbb{E}[x] - c_2\mathbb{E}[x]^{-\frac{2}{\alpha}}\right) \tag{4.41}$$

with $\mathbb{E}[x] = \mathbb{E}_r[r^{-\alpha}] = \int_0^R r^{-\alpha}\frac{2r}{R^2}\mathrm{d}r = \frac{2}{2+\alpha}R^{\alpha}$ [66]. Then by combining (4.40) and (4.41), we have

$$p_c(\gamma_c) \geq \exp\left(-c_1\frac{2}{2+\alpha}R^{\alpha} - c_2\left(\frac{2}{2+\alpha}\right)^{-\frac{2}{\alpha}}R^2\right). \tag{4.42}$$

The upper bound of $p_c(\gamma_c)$ is obtained as follows:

$$\begin{aligned} p_c(\gamma_c) = \int_0^R \exp\left(-c_1 r^{-\alpha} - c_2 r^2\right)\frac{2r}{R^2}\mathrm{d}r &\leq \int_0^{R^2}\frac{e^{-c_2 x}}{R^2}\mathrm{d}x \\ &= \frac{1-e^{-c_2}R^2}{c_2 R^2}. \end{aligned} \tag{4.43}$$

In (4.43), we use the inequality $\exp(-c_1 r^{-\alpha}) \leq 1$ and apply the variable transformation $x = r^2$. From (4.42) and (4.43), we obtain (4.24). The lemma is therefore proved.

4.7.3 Proof of Lemma 7

We approximate the coverage probability (4.29) as

$$\begin{aligned} p_d(\gamma_d) &\approx \mathbb{E}_r[p_t(r)]\mathbb{E}_r\left[e^{-r^{-\alpha}P_d^{-1}\gamma_d(p_t(r)\beta P_d+\sigma^2)}\right]\mathbb{E}_r\left[\frac{e^{-\frac{2\pi}{\mathrm{sinc}\left(\frac{2}{\alpha}\right)}\lambda_d\gamma_d^{-\frac{2}{\alpha}}r^2 p_t(r)}}{1+r^2\gamma_d^{-\frac{2}{\alpha}}\left(\frac{P_c}{P_d}\right)^{-\frac{2}{\alpha}}\left(\frac{128R}{45\pi}\right)^{-2}}\right] \\ &\approx \overline{p}_t e^{-\mathbb{E}_r[r]^{\alpha/2}P_d^{-1}\gamma_d(\overline{p}_t\beta P_d+\sigma^2)}\mathbb{E}_r\left[\frac{e^{-\frac{2\pi}{\mathrm{sinc}\left(\frac{2}{\alpha}\right)}\lambda_d\gamma_d^{-\frac{2}{\alpha}}r^2\overline{p}_t}}{1+r^2\gamma_d^{-\frac{2}{\alpha}}\left(\frac{P_c}{P_d}\right)^{-\frac{2}{\alpha}}\left(\frac{128R}{45\pi}\right)^{-2}}\right], \end{aligned} \tag{4.44}$$

where (4.44) comes from the approximation

$$\mathbb{E}_r\left[\exp\left(-r^{-\alpha}P_d^{-1}\gamma_d(p_t(r)\beta P_d+\sigma^2)\right)\right] \approx \exp\left(-\mathbb{E}_r[r]^{\alpha/2}P_d^{-1}\gamma_d(\overline{p}_t\beta P_d+\sigma^2)\right).$$

Moreover, in (4.44), $\mathbb{E}_r[r] = \mathbb{E}\left[d_{0,k}^{(\mathrm{r})}\right] = \frac{128R}{45\pi}$. To simplify (4.44) further, we can approximate the distance PDF in (4.38) by a Rayleigh distribution function by $f_d(r) \approx \frac{r}{\mu^2}\exp(-r^2/(2\mu^2))$, $0 \leq$

$r \leq d_{\max}$. Here, the scale parameter μ is determined by the moment matching method. The motivation behind this idea comes from the fact that the closest distance of two points generated from a PPP in $\mathbb{R}^2$ follows a Rayleigh distribution [128]. Note that the scale parameter μ is obtained by fitting two distributions so that they have the same mean value. As a result, $\mu = \frac{128\sqrt{2}R}{48\pi\sqrt{\pi}}$. As such, the last expectation in (4.44) can be approximated as

$$\mathbb{E}_r\left[\frac{e^{-\frac{\pi}{\mathrm{sinc}\left(\frac{2}{\alpha}\right)}\lambda_d\gamma_d^{-\frac{2}{\alpha}}r^2 2\overline{p}_t}}{1+r^2\gamma_d^{-\frac{2}{\alpha}}\left(\frac{P_c}{P_d}\right)^{-\frac{2}{\alpha}}\left(\frac{128R}{45\pi}\right)^{-2}}\right] \approx \int_0^{d_{\max}} \frac{e^{-\frac{\pi}{\mathrm{sinc}\left(\frac{2}{\alpha}\right)}\lambda_d\gamma_d^{-\frac{2}{\alpha}}r^2 2\overline{p}_t}}{1+r^2\gamma_d^{-\frac{2}{\alpha}}\left(\frac{P_c}{P_d}\right)^{-\frac{2}{\alpha}}\left(\frac{128R}{45\pi}\right)^{-2}} \frac{de^{-r^2/(2\mu^2)}\mathrm{d}r}{\mu^2\mathbb{P}\left(r \leq d_{\max}\right)}$$

$$= \frac{e^{A/B}}{B}\mathrm{E}_i(-(A/B)(x+1))\Big|_{x=0}^{x=BC}. \tag{4.45}$$

Finally, substituting (4.45) to (4.44) yields (4.30), which completes the proof.

Chapter 5

Performance Analysis of Full-Duplex D2D Cellular Networks in Multi-Cell Setting [1]

5.1 Introduction

In this chapter, we extend the single-cell setting in Chapter 4 into a multi-cell system to rigorously study the benefits of incorporating D2D transmission into cellular networks. The focus is on underlaid FD D2D cellular networks where cellular uplinks and D2D links use HD and FD operations, respectively (i.e., cellular links transmit in the HD mode and D2D links use the FD mode); and they share the same time-frequency resources. We introduce a tractable hybrid multi-cell network model in which the BSs are distributed uniformly according to a hexagonal grid, while the locations of cellular and D2D users are modeled by Poisson point processes (PPPs). As discussed in Chapter 2, the use of such a PPP model allows to capture the random and unpredictable D2D/cellular positions, which has been validated and extensively adopted in literature (e.g., [68–70]). In each cell, multiple FD D2D links communicate simultaneously by sharing the uplink spectrum with *one* cellular uplink. Furthermore, a universal frequency reuse (UFR) mode is employed, i.e., every cells use the same time-frequency resource in each channel. Given the random network model, we are interested in studying the key performance metrics including the coverage probabilities of both cellular and D2D links and the sum-rate of D2D links. More specifically, we derive the coverage probabilities and ergodic sum-rates of cellular and D2D links, as well as the spectrum efficiency gain by underlaid FD D2D in cellular networks compared to the HD counterpart. Toward this end, we utilize the tools of stochastic geometry to derive the approximations of cellular/D2D coverage

[1] Parts of Chapter 5 have been presented at the 2019 IEEE International Symposium on Personal, Indoor and Mobile Radio Communications (PIMRC) [27] and published in the IEEE Access [24].

probabilities and ergodic sum-rates of cellular and D2D links, which can be effectively calculated by computable integrals. Such approximations can be simplified to closed-form expressions when the D2D link density is sufficiently large, allowing to study the effects of network parameters such as D2D link distance, D2D user density, target SINR, and self-interference cancellation level of FD operation on the cellular/D2D coverage and sum-rate behaviors, and numerical results are also provided to confirm such behaviors. Our numerical results show the amount of self-interference cancellation (SIC) to determine if HD or FD D2D is preferable. And with a sufficiently low SIC level, FD D2D can offer substantial spectral efficiency gain over HD D2D. In addition, the underlaid D2D networking feature offers a significant spectral efficiency gain when it is incorporated into existing cellular networks.

Our analysis for coverage probabilities and achievable sum-rates can be modified to derive the expressions for frequency reuse modes including standard (i.e., fixed) frequency reuse (SFR) and fractional frequency reuse (FFR). The obtained results show how the use of frequency reuse affects the network performance metrics. Specifically, the effect of newly introduced parameters due to the use of SFR and FFR, such as reuse factor and spectrum fraction allocated to each sub-band, is characterized. The employment of SFR and FFR provides an improvement on both D2D and cellular coverage probabilities, but at the cost of degrading in the sum-rates of D2D links.

The remainder of this chapter is organized as follows. In Section 5.2, we describe the system model of interest and define the key performance metrics. Sections 5.3 and 5.4 focus on the development of these metrics for cellular and D2D transmission, respectively. Extension to frequency reuse modes is considered in Section 5.5. Numerical results are given in Section 5.6 to confirm our analysis. Finally, Section 5.7 concludes the chapter.

5.2 System Model and Performance Metrics

In this section, we provide a baseline model for the considered underlaid D2D cellular networks and define the desired performance metrics.

5.2.1 System Model

As illustrated in Fig. 5.1, we consider a hybrid network including cellular uplinks and D2D links operating in HD and FD modes, respectively. In addition, the underlaid FD D2D links share the same time-frequency resource with the cellular uplink. The network consists of BSs arranged according to a hexagonal grid as in [68] in which the area of a hexagonal cell is $1/\lambda_b$, thus λ_b represents the average number of BSs per unit area. The cellular users are randomly distributed and

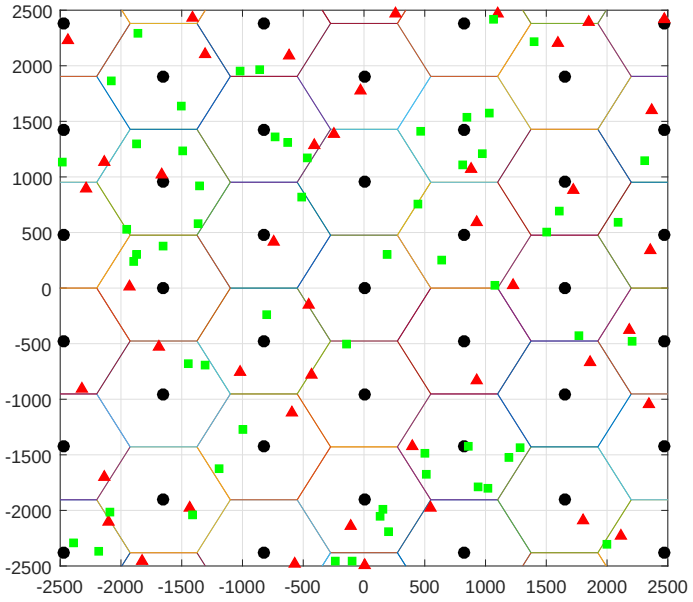

Fig. 5.1 A underlaid D2D cellular network with multi-cell setting (black circle: BS, red triangle: cellular uplink user, green square: D2D user).

modeled by a homogeneous PPP $\Phi_c = \{X_i^{(c)}\} \in \mathbb{R}^2$ having the density λ_c, and $\{X_i^{(c)}\}$ denote the spatial locations of cellular users. We assume that the spectrum is allocated orthogonally to cellular users so that only one cellular user is active in a given channel and universal frequency reuse (UFR) scheme is deployed. This assumption, however, yields a dependent thinning of PPP Φ_c, which makes the analysis intractable, so some approximations are needed to simplify the considered network model. Specifically, we approximate the coverage region of a hexagonal cell by a disk having the same area, i.e., a circle centered at the cell origin with the radius $R = \sqrt{\frac{1}{\pi\lambda_b}}$. Moreover, the typical cellular transmitter is always uniformly distributed within the cell coverage, which can be ensured by assuming that the density of cellular transmitters is significantly higher than that of BSs, i.e., $\lambda_c \gg \lambda_b$. Also, the locations of active cellular users form a PPP $\Phi_{c,a}$ with density λ_b, and the cellular interferers are located outside the coverage region of typical cellular link.

With regard to the underlaid D2D transmission, we consider a marked PPP $\hat{\Phi} = \{X_i^{(d)}, m(X_i^{(d)})\} \in \mathbb{R}^2 \times \mathbb{R}^2$, where the ground process $\Phi = \{X_i^{(d)}\}$ that models the spatial locations of the D2D transceivers forms a PPP with the density λ. Here, λ is the density of potential D2D links that wish to operate in D2D mode; the number of potential D2D links N is a Poisson random variable (RV) having the mean $\mathbb{E}[N] = \lambda A$ with A being the area of considered network. The mark $m(X_i^{(d)})$ denotes the respective locations of D2D users whose $X_i^{(d)}$ communicate with, and we also

assume $m(X_i^{(d)})$ are uniformly placed in the whole $\mathbb{R}^2$ plane. Correspondingly, $m(X_i^{(d)})$ also form a PPP with the density λ, denoted as $m(\Phi)$. Furthermore, the location distributions of a typical D2D node in Φ and $m(\Phi)$ are identical. Therefore, to slightly avoid abuse of notations, we use $\hat{\Phi}_d = \Phi_d \cup m(\Phi_d)$ and $X_i^{(d)} \in \hat{\Phi}_d$ to represent the locations of D2D users in both two PPPs Φ_d and $m(\Phi_d)$. We also should note that the consideration of marked PPP $\hat{\Phi}$ is to guarantee that the instantaneous number of D2D nodes in Φ_d and $m(\Phi_d)$ are equal in each network realization.

In this chapter, we adopt a distance-based D2D mode selection in which the D2D mode of a potential D2D link can only be established if and only if (iff) the link distance d is in the range $[d_{\min}, d_{\max}]$. Suppose that K out of N potential D2D links satisfy the distance constraint, the average number of operating D2D links is $\mathbb{E}[K] = p\mathbb{E}[N]$ with $p = \mathbb{P}(d_{\min} \leq d \leq d_{\max})$ being the probability that the D2D link distance is in the range $[d_{\min}, d_{\max}]$. As potential D2D links are active in D2D mode, their transceivers are the thinned processes of Φ and $m(\Phi)$ and form two corresponding PPPs Φ_d and $m(\Phi_d)$ with the same density $\lambda_d = p\lambda$.

Constant powers P_c and P_d are assumed for cellular and D2D transmitters. The path-loss is computed as $Cr^{-\alpha}$ where r is the distance, $\alpha > 2$ is the path-loss exponent, and C denotes the reference path-loss determined by the carrier frequency and reference distance. As the D2D links operate in FD mode, there exists residual self-interference (SI) due to FD operation that hurts the D2D communications. In this chapter, we also adopt an SI model in which the residual interference is reflected in the self-interference-to-power-ratio (SIPR) β introduced in Chapter 4.

We assume that the typical receiver (either cellular or D2D) is located at the origin o, then the SINRs at a typical cellular BS and a D2D receiver (either in Φ or $m(\Phi)$) are written as

$$\text{SINR}_c = \frac{P_c C |X_0^{(c)}|^{-\alpha} g_0^{(c)}}{I_c^{(c)} + I_d^{(c)} + \sigma_c^2}, \tag{5.1}$$

$$\text{SINR}_d = \frac{P_d C |X_0^{(d)}|^{2} g_0^{(d)}}{I_c^{(d)} + I_d^{(d)} + \beta P_d + \sigma_d^2}, \tag{5.2}$$

where the aggregate interference powers are provided by

$$I_c^{(c)} = \sum_{X_i^{(c)} \in \Phi_{c,a} \setminus \{o\}} P_c C |X_i^{(c)}|^{-\alpha} g_i^{(c)}, \quad I_d^{(c)} = \sum_{X_i^{(d)} \in \hat{\Phi}_d} P_d C |X_i^{(d)}|^{-\alpha} g_i^{(d)},$$
$$I_c^{(d)} = \sum_{X_i^{(c)} \in \Phi_{c,a}} P_c C |X_i^{(c)}|^{-\alpha} g_i^{(c)}, \quad I_d^{(d)} = \sum_{X_i^{(d)} \in \hat{\Phi}_d \setminus \{o\}} P_d C |X_i^{(d)}|^{-\alpha} g_i^{(d)}.$$

In (5.1), the subscript 0 is used for the typical cellular/D2D link. Further, $I_c^{(c)}$ and $I_d^{(c)}$ are the

interference powers from cellular and D2D transmitters to the considered BS, repetitively. Likewise, $I_c^{(d)}$ and $I_d^{(d)}$ present the interference power at typical D2D receiver from cellular and D2D transmitters, respectively. $g_y^{(z)}$, $z \in \{c, d\}$, denotes the fading power gain associated with the communication link from transmitter $X_y^{(z)}$ to the typical receiver. For simplicity, we consider Rayleigh fading where all channel power gains follow an exponential distribution with unit parameter, i.e., $g_y^{(z)} \sim \exp(1)$. In addition, the additive thermal noises at cellular and D2D receivers are modeled as $\mathcal{CN}(0, \sigma_z^2)$, $z \in \{c, d\}$, where σ_z^2 is the noise power. Here, the term βP_d represents the residual self-interference power due to its own transmit power when these D2D links communicate to each other in FD simultaneously using the same time-frequency resource.

5.2.2 Performance Metrics

In this chapter, we are interested in the coverage probabilities of cellular and D2D links, defining as complementary cumulative distribution functions (CCDFs)

$$p_c(\gamma) = \mathbb{P}\left(\text{SINR}_c \geq \gamma\right), \tag{5.3}$$

$$p_d(\gamma) = \mathbb{P}\left(\text{SINR}_d \geq \gamma\right), \tag{5.4}$$

where γ denotes the minimum target SINR for reliable transmission at cellular uplink and D2D connections. Such coverage probabilities indicate the probability that a typical D2D/cellular link can achieve the required SINR γ [128].

Under the assumption that Gaussian signaling schemes are used at all the transmitters, the interferences, conditioned on the user locations and fading gain, are also Gaussian distributed. Therefore, we can define the instantaneous sum-rates over a cell that cellular and D2D links can achieved at a given target SINR γ as

$$R_c(\gamma) = \log_2(1+\gamma)\, p_c(\gamma), \tag{5.5}$$

$$R_d(\gamma) = 2S \log_2(1+\gamma)\, p_d(\gamma), \tag{5.6}$$

where S represents the average number of active D2D links in a cell. The ergodic sum-rates of cellular and D2D links (per cell) can also be defined by invoking the Shannon's capacity formula as

$$\overline{R}_c = \mathbb{E}\left[\log_2(1+\text{SINR}_c)\right], \tag{5.7}$$

$$\overline{R}_d = S\,\mathbb{E}\left[2\log_2(1+\text{SINR}_d)\right], \tag{5.8}$$

where the expectation is taken over the SINR distribution.

Before closing this section, we should note that, because we use the approximate approach for the spatial distribution of cellular transmitters, the analytical results in this work are purely approximations. Thus, for simplicity and clarity on representation of the equations, we will use the equalities instead of the more cumbersome approximations in the sequel to present the analytical expressions of performance metrics.

5.3 Coverage and Sum-Rate Analysis of Cellular Link

5.3.1 Coverage Probability

In this section, we analyze the coverage probability of a typical cellular link. Recall that we adopt an approximation on the distribution of cellular nodes that the coverage region of a hexagonal cell is approximated by a circle with radius $R = \sqrt{\frac{1}{\pi\lambda_b}}$. As a result, the probability density function (PDF) of cellular link distance is given by

$$f_c(r) = \begin{cases} \frac{2r}{R^2}, & \text{if } 0 \leq r \leq R \\ 0, & \text{otherwise.} \end{cases} \tag{5.9}$$

Conditioned on the distance of cellular link $|X_0^c| = r$ and note that $g_0^{(c)} \sim \exp(1)$, the CCDF of typical cellular uplink at the instantaneous SINR of γ can be computed as

$$\begin{aligned} \mathbb{P}(\text{SINR}_c \geq \gamma || X_0^c| = r) &= \mathbb{P}\left(\frac{P_c C r^{-\alpha} g_0^{(c)}}{I_c^{(c)} + I_d^{(c)} + \sigma_c^2} \geq \gamma\right) \\ &= \mathbb{E}\left[\exp\left(-s\left(I_c^{(c)} + I_d^{(c)} + \sigma_c^2\right)\right)\right] \\ &= e^{-s\sigma_c^2}\, \mathcal{L}_{I_c^{(c)}}(s)\, \mathcal{L}_{I_d^{(c)}}(s), \end{aligned} \tag{5.10}$$

where $s = P_c^{-1} C^{-1} r^{\alpha} \gamma$, and $\mathcal{L}_{I_z^{(c)}}$ is the Laplace transform of interference $I_z^{(c)}$, $z \in \{c, d\}$. Con-

sidering the first Laplace transform in (5.10), it is simplified by

$$\begin{aligned}
\mathcal{L}_{I_c^{(c)}}(s) &= \mathbb{E}\left[\prod_{X_i^{(c)}\in\Phi_{c,a}\setminus\{o\}} \exp\left(-sP_cC|X_i^{(c)}|^{-\alpha}g_i^{(c)}\right)\right], \\
&= \mathbb{E}\left[\prod_{X_i^{(c)}\in\Phi_{c,a}} \exp\left(-sP_cC|X_i^{(c)}|^{-\alpha}g_i^{(c)}\mathbb{1}_{\{|X_i^{(c)}|\geq R\}}\right)\right], \\
&= \exp\left(-\int_0^{2\pi}\int_0^{\infty}\left(1-\mathbb{E}\left[e^{-sP_cgCl^{-\alpha}\mathbb{1}_{\{l\geq R\}}}\right]\lambda_b l\,\mathrm{d}l\,\mathrm{d}\theta\right)\right), \\
&= \exp\left(2\pi\lambda_b\int_R^{\infty}\left(1-\mathbb{E}\left[e^{-sP_cgCl^{-\alpha}}\right]\right)\,l\,\mathrm{d}l\right), \\
&= \exp\left(-2\pi\lambda_b\int_R^{\infty}\left(1-\frac{1}{1+sP_cCl^{-\alpha}}\right)\,l\,\mathrm{d}l\right). \qquad (5.11)
\end{aligned}$$

Here, $\mathbb{1}_{\{\cdot\}}$ denotes the indicator function. The second equality is from the assumption that only one cellular link is active in each cell, so the cellular interferers are located outside the typical cell. Furthermore, we have implemented the probability generating functional [128] of a PPP to arrive at the fourth equality, and $g\sim\exp(1)$ in the last equality.

Using a similar approach to (5.11), the last Laplace transform in (5.10) can be simplified by

$$\begin{aligned}
&\mathcal{L}_{I_d^{(c)}}(s) = \mathbb{E}\left[\prod_{X_i^{(d)}\in\hat{\Phi}_d} \exp\left(-sP_dC|X_i^{(d)}|^{-\alpha}g_i^{(d)}\right)\right], \\
&= \mathbb{E}\left[\prod_{X_i^{(d)}\in\Phi_d} \exp\left(-sP_dC|X_i^{(d)}|^{-\alpha}g_i^{(d)}\right)\right]\cdot\mathbb{E}\left[\prod_{X_i^{(d)}\in m(\Phi_d)} \exp\left(-sP_dC|X_i^{(d)}|^{-\alpha}g_i^{(d)}\right)\right], \\
&= \exp\left(-2\pi\lambda_d\int_0^{\infty}\left(1-\mathbb{E}\left[e^{-sP_dCgl^{-\alpha}}\right]\right)\,l\,\mathrm{d}l\right)\cdot\exp\left(-2\pi\lambda_d\int_0^{\infty}\left(1-\mathbb{E}\left[e^{-sP_dCgl^{-\alpha}}\right]\right)\,l\,\mathrm{d}l\right), \\
&= \exp\left(-\frac{2\pi\lambda_d}{\mathrm{sinc}\,(2/\alpha)}P_d^{\frac{2}{\alpha}}C^{\frac{2}{\alpha}}s^{\frac{2}{\alpha}}\right), \qquad (5.12)
\end{aligned}$$

where, in third equality, we have used the probability generating functional of two PPPs formed by D2D transceivers having the same density λ_d.

Substituting (5.11) and (5.12) into (5.10) yields the analytical expression of cellular coverage probability

$$p_c(\gamma) = \int_0^R \exp\left(-a_1 r^\alpha \gamma - a_2 r^2 \gamma^{\frac{2}{\alpha}} - 2\pi\lambda_b \int_R^\infty \frac{r^\alpha l}{\gamma l^\alpha + r^\alpha} \mathrm{d}l\right) \cdot \frac{2r}{R^2}\, \mathrm{d}r, \tag{5.13}$$

where

$$a_1 = \frac{\sigma_c^2}{P_c C}, \tag{5.14}$$

$$a_2 = \frac{2\pi\lambda_d}{\mathrm{sinc}\,(2/\alpha)} \left(P_d/P_c\right)^{2/\alpha}. \tag{5.15}$$

We will now consider a special case in which the number of D2D links is sufficiently large, the D2D-to-cellular interference becomes dominant that both the inter-cell interference and thermal noise can essentially be neglected at the BS. More specifically, if $I_c^{(d)} \gg I_c^{(c)} + \sigma_c^2$, the SINR of cellular receiver can be approximated as $\mathrm{SINR}_c = \frac{P_c C |X_0^{(c)}|^{-\alpha} g_0^{(c)}}{I_d^{(c)}}$. As a result, the cellular coverage probability can be effectively computed by a simple close-formed expression

$$\begin{aligned} p_c(\gamma) &= \int_0^R \exp\left(-a_2 r^2 \gamma^{\frac{2}{\alpha}}\right) \frac{2r}{R^2}\, \mathrm{d}r \\ &= \frac{1 - \exp\left(-a_2 R^2 \gamma^{\frac{2}{\alpha}}\right)}{a_2 R^2 \gamma^{\frac{2}{\alpha}}}, \end{aligned} \tag{5.16}$$

where a_2 is given in (5.15). Next we find a necessary condition on the D2D link density so that (5.16) is valid. Since the integrand of (5.13) admits an exponential expression, the closed-form (5.16) is possible to obtained from (5.13) when the term $a_2 r^2 \gamma^{\frac{2}{\alpha}}$ is sufficiently larger than $2\pi\lambda_b \int_R^\infty \frac{r^\alpha l}{\gamma l^\alpha + r^\alpha} \mathrm{d}l + a_1 r^\alpha \gamma$, e.g., $0.1 \cdot a_2 r^2 \gamma^{\frac{2}{\alpha}} \geq 2\pi\lambda_b \int_R^\infty \frac{r^\alpha l}{\gamma l^\alpha + r^\alpha} \mathrm{d}l + a_1 r^\alpha \gamma$, $\forall r \in [0, R]$. Select $r = R$, a necessary condition on the D2D link density is written as

$$\begin{aligned} \lambda_d &\geq \frac{\mathrm{sinc}\,(2/\alpha)}{2\pi} \left(\frac{P_c}{P_d}\right)^{\frac{2}{\alpha}} \left(20\pi\lambda_b \int_R^\infty \frac{R^{\alpha-2}\gamma^{\frac{2}{\alpha}} l}{\gamma l^\alpha + R^\alpha} \mathrm{d}l + \frac{10\sigma_c^2}{P_c C} R^{\alpha-2} \gamma^{\frac{\alpha-2}{\alpha}}\right), \\ &> \frac{5\sigma_c^2 \mathrm{sinc}\,(2/\alpha)}{\pi P_c C} \left(\frac{P_c}{P_d}\right)^{\frac{2}{\alpha}} R^{\alpha-2} \gamma^{\frac{\alpha-2}{\alpha}}. \end{aligned}$$

Further, the closed-formed expression (5.16) indicates that the cellular coverage probability $p_c(\gamma)$

is exponentially reduced with increasing target SINR γ.

5.3.2 Achievable Sum-Rates of Cellular Links

From (5.5), the instantaneous sum-rate of cellular link over a cell can be directly computed via the cellular coverage probability by a single integral. For the case of large D2D link deployment, such a sum-rate can be expressed in the following closed-form

$$R_c(\gamma) = \frac{\log_2(1+\gamma)}{a_2 R^2 \gamma^{\frac{2}{\alpha}}} \left(1 - \exp\left(-a_2 R^2 \gamma^{\frac{2}{\alpha}}\right)\right). \tag{5.17}$$

Since $\alpha > 2$, (5.17) indicates that the instantaneous sum-rate of cellular links $R_c(\gamma)$ increases to a maximum value and decays to 0 as γ increases, agreeing with the intuition: less number of cellular links achieves the increasing target SINR.

The ergodic sum-rate of cellular link (per cell) can be estimated via the coverage probability as follows

$$\begin{aligned}
\overline{R}_c &= \mathbb{E}\left[\log_2(1+\text{SINR}_c)\right] \\
&= \int_0^\infty \log_2(1+\gamma) \mathrm{d}p_c(\gamma), \\
&= \int_0^\infty \frac{p_c(\gamma)}{\ln(2)(1+\gamma)} \mathrm{d}\gamma, \\
&= \int_0^\infty \int_0^R \frac{2r \exp\left(-a_1 r^\alpha \gamma - a_2 r^2 \gamma^{\frac{2}{\alpha}} - 2\pi\lambda_b \int_R^\infty \frac{r^\alpha l}{\gamma l^\alpha + r^\alpha} \mathrm{d}l\right)}{\ln(2)(1+\gamma)R^2} \mathrm{d}r\, \mathrm{d}\gamma,
\end{aligned} \tag{5.18}$$

where the second equation is from the Slivynak's Theorem while the third equation is obtained from integration by parts. Further, a_1 and a_2 are provided in (5.14) and (5.15), respectively. When the number of D2D links is sufficiently large, $\overline{R}_c$ can be simplified to a more tractable expression

$$\overline{R}_c = \int_0^\infty \frac{\text{sinc}\,(2/\alpha)}{2\pi\lambda_d R^2 \gamma^{\frac{2}{\alpha}}(1+\gamma)} \left(\frac{P_c}{P_d}\right)^{\frac{2}{\alpha}} \left(1 - \exp\left(-\frac{2\pi\lambda_d R^2 \gamma^{\frac{2}{\alpha}}}{\text{sinc}\,(2/\alpha)} \left(\frac{P_d}{P_c}\right)^{\frac{2}{\alpha}}\right)\right) \mathrm{d}\gamma, \tag{5.19}$$

which can be evaluated effectively with one numerical integration. From (5.19), we observe that the cellular sum-rate depends on two D2D-related network parameters: λ_d and P_d. The integrand of expression (5.19) also implies that, as the density of D2D links λ_d increases, ergodic cellular sum-

rate $\overline{R}_c$ monotonically decays. When $\lambda_d \to \infty$, R_c decays to 0 as the D2D-to-cellular interference becomes dominant. Moreover, as the D2D transmit power P_d increases, $\overline{R}_c$ is reduced due to the increasing D2D-to-cellular interference.

5.4 Coverage and Sum-Rate Analysis of D2D Links

5.4.1 Coverage Probability

We now turn our attention to the D2D transmission and evaluate the coverage probability of a typical D2D link. As the underlaid D2D users are also assumed to be uniformly distributed within the circle having radius R, the PDF of D2D link distance can be written as follows [130]

$$f_d(r) = \frac{2r}{R^2}\left(\frac{2}{\pi}\arccos\left(\frac{r}{2R}\right) - \frac{r}{\pi R}\sqrt{1-\frac{r^2}{4R^2}}\right) \tag{5.20}$$

for $r \in [0, 2R]$. Given the range constraint on D2D link distances, this PDF can be further approximated by a more simplified Rayleigh distribution provided by [23, 26]

$$f_d(r) \approx \frac{r}{\mu^2}\exp\left(-\frac{r^2}{2\mu^2}\right), \quad r \in [d_{\min}, d_{\max}]. \tag{5.21}$$

Here, the scale parameter μ is determined by the moment matching method. The approximation (5.21) is motivated by the fact that the closest distance of two points generated from a PPP in $\mathbb{R}^2$ follows a Rayleigh distribution [128]. In addition, the scale parameter μ is obtained by fitting two distributions so that they have the same mean value. As a result, $\mu = \frac{128\sqrt{2}R}{48\pi\sqrt{\pi}}$. The probability that the distance r of a D2D link will be in the range $[d_{\min}, d_{\max}]$ can be directly obtained in closed-form from [26, Appendix A]

$$p = -y\sqrt{1-y^2}\left(4y^2+2\right)8\arccos(y)/\pi^2 - 2\arcsin(y)/\pi\Big|_{y=d_{\min}/(2R)}^{y=d_{\max}/(2R)}. \tag{5.22}$$

We now focus on the derivation of D2D coverage probability. The CCDF of typical D2D link,

conditioned on the D2D link distance $|X_0^{(d)}|= r$ and at the target SINR of γ, is provided by

$$\begin{aligned}\mathbb{P}(\text{SINR}_d \geq x||X_0^{(d)}|= r) &= \mathbb{P}\left(\frac{P_d C r^{-\alpha} g_0^{(d)}}{I_c^{(d)} + I_d^{(d)} + \beta P_d + \sigma_d^2} \geq \gamma\right) \\ &= \mathbb{E}\left[\exp\left(-s\left(I_c^{(d)} + I_d^{(d)} + \beta P_d + \sigma_d^2\right)\right)\right] \\ &= e^{-v(\beta P_d + \sigma_d^2)} \mathcal{L}_{I_c^{(d)}}(s) \mathcal{L}_{I_d^{(d)}}(s), \end{aligned} \tag{5.23}$$

where the second equality is from $g_0^d \sim \exp(1)$. Also, $v = P_d^{-1} C^{-1} r^{\alpha} \gamma$, and $\mathcal{L}_{I_z^{(d)}}$ is the Laplace transform of interference $I_z^{(d)}$, $z \in \{c, d\}$. As aforementioned, the active cellular transmitters form a PPP with density λ_b. Therefore, using similar derivations with (5.12), we can simplify the first Laplace transform in (5.23) by

$$\begin{aligned}\mathcal{L}_{I_c^{(d)}}(v) &= \mathbb{E}\left[\prod_{X_i^{(c)} \in \Phi_{c,a}} \exp\left(-v P_c C |X_i^{(c)}|^{-\alpha} g_i^{(c)}\right)\right] \\ &= \exp\left(-\frac{\pi \lambda_b}{\text{sinc}\,(2/\alpha)} P_c^{\frac{2}{\alpha}} C^{\frac{2}{\alpha}} v^{\frac{2}{\alpha}}\right). \end{aligned} \tag{5.24}$$

Simlarly, the second Laplace transform in (5.23) is given by

$$\begin{aligned}\mathcal{L}_{I_d^{(d)}}(s) &= \mathbb{E}\left[\prod_{X_i^{(d)} \in \hat{\Phi}_d \setminus \{o\}} \exp\left(v P_d C |X_i^{(d)}|^{-\alpha} g_i^{(d)}\right)\right] \\ &= \exp\left(-\frac{2\pi \lambda_d}{\text{sinc}\,(2/\alpha)} P_d^{\frac{2}{\alpha}} C^{\frac{2}{\alpha}} v^{\frac{2}{\alpha}}\right). \end{aligned} \tag{5.25}$$

Substituting (5.24) and (5.25) into (5.23), we obtain the conditional coverage probability of D2D link

$$\mathbb{P}\left(\text{SINR}_d \geq \gamma||X_0^d|= r\right) = \exp\left(-c_1 r^{\alpha} \gamma - c_2 r^2 \gamma^{\frac{2}{\alpha}}\right), \tag{5.26}$$

where the coefficients c_1 and c_2 are expressed as

$$c_1 = \frac{\beta P_d + \sigma_c^2}{P_c C} \tag{5.27}$$

$$c_2 = \left[\lambda_b \left(P_c/P_d\right)^{2/\alpha} + 2\lambda_d\right] \frac{\pi}{\text{sinc}\,(2/\alpha)}. \tag{5.28}$$

De-conditioning (5.26) over the D2D link distance r with the PDF in (5.21), the coverage probability of D2D link equals

$$p_d(\gamma) = \int_{d_{\min}}^{d_{\max}} \exp\left(-c_1 r^{\alpha}\gamma - c_2 r^2 \gamma^{\frac{2}{\alpha}}\right) \frac{2r}{p\mu^2}\,\mathrm{d}r, \tag{5.29}$$

where the distance probability p is given in (5.22).

Adopting a similar approach to the cellular transmission, a simplification of (5.29) is possible when the interference from cellular and D2D transmitters to the D2D receiver is much larger than the thermal noise and self-interference due to FD operation, i.e., $I_d^{(d)} + I_c^{(d)} \gg \beta P_d + \sigma_c^2$. In this case, the SINR at D2D receiver can be reduced to $\text{SINR}_d = \frac{P_d C |X_0^{(d)}|^2 g_0^{(d)}}{I_c^{(d)} + I_d^{(d)}}$, and subsequently the corresponding D2D coverage probability can be derived in closed-form

$$\begin{aligned} p_d(\gamma) &= \int_{d_{\min}}^{d_{\max}} \exp\left(-c_2 r^2 \gamma^{\frac{2}{\alpha}}\right) \frac{2r}{p\mu^2}\mathrm{d}r \\ &= \frac{\exp\left(-c_2 d_{\min}^2 \gamma^{\frac{2}{\alpha}}\right) - \exp\left(-c_2 d_{\max}^2 \gamma^{\frac{2}{\alpha}}\right)}{c_2 p \mu^2}. \end{aligned} \tag{5.30}$$

Here, we have used the variable transformation $x = r^2$. Furthermore, a necessary condition of the D2D densities that (5.30) is used to accurately approximate $p_d(\gamma)$ can be derived from the expression (5.29). In particular, when $c_2 r^2 \gamma^{\frac{2}{\alpha}} \gg c_1 r^{\alpha}\gamma$, e.g., $0.1 \cdot c_2 r^2 \gamma^{\frac{2}{\alpha}} \geq c_1 r^{\alpha}\gamma$, $\forall r \in \{d_{\min}, d_{\max}\}$, and let $r = d_{\max}$, a necessary condition on D2D link density is given by

$$\lambda_d \geq \frac{5\, d_{\max}^{\alpha-2} \gamma^{\frac{\alpha-2}{\alpha}} (\beta P_d + \sigma_c^2) \text{sinc}\left(\frac{2}{\alpha}\right)}{P_c C} - \frac{\lambda_b}{2} \left(\frac{P_c}{P_d}\right)^{\frac{2}{\alpha}}. \tag{5.31}$$

The closed-formed expression of D2D coverage probability $p_d(\cdot)$ in (5.30) also allows to investigate the behavior of $p_d(\cdot)$ under the effect of network parameters. For instance, we can observe that, as the target SINR γ increases, $p_d(\cdot)$ exponentially decays. Further, increasing D2D networking distance $d_{\max}$ shall decrease the D2D coverage probability. This is because the D2D transceivers, on average, are closer, thus causing more interference to each other.

5.4.2 Achievable Sum-Rate of D2D links

In this section, analytical expressions for the achievable sum-rates of D2D links are developed. The obtained expressions characterize the effect of important network parameters, such as λ_d, β, γ, and $d_{\max}$, on the D2D sum-rates.

Let S denote the average number of D2D links per cell. From $R = \sqrt{\frac{1}{\pi\lambda_b}}$, S can be expressed as $S = \lambda_d \pi R^2 = \lambda_d/\lambda_b$. Utilizing (5.6), the instantaneous sum-rate of D2D links over a cell, conditioned on the D2D link distance r and SINR target γ, can be compactly written as a function of λ_d

$$\begin{aligned} R_d(\gamma, r) &= 2S \log_2(1+\gamma)\, \mathbb{P}(\text{SINR}_d \geq \gamma || X_0^{(d)}| = r) \\ &= \theta_1 \lambda_d \exp(-\theta_2 \lambda_d), \end{aligned} \tag{5.32}$$

where

$$\theta_1 = \frac{2\lambda_d}{p\lambda_b \mu^2} \log_2(1+\gamma) \exp\left(-\frac{r^\alpha \gamma(\beta P_d + \sigma_c^2)}{P_c C} - \left(\frac{P_c}{P_d}\right)^{\frac{2}{\alpha}} \frac{\pi \lambda_b r^2 \gamma^{\frac{2}{\alpha}}}{\text{sinc}\,(2/\alpha)} \right),$$

$$\theta_2 = \frac{2\pi r^2 \gamma^{\frac{2}{\alpha}}}{\text{sinc}\,(2/\alpha)}.$$

The obtained expression (5.32) indicates that the achieved sum-rate of D2D links linearly increases but exponentially decays with the D2D link density λ_d, i.e., as λ_d increases from 0, the achieved sum-rate of D2D links increases until the maximum value of $\frac{\theta_1}{\theta_2 e}$ at $\lambda_d = \frac{1}{\theta_2}$. Beyond this point, the achieved sum-rate of D2D links is reduced to 0 as λ_d keeps increasing to $+\infty$, since when the number of D2D links is sufficiently large, the interference becomes dominant. The analytical expression (5.32) also allows to characterize the effect SIC level β on the achieved sum-rate of D2D links. In particular, the contribution of FD is indicated by the level of self-interference cancellation relative to the thermal noise in the term $\beta P_d + \sigma_d^2 = \sigma_d^2 \left(1 + \frac{\beta}{\sigma_d^2/P_d}\right)$. In this term, σ_d^2/P_d represents the D2D noise-to-signal power ratio or SNR_d^{-1}. When β is sufficiently smaller than SNR_d^{-1}, e.g., $\frac{\beta}{\sigma_d^2/P_d} \leq 0.1$, this term is approximately σ_d^2, corresponding to the best sum-rate achieved by the FD operation. From (5.32) and (5.26), one can observe that, initially in a relatively small range $[0, \gamma^\star]$ as the target SINR γ increases, the instantaneous D2D sum-rate R_d increases to a maximum value $R_d^\star$ and then decays to 0 as $\gamma \to +\infty$.

We also analyze the spectral efficiency gain achieved by FD D2D transmission over the HD D2D counterpart under different SIC levels β. Toward this end, we first consider the FD-to-HD D2D sum-rate ratio $\xi_d = R_d(\gamma, r)/R'_d(\gamma, r)$ where $R'_d(\gamma, r)$ denotes the achieved sum-rate of HD

D2D links at target SINR γ and D2D link distance r. From (5.32), the achievable sum-rate of FD D2D links at given target SINR γ and D2D link distance r can be rewritten as

$$R_d(\gamma, r) = \frac{2Sr}{p\mu^2} \log_2(1+\gamma) e^{-c_1 r^\alpha \gamma - c_2 r^2 \gamma - \frac{r^2}{2\mu^2}}. \tag{5.33}$$

For HD D2D transmission, the corresponding coverage probability of typical D2D link and subsequently the conditional D2D link sum-rate $R'_d(\gamma, d)$ are obtained by following a similar approach with the derivation of (5.33). Such a sum-rate is given in [68] by

$$R'_d(\gamma, r) = \frac{Sr}{p\mu^2} \log_2(1+\gamma) e^{-c'_1 r^\alpha \gamma - c'_2 r^2 \gamma^{\frac{2}{\alpha}} - \frac{r^2}{2\mu^2}}, \tag{5.34}$$

where $c'_1 = \frac{\sigma_d^2}{P_d C}$ and $c'_2 = \frac{\pi\lambda_b}{\text{sinc}(2/\alpha)} \left(P_c/P_d\right)^{2/\alpha} + \frac{\pi\lambda_d}{\text{sinc}(2/\alpha)}$. Taking the ratio of (5.33) and (5.34), we obtain the FD-to-HD D2D sum-rate ratio as

$$\xi_d = 2e^{-B_1\beta - B_2}, \tag{5.35}$$

where $B_1 = r^\alpha \gamma / C$ and $B_2 = \frac{\pi\lambda_d}{\text{sinc}(2/\alpha)} r^2 \gamma^{-2/\alpha}$. The result (5.35) indicates that FD-to-HD D2D sum-rate ratio exponentially increases as the self-interference cancellation level increases. Conditioned on the target SINR γ and the D2D link distance r, the maximum achievable FD-to-HD D2D sum-rate ratio can be achieved is $2\exp(-B_2)$. Further, FD D2D offers better sum-rate than HD D2D with $\beta \leq (1 - B_2)/B_1$.

From the D2D coverage probability (5.29), the instantaneous sum-rate of D2D links $R_d(\gamma)$ at a given target SINR γ can be directly derived by invoking (5.6). In the case of dense D2D link deployment, the obtained result can be approximated by a more tractable expression

$$R_d(\gamma) = \frac{2S\log_2(1+\gamma)}{c_2 p\mu^2 \gamma^{\frac{2}{\alpha}}} \left[e^{-c_2 d_{\min}^2 \gamma^{\frac{2}{\alpha}}} - e^{-c_2 d_{\max}^2 \gamma^{\frac{2}{\alpha}}} \right],$$

which exhibits a similar behavior to $R_c(\gamma)$ with respect to (w.r.t.) γ.

Using a similar approach to derive $\overline{R}_c$, the ergodic sum-rate of D2D links is given by

$$\begin{aligned}\overline{R}_d &= \int_0^\infty \frac{2Sp_d(\gamma)}{\ln(2)(1+\gamma)}\,\mathrm{d}\gamma \\ &= \int_0^\infty \int_{d_{\min}}^{d_{\max}} \frac{2\lambda_d r \exp\left(-c_1 r^\alpha \gamma - c_2 r^2 \gamma^{\frac{2}{\alpha}}\right)}{\ln(2)\lambda_b p \mu^2 (1+\gamma)}\,\mathrm{d}r\,\mathrm{d}\gamma. \end{aligned} \tag{5.36}$$

The expression (5.36) can be reduced to a single integral when the D2D link density satisfying the condition (5.31) as

$$\overline{R}_d = \int_0^\infty \frac{\exp\left(-c_2 d_{\min}^2 \gamma^{\frac{2}{\alpha}}\right) - \exp\left(-c_2 d_{\max}^2 \gamma^{\frac{2}{\alpha}}\right)}{\ln(2) c_2 p \mu^2 (1+\gamma)(\lambda_b/\lambda_d)} \mathrm{d}\gamma, \tag{5.37}$$

where c_2 is given in (5.28). From the integrand of (5.37), we observe that the D2D sum-rate exponentially decays as the maximum D2D link distance $d_{\max}$ increases.

5.5 Frequency Reuse: Coverage and Rate Trade-Off

The deployment of universal frequency reuse inevitably suffers from the inter-cell interference, hurting the performance of both cellular and D2D transmission. In commercial cellular networks, frequency reuse schemes based on spectrum partitioning is used to reduce the interfering channels, so the coverage performance can be improved. Thus, it is also of interest to study the impact of incorporating underlaid D2D transmission in existing cellular networks operating in frequency reuse modes with the reuse factor $\delta > 1$. In this work, we consider two common frequency reuse schemes for both cellular and D2D users: standard and fractional frequency reuse.

1) Standard frequency reuse (SFR): In SFR, a fixed frequency reuse pattern for a reuse factor δ is adopted in the multi-cell system so that only one band is employed per cell. By doing so, the out-of-cell cellular and D2D interferers are now separated by a further distance than those of universal frequency reuse considered in previous sections, thereby reducing the inter-cell interference. In Fig. 5.2 (left), we present a visual example to illustrate a fixed frequency reuse pattern where $\delta = 3$ for the considered network. In each cell, D2D and cellular links share the same time-frequency resource.

2) Fractional frequency reuse (FFR): FFR is a modification of SFR where the cellular users in cell-edge is allocated different sub-bands of frequencies based on a reuse factor of δ while the

cell-interior's users share a common sub-band [131]. As a result, FFR requires $(\delta + 1)$ sub-bands in total. Since the interior cellular users do not share any spectrum with cell-edge users and cell-edge users of adjacent cell use orthogonal spectrum, the interference received at both cell-edge and interior users is significantly reduced. Fig. 5.2 (right) illustrates a FFR pattern for cellular users in the hexagonal grid network model with the cell-edge reuse factor $\delta = 3$. Given cellular users in FFR mode, FFR scheme is also adopted for D2D transmission in which D2D links located in interior and cell-edge regions also operate in the same bands reserved for interior and cell-edge cellular users, respectively. As a result, the consideration of FFR classifies two types of users for both cellular and D2D communications: interior and cell-edge, based on their corresponding locations.

We should note that existing research on frequency reuse in D2D communications has focused on optimal designs of D2D cellular systems with the emphasis on reuse factor > 1 by applying advanced optimization algorithms (please see e.g. [132–135] and the references therein). At the network level, there have been few efforts that attempt to integrate frequency reuse into D2D transmission using stochastic geometry approach. For instance, Zhang *et al* in [136] studied the performance of underlaid D2D networking in cellular systems with the focus on FFR. The analysis of this work, however, can not directly apply to ours as it was assumed D2D links having a fixed distance. D2D cellular networks with FFR was also considered in [137] but only one underlaid D2D link was allowed to occupy the cellular spectrum.

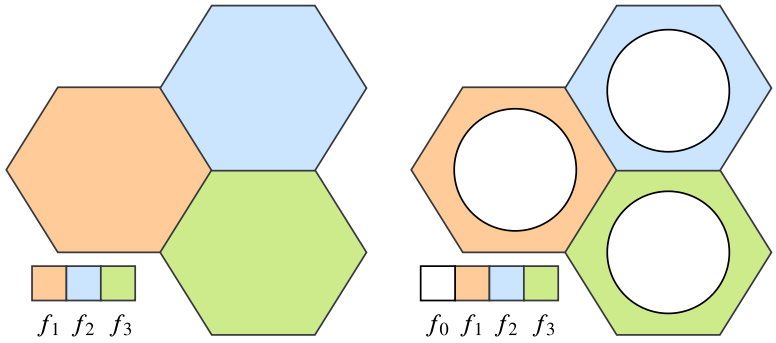

Fig. 5.2 SFR (left) and FFR (right) deployments with reuse factor $\delta = 3$ in the hexagonal grid model.

5.5.1 Standard Frequency Reuse

Cellular Link

If the standard frequency reuse scheme is adopted, it is possible to assume that the inter-cell interference at a typical BS is essentially nulled out. As a result, the cellular performance is only affected by the D2D interferers and thermal noise. In a given cell, the D2D users which share the same frequency with the typical cellular link also form two PPPs having the density λ_d, thus the coverage probability of a typical cellular link in SFR mode can be written as

$$p_c^{(\text{SFR})}(\gamma) = \int_0^R \exp\left(-a_1 r^\alpha \gamma - a_2 r^2 \gamma^{\frac{2}{\alpha}}\right) \frac{2r}{R^2}\, \mathrm{d}r. \tag{5.38}$$

Note that $a_1 = \frac{\sigma_c^2}{P_c C}$ and $a_2 = \frac{2\pi\lambda_d}{\text{sinc}(2/\alpha)} \left(P_d/P_c\right)^{2/\alpha}$. As shown in the expression (5.38), the cellular coverage does not depend on the reuse factor δ as the inter-cell D2D interference can be neglected due to low D2D transmit powers. Assuming that a fraction $1/\delta$ of total spectrum is allocated to each frequency band, the ergodic rate of cellular link over a cell is given from (5.38) by

$$\overline{R}_c^{(\text{SFR})} = \int_0^\infty \int_0^R \frac{\exp\left(-a_1 r^\alpha \gamma - a_2 r^2 \gamma^{\frac{2}{\alpha}}\right) 2r}{\delta \ln(2)(1+\gamma)R^2}\, \mathrm{d}r\, \mathrm{d}\gamma. \tag{5.39}$$

As in (5.19), the cellular rate simplifies for the case of large D2D link density and it is given by

$$\begin{aligned}\overline{R}_c^{(\text{SFR})} &= \int_0^\infty \int_0^R \frac{\exp\left(-a_2 r^2 \gamma^{\frac{2}{\alpha}}\right) 2r}{\delta \ln(2)(1+\gamma)R^2}\, \mathrm{d}r\, \mathrm{d}\gamma \\ &= \int_0^\infty \frac{\left(1 - \exp\left(-a_2 R^2 \gamma^{\frac{2}{\alpha}}\right)\right)}{\delta a_2 R^2 \ln(2) \gamma^{\frac{2}{\alpha}} (1+\gamma)}\, \mathrm{d}\gamma. \end{aligned} \tag{5.40}$$

Observe that the average rate (5.40) decreases with δ and it is maximized for $\delta = 1$, i.e., universal frequency reuse mode.

D2D Link

Given that the SFR is employed at cellular users, the effective cellular-to-D2D interference at a typical D2D receiver now is only from the cellular link that co-exists within the same cell. Further, the effective D2D interferers also constitute two PPPs with the density λ_d. Denoting the set of

such D2D interferers as $\hat{\Phi}_{d,s}$, the aggregate interference power at the typical D2D receiver equals $P_c C|X_0^{(c)}|^{-\alpha} g_0^{(c)} + \sum_{X_i^{(d)} \in \hat{\Phi}_{d,s} \setminus \{o\}} P_d C|X_i^{(d)}|^{-\alpha} g_i^{(d)}$. Using the same approach used to obtain (5.23), we need to compute two Laplace transforms $\mathbb{E}\left[e^{-vP_cC|X_0^{(c)}|^{-\alpha} g_0^{(c)}}\right]$ and $\mathbb{E}\left[e^{-v\sum_{X_i^{(d)} \in \hat{\Phi}_{d,s} \setminus \{o\}} P_d C|X_i^{(d)}|^{-\alpha} g_i^{(d)}}\right]$ in order to derive the coverage probability of D2D link.

Let first focus on $\mathbb{E}\left[e^{-vP_cC|X_0^{(c)}|^{-\alpha} g_0^{(c)}}\right]$. As we assume that both cellular and D2D users are uniformly located within the circle with radius R, the PDF of $l = |X_0^{(c)}|^{\frac{1}{2}}$, which represents the distance from the cellular transmitter to the considered D2D receiver, is identical with that of D2D link distance. It then follows that the mean of l equals $\mathbb{E}[l] = \frac{128R}{45\pi}$ [23]. Using $g = g_0^{(c)} \sim \exp(1)$, we have

$$\begin{aligned}\mathbb{E}\left[e^{-vP_cC|X_0^{(c)}|^{-\alpha} g_0^{(c)}}\right] &= \mathbb{E}_l\left[\int_0^\infty e^{-vCgl^{-\alpha}}\,\mathrm{d}l\right] \\ &= \mathbb{E}_l\left[\frac{1}{1+vP_cCl^{-\alpha}}\right] \\ &\approx \frac{1}{1+vP_cC\left(\frac{45\pi}{128R}\right)^2}. \end{aligned} \tag{5.41}$$

where the last result is from the approximation of $\mathbb{E}_l\left[\frac{1}{1+a/l^\alpha}\right] \approx \frac{1}{1+a^{2/\alpha}/\mathbb{E}[l]^2}$ given in [66].

With a similar derivation as in (5.25), the Laplace transform of D2D interference can be written as

$$\mathbb{E}\left[e^{-v\sum\limits_{X_i^{(d)} \in \hat{\Phi}_{d,s} \setminus \{o\}} P_d C|X_i^{(d)}|^{-\alpha} g_i^{(d)}}\right] = e^{-\frac{2\pi\lambda_d}{\delta \mathrm{sinc}\left(\frac{2}{\alpha}\right)} P_d^{\frac{2}{\alpha}} C^{\frac{2}{\alpha}} v^{\frac{2}{\alpha}}}. \tag{5.42}$$

Using (5.41) and (5.42) and noting that $\mu = \frac{128\sqrt{2}R}{48\pi\sqrt{\pi}}$, the coverage probability of the typical D2D link is given by

$$p_d^{(\mathrm{SFR})}(\gamma) = \int_{d_{\min}}^{d_{\max}} \exp\left(-\frac{r^\alpha \gamma(\beta P_d + \sigma_d^2)}{P_c C} - \frac{2\pi\lambda_d r^2 \gamma^{\frac{2}{\alpha}}}{\mathrm{sinc}\left(\frac{2}{\alpha}\right)}\right) \cdot \frac{2r}{p\mu^2\left(1 + \frac{P_c r^\alpha \gamma}{P_d}\left(\frac{45\pi}{128R}\right)^2\right)}\,\mathrm{d}r. \tag{5.43}$$

Since in each frequency band, the D2D links are allocated a fraction $1/\delta$ of the total spectrum, we can obtain the achievable sum-rate of D2D links over a cell by substituting (5.43) into (5.8) as

follows

$$\overline{R}_d^{(\mathrm{SFR})} = \int_0^{\infty} \int_{d_{\min}}^{d_{\max}} \exp\left(-\frac{r^{\alpha}\gamma(\beta P_d + \sigma_d^2)}{P_c C} - \frac{2\pi\lambda_d r^2 \gamma^{\frac{2}{\alpha}}}{\mathrm{sinc}\left(\frac{2}{\alpha}\right)} \right) \times \frac{2\lambda_d r}{\delta p \mu^2 \ln(2) \lambda_b (1+\gamma) \left(1 + \frac{P_c r^{\alpha}\gamma}{P_d}\left(\frac{45\pi}{128R}\right)^2\right)} \mathrm{d}r\, \mathrm{d}\gamma. \tag{5.44}$$

We observe that, as the number of sub-bands δ increases to $+\infty$, the achievable sum-rate $\overline{R}_d^{(\mathrm{SFR})}$ decays to 0, achieving its limit at $\delta = 1$, i.e., universal frequency reuse mode.

5.5.2 Fractional Frequency Reuse

Let f_0 denote the sub-band allocated to cellular users in the cell interior region and $\{f_1, \ldots, f_\delta\}$ is the set of δ sub-bands employed in the cell-edge of multi-cell networks. We assume that f_0 is assigned a fraction ε of the total spectrum, while the remaining spectrum fraction $(1-\varepsilon)$ is equally allocated to the cell-edge bands, i.e., each band f_k, $k = 1, \ldots, \delta$, occupies $\frac{1-\varepsilon}{\delta}$ of the total spectrum. In the following, we shall analyze the coverage probabilities and ergodic sum-rates of cellular and D2D links when the FFR mode is adopted.

Cellular Link

As the cell-edge cellular users operating in the same spectrum are separated by large distances, a typical cellular user in cell-edge region now only experiences the interference from the underlaid D2D transmission sharing the same channel. When D2D users are located in the cell-edge region, many D2D links now will be separated from the BS by large distances, thus the D2D-to-cellular interference from such D2D links can be neglected. As a result, we shall tightly approximate the coverage probability of a typical cell-edge cellular user by assuming that the cell-edge cellular link is only affected by the interference from one D2D link which is uniformly placed within the considered cell. Denoting the radius of interior region as $\hat{R} \in [0, R]$, the coverage probability of a typical cell-edge cellular link can be obtained directly from the derivations of $p_d^{(\mathrm{SFR})}(\gamma)$ in (5.43) as follows

$$p_{c,e}^{(\mathrm{FFR})}(\gamma) = \int_{\hat{R}}^{R} \frac{\exp\left(-\frac{\sigma_c^2}{P_c C} r^{\alpha}\gamma\right)}{\left(1 + \frac{P_d r^{\alpha}\gamma}{P_c}\left(\frac{45\pi}{128R}\right)^2\right)} \frac{2r}{R^2}\, \mathrm{d}r, \tag{5.45}$$

We observe that $p_{c,e}^{(\text{FFR})}(\gamma)$ is maximized for $\hat{R} = 0$, corresponding to the mode of standard frequency reuse.

For the cellular users located in cell interior, we assume that they are uniformly distributed within the circle with radius $\hat{R}$. Subsequently the coverage probability of inner cellular user can be found in the same manner as in the case of SFR, and it is given from (5.38) by

$$p_c^{(\text{SFR})}(\gamma) = \int_0^{\hat{R}} \exp\left(-a_1 r^{\alpha}\gamma - a_2 r^2 \gamma^{\frac{2}{\alpha}}\right) \frac{2r}{\hat{R}^2}\, \mathrm{d}r. \tag{5.46}$$

where $a_1 = \frac{\sigma_c^2}{P_c C}$ and $a_2 = \frac{2\pi\lambda_d}{\text{sinc}(2/\alpha)} \left(P_d/P_c\right)^{2/\alpha}$. We also present the special case when the D2D interference becomes dominant as compared to the cellular interferer and noise powers. Given that, the coverage probability result of interior user will reduce to the simple expression

$$p_{c,i}^{(\text{FFR})}(\gamma) = \frac{1 - \exp\left(-a_2 \hat{R}^2 \gamma^{\frac{2}{\alpha}}\right)}{a_2 \hat{R}^2 \gamma^{\frac{2}{\alpha}}}. \tag{5.47}$$

Observe that $p_{c,i}^{(\text{FFR})}(\gamma)$ decays as the inner radius $\hat{R}$ reduces to 0, which implies that smaller cell interior region results in better coverage for inner cellular users. This is because, in this case, the users are placed (in average) closer to the BS.

Denoting $\overline{R}_{c,e}^{(\text{FFR})}$ and $\overline{R}_{c,i}^{(\text{FFR})}$ as the achievable sum-rates of cell-edge and interior cellular users over a cell, the total sum-rate of cellular links can be computed from (5.45) and (5.46) by the following integral equation

$$\begin{aligned} \overline{R}_c^{(\text{FFR})} &= \frac{1-\varepsilon}{\delta}\overline{R}_{c,e}^{(\text{FFR})} + \varepsilon \overline{R}_{c,i}^{(\text{FFR})} \\ &= \int_0^{\infty} \frac{\left(\frac{1-\varepsilon}{\delta} p_{c,e}^{(\text{FFR})}(\gamma) + \varepsilon p_{c,i}^{(\text{FFR})}(\gamma)\right) \log_2(1+\gamma)}{\ln(2)(1+\gamma)}\, \mathrm{d}\gamma. \end{aligned} \tag{5.48}$$

Given (5.48), it is interesting to investigate effects of FFR parameters, such as reuse factor δ and frequency partition parameter ε on the achievable sum-rate $\overline{R}_c^{(\text{FFR})}$. It is straightforward that $\overline{R}_c^{(\text{FFR})}$ is maximized for $\delta = 1$. Furthermore, considering the integrand numerator of (5.48), it is rewritten as $\left(p_{c,e}^{(\text{FFR})}(\gamma) + \varepsilon\left(p_{c,i}^{(\text{FFR})}(\gamma) - \frac{1}{\delta}\cdot p_{c,e}^{(\text{FFR})}(\gamma)\right)\right)\log_2(1+\gamma)$. When $\delta \geq p_{c,e}^{(\text{FFR})}(\gamma)/p_{c,i}^{(\text{FFR})}(\gamma)$, $\overline{R}_c^{(\text{FFR})}$ increases to its limit as ε increases to 1, implying that more spectrum should be allocated to the interior cellular users in order to achieve the improved sum-rates. Otherwise, for $\delta < p_{c,e}^{(\text{FFR})}(\gamma)/p_{c,i}^{(\text{FFR})}(\gamma)$, $\overline{R}_c^{(\text{FFR})}$ decays as ε increases, so less spectrum should be assigned to the

interior users.

D2D Link

When a D2D user is located in the cell-edge region, it suffers from the interference caused by the cellular transmitter and other D2D users operate in the same sub-band. We will adopt an approximate approach that the active D2D users in cell-edge regions now constitute a PPP with the density $\hat{\lambda}_d = \lambda_d \left(1 - \frac{\hat{R}^2}{R^2}\right)$. It follows that, by adopting a similar approach with the derivation of D2D coverage probability in SFR mode, the coverage probability of a typical cell-edge D2D link can be obtained from (5.43) as follows:

$$p_{d,e}^{(\text{FFR})}(\gamma) = \int_{d_{\min}}^{d_{\max}} \exp\left(-\frac{r^{\alpha}\gamma(\beta P_d + \sigma_d^2)}{P_c C} - \frac{2\pi\hat{\lambda}_d r^2 \gamma^{\frac{2}{\alpha}}}{\text{sinc}\left(\frac{2}{\alpha}\right)}\right) \times \frac{2r}{p\mu^2\left(1 + \frac{P_c r^{\alpha}\gamma}{P_d}\left(\frac{45\pi}{128R}\right)^2\right)}\,\mathrm{d}r. \quad (5.49)$$

As $\hat{\lambda}_d = \lambda_d \left(1 - \frac{\hat{R}^2}{R^2}\right)$, $p_{d,e}^{(\text{FFR})}(\gamma)$ monotonically increases as $\hat{R}$ increases and it reaches the limit at $\hat{R} = R$.

Now we turn our attention to the interior D2D users in the case of FFR. The aggregate interference at a typical D2D receiver is from a cellular transmitter and co-channel D2D users. Assuming that both cellular and D2D users are uniformly distributed within the circle having radius $\hat{R}$ and D2D users also form a PPP with density λ_d, the coverage probability of an interior D2D user can be obtained by using a similar approach as (5.43), and it is expressed as

$$p_{d,i}^{(\text{FFR})}(\gamma) = \int_{d_{\min}}^{d_{\max}} \exp\left(-\frac{r^{\alpha}\gamma(\beta P_d + \sigma_d^2)}{P_c C} - \frac{2\pi\lambda_d r^2 \gamma^{\frac{2}{\alpha}}}{\text{sinc}\left(\frac{2}{\alpha}\right)}\right) \times \frac{2r}{p\mu^2\left(1 + \frac{P_c r^{\alpha}\gamma}{P_d}\left(\frac{45\pi}{128\hat{R}}\right)^2\right)}\,\mathrm{d}r, \quad (5.50)$$

which is also maximized for $\hat{R} = 0$.

The average numbers of D2D links located in inner and cell-edge regions are provided as $\frac{\hat{R}^2\lambda_d}{R^2\lambda_b}$ and $\frac{(R^2-\hat{R}^2)\lambda_d}{R^2\lambda_b}$. Utilizing the derivations of (5.18) and (5.48), the average sum-rate of D2D links per cell is given by

$$\overline{R}_d^{(\text{FFR})} = \int_0^{\infty} \frac{\frac{1-\varepsilon}{\delta}(R^2 - \hat{R}^2)p_{d,e}^{(\text{FFR})}(\gamma) + \varepsilon\hat{R}^2 p_{d,i}^{(\text{FFR})}(\gamma)}{(\ln(2)/2)(1+\gamma)R^2(\lambda_b/\lambda_d)}\,\mathrm{d}\gamma. \quad (5.51)$$

As a function of δ, $\overline{R}_d^{(\text{FFR})}$ decays as δ increases, so $\overline{R}_d^{(\text{FFR})}$ achieves its maximum at $\delta = 1$, corresponding to the case of universal frequency reuse.

To have a clear insight into the impact of ε and $\hat{R}$ on $\overline{R}_d^{(\text{FFR})}$, we rewrite the numerator of integrand in (5.51) as

$$\frac{R^2 - \hat{R}^2}{\delta} p_{d,e}^{(\text{FFR})}(\gamma) + \varepsilon \left(\hat{R}^2 p_{d,i}^{(\text{FFR})}(\gamma) - \frac{R^2 - \hat{R}^2}{\delta} p_{d,e}^{(\text{FFR})}(\gamma) \right).$$

For $\hat{R}^2 p_{d,i}^{(\text{FFR})}(\gamma) \geq (R^2 - \hat{R}^2) p_{d,e}^{(\text{FFR})}(\gamma)\delta^{-1}$, i.e, $\hat{R} \geq R(p_{d,e}^{(\text{FFR})}(\gamma)/(\delta p_{d,i}^{(\text{FFR})}(\gamma) + p_{d,e}^{(\text{FFR})}(\gamma)))^{\frac{1}{2}}$, $\overline{R}_d^{(\text{FFR})}$ is improved by increasing ε. This result implies that, as the area of inner cell region increases, more spectrum should be assigned to the inner D2D users and vise versa.

5.6 Illustrative Results

In this section, numerical results are provided to confirm the approximations of performance metrics and illustrate their behaviors discussed in previous sections. A comparison between FD D2D networks, HD D2D networks, cellular network without D2D transmission as well as SFR and FFR is also made to demonstrate the benefits of FD D2D operations.

Our Monte Carlo simulations are performed as follows. Consider a network having square coverage area of A, the BSs are dropped according to a hexagonal grid in the network coverage; so the area of a hexagon is $1/\lambda_b$. The cellular users are placed according to a PPP having density λ_c within the network region. For each BS, we randomly schedule a cellular transmitter so that there is always one cellular transmitter per cell, which can be ensured by choosing $\lambda_c \gg \lambda_b$. The D2D users are placed according to a marked PPP with density $\lambda = \lambda_d/p_s$, where p_s denotes the probability that the distance between two uniformly distributed points within the square region lies in the range $[d_{\min}, d_{\max}]$. Such a probability is provided as $p_s = \int_{d_{\min}}^{d_{\max}} \left(\frac{2\pi l}{A} + \frac{2l^3}{A^2} \right) \mathrm{d}l = \frac{\pi d_{\max}^2 - \pi d_{\min}^2}{A} + \frac{d_{\max}^4 - d_{\min}^4}{2A^2}$, where A is the network area. Given the D2D nodes, we then select the D2D links having distances in the range $[d_{\min}, d_{\max}]$. The Rayleigh channel power gains are generated independently according to an exponential distribution with unit parameter. In our simulations, we assume the cellular and D2D users use constant transmit powers P_c and P_d, respectively. Regarding the SFR and FFR, we select the reuse factor $\delta = 3$. In particular, we adopt the reuse patterns as in Fig. 5.2 for both cellular and D2D users. In the FFR scheme, we choose the spectrum partition parameter equal to the ratio of areas between the inner region and the cell, i.e, $\varepsilon = \hat{R}^2/R^2$. In all frequency reuse modes, the SINR statistics of cellular and D2D links are collected in the central

hexagonal cells to avoid the boundary effect [68]. Unless state otherwise, Table 5.1 summarizes the numerical values of parameters used in our simulations.

Table 5.1 Simulation Parameters

Network area A	5^2 km^2
BS density λ_b	$(\pi 0.5^2)^{-1}$ km^{-2}
Cellular user density λ_c	$20 \cdot (\pi 0.5^2)^{-1}$ km^{-2}
Carrier frequency	2 GHz
Density of D2D links λ_d	40 links/km^2
Maximum D2D link distance $d_{\max}$ [20]	50 m
Minimum D2D link distance $d_{\min}$ [20]	3 m
Path-loss exponent α [138]	3.76
Reference path-loss C [138]	-15.3 dB
Cellular transmit power P_c	200 mW
D2D transmit power P_d	0.1 mW
Channel bandwidth	10 MHz
Noise PSD	-174 dBm/Hz
BS receiver noise figure	5 dB
User receiver noise figure	9 dB
Self-interference-to-power-ratio β	-80 dB
Frequency reuse factor δ	3
Radius of interior cell region $\hat{R}$	$0.7 \cdot R$
Spectrum partition parameter ε	0.7^2
Number of network realizations	$10,000$

5.6.1 Universal Frequency Reuse

Let first consider the case when the reuse factor $\delta = 1$, i.e., universal frequency reuse (UFR). In the considered network, the average numbers of BSs *per* km^2 and equivalently cellular links become $\lambda_b A = (\pi 0.5^2)^{-1} \cdot 5^2 = 31$. The link density is selected as $\lambda_d = 40$ links/km^2. The average number of underlaid D2D links (per km^2) over a cell is therefore $\mathbb{E}[K] = 32$.

In Fig. 5.3, we first plot the coverage probabilities versus target SINR of the cellular uplink for $\lambda_d = 40$ links/km^2. To validate our approximation of coverage probability of cellular link in (5.13), Fig. 5.3 shows this approximation and corresponding coverage probability obtained by Monte Carlo simulation over a wide range of SINRs. The tightness of approximation in (5.13) is clearly observed. In addition, the cellular coverage probability performances under HD D2D links and pure cellular transmission (i.e., in absence of D2D communications) are also shown in Fig. 5.3. In general, the link coverage probability $\mathbb{P}$(instantaneous SINR $\geq$ target SINR) is reduced

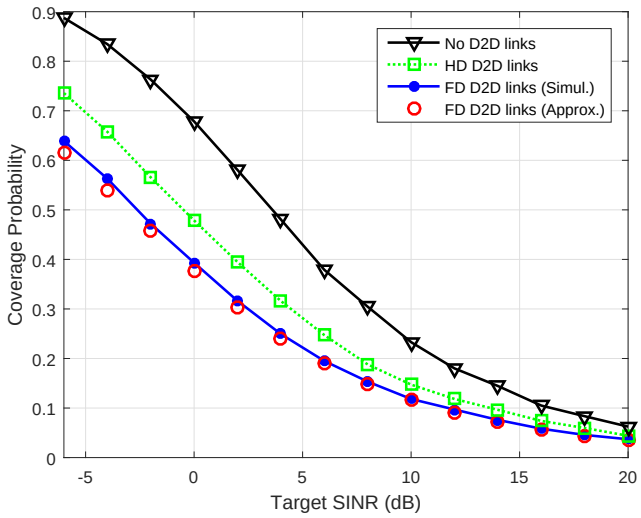

Fig. 5.3 Coverage probability performance of the cellular link for $\lambda_d = 40$ links/km^2.

as target SINR increases. In Fig. 5.3, without D2D links, the cellular uplink uses its allocated frequency with only inter-cell cellular interference, and it is exponentially reduced the coverage probability versus increasing target SINR. In presence of interference of D2D links sharing the same frequency, the coverage probability is further reduced. Since a HD D2D link shares the same frequency in only one direction while a FD D2D link uses the same frequency in both two directions, more interference in the case of FD D2D degrades the coverage probability of cellular link as compared to the case of HD D2D. We should note that, in this work, the results related to HD D2D links are obtained by simulations.

In Fig. 5.4, we also plot the approximation of corresponding coverage probability of D2D link in (5.29) with simulation result as well as with HD D2D transmission for $\lambda_d = 40$ links/km^2. As shown in Fig. 5.4, the proposed approximation is fairly tight with simulation result, so the obtained result is sufficiently accurate to approximate the coverage probability. When the D2D links use HD mode, the coverage probability is improved as compared to FD D2D transmission.

Fig. 5.5 illustrates the instantaneous sum-rates of cellular and D2D links for both HD and FD D2D operations. The numerical results in Fig. 5.5 verify the behaviors of the sum-rates analyzed in previous sections and shows the trade-off in terms of throughput when D2D networking is incorporated into existing cellular networks. Specifically, as target SINR γ increases to $+\infty$, the sum-rate of cellular (D2D) increases (decays) to the limit at $\gamma = 6$ dB and monotonically decays (increases) to 0. In Fig. 5.5, we also include both numerical and analytical results of cellular and D2D sum-rates, as well as the results of HD D2D links obtained by simulations. We observe that

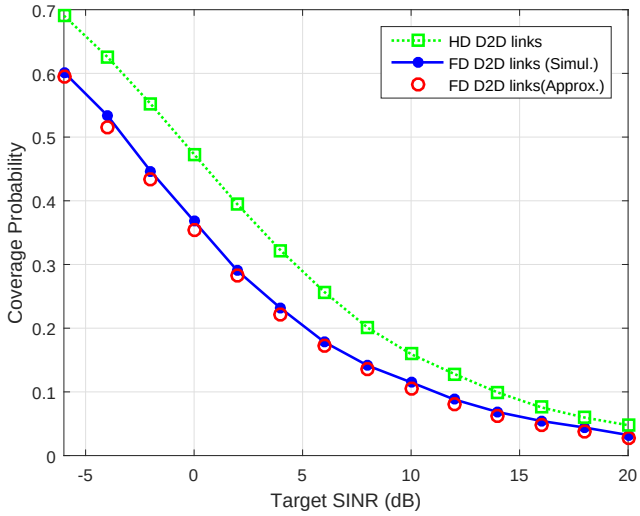

Fig. 5.4 Coverage probability performance of the D2D link versus target SINR.

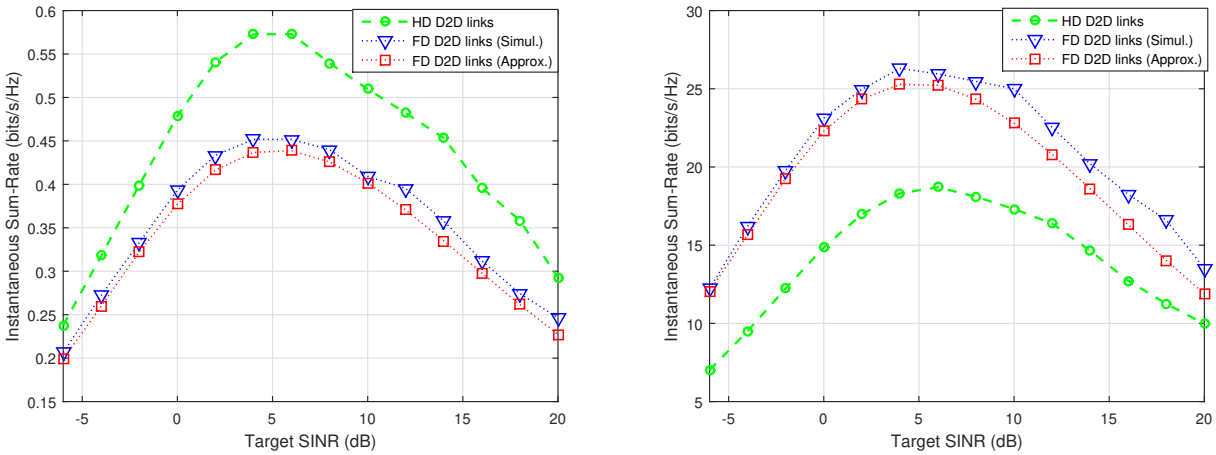

(a) Cellular link (b) D2D link

Fig. 5.5 Instantaneous sum-rates of cellular and D2D links versus target SINR.

HD D2D allows to improve the cellular throughput but significantly reduces the D2D sum-rate. This is intuitive since HD D2D yields less D2D-to-cellular interference.

Similar results are also obtained for the ergodic sum-rates of cellular and D2D links. Specifically, Fig. 5.6 compares the cellular and D2D link sum-rates obtained by using the analytical expressions (5.18) and (5.36) to those obtained by Monte Carlo simulations for various D2D link densities. It can be seen from Fig. 5.6 that the two results are fairly close. As such, the proposed approximations can be used effectively as accurate system benchmarks. Fig. 5.6 also illustrates

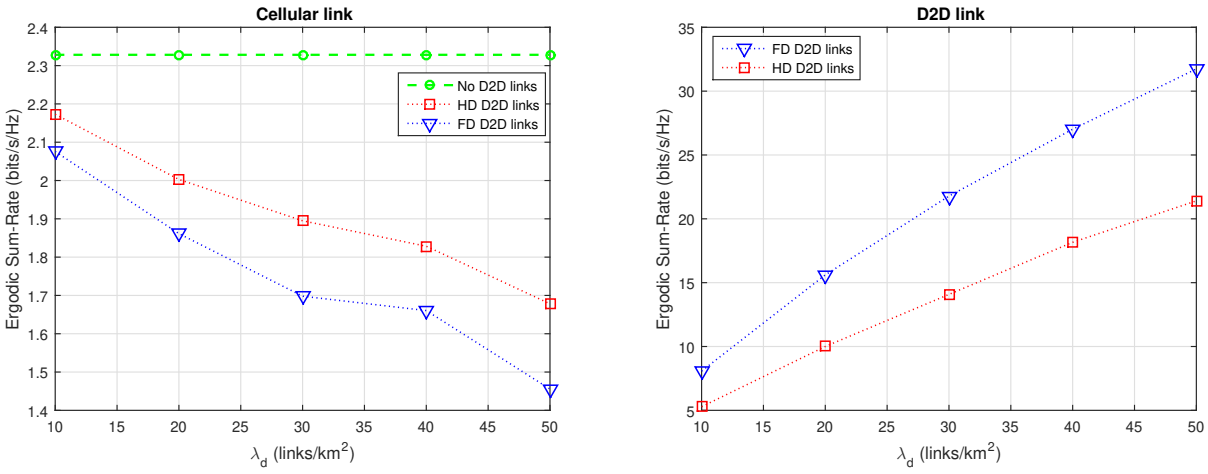

(a) Cellular link (b) D2D link

Fig. 5.6 Ergodic sum-rates of D2D and cellular links versus D2D link densities.

the ergodic sum-rates when D2D links use HD transmission. As illustrated in Fig. 5.6a, FD D2D inevitably hurts the cellular sum-rate performance due to the increasing D2D-to-cellular interference as compared to the HD counterpart. The loss in terms of cellular throughput, however, can be compensated by significant D2D sum-rate gains obtained by FD D2D operation, as shown in Fig. 5.6b. Further, Fig. 5.6 shows that D2D links can offer substantially higher sum-rates than cellular links, indicating a large spectral efficiency gain by incorporating the D2D option.

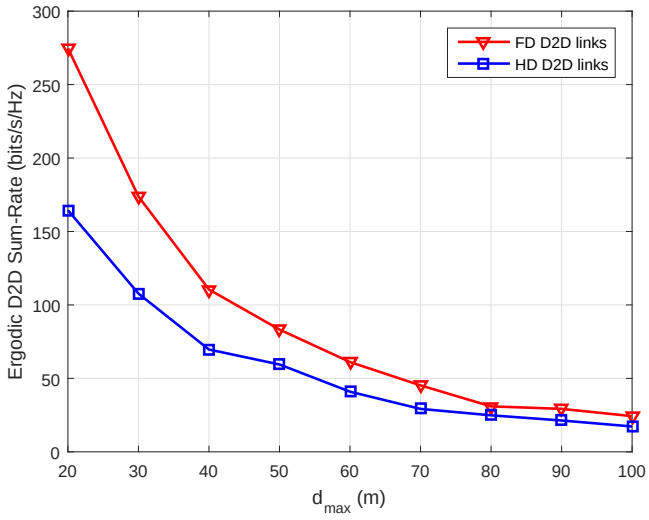

Fig. 5.7 Ergodic D2D link sum-rate for different maximum D2D link distances.

In Fig. 5.7, we plot the ergodic sum-rate of D2D links versus maximum D2D link distance for

$\lambda_d = 40$ links/km^2. The results show a significant D2D link sum-rate achieved, especially with FD D2D at short distances. As maximum D2D link distance increases, the achieved D2D sum-rate exponentially reduces, which is in agreement with our previous discussion.

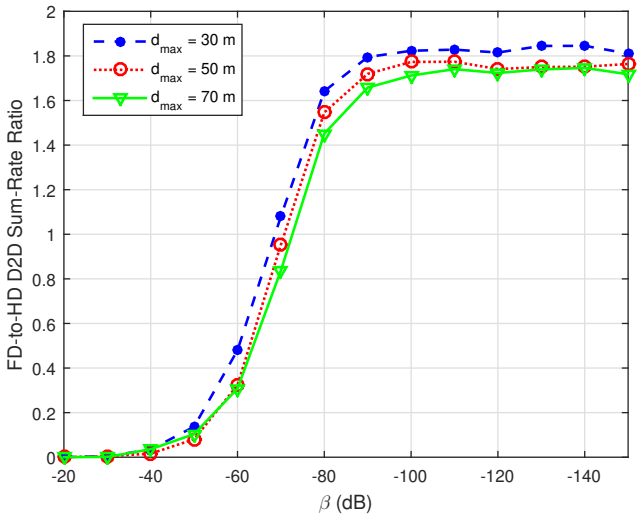

Fig. 5.8 FD-to-HD sum-rate ratio versus SIC for various maximum D2D link distance $d_{\max} = \{30\,\text{m}, 50\,\text{m}, 70\,\text{m}\}$.

For FD and HD D2D performance comparison, we establish the FD-to-HD D2D sum-rate ratio and plot it versus the self-interference cancellation (SIC) in dB for different maximum D2D distances: $30\,$m, $50\,$m and $70\,$m in Fig. 5.8 for $\lambda_d = 40$ links/km^2. The results show that FD D2D can offer better sum-rate than HD D2D with sufficiently large SIC and shorter range, e.g., 1.7 times better at $70\,$m, 1.76 times better at $50\,$m and 1.8 times better at $30\,$m with SIC of $100\,$dB. However, for SIC larger than $100\,$dB, the FD-to-HD D2D sum-rate ratio seems to get stable at 1.8. Further, the results in Fig. 5.8 also indicate that the SIC of $100\,$dB is sufficient to achieve the best FD-to-HD D2D sum-rate ratio.

By defining this spectral efficiency gain as the ratio of the achieved total sum-rate (of both cellular uplink and D2D links) to the achieved rate of only cellular uplink (operating alone without D2D links in the same environmental conditions), Fig. 5.9 plots the resulting spectral efficiency gain versus D2D link density. The results in Fig. 5.9 indicate that, over the wide D2D link density range from 10 to $50\,$links/km^2, the spectral efficiency gain linearly increases with the D2D link density for the cases of HD D2D and FD D2D with SIC of $80\,$dB. With better SIC of $100\,$dB, FD D2D offers a substantial improvement in the spectral efficiency gain as compared to HD D2D. For example, in Fig. 5.9, for a D2D link density of 40 links/km^2, HD D2D achieves a spectral spectrum gain of 22 while FD D2D can offer 33.5 with SIC of $80\,$dB and 40 with SIC of $100\,$dB.

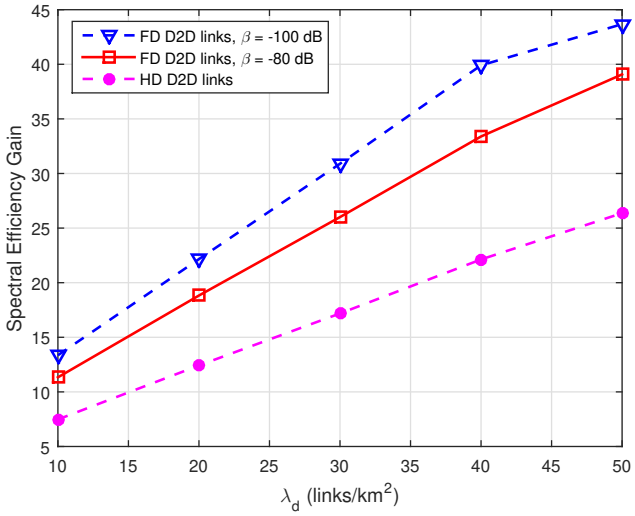

Fig. 5.9 Spectral efficiency gain versus D2D link density when D2D links operate in FD and HD modes with $d_{\max} = 50\,\text{m}$.

It is also noticed that for D2D link density of higher 40 links/km^2, increase in sum-rate (and in spectral efficiency gain) of FD D2D with SIC of $100\,\text{dB}$ gets compressed. This can be explained by the fact that co-channel interference becomes dominant at higher D2D link density. In general, it is expected that the increase in sum-rate (and in spectral efficiency gain) of FD/HD D2D will get compressed and saturated at a certain sufficiently high D2D link density due to the dominant interference generated in the network.

5.6.2 Comparison with SFR and FFR

In this section, we represent the key performance metrics including coverage probabilities of cellular and D2D links and ergodic sum-rates of cellular and D2D links when standard and fractional frequency reuse schemes are employed in the considered network. The results are then compared to those obtained in the case of universal frequency reuse to demonstrate the trade-off between coverage and sum-rate.

In Fig. 5.10, we first plot the coverage probabilities of cellular link under FFR, SFR and UFR for the D2D link density $\lambda_d = 40$ links/km^2. In addition, we consider both HD and FD D2D transmission. It can be seen from Fig. 5.10 that the use of frequency reuse modes improves the coverage probabilities of cellular link, which is intuitive since the cellular receiver no longer suffers from the inter-cell interference. Further, the performance of interior cellular user in FFR outperforms that of typical user in SFR. Interestingly, we observe that the coverage probabilities of cell-edge cellular link in the cases of FD and HD D2D transmission are identical, implying that

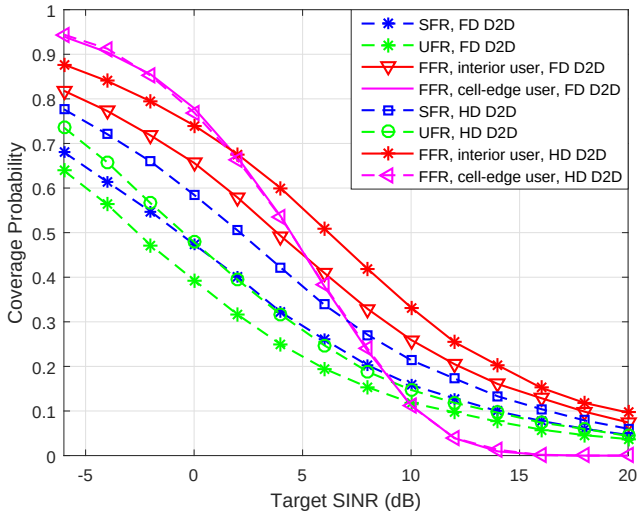

Fig. 5.10 Coverage probabilities of typical cellular link versus target SINR in SFR, FFR and UFR modes for both FD and HD D2D transmission.

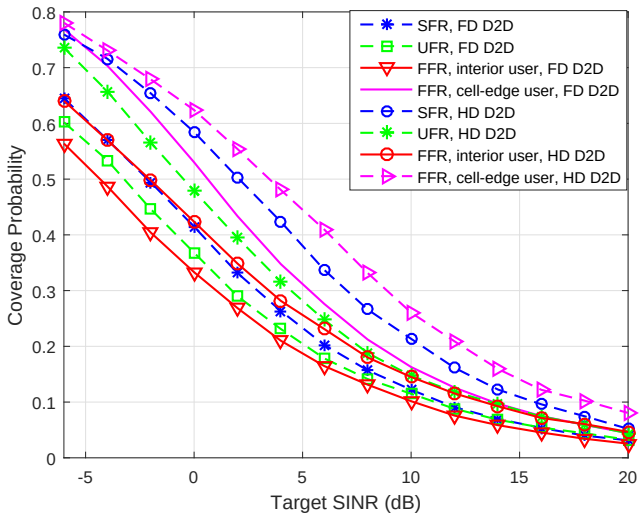

Fig. 5.11 Coverage probabilities of typical D2D link versus target SINR in SFR, FFR and UFR modes for both FD and HD D2D transmission.

the coverage performance of a typical cellular link located in the cell-edge region shall essentially not be affected by the D2D interference. This is because, in this case, D2D links are placed (in average) far from cellular link. Similar observations are obtained in Fig. 5.11 where we plot the corresponding coverage probabilities of typical D2D link under FFR, SFR and UFR for $\lambda_d = 40$ links/km^2. An improvement in D2D coverage can be observed when frequency reuse is employed. The performance of typical interior D2D user in FFR, however, is lower than the UFR counterpart.

This is because, in the interior region of FFR, the cellular transmitter is located closer to the D2D users than in UFR mode.

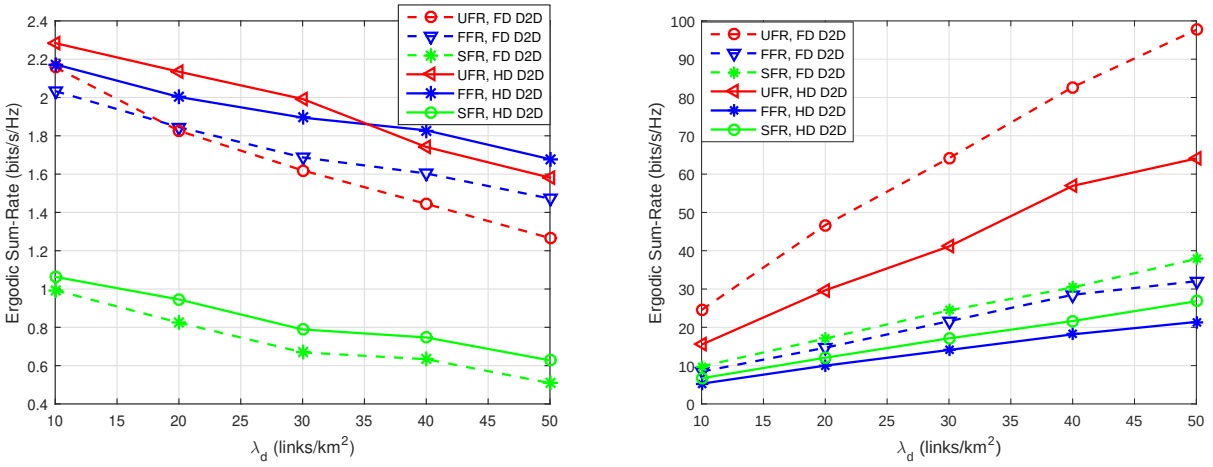

(a) Cellular link (b) D2D link

Fig. 5.12 Ergodic sum-rates of cellular and D2D links versus D2D link densities under difference frequency reuse schemes for both FD and HD D2D transmission.

Finally, Fig. 5.12 compares the ergodic sum-rates of cellular and D2D links between FFR, SFR and UFR for HD and FD D2D transmission. It is shown that the sum-rate of D2D links (both FD and HD operation) with FFR and SFR is significantly lower than that with UFR. While FFR provides an improved cellular rate as compared to SFR, the D2D sum-rates with FFR and SFR are close in both cases of HD and FD D2D transmission.

5.7 Concluding Remarks

In this chapter, we have studied the benefits of integrating FD D2D communications into existing cellular network under the multi-cell setting where the BSs are regularly placed according to a hexagonal grid and the locations of users were distributed according to Poisson point processes. Given the network model, analytical expressions of coverage probability and ergodic sum-rate of both cellular and D2D links were derived and the effect of network parameters to the cellular/D2D sum-rates was investigated. Our results revealed that significant performance gains in term of spectral efficiency can be achieved in the considered FD network as compared to the HD counter part with sufficient self-interference cancellation. Further, D2D services can offer significant spectral efficiency gain as compared to pure cellular transmission. We also shown that, when standard and fractional frequency reuse schemes were employed, it helped enhance the rate of cellular link as

well as the coverage of both cellular and D2D links, but substantially degraded the D2D throughput performance.

Chapter 6

Underlaid Full-Duplex D2D Communications in Massive MIMO Systems via Joint Beamforming and Power Allocation

6.1 Introduction

Chapters 4 and 5 focused on the integration of FD D2D services in cellular uplink resources; and BS uses an omni-directional antenna. This chapter focuses on exploring impact of incorporating underlaid FD D2D services into cellular downlink transmission of existing multi-cell networks where BSs are equipped with massive MIMO transmission. As discussed in Chapters 1, when D2D communications is allowed to occupy the downlink resources, the receiving D2D user experiences strong interference from the BSs. Meanwhile, D2D transmitter may cause high interference to the co-channel cellular user who receives the downlink traffic. Thus, interference management is essential to ensure a harmonious co-existence between D2D and cellular services. Under the assumption of uniform linear array (ULA) antennas equipped at each BS, our objective is to design a joint beamforming and power allocation algorithm so as to alleviate the interference between cellular and D2D transmission and optimize the overall network sum-rate. The proposed algorithm is based on the fractional programming (FP) approach, which is developed to solve general noncovex optimization problems with the corresponding objective functions being in form of the sum-functions-of-ratio. In wireless communications systems, FP has recently been employed extensively to solve the energy and spectral efficient optimization problems (e.g., [84, 139–141] and

the references therein). The FP-based algorithm takes advantage of the fractional structure of the nonconvex optimization problem by directly looking at the objective function decomposition. The form of the original objective function naturally lends itself to this choice of fractional decomposition. More specifically, the FP-based algorithm approximates the nonconvex optimization problem by applying a quadratic transformation to the fractional argument terms of the objective function to ensure that the transformed objective function is concave. The FP-based algorithm is operated in a centralized manner and requires full knowledge of CSI at the central controllers. While our algorithm utilizes the FP theory developed in [141] applied to separate power control and beamforming design in cellular systems, the extension to joint beamforming and power allocation in underlaid D2D cellular networks is not trivial and requires new derivations.

Based on the developed FP-based algorithm, the benefits of incorporating underlaid FD D2D networking into massive MIMO cellular systems are investigated. In particular, we shall study the average network sum-rates per cell under the impact of important network parameters including SIC levels, number of antennas equipped at each BS, D2D link distances, and number of active D2D links in each cell. We adopt the network sum-rates (over a cell) of HD D2D cellular systems and pure cellular systems (in absence of D2D), both also employing the FP-based algorithm, as the benchmarks to characterize the benefits offered by the FD D2D transmission. For completeness, we consider two scenarios in which D2D users are either located inside or outside of the buildings in urban area. An interesting observation is that adopting the FP-based algorithm to FD D2D cellular systems significantly improves the achievable network throughput (over a cell) and vastly outperforms that achieved by the HD D2D counterpart and pure cellular systems, but only under sufficiently high SIC levels. Based on the numerical results, a comparison with the scenario in which omni-directional transmission is employed at the cellular link is also made to demonstrate the advantage of ULA-equipped BS.

The remainder of this chapter is organized as follows. Section 6.2 describes the system model of interest and formulate the optimization problem. Section 6.3 focuses on the development of joint beamforming and power allocation algorithm to solve this problem. Numerical results are given in Section 6.4 to illustrate the sum-rate objective obtained by our proposed algorithm and the impact of network parameters on this sum-rate objective. Finally, Section 6.5 concludes the chapter.

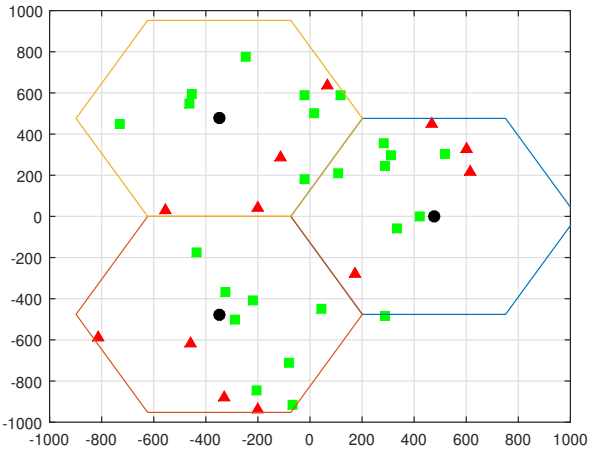

Fig. 6.1 A underlaid D2D cellular network with multi-cell setting (black circle: BS, red triangle: cellular user, green square: D2D transceiver).

6.2 System Model and Problem Formulation

6.2.1 System Model

As illustrated in Fig. 6.1, we consider a hybrid network including cellular downlinks and D2D links operating in HD and FD modes, respectively. The network consists of B base-stations (BSs) located in multiple hexagonal cells. We assume that both multiple cellular and D2D transceivers are randomly located within the cell region. The associated receiver with a D2D transceiver is located at a fixed distance away with an isotropic direction. This chapter considers single antenna transmission at all cellular/D2D users, while each BS is equipped with A antennas. Each BS is capable of serving M cellular users simultaneously in a time-frequency slot ($A \geq M$). In addition, the downlink frequency-time resources are fully reused by multiple underlaid FD D2D links, and the universal frequency reuse scheme (UFR) is employed. The sets of cellular users served by the BS b are denoted as $\mathcal{C}_b$, $b = 1, \ldots, B$. Meanwhile, let $\mathcal{D}$ be the collection of all D2D transceivers in the network. As a result, $N = |\mathcal{D}|/(2B)$ is the number of D2D links per cell.

The transmit power vector of D2D users in the same time-frequency slot is defined as $\mathbf{p} = [P_1, \ldots, P_{2BN}] \in \mathbb{R}_+^{2BN}$, where P_n denotes the transmit power at D2D transceiver n. The path-loss L is computed as $L = Cr^{-\alpha}$ where r is the distance, $\alpha > 2$ is the path-loss exponent, and C denotes the reference path-loss determined by the carrier frequency and reference distance. Furthermore, the system uses the time division multiplexing (TDD); we assume channel reciprocity, i.e., the downlink channel is Hermitian transpose of the uplink channel.

Given the system model, the received signals at cellular user m in cell b is given by

$$y_{bm}^{(\mathrm{c})} = L_{b,bm}^{(\mathrm{cc})}\left(\mathbf{h}_{b,bm}^{(\mathrm{cc})}\right)^{\mathsf{H}}\mathbf{v}_{bm}x_{bm}^{(\mathrm{c})} + \underbrace{\sum_{j\in\mathcal{C}_b\setminus\{m\}} L_{b,bm}^{(\mathrm{cc})}\left(\mathbf{h}_{b,bm}^{(\mathrm{cc})}\right)^{\mathsf{H}}\mathbf{v}_{bj}x_{bj}^{(\mathrm{c})}}_{\text{Intra-cell cellular interference}}$$
$$+ \underbrace{\sum_{i\neq b}\sum_{j\in\mathcal{C}_i} L_{i,bm}^{(\mathrm{cc})}\left(\mathbf{h}_{i,bm}^{(\mathrm{cc})}\right)^{\mathsf{H}}\mathbf{v}_{ij}x_{ij}^{(\mathrm{c})}}_{\text{Inter-cell cellular interference}} + \underbrace{\sum_{j\in\mathcal{D}} L_{j,bm}^{(\mathrm{dc})}h_{j,bm}^{(\mathrm{dc})}x_{j}^{(\mathrm{d})}}_{\text{D2D-to-cellular interference}} + z_{bm}^{(\mathrm{c})}, \tag{6.1}$$

where $\mathbf{h}_{l,bm}^{(\mathrm{cc})} \in \mathbb{C}^A$ ($L_{l,bm}^{(\mathrm{cc})} \in \mathbb{R}_+$), $l \in \{b, i\}$, denotes the channel fading vector (path-loss) from for cellular user m in cell b to the BS l. Correspondingly, $\mathbf{v}_{uv} \in \mathbb{C}^A$, $uv \in \{bm, bj, ij\}$, is the downlink precoding/beamforming vector for cellular user v in cell u. We use $h_{j,bm}^{(\mathrm{dc})} \in \mathbb{C}$ ($L_{j,bm}^{(\mathrm{dc})} \in \mathbb{R}_+$) to denote the channel (path-loss) from D2D transceiver j to cellular user m in cell b. Further, $x_j^{(\mathrm{d})} \in \mathbb{C}$ refers to the signals sent by D2D transceiver j, while $x_{uv}^{(\mathrm{c})} \in \mathbb{C}$, $uv \in \{bm, bj, ij\}$, denotes the signal from BS u intended to transmit to the cellular user v. In addition, we assume that all transmitted signals are normalized so that $|x_{uv}^{(\mathrm{c})}|^2 = |x_j^{(\mathrm{d})}|^2 = 1$, $u = 1, \ldots, B, \forall v \in \mathcal{C}_u$, $\forall j \in \mathcal{D}$. Further, $z_{bm}^{(\mathrm{c})} \in \mathbb{C}$ refers to the thermal noise at cellular user m in cell b, and it is distributed as $z_{bm}^{(\mathrm{c})} \sim \mathcal{CN}(0, \sigma_c^2)$.

Let's consider a typical D2D link constituted by two D2D transceivers n and n' which can communicate simultaneously in both directions in a spectrum-time slot. Using a similar approach, the received signal at D2D transceiver $n \in \mathcal{D}$ is given by

$$y_n^{(\mathrm{d})} = \sqrt{P_n}L_{n',n}^{(\mathrm{dd})}h_{n',n}^{(\mathrm{dd})}x_n^{(\mathrm{d})} + \underbrace{\sum_{b=1}^{B}\sum_{m\in\mathcal{C}_b} L_{b,n}^{(\mathrm{cd})}\left(\mathbf{h}_{b,n}^{(\mathrm{cd})}\right)^{\mathsf{H}}\mathbf{v}_{bm}x_{bm}^{(\mathrm{c})}}_{\text{Cellular-to-D2D interference}}$$
$$+ \underbrace{\sum_{j\in\mathcal{D}\setminus\{n,n'\}} \sqrt{P_j}L_{j,n}^{(\mathrm{dd})}h_{j,n}^{(\mathrm{dd})}x_j^{(\mathrm{d})}}_{\text{Intra-D2D interference}} + s_n + z_n^{(\mathrm{d})}, \tag{6.2}$$

where $x_u^{(\mathrm{d})} \in \mathbb{C}$, $u \in \{n, j\}$, denotes the signal sent by the D2D transceiver $u \in \mathcal{D}$, and $\mathbf{h}_{b,n}^{(\mathrm{cd})} \in \mathbb{C}^A$ ($L_{b,n}^{(\mathrm{cd})} \in \mathbb{R}_+$) denotes the vector channel (path-loss) from D2D transceiver n to the BS b. In addition, $h_{j,n}^{(\mathrm{dd})} \in \mathbb{C}$ ($L_{j,n}^{(\mathrm{dd})} \in \mathbb{R}_+$) denotes the channel (path-loss) from D2D transceiver j to the D2D transceiver n. Here, s_n is the residual self-interference (SI) caused by imperfect cancellation of FD operation. We adopt an SI model in which the residual interference is reflected in the self-interference-to-power-ratio (SIPR) β so that $|s_n|^2 = \beta P_n$ given by [71, 122] with P_n being the instantaneous transmit power at the D2D transceiver n. $z_n^{(\mathrm{d})} \in \mathbb{C}$ is the thermal noise at D2D

transceiver n and it is also distributed as $z_n^{(\mathrm{d})} \sim \mathcal{CN}(0, \sigma_d^2)$, $\forall n \in \mathcal{D}$, with σ_d^2 being the noise power at the D2D receiver. From (6.2), the received signal at other D2D transceiver n' can be obtained by replacing the index n with n' and vise versa, but we omit its derivation here for the sake of a concise presentation. In this chapter, as D2D and cellular transmission operate in downlink, we can assume that the D2D and cellular receivers have identical noise powers, denoted as $\sigma^2 \triangleq \sigma_d^2 = \sigma_c^2$.

This work assumes uniform linear array (ULA) antennas being employed at each BS. We model the channel vector $\mathbf{h}^{(\cdot)}$ from D2D/cellular users to BS as [142] $\mathbf{h}^{(\cdot)} = [\mathbf{A} \quad \mathbf{0}_{A\times A-P}] \times \hat{\mathbf{h}}^{(\cdot)}$, where $\hat{\mathbf{h}}^{(\cdot)}$ denotes the fast fading channel vector. Each vector element is independent and identically distributed (i.i.d.) and follows the Rayleigh distribution with zero mean and unit variance. Additionally, $\mathbf{0}_{A\times A-P}$ is the $A \times A - P$ zero matrix. Here, P represents the fixed number of angular dimensions. The steering matrix $\mathbf{A} = [\mathbf{a}(\phi_1), \ldots, \mathbf{a}(\phi_P)] \in \mathbb{C}^{A\times P}$ is composed of the steering vectors $\mathbf{a}(\phi)$ defined as

$$\mathbf{a}(\phi) = \frac{1}{\sqrt{P}} \left[1, e^{-\mathrm{i}2\pi w \sin(\phi)}, \ldots, e^{-\mathrm{i}2\pi w(A-1)\sin(\phi)}\right],$$

where w is the antenna spacing in multiples of the wavelength and $\phi_p = -\pi/2 + (p-1)\pi/P$, $p = 1, \ldots, P$, are uniformly distributed angles of transmission.

Before processing further, to avoid cumbersome equations with many denotations in our subsequent derivations, we define the overall channel power gains as

$$\begin{aligned} g_{j,bm}^{(\mathrm{dc})} &\triangleq L_{j,bm}^{(\mathrm{dc})} h_{j,bm}^{(\mathrm{dc})}, \\ g_{u,n}^{(\mathrm{dd})} &\triangleq L_{u,n}^{(\mathrm{dd})} h_{u,n}^{(\mathrm{dd})},\ u \in \{n', j\}, \\ \left(\mathbf{g}_{b,n}^{(\mathrm{cd})}\right)^{\mathsf{H}} &\triangleq L_{b,n}^{(\mathrm{cd})} \left(\mathbf{h}_{b,n}^{(\mathrm{cd})}\right)^{\mathsf{H}}, \\ \left(\mathbf{g}_{l,bm}^{(\mathrm{cc})}\right)^{\mathsf{H}} &\triangleq L_{l,bm}^{(\mathrm{cc})} \left(\mathbf{h}_{l,bm}^{(\mathrm{cc})}\right)^{\mathsf{H}},\ l \in \{b, i\}. \end{aligned} \tag{6.3}$$

6.2.2 Problem Formulation

Given the system model, we now define the desired performance metrics, including SINR and sum-rate of cellular/D2D links, and correspondingly formulate the optimization problem. From the received signal in (6.1), the SINR at the cellular receiver m in cell b can be written as

$$\mathrm{SINR}_{bm}^{(\mathrm{c})} = \frac{\left|\left(\mathbf{g}_{b,bm}^{(\mathrm{cc})}\right)^{\mathsf{H}} \mathbf{v}_{bm}\right|^2}{I_{bm}^{(\mathrm{c})} + \sigma^2}, \tag{6.4}$$

where the term $I_{bm}^{(\mathrm{c})}$ represents the aggregate interference power caused by both cellular and D2D transmission, and it is given by

$$I_{bm}^{(\mathrm{c})} = \sum_{j \in \mathcal{C}_b \setminus \{m\}} \left| \left(\mathbf{g}_{b,bm}^{(\mathrm{cc})} \right)^{\mathsf{H}} \mathbf{v}_{bj} \right|^2 + \sum_{i \neq b} \sum_{j \in \mathcal{C}_i} \left| \left(\mathbf{g}_{i,bm}^{(\mathrm{cc})} \right)^{\mathsf{H}} \mathbf{v}_{ij} \right|^2 + \sum_{j \in \mathcal{D}} P_j \left| g_{j,bm}^{(\mathrm{dc})} \right|^2. \tag{6.5}$$

Treating the interference as noise, the achievable rate of cellular link m in cell b can be computed by invoking the Shannon's capacity formula as

$$R_{bm}^{(\mathrm{c})} = \log_2 \left(1 + \mathrm{SINR}_{bm}^{(\mathrm{c})} \right). \tag{6.6}$$

Meanwhile, for a FD D2D link constituted by D2D transceivers n and n', the received SINR of D2D the transceiver n can be written from (6.2) as

$$\mathrm{SINR}_{n}^{(\mathrm{d})} = \frac{P_n \left| g_{n',n}^{(\mathrm{dd})} \right|^2}{I_n^{(\mathrm{d})} + \beta P_n + \sigma^2}, \tag{6.7}$$

where

$$I_n^{(\mathrm{d})} \triangleq \sum_{b=1}^{B} \sum_{m \in \mathcal{C}_b} \left| \left(\mathbf{g}_{b,n}^{(\mathrm{cd})} \right)^{\mathsf{H}} \mathbf{v}_{bm} \right|^2 + \sum_{j \in \mathcal{D} \setminus \{n,n'\}} P_j \left| g_{j,n}^{(\mathrm{dd})} \right|^2 \tag{6.8}$$

denotes the aggregate interference power caused by other D2D and cellular transmission. Likewise, the received SINR at D2D the transceiver n', denoted as $\mathrm{SINR}_{n'}^{(\mathrm{d})}$, can be obtained by replacing the index n with n' in (6.7) and (6.8) and vise versa. As a result, the achievable rate of corresponding FD D2D link is given by

$$R_n^{(\mathrm{d})} = \log_2 \left(1 + \mathrm{SINR}_{n}^{(\mathrm{d})} \right) + \log_2 \left(1 + \mathrm{SINR}_{n'}^{(\mathrm{d})} \right). \tag{6.9}$$

This thesis uses the network sum-rate of both cellular and D2D links over a cell as the optimization objective under the constraints on the target (minimum required) SINR at both cellular and D2D transmission and maximum transmit powers of D2D transmitters and BSs, denoted as P_d and P_c, respectively. Without generality, we can assume that D2D (cellular) users have equal

target SINR γ_d (γ_c). The optimization problem therefore can be mathematically formulated as

$$\max_{\mathbf{p},\mathbf{V}} \quad R \triangleq \frac{1}{B}\sum_{b=1}^{B}\sum_{k\in\mathcal{C}_b} R_{bm}^{(\mathrm{c})} + \frac{1}{B}\sum_{n\in\mathcal{D}} R_n^{(\mathrm{d})} \tag{6.10a}$$

$$\text{s.t.} \quad \mathrm{SINR}_{bm}^{(\mathrm{c})} \geq \gamma_c,\ b = 1,\ldots,B,\ \forall m \in \mathcal{C}_b, \tag{6.10b}$$

$$\mathrm{SINR}_n^{(\mathrm{d})} \geq \gamma_d,\ \forall n \in \mathcal{D}, \tag{6.10c}$$

$$\sum_{m\in\mathcal{C}_b} |\mathbf{v}_{bm}|^2 \leq P_c,\ b = 1,\ldots,B, \tag{6.10d}$$

$$P_n \leq P_d,\ \forall n \in \mathcal{D}, \tag{6.10e}$$

where $\mathbf{V}$ refers to the beamformer collection $\{\mathbf{v}_{bm}\}$ and $\mathbf{p}$ is the D2D transmit power vector.

6.3 Joint Beamforming and Power Allocation Algorithm

In this section, we focus on addressing the optimal solution of (6.10a-e). The problem (6.10a-e) involves continuous nonconvex optimization, and it is not possible to directly obtain the globally optimal solution. To overcome this issue, we propose to apply fractional programming (FP) tools [141] to transform (6.10a-e) into a sequence of convex problems in which each problem can be solved effectively by standard convex optimization techniques. More specifically, the FP-based approach exploits the fractional structure of the objective function so that we can develop a sequential convex programming algorithm that approximately locates the globally optimal point with a low complexity. Such an approach is possible when the objective function exhibits a sum-ratio form of $\sum_n f\left(A_n(\mathbf{x})/B_n(\mathbf{x})\right)$. Additionally, $f(\cdot)$ is a nondecreasing and concave function, while the functions $A_n(\mathbf{x}) : \mathbb{C}^u \to \mathbb{R}$ and $B_n(\mathbf{x}) : \mathbb{C}^u \to \mathbb{R}$, $u \geq 1$, are convex and concave w.r.t. $\mathbf{x}$, respectively.

Let first consider the case in which the numerator function $A_n(\cdot)$ can be represented by a quadratic form $A_n(\mathbf{x}) = a_n^2(\mathbf{x})$ with $a_n(\mathbf{x}) : \mathbb{C}^u \to \mathbb{R}$ being a multidimensional and real-valued function. By adopting the quadratic transform of A_n/B_n to $2q_n a_n - q_n^2 B_n$ [141], the optimization problem

$$\max_{\mathbf{x}} \quad \sum_n f\left(A_n(\mathbf{x})/B_n(\mathbf{x})\right) \tag{6.11}$$

$$\text{s.t.} \quad \mathbf{x} \in \mathcal{X},$$

where $\mathcal{X}$ represents the nonempty convex set of constraints, is equivalent to [141]

$$\begin{aligned} \max_{\mathbf{x},q_n} \quad & \sum_n f\left(2q_n a_n(\mathbf{x}) - q_n^2 B_n(\mathbf{x})\right) \\ \text{s.t.} \quad & \mathbf{x} \in \mathcal{X}. \end{aligned} \tag{6.12}$$

In (6.12), $q_n \in \mathbb{R}$ refers to an auxiliary variable, and it is optimized when $\mathbf{x}$ is held fixed as $q_n^\star = a_n(\mathbf{x})/B_n$.

For an alternative case in which the numerator of f is represented by an expanded multiplication $A_n(\mathbf{x}) = a_n(\mathbf{x})\bar{a}_n(\mathbf{x})$ with $a_n(\mathbf{x}) : \mathbb{C}^u \to \mathbb{C}$ being a multidimensional and complex-valued function, the problem (6.11) is now equivalent to [141]

$$\begin{aligned} \max_{\mathbf{x},q_n} \quad & \sum_n f\left(2\text{Re}\left(\bar{q}_n a_n(\mathbf{x})\right) - \bar{q}_n B_n(\mathbf{x}) q_n\right) \\ \text{s.t.} \quad & \mathbf{x} \in \mathcal{X}, \end{aligned} \tag{6.13}$$

where the auxiliary variables $q_n \in \mathbb{C}$ are also optimized at $q_n^\star = a_n(\mathbf{x})/B_n(\mathbf{x})$.

The argument function of each outer function f is now convex w.r.t. $\mathbf{x}$ and fixed q_n, and the transformed optimization problems (6.12) and (6.13) become convex. As a result, the global optimal solution can be achieved by solving a sequence of convex optimization subproblems that find the optimal $\mathbf{x}$ and q_n in an iterative fashion.

Based on the transformed convex problems (6.12) and (6.13), we now focus on resolving the joint beamforming and power allocation problem (6.10). Although the argument in each cellular/D2D link rate component of the objective function in (6.10) is not in a direct ratio form (i.e., $1 +$ SINR), the SINR terms of such objective function are in fractional form. Since the logarithm function $\log_2(\cdot)$ is nondecreasing and concave and each SINR term resides in the logarithm function, the quadratic transforms can be directly applied to the SINR terms [141]. The detailed procedure is provided as follows.

Applying the quadratic transform to each SINR term and following (6.12) and (6.13), the optimization problem (6.10) can be transformed to

$$\begin{aligned} \max_{\mathbf{p},\mathbf{V},\{q_{bm}^{(\text{c})}\},\{q_n^{(\text{d})}\}} \quad & f_{\text{FR}} = \frac{1}{B}\sum_{b=1}^{B}\sum_{m\in\mathcal{C}_b} f_{bm}^{(\text{c})} + \frac{1}{B}\sum_{n\in\mathcal{D}} f_n^{(\text{d})}. \\ \text{s.t.} \quad & (6.10b) - (6.10e). \end{aligned} \tag{6.14}$$

Here, $\{q_{bm}^{(\text{c})}\}$ and $\{q_n^{(\text{d})}\}$ refer to the collections of auxiliary variables corresponding to the cellular

and D2D sum-rates, respectively. In the objective function of (6.14), using $\left|\left(\mathbf{g}_{b,bm}^{(\mathrm{cc})}\right)^{\mathsf{H}}\mathbf{v}_{bm}\right|^2 = \left(\mathbf{g}_{b,bm}^{(\mathrm{cc})}\right)^{\mathsf{H}}\mathbf{v}_{bm}\left(\mathbf{v}_{bm}\right)^{\mathsf{H}}\mathbf{g}_{b,bm}^{(\mathrm{cc})}$, the component $f_{bm}^{(\mathrm{c})}$ can be expressed from (6.13) as follows:

$$f_{bm}^{(\mathrm{c})} = \log_2\left(1 + 2\mathrm{Re}\left(2\bar{q}_{bm}^{(\mathrm{c})}\left(\mathbf{g}_{b,bm}^{(\mathrm{cc})}\right)^{\mathsf{H}}\mathbf{v}_{bm}\right) - \bar{q}_{bm}^{(\mathrm{c})}\left(I_{bm}^{(\mathrm{c})} + \sigma^2\right)q_{bm}^{(\mathrm{c})}\right). \tag{6.15}$$

Meanwhile, the component $f_n^{(\mathrm{d})}$ is provided from (6.12) by

$$f_n^{(\mathrm{d})} = \log_2\left(1 + 2q_n^{(\mathrm{d})}\sqrt{P_n}\left|g_{n',n}^{(\mathrm{dd})}\right| - 2\left(q_n^{(\mathrm{d})}\right)^2\left(I_n^{(\mathrm{d})} + \beta P_n + \sigma^2\right)\right). \tag{6.16}$$

From (6.15) and (6.16), we observe that, as the logarithmic function $\log_2(\cdot)$ is nondecreasing and concave, the optimization problem (6.14) is a convex problem of $\mathbf{V}$ and $\mathbf{p}$ when the auxiliary variables $\{q_{bm}^{(\mathrm{c})}\}$ and $\{q_n^{(\mathrm{d})}\}$ are held fixed. It follows that, the optimal $q_{bm}^{(\mathrm{c})}$ and $q_n^{(\mathrm{d})}$ for fixed $\mathbf{v}_{bm}$ and P_n are given by

$$q_{bm}^{(\mathrm{c})} = \left(\mathbf{g}_{b,bm}^{(\mathrm{cc})}\right)^{\mathsf{H}}\mathbf{v}_{bm}\left(I_{bm}^{(\mathrm{c})} + \sigma^2\right)^{-1}, \quad b = 1,\ldots,B, \forall m \in \mathcal{C}_b, \tag{6.17}$$

$$q_n^{(\mathrm{d})} = \sqrt{P_n}\left|g_{n',n}^{(\mathrm{dd})}\right|\left(I_n^{(\mathrm{d})} + \beta P_n + \sigma^2\right)^{-1}, \quad \forall n \in \mathcal{D}. \tag{6.18}$$

The convex optimization problem (6.14) allows to develop an iterative algorithm in order to solve (6.10) as follows. The iterative algorithm generates a sequence $\mathbf{V}$ and $\mathbf{p}$ to improve the optimal solutions. From the first feasible solution of $\mathbf{V}$ and $\mathbf{p}$ that is randomly generated, at each iteration, we compute the optimal values of $\{q_{bm}^{(\mathrm{c})}\}$ and $\{q_n^{(\mathrm{d})}\}$ and subsequently locate the optimal solution of the convex program (6.14), which can be solved effectively by using standard convex programming techniques. Because the constraint set $(6.10b) - (6.10e)$ is convex, the sequence $\mathbf{V}$ and $\mathbf{p}$ always converges [141]. We can set to stop the iterative algorithm when the objective function f_{FR} converges, i.e., its absolute improvement is less than a desired (pre-selected) threshold ϵ. For convenience, the iterative joint beamforming and power allocation algorithm based on FR programming is summarized in Algorithm 2.

Algorithm 2 Iterative FP-based algorithm

1: Initiate a feasible solution of $\mathbf{v}_{bm}$ and $\mathbf{p}$ and choose ϵ.
2: **repeat**
3: Compute $\{q_{bm}^{(\mathrm{c})}\}$ and $\{q_n^{(\mathrm{d})}\}$ given by (6.17) and (6.18).
4: Solve the convex program (6.14) to obtain optimal $\mathbf{V}^\star$, $\mathbf{p}^\star$, and $f_{\mathrm{FR}}^\star$.
5: **until** f_{FR} converges, i.e., $|f_{\mathrm{FR}} - f_{\mathrm{FR}}^\star| \leq \epsilon$

6.4 Illustrative Results

In this section, numerical results are presented to compare the achievable network sum-rates (per cell) of both cellular and D2D links, provided by FP-based algorithm developed in previous section, for the FD D2D, HD D2D, and pure massive MIMO cellular systems (in absence of D2D transmission). The behaviors of such sum-rates under the effect of various networking parameters such as SIC level, D2D link distance, and number of active D2D links per cell are also illustrated.

Our Monte Carlo simulations are performed as follows. We consider a multi-cell network consisting of three hexagonal-cells as shown in Fig. 6.1. The cellular users and D2D transceivers are dropped randomly within the cell region. Each D2D transceiver is located uniformly in the circle where the radius equals a fixed D2D link distance r and the corresponding D2D transceiver is located at the origin. The path-loss parameters correspond to a carrier frequency of 2 GHz, while the channel fast fading are generated independently according to a complex Gaussian distribution with unit variance. With regards to the steering matrix $\mathbf{A}$, we select the number of angular dimension $P = A/2$ and the antenna spacing $w = 0.3$ provided in [142]. In FP-based algorithm, the rate improvement threshold of iterative algorithm is chosen as ϵ.

In our simulations, we assume that cellular users are located outside of the buildings (i.e., outdoor) and in the urban macrocells. In addition, we consider two D2D-related propagation scenarios in which the D2D users are located either outside or inside of the buildings in urban areas (i.e., outdoor and indoor, respectively). We denote these two scenarios as outdoor and indoor D2D transmission, respectively. For outdoor D2D transmission, we consider a similar channel model to that of Chapter 5, yet focusing on downlink, in which 3GPP macrocell propagation model (urban area) is adopted [20, 138]. For indoor D2D transmission, we consider the setting where the D2D transceivers are located inside indoor RRH/Hotzone [20, 143]. Unless stated otherwise, the network parameters used in both outdoor and indoor D2D transmission scenarios are provided in Tables 6.1.

6.4.1 Outdoor D2D Transmission

In this section, the illustrative results of outdoor D2D transmission scenario will be represented. The path-loss parameters for this scenario are provided in Tables 6.2. We should note that, for a concise representation, we denote UE as either cellular user (CU) or D2D user.

For FD and HD D2D performance comparison, we first establish the FD-to-HD network sum-rate ratio and plot it versus SIPR β in dB in Fig. 6.2. The numbers of cellular and D2D links per cell are chosen as $M = 4$ and $N \in \{14, 30\}$ links/cell, respectively. In addition, the D2D link

Table 6.1 Common Simulation Parameters of Outdoor and Indoor D2D

Carrier frequency	2 GHz
Channel bandwidth	10 MHz
Cell area	$\pi 500^2$ m^2
Number of cells	3
Number of antennas at BS A	$\{16, 32\}$
Number of angular dimension $P = A/2$ [142]	$\{8, 16\}$
Antenna spacing ω [142]	0.3
Number of cellular users per cell M	4
Number of D2D links per cell N	$[10,\ 40]$
D2D link distance r [20]	$\{20, 50\}$ m
Total BS transmit power P_c [138]	46 dBm
Maximum D2D transmit power P_d	23 dBm
Noise PSD	-174 dBm/Hz
Receiver noise figure	9 dB
Self-interference-to-power-ratio β	$[-120, -60]$ dB
Target SINR $\gamma_c = \gamma_d$	0 dB
Improvement threshold ϵ	10^{-5} dB

Table 6.2 Path-Loss Parameters of Outdoor D2D Transmission

Path-loss of BS-UE channels [20, 138]	$15.3 + 37.6 \log(r)$, r in m
Path-loss of UE-UE channels [20, 138]	$15.3 + 37.6 \log(r)$, r in m

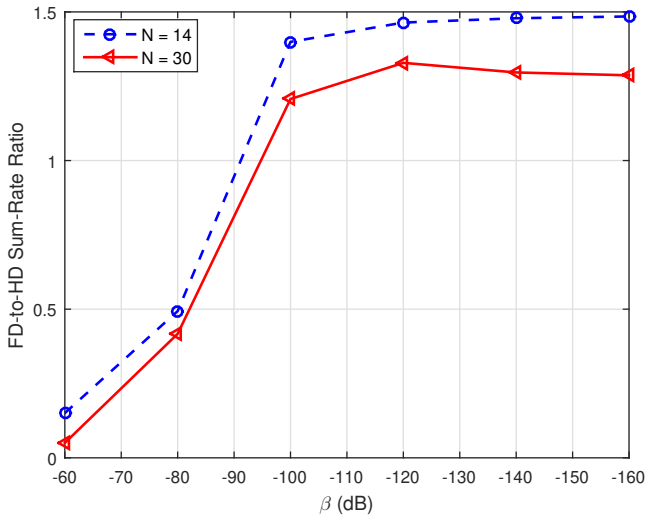

Fig. 6.2 FD-to-HD network sum-rate ratio versus SIPR.

distance is $r = 50$ m, while the number of antennas equals $A = 16$. The obtained results show that FD D2D can offer better sum-rate than HD D2D with SIPR $\beta \leq -95$ dB. For $\beta \leq -100$ dB, the FD-to-HD D2D sum-rate ratios seem to be fixed around 1.45 and 1.30 for $N = 14$ and $N = 30$ links/cell, respectively. From the obtained results, we observe that, for outdoor D2D transmission scenario, the SIC level of 100 dB is sufficient to provide the best sum-rate ratio.

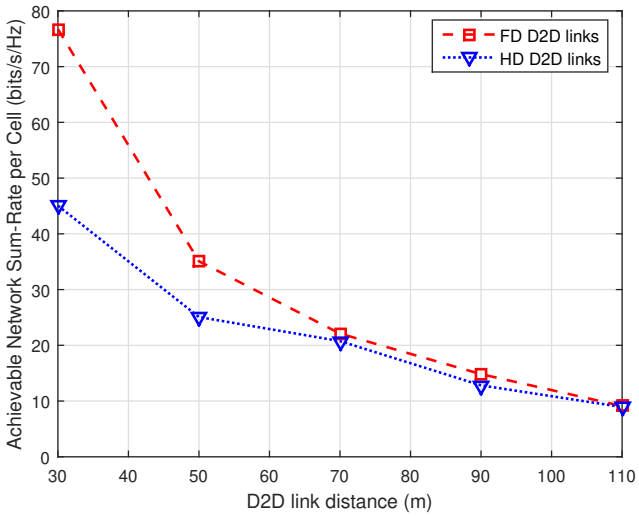

Fig. 6.3 Achievable network sum-rate (per cell) for different D2D link distances.

In Fig. 6.3, we plot network sum-rate (over a cell) for both FD and HD D2D transmission versus maximum D2D link distance for $N = 14$ links/cell, $A = 16$ antennas, and $\beta = -100$ dB. The obtained results demonstrate a significant D2D link sum-rate achieved, especially with FD D2D at short distances. As the D2D link distance increases, the achieved network sum-rate exponentially reduces. Interestingly, we observe that, as the D2D link distance exceeds 70 m, the sum-rate performances of FD and HD D2D are almost identical. This result indicates that, with sufficiently large D2D link distances, FD D2D is no longer beneficial in terms of spectral efficiency gain as compared to HD D2D operated in the same outdoor environment. This is because, with increasing D2D link distance, D2D transceivers, in average, are located closer, thus causing more interference to each other.

In Fig. 6.4, we plot the achieved network sum-rate versus the number of D2D links over a cell under the consideration of FD and HD D2D. Furthermore, various numbers of antennas equipped at BSs are considered, i.e., $A \in \{1, 16, 32\}$, in order to demonstrate the advantage of ULA. Here, the case $A = 1$ corresponds to the omni-directional transmission at BSs. In the simulations for Fig. 6.4, we assume the D2D link distance as $r = 50$ m, while the numbers of D2D links are from

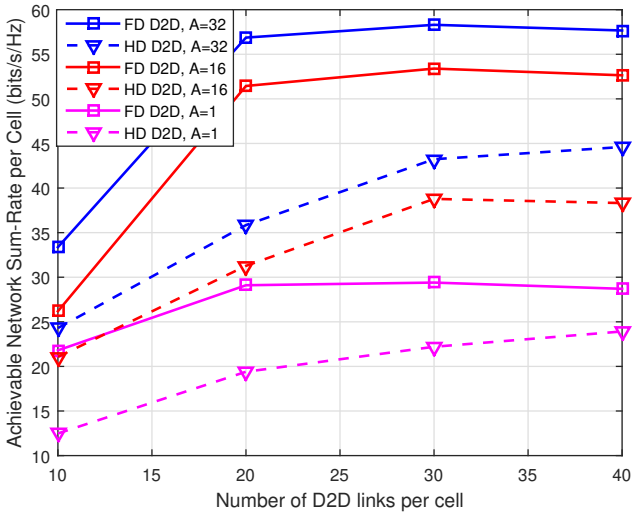

Fig. 6.4 Achievable network sum-rate versus number of D2D links (per cell) when D2D links operate in FD and HD modes.

$N = 10$ to $N = 40$ links/cells. In addition, the SIC level is chosen as $\beta = -100$ dB. From Fig. 6.4, it can be seen that the network sum-rate for both FD and HD D2D increases as the number of D2D links N increases. However, such an increase in sum-rate performance gets compressed when N is beyond a certain threshold. For instance, the sum-rates of FD and H2D D2D links reach the limit at $N = 20$ links/cell and $N = 30$ links/cell, respectively. In particular, at $N = 30$ links/cell and $A = 16$ antennas, the network sum-rates (over all cell) for FD and HD D2D are 53.40 and 30.16 bits/s/Hz, respectively. Hence, with $N \geq 30$ links/cell and $A = 16$ antennas, the FD-to-HD sum-rate ratio is fixed around 1.77. This can be explained by the fact that the number of D2D links satisfying the SINR constraints will stop increasing at a sufficiently high D2D link density. We also observe that the network sum-rates offered by ULA-equipped BSs (i.e., $A \in \{16, 32\}$ antennas) significantly outperform those achieved by omni-directional transmission (i.e., $A = 1$ antenna) at BSs in both FD and HD D2D. For instance, at $N = 40$ links/cells and $A = 16$ antennas ($A = 32$ antennas), the ULA-equipped BSs provide 1.83 (2.01) and 1.60 (1.86) times better in terms of network sum-rate as compared to omni transmission for FD and HD D2D, respectively. Not surprisingly, increasing the number of equipped antennas at BSs allows to improve the sum-rate performance since narrower beams can be formed, thus reducing the interference caused by the cellular transmission. However, in agreement with the case of $A = 16$ antennas, the offered network sum-rate with $A = 32$ antennas also stops increasing at $N \geq 20$ links/cell ($N \geq 30$ links/cell) for FD (HD) D2D due to the intra-D2D interference.

By defining the spectral efficiency gain as the ratio of the network sum-rate (provided in Fig.

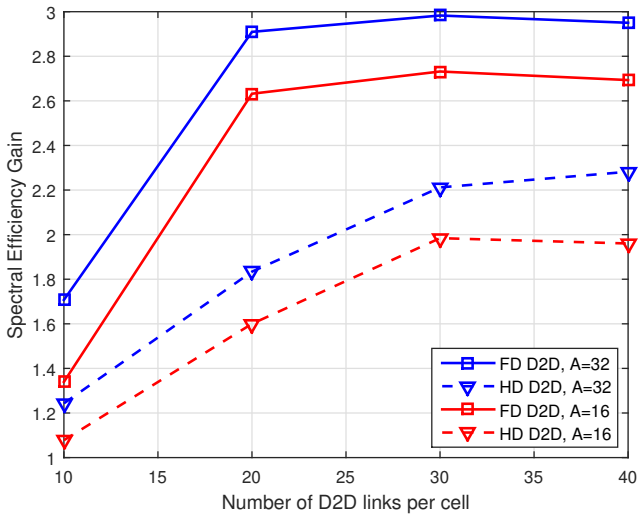

Fig. 6.5 Spectral efficiency gain versus number of D2D links (per cell) when D2D links operate in FD and HD modes.

6.4) to the achievable sum-rate of only cellular links (operating alone without D2D links in the same environmental conditions), Fig. 6.5 plots the resulting spectral efficiency gain versus the number of active D2D link over a cell. Given the D2D link distance $r = 50\,\text{m}$, SIC level $\beta = -100\,\text{dB}$, and number of antennas equipped at BSs $A \in \{16, 32\}$, the results in Fig. 6.5 indicate that, over the wide D2D link density range from 10 to 40 links/cell, the spectral efficiency gain linearly increases with the D2D link number for the cases of FD and HD D2D to a sufficiently high number of active D2D links. Additionally, it is beneficial to employ more antennas at BSs since the spectral efficiency gain is improved when the number of antennas increases from $A = 16$ to $A = 32$. For instance, at the D2D link number of 20 links/cell and $A = 16$ antennas ($A = 32$ antennas), FD D2D offers a spectral efficiency gain of 2.61 (2.91) as compared to pure cellular transmission. Meanwhile, HD D2D provides a spectral efficiency gain of 2.00 (2.21) at the D2D link number of 30 links/cell and $A = 16$ antennas ($A = 32$ antennas). Similar to the observation in Fig. 6.4, for the number of active FD (HD) D2D links beyond 20 (30) links/cell, the increase in spectral efficiency gain will eventually get compressed, which implies that the increase in number of underlaid D2D links will not bring further sum-rate improvement. This result illustrates the number of active D2D links should be chosen to optimize spectral efficiency gains offered by the underlaid D2D services.

6.4.2 Indoor D2D Transmission

In this section, we provide the numerical results for the indoor D2D transmission scenario in which D2D users are located inside of the building, while CUs are located outside in urban macro-cell environment. As aforementioned, D2D transceivers are located inside indoor RRH/Hotzone [20, 143]. The direct D2D transmission is assumed to be inside the same building as the indoor RRH/Hotzone, while the transmission from a D2D transmitter to cellular users or interfered D2D receivers is assumed to be outside the same building as the indoor hotzone. The path-loss, penetration loss, and lognornal shadowing parameters for the indoor D2D transmission scenario are provided in Tables 6.3 where the indoor RRH/Hotzone-related parameters are given in [143, Table A.2.1.1.5].

Table 6.3 Path-Loss and Shadowing Parameters of Indoor D2D Transmission

BS-CU channels [138]	Path-loss Lognormal Shadowing σ	$15.3 + 37.6\log(r)$, r in m 7 dB
BS-D2D channels [143]	Path-loss Penetration loss Lognormal Shadowing σ	$2.7 + 42.8\log(r)$, r in m 20 dB 10 dB
Direct D2D channels [143]	Path-loss Lognormal Shadowing σ	$17.5 + 43.3\log(r)$, r in m 4 dB
D2D-UE channels [143]	Path-loss Penetration loss Lognormal Shadowing σ	$\max\{17.5 + 43.3\log(r), 2.7 + 42.8\log(r)\}$, r in m 20 dB 10 dB

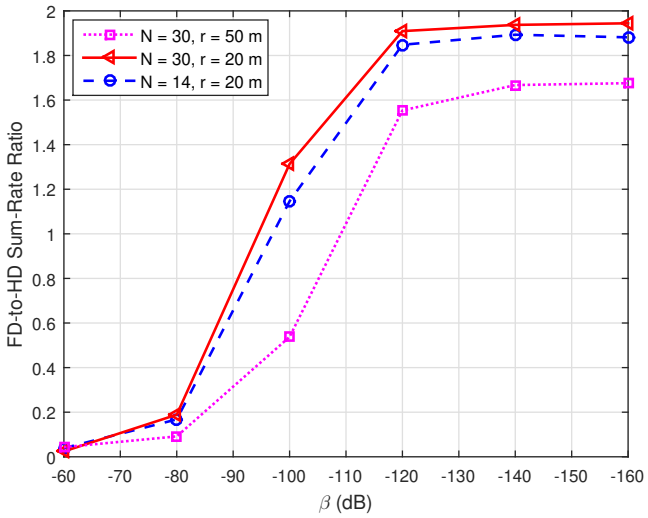

Fig. 6.6 FD-to-HD network sum-rate ratio versus SIPR.

In Fig. 6.6, we first demonstrate the FD-to-HD network sum-rate ratio versus SIPR β in dB so as to compare FD and HD D2D sum-rate performances. The numbers of cellular and D2D links per cell are chosen as $M = 4$ and $N \in \{14, 30\}$, respectively. In addition, the D2D link distance is chosen as $r \in \{20, 50\}$ m for $N = 30$ links/cell. Meanwhile, the number of antennas equipped at BSs is $A = 16$. The results show that FD D2D can offer better sum-rate than HD D2D with SIPR $\beta \leq -100$ dB. We also observe that, for indoor D2D transmission, FD D2D can offer significant sum-rate improvement (as compared to HD D2D) when $\beta \leq -120$ dB. Further, as $\beta \leq -120$ dB and D2D link distance $r = 20$ m, the FD-to-HD D2D sum-rate ratios seem to stop improving and get fixed around 1.85 and 1.90 for $N = 14$ and $N = 30$ D2D links/cell, respectively. When the D2D link distance increases to $r = 50$ m, the FD-to-HD D2D sum-rate ratio reduces to 1.6 for $\beta \leq -120$ dB. This result indicates that the SIC level of $\beta = -120$ dB is sufficient to achieve the best FD-to-HD D2D sum-rate ratio for indoor D2D transmission.

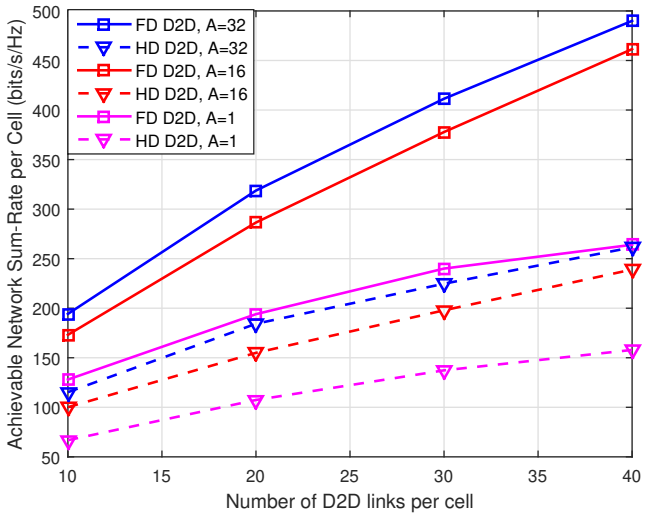

Fig. 6.7 Achievable network sum-rate versus number of D2D links (per cell).

In Fig. 6.7, we plot the network sum-rate (over a cell) versus number of D2D links per cell for D2D link distance $r = 20$ m and SIPR $\beta = -120$ dB. The range of D2D link numbers is chosen as $N \in [10, 40]$ links/cell. Similar to the case of outdoor D2D transmission, to demonstrate the benefit of ULA-equipped BSs, we also compare the network sum-rates between the cases of beamforming and omni-directional transmission under various number of antennas at BSs, i.e., $A \in \{1, 16, 32\}$ antennas. Fig. 6.7 illustrates that, as the number of D2D link increases, the achieved network sum-rate linearly increases. For instances, at $N = 10$ and $N = 40$ links/cell with $A = 16$ antennas, the achievable network sum-rates (per cell) for FD D2D are 173.13 and 461.47 bits/s/Hz, respectively,

while the network sum-rates for HD D2D are 100.10 and 235.77 bits/s/Hz, respectively. These results imply that, at $N = 10$ and $N = 40$ links/cell, FD D2D offers 1.73 and 1.95 times better in terms of network sum-rate, as compared to the HD D2D counterpart operating in the same indoor D2D environment. Fig. 6.7 also shows significant network sum-rates achieved by ULA-equipped BSs as compared to the omni-directional transmission. For instance, at $N = 40$ links/cell and $A = 16$ antennas ($A = 32$ antennas), ULA-equipped BSs offer 1.74 (1.86) and 1.51 (1.66) times better (in terms of network sum-rate) than the omni-directional transmission for FD and HD D2D services, respectively. Similar to the outdoor D2D scenario, as the number of D2D links increases further, these sum-rate gains will eventually converge since the number of D2D links satisfying the target SINR will stop increasing beyond a certain D2D link density.

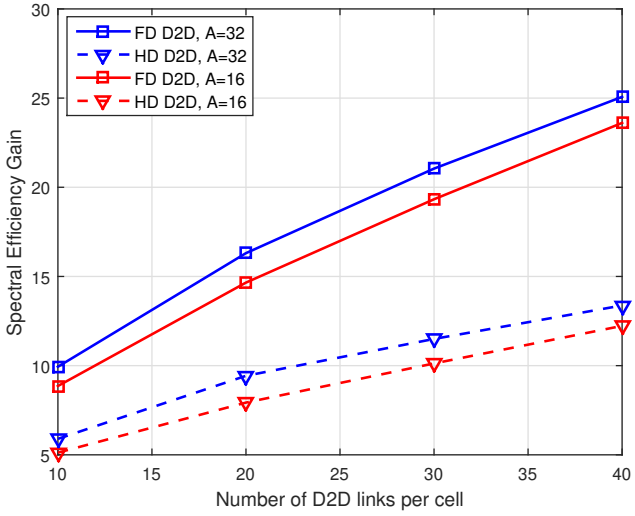

Fig. 6.8 Spectral efficiency gain versus number of D2D links (per cell).

Fig. 6.8 illustrates the resulting spectral efficiency gain versus the number of D2D links over a cell for D2D link distance $r = 20\,\text{m}$, the numbers of antennas equipped at BSs $A \in \{16, 32\}$, and SIPR $\beta = -120\,\text{dB}$. Recall that the spectral efficiency gain is computed as the ratio of the network sum-rate to the achievable sum-rates of cellular links. We observe that, over various number of D2D links ranging from $N = 10$ to $N = 40$ links/cell, the spectral efficiency gain linearly increases with the number of D2D links for both HD and FD D2D. With a better SIC level of $120\,\text{dB}$, FD D2D offers a substantial improvement in the spectral efficiency gain as compared to HD D2D. For example, in Fig. 6.8, for a D2D link number of 40 links/cell with $A = 16$ antennas ($A = 32$ antennas), HD D2D achieves a spectral gain of 12.0 (13.37) while FD D2D can offer 23.6 (25.07). However, as the number of D2D links increases further, such a gain will reach the limit at

a sufficiently high D2D link density due to the dominant D2D interference.

6.5 Concluding Remarks

In this chapter, we have focused on multi-cell massive MIMO cellular networks being underlaid by FD D2D transmission. Specifically, we proposed a joint beamforming and power allocation scheme that maximizes the network sum-rate while protecting the D2D and cellular link. To deal with the non-convexity of the problem, a FP-based method was developed to transform the problem into a sequence of convex subproblems, which can be solved efficiently. For both indoor and outdoor D2D transmission, simulation results revealed that significant performance gains in term of spectral efficiency can be achieved in the considered FD network, especially in the indoor D2D scenario, as compared to the HD D2D counterpart and pure cellular transmission (in absent of D2D) with sufficient self-interference cancellation levels.

Chapter 7

Multi-Agent Reinforcement Learning Approach to Joint Channel Assignment and Power Allocation in Platoon-Based C-V2X Systems

7.1 Introduction

In this chapter, the focus is shifted from underlaid D2D services to highly mobile D2D-based C-V2X systems that support the communications between the vehicles in proximity as well as provide the connections from the vehicles to the networks. As discussed in Chapter 1, 3GPP enables the V2V services in cellular networks via D2D communications to satisfy the stringent latency requirement, reliable packet delivery, and high throughput demand of the C-V2X systems. In this chapter, we consider a single-cell C-V2X setting comprised of multiple V2V links who wish to reuse the time-frequency slots currently occupied by the existing (cellular) V2I uplinks. Additionally, we are interested in an innovative V2V transmission paradigm called V2V platooning in which multiple vehicles are grouped into a train-like platoon and the communications between participants is organized by a vehicle leader. In existing research, this paradigm has received increasing interest due to its significant benefits including reducing traffic congestion, saving vehicle fuel, and enhancing driving experience [7, 144]. Given the platoon-based C-V2X systems, we explore the coordination across the (vehicle) leaders where multiple V2V platoons are allowed to operate in the same time-frequency resources of the active V2I uplinks. In each time step, each platoon leader flexibly selects a V2I channel and adapts its transmit power accordingly so as to optimize the de-

sired objectives. In C-V2X systems, this mode is formally referred to as Mode 4 in which a V2V link can autonomously choose from a pool of radio resources to communicate [145, 146].

This chapter formulates a joint channel assignment and power allocation problem in which each platoon leader selects a combination of channel and transmit power from an available set of sub-bands and discrete power levels in order to simultaneously maximize the achievable sum-rate of V2I links and the packet delivery probability of V2V links. As mentioned in Chapter 2, the V2I sum-rate objective is chosen to represent the high throughput demand in the C-V2X applications, while the packet delivery probability objective of V2V service reflects the stringent latency constraint on safety message exchange between the vehicles. We define the V2V packet delivery probability as the probability of successfully transmitting a payload having size B within the time limitation T (i.e., latency constraint) [92–94].

In this chapter, we utilize reinforcement learning (RL), a distributed approach, to tackle the challenge of high CSI overhead in centralized optimization methods. Further, RL can work well with the hard-to-model objective function, e.g., the probability of successfully transmitting a payload having size B within the time limitation T, which is generally difficult to address by traditional distributed optimization approach. The RL approach allows to recast the original optimization problem as a multi-agent RL problem where each platoon leader, acting as an agent, gradually refines its channel and transmit power selection strategy via trial-and-error interacting with the vehicular environment. The proposed multi-agent RL approach is based on deep Q-learning, a well-known RL algorithm initially developed to deal with discrete control in video games [147]. In distributed resource allocation for the C-V2X services, deep Q-learning has been extensively adopted in joint channel assignment and power allocation design, e.g., in [92, 93], to which our work is most related. Ye *et al* in [92] focused on multi-agent RL in unicast and broadcast V2V communications in which a common deep Q-network (DQN) was shared among the agents. Subsequent work [93] was also concerned with the multi-agent RL design, yet a separate DQN was employed at each agent. In [92], the network trainer trained a single DQN by using the *global* states collected from all agents, while [93] only required *local* states to train the DQN at each agent with limited parameter exchange. Thus, the latter approach is more practical in training. Similar to [93], we adopt the multi-agent RL with a separate deep-Q network at each agent, and assume that all agents act simultaneously to optimize a common reward in each time step. However, we shall consider a different reward function design to that of [93]. More specifically, beside the weighted sum-rates of V2I and V2V links as in [93], we propose to incorporate the transmission time of the agents into the common reward function as a charged price. In the context of platoon-based V2V communications, the proposed reward design allows to improve the probability of successful V2V

payload delivery (as compared to that offered by the reward design in [93]), while satisfying the high sum-rate demand at V2I links.

Illustrative results show that the RL-based resource allocation algorithm can successfully learn and enable the V2V links to share the channels (time-frequency resources) with the V2I uplinks. As a result, the interference between V2V and V2I transmission can be effectively alleviated. Further, we demonstrate that, in terms of both successful V2V packet delivery probability and V2I sum-rate, the performance of multi-agent RL approach is close to that obtained by the centralized benchmark, particularly the exhaustive search algorithm. It is also worth to note that, the exhaustive search algorithm requires the global CSI at central controller, while the proposed RL-based algorithm only requires the local CSI available at each platoon leader.

The remainder of this chapter is organized as follows. In Section 7.2, we describe the system model of interest and formulate the optimization problem. Section 7.3 briefly introduces the concepts of RL and deep Q-learning, and represents the development of multi-agent RL algorithm. Numerical results are given in Section 7.4 to demonstrate the achieved performances. Finally, Section 7.5 concludes the chapter.

7.2 System Model and Problem Formulation

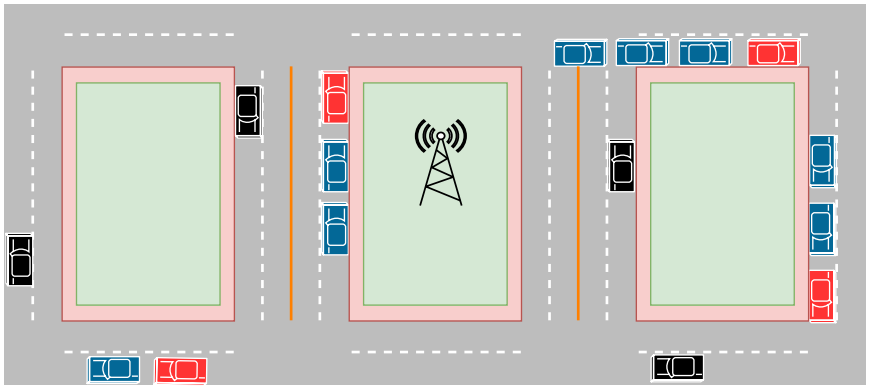

Fig. 7.1 An illustrative C-V2X system in single-cell setting for the urban environment (blue vehicle: platoon member, red vehicle: platoon leader, black vehicle: cellular (V2I) user).

As illustrated in Fig. 7.1, we consider C-V2X systems in a single-cell setting for the urban environment consisting of multiple V2I and V2V links. While the V2I links operate in the cellular uplink to connect the vehicles to the BS, the V2V links operate in a platoon fashion in which several vehicles are grouped into a train-like platoon to share common mobility modes [144]. In

addition, the communications between platoon members is organized by a leader; and the V2V communications is formed as the platoon leader periodically and simultaneously transmits the safety messages to all platoon members. Before processing further, to avoid confusion on the names of vehicle types, we denote the vehicle of a V2I link as cellular user, while the vehicle leader and member of a platoon are simply called platoon leader and platoon member, respectively.

In the considered vehicular network, let M be the overall number of cellular users and correspondingly V2I links. In addition, we assume that the cellular users transmit at a constant power P_c. Meanwhile, in the V2V platoons, the vehicles are in the same lane and maintain very close distances (e.g., few meters) between two adjacent vehicles. We denote the set of receiving members in a platoon as $\mathcal{V}_n$, $n = 1, \ldots, N$, i.e., there are N platoons and correspondingly N platoon leaders. The number of V2V links in platoon n is denoted as $V_n \triangleq |\mathcal{V}_n| - 1$. The transmit power vector of platoon leaders is defined as $\mathbf{p} = [P_1, \ldots, P_N] \in \mathbb{R}_+^N$, where P_n denotes the transmit power of leader in platoon n. Further, we assume that both cellular and platoon transceivers use single antenna to transmit and receive their signals.

Suppose that, at a given time slot, orthogonal carrier frequencies are assigned to the cellular users, i.e., each V2I link occupies a separate sub-band. Without the loss of generality, we assume that the V2I link m operates in the sub-band m (i.e., channel m). As a result, the number of channels equals M. In this chapter, the V2V platoons shall reuse the channels currently occupied by the cellular users. More specifically, in each time step, each platoon leader flexibly selects an active V2I channel and adapts its transmit power accordingly so as to simultaneously maximize the achievable sum-rate of V2I links and the successful packet delivery probability of V2V links.

Given the system model, we now define the desired performance metrics, including SINR and achievable rate of V2I and V2V links, and formulate the optimization problem. As each V2I link occupies a separate channel, the corresponding V2I receiver (i.e., BS) only experiences the interference caused by the platoon leaders. It follows that the SINR of a typical V2I link m can be written as

$$\text{SINR}_m^{(\text{c})} = \frac{P_c L_m^{(\text{cc})} g_m^{(\text{cc})}}{\sum\limits_{n=1}^{N} \rho_n(m) P_n L_{n,m}^{(\text{dc})} g_{n,m}^{(\text{dc})} + \sigma_c^2}, \tag{7.1}$$

where $L_m^{(\text{cc})}$ denotes the large-scale fading power, caused by path-loss and log-normal shadowing, of V2V link m. Similarly, $L_{n,m}^{(\text{dc})}$ refers to the large-scale fading power from platoon leader n to the receiver of V2I link m. Meanwhile, $g_m^{(\text{cc})}$ denotes to the small-scale fading power of link V2I m; and $g_{n,m}^{(\text{dc})}$ is the small-scale fading power from platoon leader n to the receiver of V2I link m. In

this work, we consider Rayleigh fading, i.e., the small-scale fading powers follow an exponential distribution with unit mean. Further, σ_c^2 is the noise power at BS. In the denominator of (7.1), $\rho_n(m)$ represents the indicator function defined as

$$\rho_n(m) = \begin{cases} 1, & \text{if V2V link } n \text{ reuses the sub-band } m, \\ 0, & \text{otherwise.} \end{cases} \tag{7.2}$$

Suppose that the platoon leader n reuses the sub-band m, the received SINR of platoon member i in platoon n can be expressed as follows

$$\text{SINR}_{ni}^{(\text{d})} = \frac{P_n L_{ni}^{(\text{dd})} g_{ni}^{(\text{dd})}}{\rho_n(m) P_c L_{m,ni}^{(\text{cd})} g_{m,ni}^{(\text{cd})} + \sum\limits_{l \neq n} \rho_l(m) P_l L_{l,ni}^{(\text{dd})} g_{l,ni}^{(\text{dd})} + \sigma_d^2}, \tag{7.3}$$

where $g_{ni}^{(\text{dd})}$ ($L_{ni}^{(\text{dd})}$) refers to the small-scale (large-scale) fading power from the leader to the member i of platoon n. Similarly, $g_{m,ni}^{(\text{cd})}$ ($L_{m,ni}^{(\text{cd})}$) denotes the small-scale (large-scale) fading power from V2I link m to the member i of platoon n, while $g_{l,ni}^{(\text{dd})}$ ($L_{l,ni}^{(\text{dd})}$) denotes the small-scale (large-scale) fading power from platoon leader l to the member i of platoon n. Further, σ_d^2 is the noise power at a vehicle. For simplicity, we assume that the noise powers at all vehicles are identical.

Treating the interference as noise, the achievable rate of V2I link m at time step t is given by invoking Shannon's capacity equation as

$$R_m^{(\text{c})}(t) = W \log_2 \left(1 + \text{SINR}_{mn}^{(\text{c})}(t)\right), \tag{7.4}$$

where W represents the bandwidth of each sub-band.

Likewise, the achievable rate of the V2V link i in platoon n at time step t is given by

$$R_{ni}^{(\text{d})}(t) = W \log_2 \left(1 + \text{SINR}_{ni}^{(\text{d})}(t)\right). \tag{7.5}$$

This work considers a multi-objective optimization problem in which we simultaneously maximize the achievable sum-rate of V2I links and the reliability of each V2V link under a latency constraint. As aforementioned, such objective functions are chosen to reflect the high data-rate and reliable message delivery demands of V2I (e.g., video streaming and gaming) and V2V (e.g., safety-message exchange for dynamic map construction) applications, respectively. While the

achievable sum-rate of V2I links is simply given by

$$\sum_{m=1}^{M} R_m^{(\mathrm{c})}(t), \tag{7.6}$$

the reliability of a typical V2V link is defined as the successful delivery of packets having size B within the time constraint T [92,93]. More specifically, the successful packet delivery of V2V link i of platoon n within the time constraint T is given by

$$\mathbb{P}\left(\sum_{t=1}^{T} R_{ni}^{(\mathrm{d})}(t) \geq B\right), \quad \text{for } n = 1, \ldots, N, i = 1, \ldots, V_n. \tag{7.7}$$

To enable spectrum sharing between V2V and V2I transmission, we aim to find the joint channel assignment and power allocation scheme at V2V platoon leaders that simultaneously maximizes the objective functions, expressed through the binary variables $\rho_n(m)$, $n = 1, \ldots, N$, $m = 1, \ldots, M$, and transmit power P_n, $n = 1, \ldots, N$. The multi-objective optimization generally is difficult to obtain an exact solution. In the following section, we shall adopt a multi-agent deep RL approach to address this challenge.

7.3 Deep Reinforcement Learning for Resource Allocation

7.3.1 Reinforcement Learning and Deep Q-Learning

In this section, we represent the concept of RL [148] and subsequently deep Q-learning [147], a well-known algorithm used to develop the RL agent in discrete optimization problems.

RL is a machine learning (ML) paradigm that allows an agent to learn the optimal action policy via trial-and-error interactions with the environment, in order to maximize a cumulative reward. In RL, the interaction between the agent and the environment is mathematically modeled as a Markov decision process (MDP). Typically, a MDP includes a set of environment states $\mathcal{S}$, a set of available actions $\mathcal{A}$, and a set of stochastic reward functions $\mathcal{R}$. In MDP, a policy is defined as a mapping function from a state s to an action a, generally represented by the conditional probability distribution $\pi(a|s)$ to specify the action a to be taken in the state s. At the time step t, let the random variables (RVs) $s_t \in \mathcal{S}$, $a_t \in \mathcal{A}$, and $r_t(s_t, a_t) \in \mathcal{R}$ denote the instantaneous state and action, and reward in the MDP, respectively. The agent observes the state s_t of the environment and chooses an action a_t. After that, the agent receives an immediate reward r_t and moves on to the next state $s_{t+1} \in \mathcal{S}$ as a result of the taken action a_t. For a concise representation, the states, action, and

reward are denoted by the tuple $e_t = [s_t, a_t, r_t, s_{t+1}]$.

The goal of agent in RL is to maximize the cumulative return R_t from time step t to future, given by [148]

$$R_t = \sum_{k=0}^{\infty} \gamma^k r_{k+t}, \tag{7.8}$$

where $\gamma \in [0, 1]$ denotes the discount factor, which represents how much the agent concerns about the rewards in the future. If $\gamma = 0$, the agent only cares about maximizing the immediate reward. As γ increases to 1, the agent is more farsighted as the future rewards are taken into account more strongly.

The action-value function, called Q-function, of a state-action pair (s, a) is defined as the expected return achievable by an action a in the state s with policy π

$$Q^{\pi}(s, a) = \mathbb{E}[R_0 | s_0 = s, a_0 = a, \pi], \tag{7.9}$$

where s_0 is the initial state. In addition, the expectation $\mathbb{E}[\cdot]$ is taken over all possible the state-action transitions following the policy distribution π.

At an instantaneous state s and action a, the goal of agent can be obtained via finding the optimal policy $\pi^{\star}$ that provides the maximum expected cumulative reward, i.e.,

$$\pi^{\star} = \arg\max_{\pi} Q^{\pi}(s, a). \tag{7.10}$$

Toward this end, various RL algorithms can be utilized. In this chapter, we focus on the deep Q-learning algorithm [147].

Q-learning is a value-based algorithm that finds the optimal value of each action a, given that such an action is taken at the state s. For each action a, the agent learns the action-value function (i.e., Q-function) by interacting with the environment until it converges to the optimal Q-function $Q^{\star}(s, a)$. It follows that the optimal policy $\pi^{\star}$ corresponds to select the greedy action $a^{\star}$ that results in the highest value of optimal Q-function $Q^{\star}(s, a)$ at the state s, given by

$$a^{\star} = \arg\max_{a} Q^{\star}(s, a).$$

It is apparent that, in order to find $a^{\star}$, the function $Q^{\star}(s, a)$ needs to be accurately estimated. The deep Q-learning algorithm utilizes a deep neural network (DNN) as the functional approximator of $Q^{\star}(s, a)$. As shown in Fig. 7.2, such a DNN, called deep Q-network Q_{θ}, takes the state s as input

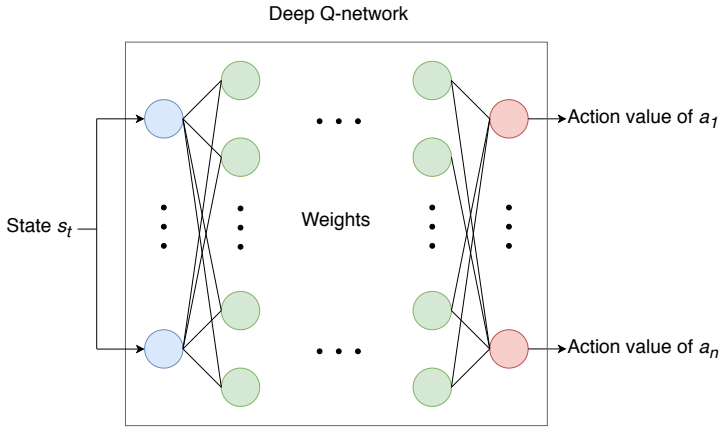

Fig. 7.2 Structure of deep Q-network.

and produces a separate output for each action $a \in \mathcal{A}$. As a result, the optimal action $a^\star$ can be easily obtained. The procedure to find the weight parameter θ of DNN Q_θ is provided as follows.

The optimal Q-function is expressed by the Bellman optimality equation in a recursive form as follows [149]

$$Q^\star(s,a) = \mathbb{E}\left[r_t + \gamma \max_{\hat{a}\in\mathcal{A}} Q^\star(s_{t+1},\hat{a}) | s_t = a, a_t = a\right], \tag{7.11}$$

which provides a necessary and sufficient condition that a Q-function is optimal.

In this chapter, we assume that the agent uses the ϵ-greedy policy to select the action a at the time step t. Specifically, given an observed state s_t at time step t, the agent chooses an action $a \in \mathcal{A}$ with a probability ϵ. Otherwise, it selects the greedy action $a^\star = \arg\max_{a\in\mathcal{A}} Q^\star(s_t,a)$.

For an experience $e_t = [s_t, a_t, r_t, s_{t+1}]$ in which the transition from s_t to s_{t+1} follows the ϵ-greedy policy, we can effectively calculate $Q_\theta(s_t,a_t)$ and $Y_t^\theta \triangleq r_t + \gamma \max_{\hat{a}\in\mathcal{A}} Q_\theta(s_{t+1},\hat{a})$. We refer $Q_\theta(s_t,a_t)$ and Y_t^θ as the online and target Q-values, respectively. From the Bellman equation, we are interested in finding the DNN parameter θ so that the online and target Q-values are identical, i.e., the optimal Q-function can be accurately computed via the deep Q-network Q_θ. This can be achieved by minimizing the loss function

$$L(\theta) = \frac{1}{2}|Y_t^\theta - Q_\theta(s_t,a_t)|^2. \tag{7.12}$$

A standard approach to minimize (7.12) is the gradient descent algorithm. In ML applications, the stochastic gradient descent (SGD) technique is often used to approximate the gradient and update the DNN parameter θ.

Using a DNN to estimate both online and target Q-values can cause an overestimation problem due to the high correlation between the target value and the parameter θ in some cases. To overcome this issue, two separate DNNs are used in the action selection and evaluation [150]. More specifically, let Q_{θ_1} and Q_{θ_2} denote the DNNs used in the action selection and evaluation, respectively. It follows that the target Q-value is updated by two DNNs as

$$Y_t^{\theta_1,\theta_2} = r_t + \gamma Q_{\theta_2}(s_{t+1}, \arg\max_{\hat{a}} Q_{\theta_1}(s_t, \hat{a})). \tag{7.13}$$

7.3.2 Multi-Agent Resource Allocation Algorithm

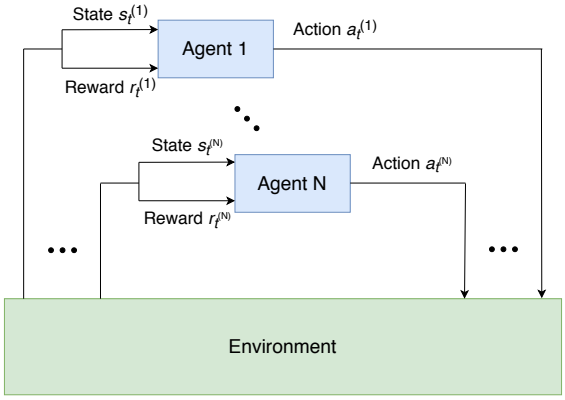

Fig. 7.3 Structure of multi-agent RL problem (to slightly abuse the notation, we include the superscripts to indicate the indexes of N agents).

As illustrated in Fig. 7.3, we reformulate the joint channel assignment and power allocation problem as a multi-agent RL problem in which each platoon leader acts as an agent. The agents collectively learn the environment via trial-and-error interaction and accordingly adjust the sub-bands and transmit powers based on their observed environment states. As a result, the optimization problem appears as a collaborative game in which the agents aim to obtain a common reward.

The multi-agent RL approach typically consists of two phases, namely training and testing. The training phase is centralized, where the common reward function is available for each agent in order to train the deep Q-network. We assume that each agent has a separate DNN (to represent the deep Q-network). Meanwhile, the testing phase is operated in a distributed fashion, where each agent receives the local state and selects the action (i.e., sub-band and transmit power) via the trained DNN in each coherent time step.

Before processing to the training and testing phases, we first define the state space, action space, and reward function used in the deep Q-learning algorithm to train each agent.

State Space

In this section, we shall characterize the state space of the agents (i.e., platoon leaders). In our state design, we include the channel measurements from the last step. Specifically, the current state space of agent n at time step t, denoted as $Z_n(t)$, consists of the following groups:

- *Direct channel information:* This group includes the direct channels of the V2V links corresponding to the agent n in the last time step. Mathematically, the direct channels of the leader n to the co-platoon members include both large- and small-scale fading powers, and they are given by the following set $\left\{L_{ni}^{(\text{dd})}, g_{ni}^{(\text{dd})}\right\}_{i\in\mathcal{V}_n}$, where $\mathcal{V}_n$ denotes the set of members in the platoon n.

- *V2V interfering channel information:* This group includes the interfering channels from other platoon leaders and cellular users sharing the same sub-band with the agent n. Assuming that the agent n occupies the sub-band m, this group is provided by

$$\left\{\rho_l(m)L_{l,ni}^{(\text{dd})}, \rho_l(m)g_{l,ni}^{(\text{dd})}, L_{m,ni}^{(\text{cd})}, g_{m,ni}^{(\text{cd})}\right\}_{i\in\mathcal{V}_n, l\neq n}.$$

- *Received interference and noise:* This group simply includes the aggregate interference and noise power at the corresponding receivers of agent k, given by $\left\{I_{ni}^{(\text{d})}\right\}_{i\in\mathcal{V}_n}$. Here, the aggregate interference plus noise power $I_{ni}^{(\text{d})}$ is provided by

$$I_{ni}^{(\text{d})} = \rho_n(m)P_c L_{m,ni}^{(\text{cd})} g_{m,ni}^{(\text{cd})} + \sum_{l\neq n}\rho_l(m)P_l L_{l,ni}^{(\text{dd})} g_{l,ni}^{(\text{dd})} + \sigma_d^2.$$

- *V2V-to-BS interference:* This group includes the interference caused by the agent n to the BS in the sub-band m, provided by $\left\{L_{n,m}^{(\text{dc})}, g_{n,m}^{(\text{dc})}\right\}$.

- *Payload delivery information:* This group includes the remaining payload and the remaining time limitation after the current time-step.

- *Policy related information:* This group represents a low-dimensional fingerprint that tracks the trajectory of policy change of other agents. In particular, we shall include the training iteration number e and the probability of random action selection ϵ in the state space of agent n. In multi-agent RL systems, this information allows to avoid the nonstationary environment that the agents might face while simultaneously making their actions [151].

Action Space

In our algorithm, each agent has an identical action space $\mathcal{A}$ where the corresponding action is a combination of the occupied sub-band and transmit power of the platoon leader. The sub-band space $\mathcal{A}_s$ simply includes M disjoint sub-bands, i.e., $\mathcal{A}_s = \{1, \ldots, M\}$. Meanwhile, we assume that the power space $\mathcal{A}_p$ is broken down into multiple discrete levels within the range $[0, P_d]$ where P_d denotes the maximum transmit power at each vehicle. The action space of a typical agent is expressed as $\mathcal{A} = \{(m, P_n)|m \in \mathcal{A}_s, P_n \in \mathcal{A}_p\}$. As a result, the dimension of action space is $|\mathcal{A}| = |\mathcal{A}_s| \cdot |\mathcal{A}_p|$.

Reward Function Design

In the considered multi-agent RL algorithm, the agents shall use a common reward function to enable their collaboration. The reward function design is based on a principal that each agent (i.e., platoon leader) should choose a combination of sub-band and transmit power that alleviates the interference to both V2I and V2V receivers, while preserving a sufficient resource to satisfy the latency requirement. To measure the interference to V2I receiver (i.e., BS), we simply include the V2I link sum-rate in the reward function. Meanwhile, the interference to other V2V receivers is reflected in the following V2V sum-rate function [93]

$$U_{ni}(t) = \begin{cases} \sum_{t=1}^{T} R_{ni}^{(\mathrm{d})}(t), & \text{if } B_{ni}(t) \geq 0, \\ U, & \text{otherwise.} \end{cases} \tag{7.14}$$

Here, the fixed sum-rate U is a hyperparameter that needs to be empirically adjusted in the simulation [93]. Meanwhile, $B_{ni}(t)$ is the remaining payload the V2V link formed by the leader and member i of platoon n at time step t. Regarding the latency condition, we use the penalty assigned to a time constraint violation up to the current time step. The reward function is therefore given by

$$r_t = w_c \sum_{m=1}^{M} R_m^{(\mathrm{c})}(t) + w_d \sum_{n=1}^{N} \sum_{i=1}^{V_n} U_{ni}(t) - w_t(T - \Delta T(t)), \tag{7.15}$$

where $w_c, w_d, w_t \in [0, 1]$ are the weights added to balance the V2I- and V2V-related objectives. Here, $\Delta T(t) \in [0, T]$ in multiples of the time step refers the remaining transmission time of the V2V links. As a result, the term $T - \Delta T(t)$ represents the increasing price as the transmission time of the V2V links grows.

Multi-Agent Reinforcement Learning Algorithm

In both learning and testing phases of the multi-agent reinforcement learning algorithm, we shall focus on the episodic setting with the time limitation T of the V2V transmission. In addition, each episode consists of multiple time steps t, and starts by randomly generating the environment state including large- and small-scale fading. The path-loss and shadowing of large-scale fading are fixed during the episode, while the small-scale Rayleigh fading (i.e., Rayleigh fading) is updated in each time step. This shall trigger the transition of the environment states and cause the agents to simultaneously adjust their action. In an episode, each agent learns to find an optimal combination of sub-band and transmit power level so as to maximize the common reward. Once the payload has been successfully delivered, the agent will terminate its transmission.

Training Phase: In the training phase, deep Q-learning is adopted to train the agents. Further, each agent stores its experience tuple e_t in a replay memory. In each episode, a mini-batch of experience $\mathcal{D}$ is uniformly sampled from the replay memory for updating the deep Q-network parameter, using the stochastic gradient descent method. The use of experience replay in our algorithm allows to break the correlation in successive updates, thus stabilizing the learning process [147]. The training algorithm is summarized in Algorithm 3.

Algorithm 3 Training Algorithm

Initiate the environment, generating the V2I links and V2V platoons
Initiate the DNN with random parameters θ
for each episode **do**
    Update the vehicle locations and large-scale fading
    for each time step t **do**
        for each agent n **do**
            Observe the state $s_t = Z_n(t)$
        end for
        All agents take actions simultaneously according the $\epsilon-$greedy policy and receive the reward r_t
        Update channel small-scale fading
        for each agent n **do**
            Observe the next state $s_{t+1} = Z_n(t+1)$
            Store $e_t = [s_t, a_t, r_t, s_{t+1}]$ in the replay memory
        end for
    end for
    for each agent n **do**
        Uniformly sample mini-batch data $\mathcal{D}$ from replay memory
        Train the deep Q-network using the mini-batch data.
    end for
end for

Testing Phase: During the testing phase that implements the resource allocation algorithm, each agent n first collects the local information $Z_n(t)$ at the time step t. Such local information is served as the input of deep Q-network, and the output of which provides the optimal action. From this action, each agent selects the corresponding sub-band and power level to transmit its signal.

7.4 Illustrative Results

In this section, we present the simulation results to illustrate the performance of the developed algorithm for the platoon-based C-V2X systems. A single-cell urban scenario with the carrier frequency of 2 GHz is considered. The simulation setup is detailed in 3GPP TR 36.885 [18] and [93] which provide the vehicle speed, drop model, and direction of movement, as well as the V2I and V2V channel models including path-loss model and shadowing distribution. In addition, the small-scale fading follows the Rayleigh distribution; and the corresponding channel power gains are generated i.i.d. in each time step according to an exponential distribution with unit parameter. Each V2V platoon consists of one leader and two members. We assume the length of each vehicle is 4 m, while the distance between two adjacent vehicles (either member or leader) of the platoon is 1 m. In addition, the transmit/receive antenna is placed in the middle point of each vehicle. Similar to [18, 93], we also update the slow- and fast-fading every 100 ms and 1 ms, respectively, but reducing the time limitation of V2V transmission to 10 ms in the testing phase to meet the latency requirement of V2V platoon-based applications proposed in [7]. Unless stated otherwise, the main simulation parameters can be found in Table 7.1 [18, 93]. We also note that, in Table 7.1, the value -100 dBm of V2V transmit power P_n effectively indicates that the V2V platoon leader n stops transmitting its signals.

In the developed multi-agent RL algorithm, the structure of deep Q-network consists of a five-layer fully connected DNN with three hidden layers. The numbers of neurons in the three hidden layers are chosen as 500, 250, and 120, respectively [92, 93]. The rectified linear unit (ReLU) function, defined as $f_{\text{ReLU}}(x) = \max\{0, x\}$, is used as the activation function, while the RMSProp optimizer with a learning rate of 0.001 is adopted as the stochastic gradient descent algorithm to train the deep Q-networks [152]. In the learning phase, we assume $1,500$ training episodes with 10 steps per episode, while we consider 100 episodes in the testing phase. Based on the empirical experience, the probability ϵ in $\epsilon-$greedy policy linearly decreases from 1 to 0.02 over first $1,200$ episodes and keeps the constant value 0.02 afterward. Moreover, the discount factor is chosen as $\gamma = 1$ so that the agents are farsighted with the future rewards. Given the parameters provided in 7.1 and based on experiment, we choose the constant sum-rate U in (7.14) as $U = 10$; and the

Table 7.1 Simulation Parameters of C-V2X System

Carrier frequency	2 GHz
Bandwidth of each sub-band	1 MHz
Number of sub-bands	4
Number of V2I links M	4
Number of V2V platoons N	4
Number of vehicles per platoon	3
Vehicle velocity	36 km/h
Transmit power of V2I cellular user P_c	23 dBm
Transmit power of V2V platoon leader P_n	$[23, 10, 5, -100]$ dBm
BS noise figure	5 dB
Vehicle noise power σ_d^2	-114 dBm
V2V time limitation T	10 ms
V2V payload B	$[1, 8] \cdot 1060$ bytes

weights $\{w_c, w_v, w_t\}$ are selected so that the reward function (7.15) is clipped within the range $[-1, 1]$ to stabilize the training. As a result, the following normalized reward function is used in our simulations

$$r_t = \frac{w_c}{10M} \sum_{m=1}^{M} R_m^{(c)}(t) + \frac{w_d}{10N} \sum_{n=1}^{N} \sum_{i=1}^{V_n} U_{ni}(t) - w_t \left(1 - \frac{\Delta T(t)}{T}\right). \tag{7.16}$$

We adopt exhaustive search and the random allocation operating in centralized and distributed manners, respectively, as a benchmark for comparison with the developed RL learning algorithm. The exhaustive search divides the time constraint T into multiple time steps and performs exhaustive search for the decision making of delivering the payload B in each time step. If the payload has not yet delivered at a V2V link, the exhaustive search finds the optimal action from the action space that maximizes the V2V sum-rate. Otherwise, it terminates the V2V transmission. Beside the requirement of global CSI at the central controller, this method also incurs an extremely high complexity. For instance, with M sub-bands, P discrete power levels, and N platoons, the dimension of search place equals $(MP)^N$, which exponentially grows with the increasing number of platoons. Meanwhile, the random allocation scheme randomly assigns the sub-band and transmit power level to each platoon leader in each time step.

In Figs. 7.4a and 7.4b, we plot the cumulative reward per episode and training loss of the deep Q-network versus the number of episodes in the training phase, respectively. The payload size is chosen as $B = 2 \cdot 1060$ bytes. It is shown in Fig. 7.4a that the reward improves and gets stable at episode $1,000$ as the number of episodes increases further. The training exhibits some fluctuations

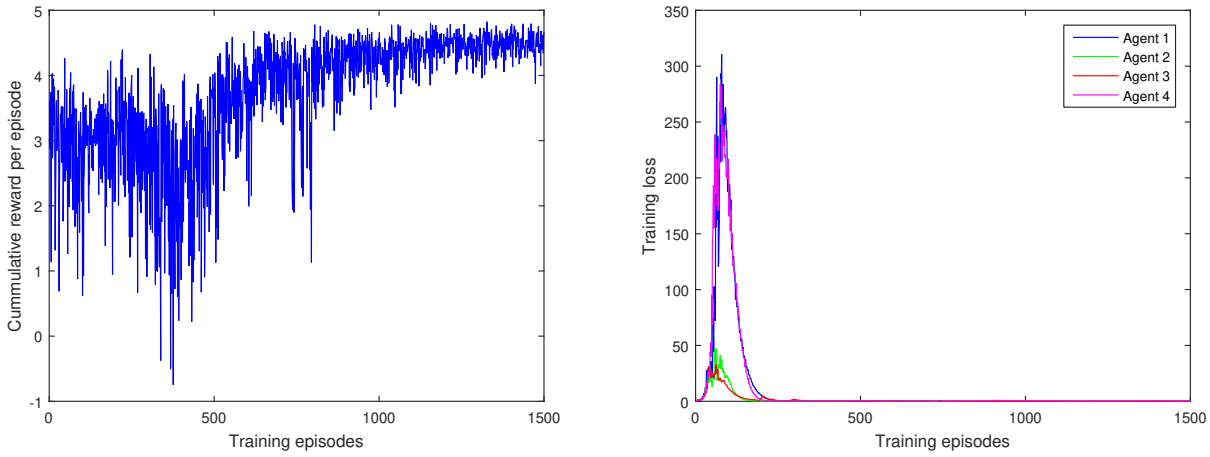

(a) Cumulative reward per episode

(b) Training loss

Fig. 7.4 Cumulative reward per episode and training loss versus number of episodes for the payload $B = 2 \cdot 1060$ bytes.

at the beginning but eventually converges. Meanwhile, Fig. 7.4b illustrates the training loss represented by the function $L(\theta)$ in (7.12), corresponding to the deep Q-network of each agent (i.e., each platoon leader). We observe that, as the training episode increases, the losses of all agents also increase to relatively large values at the beginning of the training process, but quickly get saturated and converge to around 0 beyond episode 500. This result indicates that the proposed deep Q-network can accurately approximate the optimal Q-function. Thus, given a sufficient number of training episodes (e.g., $1,500$), each agent can learn to find the optimal sub-band and power selection strategy to jointly optimize the common reward. Based on the observation of reward and loss behaviors in Figs. 7.4a and 7.4b, to safely ensure the convergence, we shall train the deep Q-network of each agent for $1,500$ episodes to evaluate the performances of V2I and V2V links in our simulations.

Figs. 7.5a and 7.5b illustrate the successful delivery probability of V2V links and corresponding sum-rate of V2I links under various payload sizes ($B \in [1, 8] \cdot 1060$ bytes), respectively, for different channel assignment and power allocation schemes including exhaustive search, RL algorithm, and random allocation. The sum-rate and probability results of Figs. 7.5a and 7.5b are averaged over 100 test episodes. Additionally, with regards to the RL algorithm, the weight combination of normalized reward function (7.16) is chosen as $(w_c, w_d, w_t) = (0, 1, 0.5)$ to favor the successful delivery of safety messages in V2V platoons. Given the latency constraint $T = 10\,\text{ms}$, Fig. 7.5a shows that the exhaustive search achieves a perfect delivery probability of 1 over the whole payload range. As the payload size B increases, the RL algorithm also achieves the perfect

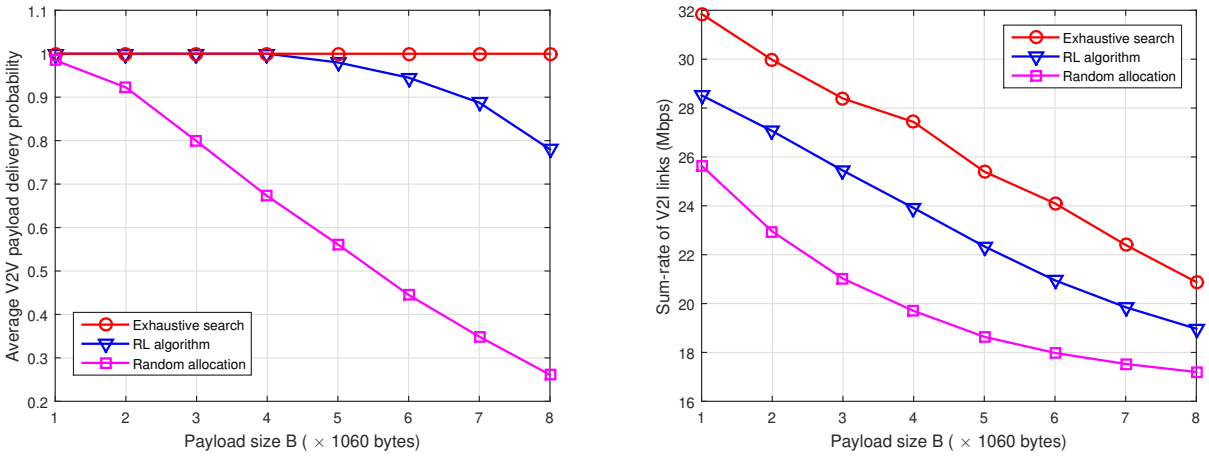

(a) Average V2V payload delivery probability

(b) Average sum-rate of V2I links

Fig. 7.5 Average V2V payload delivery probability and V2I sum-rate versus payload size B.

delivery probability of 1 up to $B = 4 \cdot 1060$ bytes and eventually gets saturated. Meanwhile, the payload delivery probability of random allocation scheme is linearly reduced with increasing payload size. We also observe that the payload delivery probability offered by the RL algorithm significantly outperforms that of the random allocation scheme. For instance, at the payload size $B = 5 \cdot 1060$ bytes, the RL algorithm and random allocation scheme provide delivery probabilities of 0.98 and 0.56, respectively. In Fig. 7.5b, we plot the corresponding sum-rate of V2I links for difference resource allocation methods. It is shown that the V2I sum-rate performances degrade with growing payload sizes. This is because a higher payload size requires a longer transmission duration of each V2V link, and hence, causing more interference to the BS. Similar to the case of V2V delivery probability, one can observe that the V2I sum-rate performance provided by exhaustive search outperforms those of RL algorithm and random allocation scheme. This is because, as each V2V link terminates its transmission once the payload has been completely delivered and the exhaustive search aims to maximize the V2V sum-rate, the average number of inactive V2V links over each time step of the latency constraint T is higher than those of RL algorithm and random allocation scheme, thus alleviating the interference to V2I transmission.

To understand why the developed RL algorithm provides a better sum-rate performance than random allocation scheme, yet lower than the exhaustive search method, we select an episode in the testing phase as well as a V2V link constituted by the leader and furthest member in the first platoon under the assumption of payload size $B = 8 \cdot 1060$ bytes. In Figs. 7.6a and 7.6b, we plot the instantaneous rate of V2V link and the remaining payload over increasing time steps of chosen

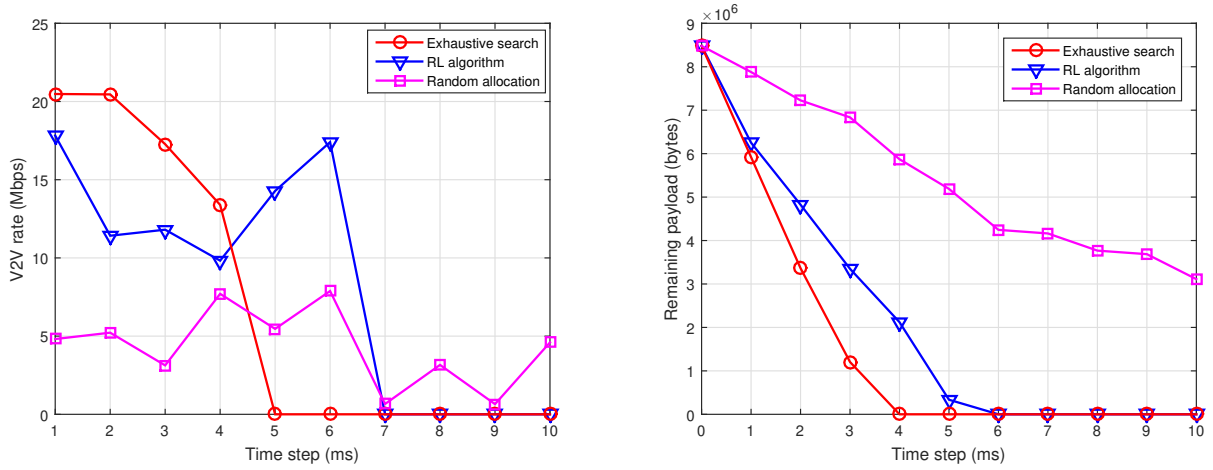

(a) V2V rate (b) Remaining payload

Fig. 7.6 V2V rate and remaining payload versus time step t.

episode, respectively. For each time step, the remaining payload is computed by subtracting the V2V rate in the remaining payload of last time step. If the V2V link has completed delivering the payload, we assign the remaining payload to 0 and terminate the transmission. It is shown in Fig. 7.6b that remaining payload is reduced with increasing number of time steps. As the exhaustive search scheme essentially finds the sub-band and power level to maximize the V2V sum-rate in each time-step, the corresponding payload delivery is completed early, i.e., at time step 4 ms. Beyond this time step, the V2V rate offered by exhaustive search vanishes to 0, indicating that the interference at BS caused by V2V transmission is mitigated. For the RL algorithm, Figs. 7.6a and 7.6b illustrate that the payload delivery of V2V link ends at time step 6 ms, resulting in the termination of V2V transmission beyond this time step (i.e, ≥ 7 ms). In this episode, both exhaustive search and RL algorithm achieve the delivery probability of 1, but exhaustive search shall provide a better V2I sum-rate due to its early payload delivery completion. Meanwhile, we observe that the random allocation scheme provides relatively low V2V rate, thus failing to delivery the safety messages in the considered episode.

Figs. 7.7a and 7.7b show the average V2V payload delivery probability and corresponding V2I sum-rate versus payload size B, offered by the developed RL algorithm, under various combinations of reward weights, i.e., $(w_c, w_d, w_t) \in \{(0,1,0),(0,1,0.5),(0.5,0.5,0.5)\}$. We should note that the case $w_t = 0$ corresponds to the reward function design in [93]. Interestingly, for identical weights w_c and w_d in the cases $(w_c, w_d, w_t) \in \{(0,1,0),(0,1,0.5)\}$, the incorporation of latency-based price represented by the weighted V2V transmission time $w_t\left(1-\frac{\Delta T(t)}{T}\right)$, $w_t > 0$, in the reward function design allows to improve both the V2V payload delivery probability of safety

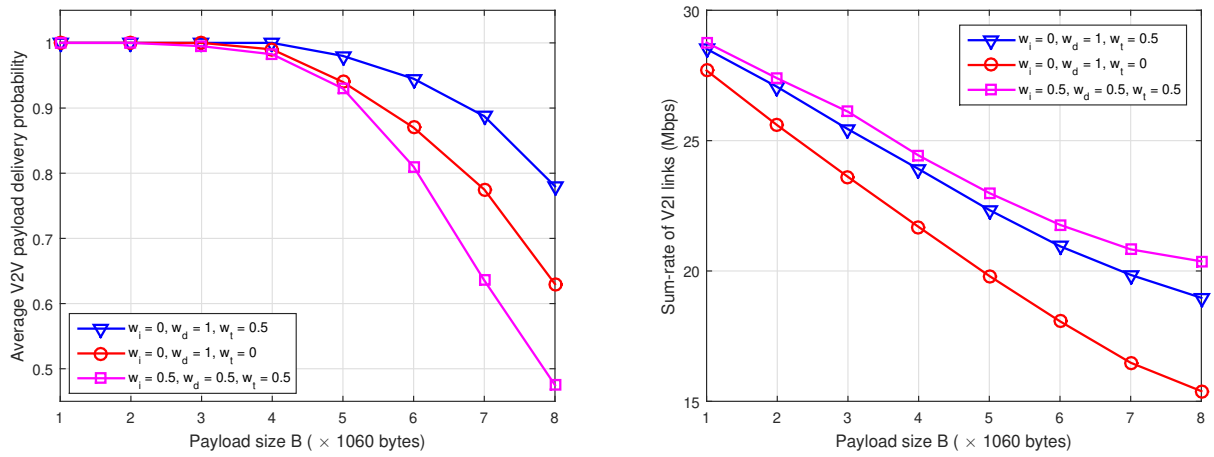

(a) Average V2V payload delivery probability

(b) Average sum-rate of V2I links

Fig. 7.7 Average V2V payload delivery probability and V2I sum-rate versus payload size B for different reward weight parameters.

message transmission and the achievable sum-rate of V2I links. It is also illustrated that, as compared to case $(w_c, w_d, w_t) = (0, 1, 0.5)$ (in absence of V2I-related reward), the case $(w_c, w_d, w_t) = (0.5, 0.5, 0.5)$ equally favors optimizing both the V2I and V2V sum-rates, leading to the V2I sum-rate improvement, yet, at the same time, substantially degrading the delivery probability of V2V links.

7.5 Concluding Remarks

In this chapter, a distributed joint channel assignment and power allocation algorithm has been proposed for the platoon-based C-V2X systems where multiple V2V platoons were allowed to reuse the spectrum of V2I transmission. The developed algorithm was based on a multi-agent deep reinforcement learning approach where each platoon leader, defined as an agent, made its own decisions to find optimal sub-band and power to transmit the signals to the corresponding platoon members. Since the proposed method was decentralized, the global channel information were not required for the agents to make their decisions, thus significantly reduced the signaling overhead. Simulation results showed that each agent can learn how to satisfy the latency limitation under a wide range of payload requirements for safety message delivery, while minimizing the interference to V2I transmission.

Chapter 8

Conclusions

8.1 Summary

D2D communications is an innovative feature that will be incorporated in cellular networks. However, adding the D2D feature to existing cellular networks poses many challenges and risks. In particular, when D2D and cellular users are allowed to operate simultaneously in a time-frequency resource, increasing the amount of resource sharing causes additional interference but, at the same time, offers substantial spectral efficient gains with necessary interference management. This thesis focused on studying the spectral efficiency benefits offered by underlaid D2D via performance analysis and sum-rate maximizing resource allocation algorithms. D2D links operate in the underlaid mode in which the D2D transmission fully reuses the time-frequency resources that are currently occupied by the cellular transmission.

In Chapter 3, we adopted the additive GM channels to model the D2D link channel in a simple underlaid HD D2D cellular network consisting of one D2D and one cellular users. This model captured the effect of interference generated by the cellular transmitter which uses discrete constellations to transmit the signals. Given the proposed GM channel model, we carried out a fundamental analysis of capacity-achieving input distribution and corresponding D2D channel capacity computation, which provides better insight into the optimal transmit codebook design for practical underlaid D2D transmission at the link level.

Chapter 4 was dedicated to studying the achievable rate at network level where multiple FD D2D links and a cellular link share the same time-frequency resources in the context of single-cell setting. Based on a stochastic geometry approach, a random network model was proposed, taking into account the randomness and unpredictable of D2D/cellular user locations. We investigated the spectral efficiency offered by FD D2D via both centralized and distributed power allocation.

In Chapter 5, we adapted the random network model to a multi-cell setting and further studied the spectrum sharing between cellular uplink and D2D communications. We derived analytical expressions of achievable cellular/D2D sum-rates and applied them to characterize the impact of network parameters under the consideration of various frequency reuse schemes.

In Chapter 6, the focus was shifted from uplink to downlink cellular transmission being underlaid by the D2D services. Moreover, we extended the baseline single-antenna network model to multi-antenna transmission to include the massive MIMO equipped BSs. To address the challenge of interference management, we developed joint beamforming and power allocation algorithms in underlaid D2D cellular networks where massive MIMO equipped BSs and underlaid FD D2D networking co-existed.

Chapter 7 utilized the reinforcement learning approach to address the distributed resource allocation challenge in D2D-based C-V2X systems where V2V users operate in a platoon fashion. We developed a joint channel assignment and power allocation algorithm based on deep Q-learning so as to simultaneously maximize the achievable sum-rate of V2I links and the successful packet delivery probability of V2V links over a desired latency constraint.

8.2 Potential Future Research

The main focus of this thesis has been on improving the spectral efficiency of cellular networks via underlaid D2D services. This section discusses some potential future works related to the research studied in this thesis. The following three extensions are interesting in the context of 5th generation mobile networks (5G). The first is to develop joint channel assignment and power allocation schemes in large C-V2X networks, the second is to design distributed algorithms for continuous resource allocation problems in C-V2X systems by utilizing RL tools, and the third is to enable vehicular communications of C-V2X systems in millimeter wave (mmWave) bands.

In the context of single-cell setting, the RL-based algorithm in Chapter 7 allows the V2V platoons to reuse the time-frequency slots of V2I links. Toward this end, the state space of each agent (i.e., platoon leader) must include the CSI of interfering V2V links as well as the aggregate interference at the BS caused by V2V transmitters. In C-V2X networks comprised of multiple cells and dense V2V/V2I link deployment, such information cannot be accurately estimated due to substantially increasing number of V2V/V2I users and fast channel variations of vehicular environment. Therefore, an area of potential future work includes extending the RL-based algorithm in Chapter 7 to develop large-scale channel assignment and power allocation algorithms in C-V2X systems.

In this thesis, the RL-based resource allocation for joint channel assignment and power alloca-

tion in C-V2X systems was essentially based on an assumption that the action set (i.e., sub-bands and transmit power levels) was discrete. As a result, the developed multi-agent RL algorithm in Chapter 7 is not viable for continuous optimization problems. For instance, considering a joint power allocation and beamforming design problem as in Chapter 6, yet applied to the C-V2X systems in which the transmit powers and beamformers are allowed to take on any values within given ranges. A straightforward solution to address this challenge is dividing the transmit power range into multiple discrete levels so the deep Q-learning algorithm developed for the transmit power set can be directly applied to approximately solve the continuous optimization problem [98]. This approach, however, cannot be expanded to include the discrete beamfomers as the size of joint transmit power and beamformer space grows w.r.t. the number of equipped antennas and V2I links, to which the deep Q-learning algorithm becomes computationally infeasible in the dense C-V2X deployment. How to adopt the multi-agent RL approach to effectively solve the continuous optimization problems in C-V2X systems, particularly in joint power allocation and beamforming design, is still largely open.

In future intelligent transportation systems, vehicles will be equipped with large number of sensors to improve the automated driving applications such as object detection, visual cameras as virtual mirrors, as well as constructing high resolution depth associated range maps for safe driving [153]. As connected vehicles will use the V2V communications to exchange the raw sensor data, increasing number of integrated sensors will result in a higher data-rate demand, e.g., gigabit-per-second (Gbps). While the focus of this thesis is on enabling the D2D and D2D-based vehicular communications into existing cellular networks, the illustrative results are dedicated to microwave frequencies, particularly at 2 GHz, which, unfortunately, does not support such a data-rate requirement. Higher carrier frequencies, particularly mmWave bands, have been proposed as a viable approach to enable the Gbps data-rates in future C-V2X systems. The first step of adopting the mmWave bands in C-V2X systems is to develop accurate channel models for mmWave V2V transmission among the connected vehicles. Although the channel propagation between vehicles has been analyzed at the carrier frequencies below 6 GHz, the propagation characteristics of mmWave frequencies are fundamentally different to those of microwave frequencies. MmWave signals have much smaller wavelength, thus mmWave V2V transmission will experience the high path-loss as the signals cannot penetrate most solid materials. To compensate the high path-loss, mmWave transmitters are equipped with large number of antennas aiming toward the intended receivers with suitable beamforming designs [154]. It follows that many aspects should be considered and integrated into mmWave V2V channel modeling such as the effects of antenna location, vehicle speeds, and blockage caused by nearby pedestrians, vehicles, buildings, and other obstacles. Once

the channel models are characterized, network level analysis (e.g., based on stochastic geometry approach) and optimization in underlaid D2D communications in this thesis can be adopted and modified for the mmWave C-V2X systems.

References

[1] Deutsche Telekom AG, Orange Silicon Valley, Qualcomm Technologies Incorporated, Tagged Incorporated, and Samsung Electronics, "LTE Direct workshop white paper," *[Online] Available: https://www.qualcomm.com/media/documents/files/lte-direct-whitepaper.pdf*, May 2013.

[2] M. S. Corson, R. Laroia, J. Li, V. D. Park, T. Richardson, G. Tsirtsis, and S. Uppala, "Flash-LinQ: Enabling a mobile proximal internet," *IEEE Wireless Commun.*, vol. 20, pp. 110–117, Oct. 2013.

[3] X. Wu, S. Tavildar, S. Shakkottai, T. Richardson, J. Li, R. Laroia, and A. Jovicic, "Flash-LinQ: A synchronous distributed scheduler for peer-to-peer ad hoc networks," *IEEE/ACM Transactions on Networking*, vol. 21, pp. 1215–1228, Aug. 2013.

[4] "3rd generation partnership project; Technical specification group SA; Feasibility study for proximity services (ProSe) (Release 12)," *TR 22.803 V1.0.0*, Aug. 2012.

[5] T. Doumi, M. F. Dolan, S. Tatesh, A. Casati, G. Tsirtsis, K. Anchan, and D. Flore, "LTE for public safety networks," *IEEE Commun. Mag.*, vol. 51, pp. 106–112, Feb. 2013.

[6] "3rd generation partnership project; Study on further enhancements to LTE device to device, UE to network relays for IoT and wearables," *RP-170295*, Mar. 2017.

[7] "3rd generation partnership project; Technical specification group services and system aspects; Study on enhancement of 3GPP support for 5G V2X services (Release 16)," *TR 22.886 V16.2.0*, Dec. 2018.

[8] "3rd generation partnership project; Technical specification group services and system aspects; Enhancement of 3GPP support for V2X scenarios; Stage 1 (Release 16)," *TS 22.186 V15.2.0*, June 2019.

[9] J. I. Choi, M. Jain, K. Srinivasan, P. Levis, and S. Katti, "Achieving single channel, full-duplex wireless communication," in *Proc. 16th Annu. Int. Conf. MobiCom Netw.*, pp. 1–12, 2010.

[10] D. Bharadia, E. McMilin, and S. Katti, "Full-duplex radios," in *Proc. ACM SIGCOMM*, pp. 375–386, 2013.

[11] M. Duarte, A. Sabharwal, V. Aggarwal, R. Jana, K. K. Ramakrishnan, C. W. Rice, and N. K. Shankaranarayanan, "Design and characterization of a full-duplex multiantenna system for WiFi networks," *IEEE Trans. Veh. Tech.*, vol. 63, pp. 1160–1177, Mar. 2014.

[12] M. Jain, J. Choi, T. Kim, D. Bharadia, S. Seth, K. Srinivasan, P. A. Levis, and S. R. Katti, "Practical, real-time, full-duplex wireless," in *Proc. 17th Annu. Int. Conf. MobiCom Netw.*, pp. 301–312, 2011.

[13] L. Liang, H. Peng, G. Y. Li, and X. Shen, "Vehicular communications: A physical layer perspective," *IEEE Trans. Veh. Tech.*, vol. 66, pp. 10647–10659, Dec. 2017.

[14] J. B. Kenney, "Dedicated short-range communications (DSRC) standards in the United States," in *Proc. of the IEEE*, vol. 99, pp. 1162–1182, July 2011.

[15] "Intelligent transport systems (ITS); Cooperative ITS (C-ITS) (Release 1)," *ETSI TR 101 607 V1.1.1*, May 2013.

[16] G. Araniti, C. Campolo, M. Condoluci, A. Iera, and A. Molinaro, "LTE for vehicular networking: A survey," *IEEE Commun. Mag.*, vol. 51, pp. 148–157, May 2013.

[17] H. Seo, K. Lee, S. Yasukawa, Y. Peng, and P. Sartori, "LTE evolution for vehicle-to-everything services," *IEEE Commun. Mag.*, vol. 54, pp. 22–28, June 2016.

[18] "3rd generation partnership project; Technical specification group radio access network; Study LTE-based V2X services (Release 14)," *TR 36.885 V2.0.0*, June 2016.

[19] K. Abboud, H. A. Omar, and W. Zhuang, "Interworking of DSRC and cellular network technologies for V2X communications: A survey," *IEEE Trans. Veh. Tech.*, vol. 65, pp. 9457–9470, Dec. 2016.

[20] "3rd generation partnership project; Technical specification group radio access network; Study on LTE device to device proximity services; Radio aspects (Release 12)," *TR 36.843 V12.0.1*, Mar. 2012.

[21] X. Lin, J. G. Andrews, A. Ghosh, and R. Ratasuk, "An overview of 3GPP device-to-device proximity services," *IEEE Commun. Mag.*, vol. 52, pp. 40–48, Apr. 2014.

[22] H. V. Vu, N. H. Tran, M. C. Gursoy, T. Le-Ngoc, and S. I. Hariharan, "Capacity-achieving input distributions of additive quadrature Gaussian Mixture noise channels," *IEEE Trans. Commun.*, vol. 63, pp. 3607–3620, Oct. 2015.

[23] H. V. Vu, N. H. Tran, and T. Le-Ngoc, "Full-duplex device-to-device cellular networks: Power control and performance analysis," *IEEE Trans. Veh. Tech.*, vol. 68, pp. 3952–3966, Apr. 2019.

[24] H. V. Vu and T. Le-Ngoc, "Performance analysis of underlaid full-duplex D2D cellular networks," *IEEE Access*, vol. 7, pp. 176233–176247, 2019.

[25] H. V. Vu, N. H. Tran, M. C. Gursoy, T. Le-Ngoc, and S. I. Hariharan, "Characterization of optimal input distributions for Gaussian-mixture noise channels," in *Proc. IEEE Can. Work. on Infor. Theory (CWIT)*, pp. 32–35, 2015.

[26] H. V. Vu, N. H. Tran, and T. Le-Ngoc, "On coverage probabilities and sum-rate of full-duplex device-to-device cellular networks," *Proc. IEEE Int. Conf. Commun. (ICC)*, pp. 4042–4047, 2018.

[27] H. V. Vu and T. Le-Ngoc, "Underlaid full-duplex D2D cellular networks: Modeling and analysis," in *Proc. Int. Symp. on Personal, Indoor and Mobile Radio Commun. (PIMRC)*, pp. 1–6, 2019.

[28] P. Janis, V. Koivunen, C. Ribeiro, J. Korhonen, K. Doppler, and K. Hugl, "Interference-aware resource allocation for device-to-device radio underlaying cellular networks," in *Proc. IEEE Veh. Tech. Conf. (VTC)*, pp. 1–5, 2009.

[29] C. H. Yu, O. Tirkkonen, K. Doppler, , and C. Ribeiro, "On the performance of device-to-device underlay communication with simple power control," in *Proc. IEEE Veh. Technol. Conf. (VTC)*, pp. 1–5, 2009.

[30] C. H. Yu, K. Doppler, C. Ribeiro, and O. Tirkkonen, "Resource sharing optimization for device-to-device communication underlaying cellular networks," *IEEE Trans. Wireless Commun.*, vol. 10, pp. 2752–2763, Aug. 2011.

[31] D. Stein, "Detection of random signals in Gaussian Mixture noise," *IEEE Trans. Inform. Theory*, vol. 41, pp. 1788–1801, Nov. 1995.

[32] D. A. Reynolds, "Gaussian Mixture models," MIT Lincoln Laboratory, 2009.

[33] C. R. Baker and A. F. Gualtierotti, "Likelihood ratios and signal detection for non-Gaussian processes," in *Stochastic Processes in Underwater Acoustics* (Lecture notes in Control and Information Sciences, vol. 85). Berlin, Germany: Springer-Verlag, pp. 154–180, 1986.

[34] T. Erseghe, V. Cellini, and G. Donà, "On UWB impulse radio receivers derived by modeling MAI as a Gaussian Mixture process," *IEEE Trans. Wireless Commun.*, vol. 7, pp. 2388–2396, June 2008.

[35] S. Bayram and S. Gezici, "On the performance of single-threshold detectors for binary communications in the presence of Gaussian Mixture noise," *IEEE Trans. Wireless Commun.*, vol. 58, pp. 3047–3053, Nov. 2010.

[36] J. Lin, M. Nassar, and B. L. Evans, "Impulsive noise mitigation in powerline communication using sparse Bayesian learning," *IEEE J. Sel. Areas in Commun.*, vol. 31, pp. 1172–1183, July 2013.

[37] R. Pighi, M. Franceschini, G. Ferrari, and R. Raheli, "Fundamental performance limits of communications systems impaired by impulse noise," *IEEE Trans. Commun.*, vol. 57, pp. 171–182, Jan. 2009.

[38] G. Ozcan, M. C. Gursoy, and S. Gezici, "Error rate analysis of cognitive radio transmissions with imperfect channel sensing," *IEEE Trans. Wireless Commun.*, vol. 13, pp. 1642–1655, Mar. 2014.

[39] T. Q. S. Quek, G. de la Roche, I. Güvenç, and M. Kountouris, *Small cell networks: Deployment, PHY techniques, and resource management*. Cambridge University Press., 1st ed., 2013.

[40] C. E. Shannon, "A mathematical theory of communication," *Bell System Technical Journal*, vol. 27, pp. 379–423, July 1948.

[41] J. G. Smith, "The information capacity of amplitude and variance constrained scalar Gaussian channels," *Inform. Contr.*, vol. 18, pp. 203–219, Apr. 1971.

[42] S. Shamai and I. Bar-David, "The capacity of average and peak-power-limited quadrature Gaussian channels," *IEEE Trans. Inform. Theory*, vol. 41, pp. 1060–1071, July 1995.

[43] M. Katz and S. Shamai, "On the capacity-achieving distribution of the discrete-time noncoherent and partially coherent AWGN channels," *IEEE Trans. Inform. Theory*, vol. 50, pp. 2257–2270, Oct. 2004.

[44] L. Zhang, H. Li, and D. Guo, "Capacity of Gaussian channels with duty cycle and power constraints," *IEEE Trans. Inform. Theory*, vol. 60, pp. 1615–1629, Mar. 2014.

[45] I. Abou-Faycal, M. D. Trott, and S. Shamai, "The capacity of discrete-time memoryless Rayleigh-fading channels," *IEEE Trans. Inform. Theory*, vol. 47, pp. 1290–1301, Mar. 2001.

[46] M. Gursoy, H. V. Poor, and S. Verdu, "The noncoherent Rician fading channel-Part I: Structure of capacity achieving input," *IEEE Trans. Wireless Commun.*, vol. 4, pp. 2193–2206, Sept. 2005.

[47] R. Palanki, "On the capacity-achieving distributions of some fading channels," in *Proc. 40th Allerton Conf. Commun., Control, and Comput.*, pp. 337–346, Oct. 2002.

[48] T. H. Chan, S. Hranilovic, and F. R. Kschischang, "Capacity-achieving probability measure for conditionally Gaussian channels with bounded inputs," *IEEE Trans. Inform. Theory*, vol. 51, pp. 2073–288, June 2005.

[49] A. Kenarsari-Anhari and L. Lampe, "Performance analysis for BICM transmission over Gaussian mixture noise fading channels," *IEEE Trans. Commun.*, vol. 58, pp. 1962–1972, June 2010.

[50] M. Ghosh, "Analysis of the effect of impulse noise on multicarrier and single-carrier QAM system," *IEEE Trans. Commun.*, vol. 44, pp. 145–147, Feb. 1996.

[51] X. Wang and V. Poor, "Robust multiuser detection in non-Gaussian channels," *IEEE Trans. Signal Process.*, vol. 47, pp. 289–305, Feb. 1999.

[52] D. Middleton, "Statistical-physical models of electromagnetic interference," *IEEE Trans. Electromagn. Compat.*, vol. EMC-19, pp. 106–127, Aug. 1977.

[53] J. Häring and A. Vinck, "Performance bounds for optimum and suboptimum reception under class-A impulsive noise," *IEEE Trans. Commun.*, vol. 50, pp. 1130–1136, July 2002.

[54] K. Wiklundh, P. Stenumgaard, and H. Tullberg, "Channel capacity of Middletons class A interference channel," *Electronics Letters*, vol. 45, pp. 1227–1229, Nov. 2009.

[55] S. P. Herath, N. H. Tran, and T. Le-Ngoc, "On optimal input distribution and capacity limit of Bernoulli-Gaussian impulsive noise channels," *Proc. IEEE Int. Conf. Commun. (ICC)*, pp. 3429–3433, June 2012.

[56] H. V. Vu, N. H. Tran, T. V. Nguyen, and S. I. Hariharan, "Estimating information rates of Bernoulli-Gaussian impulsive noise channels in Rayleigh fading," in *Proc. IEEE Int. Conf. Commun. (ICC)*, pp. 5859–5864, June 2014.

[57] H. V. Vu, N. H. Tran, T. V. Nguyen, and S. I. Hariharan, "Estimating Shannon and constrained capacities of Bernoulli-Gaussian impulsive noise channels in Rayleigh fading," *IEEE Trans. Commun.*, vol. 62, pp. 1845–1856, June 2014.

[58] A. Das, "Capacity-achieving distributions for non-Gaussian additive noise channels," *Proc. IEEE Int. Symp. Inform. Theory (ISIT)*, p. 420, June 2000.

[59] J. Fahs and I. Abou-Faycal, "On the capacity of additive white Alpha-stable noise channels," *Proc. IEEE Int. Symp. Inform. Theory (ISIT)*, pp. 294–298, July 2012.

[60] J. Cao, S. Hranilovic, and J. Chen, "Capacity-achieving distributions for the discrete-time Poisson channel-Part I: General properties and numerical techniques," *IEEE Trans. Commun.*, vol. 62, pp. 194–202, Jan. 2014.

[61] A. Tchamkerten, "On the discreteness of capacity-achieving distributions," *IEEE Trans. Inform. Theory*, vol. 50, pp. 2773–2778, Nov. 2004.

[62] H. Li, S. M. Moser, and D. Guo, "Capacity of the memoryless additive inverse Gaussian noise channel," *IEEE J. Sel. Areas in Commun.*, vol. 32, pp. 2315–2329, Dec. 2014.

[63] R. Zamir, "A Gaussian input is not too bad," *IEEE Trans. Inform. Theory*, vol. 50, pp. 1362–1367, June 2004.

[64] S. Ali and A. Ahmad, "Resource allocation, interference management and mode selection in device-to-device communication: A survey," *Trans. Emer. Tel. Tech.*, vol. 28, pp. 1–36, July 2017.

[65] F. A. Orakzai, M. Iqbal, M. Naeem, and A. Ahmad, "Energy efficient joint radio resource management in D2D assisted cellular communication," *Tel. Sys.*, vol. 69, pp. 505–517, Apr. 2018.

[66] N. Lee, X. Lin, J. G. Andrews, and J. Robert W. Heath, "Power control for D2D underlaid cellular networks: Modeling, algorithms, and analysis," *IEEE J. Sel. Areas in Commun.*, vol. 33, pp. 1–13, Jan. 2015.

[67] X. Lin, R. Ratasuk, A. Ghosh, and J. G. Andrews, "Modeling, analysis, and optimization of multicast device-to-device transmissions," *IEEE Trans. Wireless Commun.*, vol. 13, pp. 4346–4359, Aug. 2014.

[68] X. Lin, J. G. Andrews, and A. Ghosh, "Spectrum sharing for device-to-device communication in cellular networks," *IEEE Trans. Wireless Commun.*, vol. 13, pp. 6727–6740, Dec. 2014.

[69] H. ElSawy, E. Hossain, and M.-S. Alouini, "Analytical modeling of mode selection and power control for underlay D2D communication in cellular networks," *IEEE Trans. Commun.*, vol. 62, pp. 4147–4161, Nov. 2014.

[70] M. G. Khoshkholgh, Y. Zhang, K. Chen, K. G. Shin, and S. Gjessing, "Connectivity of cognitive device-to-device communications underlying cellular networks," *IEEE J. Sel. Areas in Commun.*, vol. 33, pp. 81–99, Jan. 2015.

[71] K. S. Ali, H. ElSawy, and M.-S. Alouini, "Modeling cellular networks with full-duplex D2D communication: A stochastic geometry approach," *IEEE Trans. Commun.*, vol. 64, pp. 4409 – 4424, Aug. 2016.

[72] X. Chai, T. Liu, C. Xing, H. Xiao, and Z. Zhang, "Throughput improvement in cellular networks via full-duplex based device-to-device communications," *IEEE Access*, vol. 4, pp. 7645–7657, 2016.

[73] S. Badri, M. Naslcheraghi, and M. Rasti, "Performance analysis of joint pairing and mode selection in D2D communications with FD radios," pp. 1–6, Apr. 2018.

[74] K. T. Hemachandra and A. O. Fapojuwo, "Duplex mode selection for throughput maximization in device-to-device underlaid cellular networks," in *Proc. IEEE Wireless Commun. and Netw. Conf. (WCNC)*, pp. 1–6, Apr. 2018.

[75] J. Gu, S. J. Bae, B.-G. Choi, and M. Y. Chung, "Dynamic power control mechanism for interference coordination of device-to-device communication in cellular networks," in *Proc. 3rd Int. Conf. Ubiquitous Future Netw.*, pp. 71–75, June 2011.

[76] S. Ali, N. Rajatheva, and M. Latva-aho, "Full duplex Device-to-Device communication in cellular networks," in *Proc. European Conf. on Netw. and Commun. (EuCNC)*, pp. 1–5, 2014.

[77] X. Huang, M. Zeng, J. Fan, X. Fan, and X. Tang, "A full duplex D2D clustering resource allocation scheme based on a K-means algorithm," *Wireless Commun. and Mobile Comput.*, vol. 2018, May 2018.

[78] S. Li, Q. Ni, Y. Sun, and G. Min, "Resource allocation for weighted sum-rate maximization in multi-user full-duplex device-to-device communications: Approaches for perfect and statistical CSIs," *IEEE Access*, vol. 5, pp. 27229–27241, Sept. 2017.

[79] J. Mirza, G. Zheng, K. Wong, and S. Saleem, "Joint beamforming and power optimization for D2D underlaying cellular networks,"," *IEEE Trans. Veh. Tech.*, vol. 67, pp. 8324–8335, Sept. 2019.

[80] J. Chen, H. Yin, L. Cottatellucci, and D. Gesbert, "Feedback mechanisms for FDD massive mimo with D2D-based limited CSI sharing," *IEEE Trans. Wireless Commun.*, vol. 16, pp. 5162–5175, Aug. 2017.

[81] H. Xu, N. Huang, Z. Yang, J. Shi, B. Wu, and M. Chen, "Pilot allocation and power control in D2D underlay massive MIMO systems," *IEEE Commun. Letters*, vol. 21, pp. 112–115, Jan. 2017.

[82] A. He, L. Wang, Y. Chen, K. Wong, and M. Elkashlan, "Spectral and energy efficiency of uplink D2D underlaid massive MIMO cellular networks," *IEEE Trans. Commun.*, vol. 65, pp. 3780–3793, Sept. 2017.

[83] A. Ghazanfari, E. Björnson, and E. G. Larsson, "Optimized power control for massive MIMO with underlaid D2D communications," *IEEE Trans. Commun.*, vol. 67, pp. 2763–2778, Apr. 2019.

[84] K. Shen, W. Yu, L. Zhao, and D. P. Palomar, "Optimization of MIMO device-to-device networks via matrix fractional programming:A minorization–maximization approach," *IEEE/ACM Trans. on Netw.*, vol. 27, no. 5, pp. 2164–2177, 2019.

[85] M. Botsov, M. Klügel, W. Kellerer, and P. Fertl, "Location dependent resource allocation for mobile device-to-device communications," in *Proc. IEEE Wireless Commun. and Netw. Conf. (WCNC)*, pp. 1679–1684, 2014.

[86] W. Sun, E. G. Ström, F. Brännström, K. C. Sou, and Y. Sui, "Radio resource management for D2D-based V2V communication," *IEEE Trans. Veh. Tech.*, vol. 65, pp. 6636–6650, Aug. 2016.

[87] W. Sun, D. Yuan, E. G. Ström, and F. Brännström, "Cluster-based radio resource management for D2D-supported safety-critical V2X communications," *IEEE Trans. Wireless Commun.*, vol. 15, pp. 2756–2769, Apr. 2016.

[88] L. Liang, G. Y. Li, and W. Xu, "Resource allocation for D2D-enabled vehicular communications," *IEEE Trans. Commun.*, vol. 65, pp. 3186–3197, July 2017.

[89] L. Liang, J. Kim, S. C. Jha, K. Sivanesan, and G. Y. Li, "Spectrum and power allocation for vehicular communications with delayed CSI feedback," *IEEE Wireless Commun. Letters*, vol. 6, pp. 458–461, Aug. 2017.

[90] R. Zhang, X. Cheng, Q. Yao, C. Wang, Y. Yang, and B. Jiao, "Interference graph-based resource-sharing schemes for vehicular networks," *IEEE Trans. Veh. Tech.*, vol. 62, pp. 4028–4039, Oct. 2013.

[91] L. Liang, S. Xie, G. Y. Li, Z. Ding, and X. Yu, "Graph-based resource sharing in vehicular communication," *IEEE Trans. Wireless Commun.*, vol. 17, pp. 4579–4592, July 2018.

[92] H. Ye, G. Y. Li, and B. F. Juang, "Deep reinforcement learning based resource allocation for V2V communications," *IEEE Trans. Veh. Tech.*, vol. 68, pp. 3163–3173, Apr. 2019.

[93] L. Liang, H. Ye, and G. Y. Li, "Spectrum sharing in vehicular networks based on multi-agent reinforcement learning," *IEEE J. Sel. Areas in Commun.*, vol. 37, pp. 2282–2292, Oct. 2019.

[94] D. Zhao, H. Qin, B. Song, Y. Zhang, X. Du, and M. Guizani, "A reinforcement learning method for joint mode selection and power adaptation in the V2V communication network in 5G," *IEEE Trans. Cognitive Commun. and Network.*, vol. 6, pp. 452–463, June 2020.

[95] M. F. Pervej and S. Lin, "Dynamic power allocation and virtual cell formation for throughput-optimal vehicular edge networks in highway transportation," in *Proc. IEEE Int. Conf. Commun. Workshops*, pp. 1–7, 2020.

[96] K. K. Nguyen, T. Q. Duong, N. A. Vien, N. Le-Khac, and M. Nguyen, "Non-cooperative energy efficient power allocation game in D2D communication: A multi-agent deep reinforcement learning approach," *IEEE Access*, vol. 7, pp. 100480–100490, 2019.

[97] Z. Li and C. Guo, "Multi-agent deep reinforcement learning based spectrum allocation for d2d underlay communications," *IEEE Trans. Veh. Tech.*, vol. 69, pp. 1828–1840, Feb. 2020.

[98] Y. S. Nasir and D. Guo, "Multi-agent deep reinforcement learning for dynamic power allocation in wireless networks," *IEEE J. Sel. Areas in Commun.*, vol. 37, pp. 2239–2250, Oct. 2019.

[99] W. Rudin, *Principles of Mathematical Analysis*. McGraw Hill:NewYork, 1964.

[100] M. Gursoy, H. V. Poor, and S. Verdu, "The capacity of the noncoherent Rician fading channel," *Princeton University Technical Report [Online]. Available: http://lcs3.syr.edu/faculty/gursoy/files/Techreport_revised.pdf*, Dec. 2002.

[101] R. L. Schilling, R. Song, and Z. Vondracek, "Bernstein functions: Theory and applications," *de Gruyter Studies in Mathematics 37, Berlin: Walter de Gruyter*, vol. 37, 2010.

[102] I. S. Gradshteyn and I. M. Ryzhik, *Table of Integrals, Series, and Products*. Academic Press, Inc., 6th ed., 2000.

[103] S. Lang, *Complex Analysis*. New York: Springer-Verlag, 2nd ed., 1985.

[104] M. D. Buhmann, *Radial Basis Functions: Theory and Implementations*. Cambridge Univ. Press, 2003.

[105] G. Fasshauer, *Meshfree approximation methods with Matlab*. World Scientific Pub. Co. Inc., 2007.

[106] C. O'Cinneide, "A property of completely monotonic functions," *J. Austral. Math. Soc. (Series A)*, vol. 42, pp. 143–486, Apr. 1987.

[107] H. Ferreira, L. Lampe, J. Newbury, and T. Swart, *Power line communications: Theory and applications for narrowband and broadband communications over power lines*. Wiley, 2010.

[108] D. G. Luenberger, *Optimization by Vector Space Methods*. New York: Wiley, 1969.

[109] H. E. Salzer and R. Zucker, "Table of the zeros and weight factors of the first fifteen Laguerre polynomials," *Bull. Amer. Math. Soc.*, vol. 55, pp. 1004–1012, Oct. 1949.

[110] M. Chung, M. S. Sim, D. K. Kim, and C. Chae, "Compact full-duplex MIMO radios in D2D underlaid cellular networks: From system design to prototype results," *IEEE Access*, vol. 5, pp. 16601–16617, 2017.

[111] M. R. A. Khandaker, C. Masouros, and K. Wong, "On coverage probabilities and sum-rate of full-duplex device-to-device cellular networks," in *Proc. IEEE Globecom Workshops (GC Wkshps)*, pp. 1–6, Dec. 2017.

[112] S. Dang, J. P. Coon, and G. Chen, "Resource allocation for full-duplex relay-assisted device-to-device multicarrier systems," *Electronics Letters*, vol. 6, pp. 166–169, Apr. 2017.

[113] S. Dang, G. Chen, and J. P. Coon, "Outage performance analysis of full-duplex relay-assisted device-to-device systems in uplink cellular networks," *IEEE Trans. Veh. Tech.*, vol. 66, pp. 4506–4510, May 2017.

[114] S. Dang, G. Chen, and J. P. Coon, "Multicarrier relay selection for full-duplex relay-assisted OFDM D2D systems," *IEEE Trans. Veh. Tech.*, vol. 67, pp. 7204–7218, Aug. 2018.

[115] H. Kha, H. Tuan, and H. Nguyen, "Fast global optimal power allocation in wireless networks by local D.C. programming," *IEEE Trans. Wireless Commun.*, vol. 11, no. 12, pp. 3510–3515, 2012.

[116] S. Huberman and T. Le-Ngoc, "Full-duplex MIMO precoding for sum-rate maximization with sequential convex programming," *IEEE Trans. Veh. Tech.*, vol. 64, pp. 5103–5112, Nov. 2015.

[117] G. Fodor *et al.*, "Design aspects of network assisted device-to-device communications," *IEEE Commun. Mag.*, vol. 50, pp. 170–177, Mar. 2012.

[118] T. Riihonen, S. Werner, and R. Wichman, "Mitigation of loopback selfinterference in full-duplex MIMO relays," *IEEE Trans. Signal Process.*, vol. 59, pp. 5983–5993, Dec. 2011.

[119] T. Riihonen, S. Werner, and R. Wichman, "Hybrid full-duplex/half-duplex relaying with transmit power adaptation," *IEEE Trans. Signal Process.*, vol. 10, pp. 3074–3085, Sept. 2011.

[120] D. Ng, E. Lo, and R. Schober, "Dynamic resource allocation in MIMO-OFDMA systems with full-duplex and hybrid relaying," *IEEE Trans. Commun.*, vol. 60, pp. 1291–1304, May 2012.

[121] L. J. Rodríguez, N. H. Tran, and T. Le-Ngoc, "Performance of full-duplex af relaying in the presence of residual self-interference," *IEEE Journal on Selected Areas in Communications*, vol. 32, pp. 1752–1764, Sept. 2014.

[122] Z. Tong and M. Haenggi, "Throughput analysis for full-duplex wireless networks with imperfect self-interference cancellation," *IEEE Trans. Commun.*, vol. 63, pp. 4490–4500, Nov. 2015.

[123] M. Duarte, C. Dick, and A. Sabharwal, "Experiment-driven characterization of full-duplex wireless systems," *IEEE Trans. Wireless Commun.*, vol. 11, no. 12, pp. 4296–4307, 2012.

[124] Z. Ma, Z. Zhang, Z. Ding, P. Fan, and H. Li, "Key techniques for 5G wireless communications: Network architecture, physical layer, and MAC layer perspectives," *SCIENCE CHINA Information Sciences*, vol. 58, pp. 1–20, 2015.

[125] A. Tang, X. Wang, and C. Zhang, "Cooperative full-duplex device to device communication underlaying cellular networks," *IEEE Trans. Wireless Commun.*, vol. 16, pp. 7800–7815, Dec. 2017.

[126] G. Zhang, K. Yang, P. Liu, and J. Wei, "Power allocation for full-duplex relaying-based D2D communication underlaying cellular networks," *IEEE Trans. Veh. Tech.*, vol. 64, pp. 4911–4916, Oct. 2015.

[127] S. Shalmashi and S. B. Slimane, "Cooperative device-to-device communications in the downlink of cellular networks," pp. 2265–2270, Apr. 2014.

[128] J. G. Andrews, F. Baccelli, and R. K. Ganti, "A tractable approach to coverage and rate in cellular networks," *IEEE Trans. Commun.*, vol. 59, pp. 3122–3134, Nov. 2011.

[129] S. Sternberg, *Dynamical Systems*. Dover, 2010.

[130] D. Moltchanov, "Distance distributions in random networks," *Ad Hoc Netw.*, vol. 10, pp. 1146–1166, Mar. 2012.

[131] Siemens, "Interference mitigation - Considerations and results on frequency reuse," *TSG-RAN WG1 Meeting #42 R1-050738*, Sept. 2005.

[132] S. N. Swain, S. Mishra, and C. S. R. Murthy, "A novel spectrum reuse scheme for interference mitigation in a dense overlay D2D network," in *Proc. Int. Symp. on Personal, Indoor and Mobile Radio Commun. (PIMRC)*, pp. 1201–1205, Aug. 2015.

[133] M. Klügel and W. Kellerer, "Determining frequency reuse feasibility in device-to-device cellular networks," in *Proc. Int. Symp. on Personal, Indoor and Mobile Radio Commun. (PIMRC)*, pp. 1503–1508, Aug. 2015.

[134] S. Gupta, S. Kumar, R. Zhang, S. Kalyani, K. Giridhar, and L. Hanzo, "Resource allocation for D2D links in the FFR and SFR aided cellular downlink," *IEEE Trans. Commun.*, vol. 64, pp. 4434–4448, Oct. 2016.

[135] D. Verenzuela and G. Miao, "Scalable device-to-device communications for frequency reuse $\gg 1$," *IEEE Trans. Wireless Commun.*, vol. 16, pp. 3435–3447, June 2017.

[136] Z. Zhang, R. Q. Hu, Y. Qian, and A. Papathanassiou, "D2D communication underlay in uplink cellular networks with fractional power control and fractional frequency reuse," in *Proc. IEEE Global Commun. Conf. (GLOBECOM)*, pp. 1–7, Dec. 2015.

[137] H. Zhu and J. Wang, "Device-to-device communication in cellular networks with fractional frequency reuse," in *Proc. IEEE Int. Conf. Commun. (ICC)*, pp. 5503–5507, June 2014.

[138] "3rd generation partnership project; Technical specification group radio access network; Evolved universal terrestrial radio access (E-UTRA); Radio frequency (RF) system scenarios (Release 14)," *TR 36.942 V14.0.0*, Mar. 2017.

[139] K. T. K. Cheung, S. Yang, and L. Hanzo, "Achieving maximum energy-efficiency in multi-relay OFDMA cellular networks: A fractional programming approach," *IEEE Trans. Commun.*, vol. 61, no. 7, pp. 2746–2757, 2013.

[140] A. Zappone and E. Jorswieck, "Energy efficiency in wireless networks via fractional programming theory," *Foundations Trends Commun. Inf. Theory*, vol. 11, pp. 185–396, June 2015.

[141] K. Shen and W. Yu, "Fractional programming for communication systems-Part I: Power control and beamforming," *IEEE Trans. Signal Process.*, vol. 66, pp. 2616–2630, May 2018.

[142] J. Hoydis, S. ten Brink, and M. Debbah, "Massive MIMO in the UL/DL of cellular networks: How many antennas do we need?," *IEEE J. Sel. Areas in Commun.*, vol. 31, pp. 160–171, Feb. 2013.

[143] "3rd generation partnership project; Technical specification group radio access network; Evolved universal terrestrial radio access (E-UTRA); Further advancements for E-UTRA physical layer aspects (Release 9)," *TR 36.814 V9.2.0*, Mar. 2017.

[144] W. Yi, Y. Liu, Y. Deng, A. Nallanathan, and R. W. Heath, "Modeling and analysis of mmWave V2X networks with vehicular platoon systems," *IEEE J. Sel. Areas in Commun.*, vol. 37, pp. 2851–2866, Dec. 2019.

[145] "3rd generation partnership project; Technical specification group services and system aspects; Study on enhancement of 3GPP support for 5G V2X services (Release 15)," *TS 22.886 v15.0.0*, Mar. 2017.

[146] R. Molina-Masegosa and J. Gozalvez, "LTE-V for sidelink 5G V2X vehicular communications: A new 5G technology for short-range vehicle-to-everything communications," *IEEE Veh. Tech. Mag.*, vol. 12, pp. 30–39, Dec. 2017.

[147] V. Mnih *et al.*, "Human-level control through deep reinforcement learning," *Nature*, vol. 518, pp. 529–533, 2015.

[148] R. S. Sutton and A. G. Barto, *Reinforcement Learning: An Introduction*. MIT Press, 1998.

[149] R. Bellman, *Dynamic Programming*. Princeton University Press, 1957.

[150] H. V. Hasselt, "Double Q-learning," *Advances in Neural Information Processing Systems*, p. 2613–2621, 2010.

[151] J. Foerster *et al.*, "Stabilising experience replay for deep multi-agent reinforcement learning," in *Proc. Int. Conf. Mach. Learn. (ICML)*, pp. 1146–1155, 2017.

[152] S. Ruder, "An overview of gradient descent optimization algorithms," *arXiv preprint arXiv:1600.04747*, 2016.

[153] J. Choi, V. Va, N. Gonzalez-Prelcic, R. Daniels, C. R. Bhat, and R. W. Heath, "Millimeter-wave vehicular communication to support massive automotive sensing," *IEEE Commun. Mag.*, vol. 54, pp. 160–167, Dec. 2016.

[154] S. Hur, T. Kim, D. J. Love, J. V. Krogmeier, T. A. Thomas, and A. Ghosh, "Millimeter wave beamforming for wireless backhaul and access in small cell networks," *IEEE Trans. Commun.*, vol. 61, pp. 4391–4403, Oct. 2013.